AD-A069 537 ROCKWELL INTERNATIONAL ANAHEIM CA ELECTRONICS RESEAR--ETC F/G 11/6
TEMPERATURE SENSITIVE OPTICAL PHENOMENA IN HEAVY METAL HALIDE F--ETC(U)
JAN 79 J D MCMULLEN, D M HEINZ, F S STEARNS DAAK70-77-C-0165

UNCLASSIFIED C79-8-501 NL

1 OF 4
AD A069537

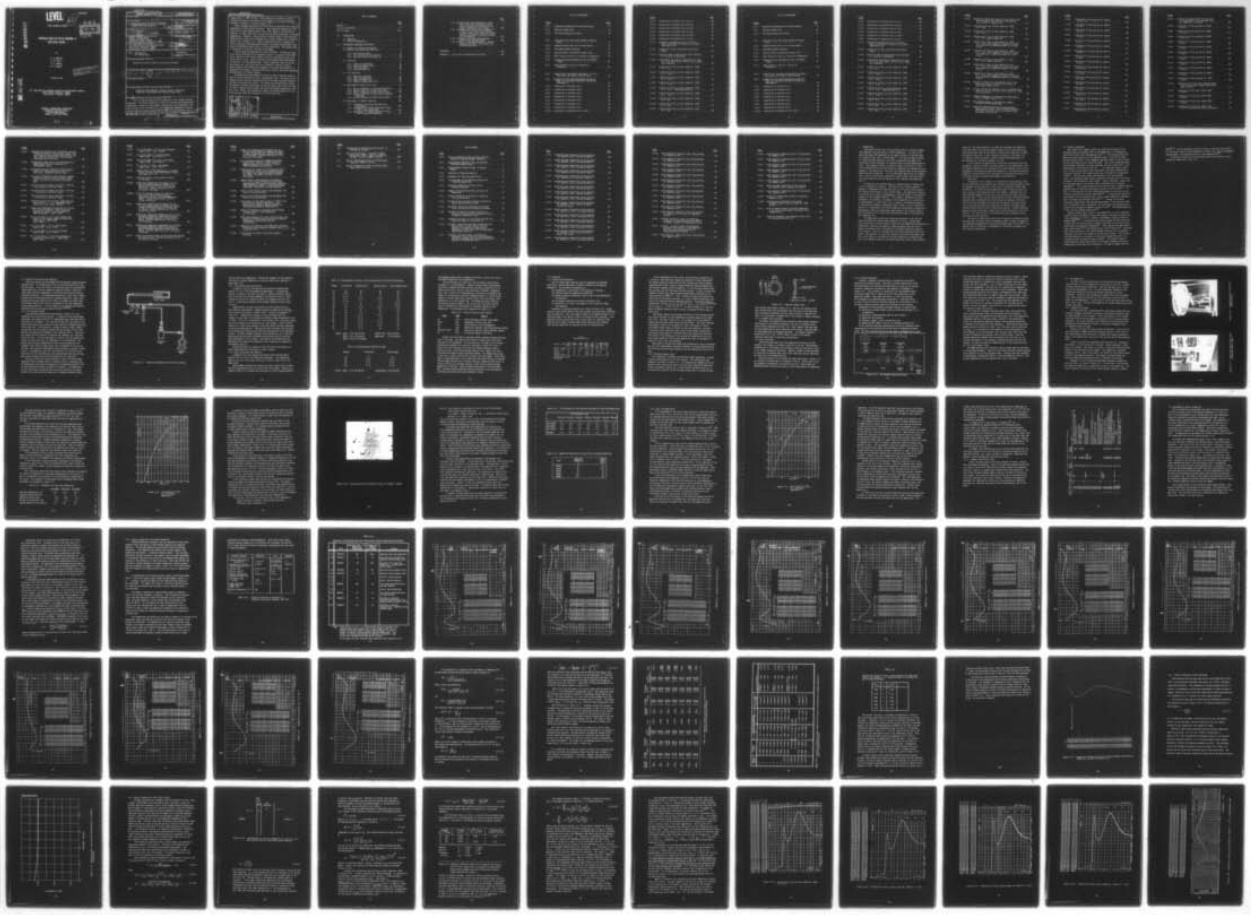

LEVEL II

C79-8-501

FINAL TECHNICAL REPORT

TEMPERATURE SENSITIVE OPTICAL PHENOMENA IN HEAVY METAL HALIDES

By

J. D. McMullen
D. M. Heinz
F. S. Stearns
B. R. Youmans

8 January 1979

U.S. Army Mobility Equipment Research and Development Command
Night Vision Laboratory, W26P8H
Fort Belvoir, Virginia 22060

ROCKWELL INTERNATIONAL CORPORATION
Electronics Research Center
3370 Miraloma Avenue
Anaheim, California 92803

UNCLASSIFIED

SECURITY CLASSIFICATION OF THIS PAGE (When Data Entered)

REPORT DOCUMENTATION PAGE		READ INSTRUCTIONS BEFORE COMPLETING FORM
1. REPORT NUMBER	2. GOVT ACCESSION NO.	3. RECIPIENT'S CATALOG NUMBER
4. TITLE (and Subtitle) (6) TEMPERATURE SENSITIVE OPTICAL PHENOMENA IN HEAVY METAL HALIDE FILMS. (14)		5. TYPE OF REPORT & PERIOD COVERED 19 September 1977 FINAL rpt -31 October 1978
		6. PERFORMING ORG. REPORT NUMBER C79-8-501
7. AUTHOR(s) (10) J. D. McMullen, D. M. Heinz, F. S. Stearns, B. R. Youmans		8. CONTRACT OR GRANT NUMBER(s) (15) DAAK70-77-C-0165 new
9. PERFORMING ORGANIZATION NAME AND ADDRESS ROCKWELL INTERNATIONAL Electronics Research Center, 3370 Miraloma Ave., Anaheim, CA 92803		10. PROGRAM ELEMENT, PROJECT, TASK AREA & WORK UNIT NUMBERS (12) 294p.
11. CONTROLLING OFFICE NAME AND ADDRESS U.S. Army Mobility Equipment R&D Command Night Vision Laboratory W26P8H Fort Belvoir, Virginia 22060 (11)		12. REPORT DATE 8 Jan 1979
		13. NUMBER OF PAGES 294
14. MONITORING AGENCY NAME & ADDRESS (if different from Controlling Office) Attn: DRSEL-NV-FIR Dr. Edward Sharp		15. SECURITY CLASS. (of this report) UNCLASSIFIED
		15a. DECLASSIFICATION/DOWNGRADING SCHEDULE

16. DISTRIBUTION STATEMENT (of this Report)

Approved for public release; distribution unlimited.

17. DISTRIBUTION STATEMENT (of the abstract entered in Block 20, if different from Report)

(9) Final technical rpt, 19 Sep 77 – 31 Oct 78

18. SUPPLEMENTARY NOTES

19. KEY WORDS (Continue on reverse side if necessary and identify by block number)

Absorption Edge Modulator, Thermal Imaging, Thermo-optic Properties, Lead Iodide Films, Mercury Iodide Films.

20. ABSTRACT (Continue on reverse side if necessary and identify by block number)

Films of PbI_2 and HgI_2 have been deposited on thin polymer and glass substrates. The thermal properties of the film materials were measured by a thermographic method to obtain thermal conductivity, heat diffusivity, and specific heat of the film materials. The temperature dependence of the absorption edge was measured between 0°C and 50°C for both materials and

over

(Cont'd.)

DD FORM 1 JAN 73 1473 EDITION OF 1 NOV 65 IS OBSOLETE

UNCLASSIFIED

SECURITY CLASSIFICATION OF THIS PAGE (When Data Entered)

ranging down to -175°C for PbI_2. These properties are needed in order to evaluate the potential application of each material as an absorption-edge-modulated transducer for thermal imaging.

Highly oriented polycrystalline films of PbI_2 are obtained with a substrate temperature of 150°C during film growth. Lower substrate temperatures yield PbI_2 films of lower apparent density and a lower degree of crystallite orientation. Parylene films used as substrates sag during depositions at elevated temperatures. Therefore, a PbI_2-parylene transducer grown at 150°C substrate temperature will need to be re-mounted onto a smaller support ring in order to obtain a taut transducer film. Optical transmission data is presented for several PbI_2-glass and PbI_2-parylene samples, including high-resolution scans across the absorption edge of PbI_2 at various tempratures. The complex index of refractive is given as a function of wavelength.

Films of HgI_2 were deposited onto glass substrates. The HgI_2 was found to be reactive with metals and evaporated rapidly in a vacuum at room temperature. Because of this latter property, physical measurements could not be carried out in vacuum. Optical transmission measurements were made between 0°C and 50°C in an unevacuated dewar. Thermal properties could not be measured because the HgI_2 films could not be thermally isolated in vacuum. Several encapsulation methods were attempted, but further development of an encapsulating overlayer is required before HgI_2 films can be used as absorption-edge modulators for thermal imaging.

The thermographic measurements are the first known contactless measurements of thermal properties of thin, rim-supported films. The theory for the steady-state and transient temperature profiles has been developed assuming a uniformly distributed heat source. This theory must be modified to include the Gaussian transverse distribution of the laser beam used to heat the films, in order to reduce the data further and obtain the thermal properties of the PbI_2 films. Thermal time constants as short as 20 ms were measured for 0.2μ thick parylene substrates covered by a 0.2μ thick PbI_2 film.

TABLE OF CONTENTS

LIST OF ILLUSTRATIONS

LIST OF ILLUSTRATIONS

LIST OF TABLES

1. INTRODUCTION

Heavy-metal halides such as PbI_2 and HgI_2 exhibit a strongly temperature dependent absorption edge at visible frequencies. The shift in the absorption edge with temperature can be used to convert an infrared image of a thermal source into a visible image.[1,2] This type of image converter, or "absorption-edge modulator," may offer considerable advantages as an infrared-to-visible transducer for forward-looking infrared imaging applications. The transducer design is relatively simple, consisting of a thin film of thermo-optically sensitive material supported by an appropriate thin substrate. The sensitivity, resolution, and response speed of the transducer depend upon the strength with which the absorption edge shifts with temperature, as well as the thermal conductivity, specific heat, and heat diffusivity of the materials, and the thinness of the transducer and supporting film.[1-5]

In operation, the infrared image of a thermal source is focused upon a film of thermo-optic material. Absorption of the infrared radiation generates a temperature distribution across the film which closely matches the intensity distribution in the infrared image. The temperature change at a particular point causes a corresponding, localized change in some physical property of the transducer material. This change is monitored at visible frequencies; for example, as a change in the transmittivity or reflectivity for monochromatic, visible light, or as a change in the photoluminescence or the electron-injection luminescence output. When a film of thermo-optic material is illuminated by an infrared image and simultaneously flooded with monochromatic light at an absorption edge frequency, the infrared image is then replicated in the visible light transmitted through or reflected from the transducer film.

The temperature distribution induced by absorption of the infrared image replicates the infrared image faithfully for only a limited time, until lateral heat diffusion begins to smear out the temperature distribution. In steady-state operation the amount of smearing depends upon the lateral thermal resistance, which is governed by the thermal conductivity and the film thickness. There are two approaches for maintaining high spatial resolution. One approach is to chop the incoming infrared beam and sample with the visible beam at a time when the localized temperature variations have built up to maximum resolution and before significant lateral heat diffusion

can occur. The second approach is to make the transducer and supporting films sufficiently thin and the thermal conductivity and heat diffusivity sufficiently small that the resistance to lateral heat conduction is large. For practical materials, a total transducer thickness of less than 0.5μ is required in order to obtain a thermal response time approaching 0.1 millisecond for a resolution element of 0.1 mm.

In this program, we address the feasibility of fabricating such thin transducers, about 0.2μ thick, with PbI_2 and HgI_2 as the thermo-optic films. The thermal properties of the transducer films are measured, as well as the dependence of the absorption edge upon temperature. The thermal and optical properties reported herein form a data base for optimizing the design of an infrared-to-visible transducer which employs these materials.

1.1. Objectives

The purpose of this program is to fabricate thin PbI_2 and HgI_2 films on thin substrates, and to measure their thermal and optical properties which are important in the operation of the films as infrared-to-visible image transducers. The films are vacuum-deposited layers of PbI_2 and HgI_2, 0.2μ thick, having a clear aperture of one inch diameter. Substrates are 0.2μ thick parylene membranes for the PbI_2 films and 18μ thick pyrex glass for the HgI_2 films. X-ray, electron microscope and electron diffraction measurements are made to determine the crystal structure, polytype, uniformity, crystallite size and degree of crystallite orientation; and these results are in turn used to optimize the deposition parameters to produce highly oriented polycrystalline films of good optical quality. Thermal properties measured include the thermal conductivity and heat diffusivity of the film material. The specific heat is calculated from these parameters and the mass density of the materials.

The optical transmission of the films is measured from 900nm to 400nm, and with high resolution across the absorption edge, in order to determine the temperature dependence of the absorption edge between 0^oC and 50^oC. The complex index of refraction is determined as a function of frequency over this range of temperatures.

1.2 Technical Background

Lead iodide (PbI_2) commonly occurs as crystalline polytype 2H with hexagonal space group symmetry $P\bar{3}m1$ at room temperature. At temperatures above 150°C several other polytypes may form.[6,7] The polytype affects the detailed optical properties of the absorption edge. At 4.5°K the strong exciton absorption peak in the fundamental absorption edge is 0.010 eV lower for the 2H polytype than for the 4H polytype.[8] PbI_2 films vacuum-evaporated onto amorphous substrates are highly oriented, with the crystallites' $\hat{c}$ axes perpendicular to the plane of the film.[9] The absorption edge at about 0.52μ (2.36eV) shifts toward longer wavelengths with higher temperatures at a rate of -0.54 meV/°K for single crystals and -0.16 meV/°K for evaporated films.[9,10] There are two primary contributions to the strong thermal shift of the absorption edge; namely, broadening of energy levels by lattice vibrations, and dilatation of the crystal.[9] Lattice vibrations always cause the absorption edge to shift toward longer wavelengths with increasing temperature.[11] The dilatation mechanism may shift the edge in either direction, depending upon the detailed energy band structure for the crystal.[9,11] For PbI_2 it is believed that the two contributions oppose in sign, but the contribution from lattice vibrations dominates.[9,12] A strong exciton transition which appears in the absorption edge is also strongly temperature dependent, both in strength and wavelength position.[13-17] A number of the above referenced investigations have reported measurements of the refractive index and its dispersion, and a comparison of the results has been reported which resolves the discrepancies apparent in earlier work.[18] The photodecomposition of PbI_2 has been studied extensively.[9-23]

Mercuric iodide (HgI_2) occurs at room temperature as a red, tetragonal (α-phase) crystal belonging to space group $P4_2/nmc$, and above the phase transition temperature of 127°C as a yellow, orthorhombic (β-phase) crystal of symmetry Bbmm.[24-26] A crystal which has passed through the phase transition exhibits poor crystalline quality, making it desirable to carry out crystal growth below the transition temperature.[25] Vapor transport has been used to grow single crystals[27-30] and polycrystalline films[31] below 127°C. The growth habit of HgI_2 along the $\hat{c}$ axis should produce oriented films on amorphous substrates, with the $\hat{c}$ axis normal to the substrate surface. Films of HgI_2 have been observed to be unstable in vacuum, with evaporation loss of I_2 attributed to the low vapor pressure of HgI_2.[32] The absorption edge of rapidly-quenched, yellow HgI_2 exhibits the strongest frequency shift with temperature of any known solid, amounting to -2.4 meV/°K between 100°K and

400°K.[25,33] Exciton absorption structure in HgI_2 is very weak, particularly for the optical electric field perpendicular to the ĉ axis, and the fundamental edge dominates the absorption curves at room temperature.[33,34]

The physical properties of PbI_2 and HgI_2 which are of interest in this program are summarized in Table 1.2-1.

Table 1.2-1. Physical properties of PbI_2 and HgI_2 which are relevant to absorption-edge transducers

Material	Absorption Edge Wavelength (μ)	Temperature Shift of Absorption Edge (meV/°K)	Coefficient of Linear Expansion $\alpha = \frac{1}{\ell}\frac{d\ell}{dT}$ ($°K^{-1}$)	Specific Heat Cp at 25°C	Mass Density (g/cm^3)
PbI_2 crystal 2H hexagonal	0.5260 (Ref. 9)	-0.5414(100-520°K) (Ref. 9)	$\alpha_a = 3.4 \times 10^{-5}$ $\alpha_c = 2.1 \times 10^{-5}$ (Ref. 18,38,39) $\langle\alpha\rangle = 3.36 \times 10^{-5}$ (Ref. 40)	0.17 (Ref. 40)	5.625 (Ref. 40)
PbI_2 film 2H hexagonal	0.5260 (Ref. 9)	-0.1624(100-300°K) (Ref. 9)			
HgI_2 crystal α-phase, red tetragonal	0.5840 (Ref. 25)	-0.7(100-200°K) -1.4(330-400°K) (Ref. 25)		0.17 (Ref. 40)	6.094 (yellow) 6.060 (red) (Ref. 40)

2. EXPERIMENTAL PROCEDURES AND RESULTS

2.1. Summary of Procedures and Results

Films of PbI_2 have been vacuum deposited on both glass and thin polymer substrates, including 0.2μ parylene and 0.05μ thick nitrocellulose substrates. Deposition parameters were optimized to produce highly oriented polycrystalline films of good optical quality. Films 0.2μ in thickness were characterized optically and by X-ray, electron microscope, and electron beam measurements. The temperature dependence of the absorption edge was determined by optical transmission measurements for temperatures between -175°C and 50°C. The complex index of refraction was calculated as a function of frequency for temperatures between 0°C and 50°C.

Original experiments were performed using a thermographic system to obtain the thermal properties of the films, including thermal conductivity and heat diffusivity. Knowledge of the actual values of these physical properties demands a more thorough analysis of the actual experimental conditions, which would be a subject of future work, because the first-cut analysis which assumed uniform sample heating proved too simplistic. The experimental data which has been taken is sufficient to yield these properties, however, and the temperature distributions and thermal time constants reported are of interest for thermal imaging applications.

Six samples of PbI_2-glass and five samples of PbI_2-nitrocellulose have been delivered. The PbI_2-parylene samples were consumed during the measurements of thermal properties.

Films of HgI_2 were deposited onto glass substrates. Because of the high vapor pressure of HgI_2, the deposition process was extremely difficult to control. Additionally, the HgI_2 films re-evaporated rapidly in vacuum during optical and thermal tests. This behavior would prevent the use of HgI_2 films as infrared-to-visible transducers because the film must be in vacuum to minimize heat transferred away from the film. Several methods were attempted to encapsulate the HgI_2 films, including overlayers of parylene, SiO_2, and photoresist. However, the high vapor pressure of solid HgI_2 makes passivation difficult. This passivation problem must be solved before thermal properties can be measured and before HgI_2 can be used in the intended thermal imaging application. Because of the high risk in obtaining stable films of HgI_2, it was agreed that emphasis in this program should be on PbI_2. Optical transmission measurements were made at temperatures between 0°C and 50°C on the HgI_2 films which were deposited.

2.2 Material Purification and Stability

Both PbI_2 and HgI_2 were purchased from the Research Organic/Inorganic Chemical Corp. The listed purity of PbI_2 was 99.99 percent and of HgI_2 was 99 percent. Since the films of PbI_2 and HgI_2 were to be prepared by vacuum deposition, and most commercial chemicals contain higher and lower vapor pressure contaminants, a preliminary purification step was considered necessary. Two evaporation-condensation cycles under reduced pressure was the technique chosen for removing impurities: higher vapor pressure constituents would be less likely to condense and lower vapor constituents would be less likely to evaporate at the same temperature as the desired material. This was found to be a preferred purification technique for PbI_2 and HgI_2 by earlier workers[27,35,36].

2.2.1 Purification System

The evaporation-condensation system shown in Figure 2.2-1 was assembled for purifying PbI_2 and HgI_2. In addition to the vacuum pumps and gauges, the system consisted of a demountable pyrex tube about 80 cm long and 4 cm in diameter. This tube was divided into four bulbs by the three constrictions, was closed at one end, and had a standard taper joint at the other end. Purification of a charge of material under vacuum in the end bulb A was initiated by heating the tube furnace, which caused material to evaporate and condense in the adjoining bulb B. Then bulb A was removed and the transport of material was repeated, this time from bulb B to bulb C. The purified material in bulb C was next removed and stored in a dark desiccator for subsequent use in evaporations. The higher vapor pressure contaminants of the as-received material were trapped in the liquid nitrogen cooled trap or condensed in bulb D, and the lower vapor pressure contaminants were discarded as residues in bulbs A and B. In preparing a tube for a purification run, filling the end bulb A was less of a problem than anticipated because both PbI_2 and HgI_2 were easily crushed and carried to the end bulb via a 6mm tube.

The key to this purification technique is the use of the minimum temperature which produces material transport within a reasonable time. Low temperatures are especially important in transporting materials such as these iodides which have a tendency to decompose. The temperature of the tube furnace surrounding the end bulb was monitored by thermocouples at the center of the furnace but no attempt was made to deter-

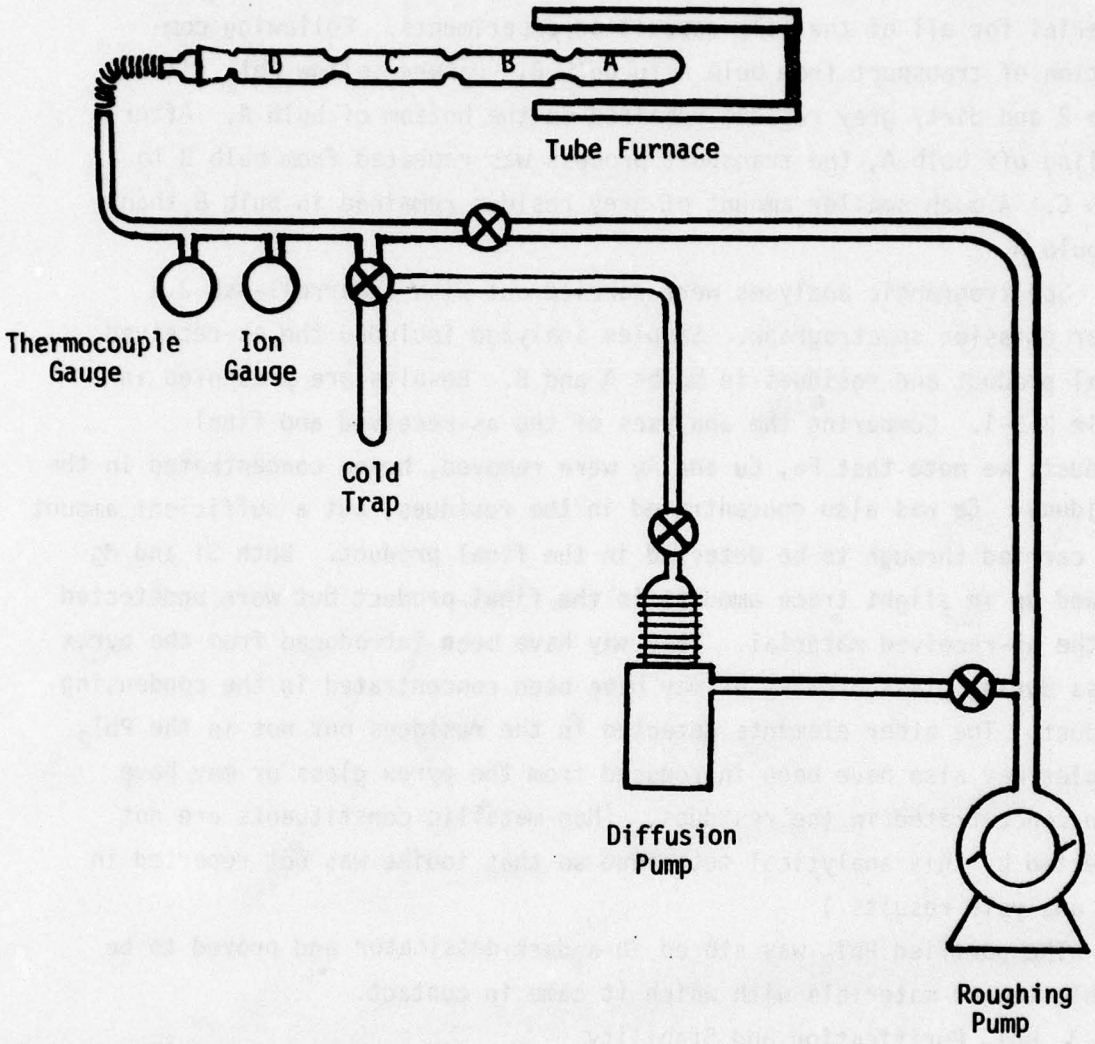

Figure 2.2-1. Evaporation-Condensation Purification System.

mine the exact bulb temperature. Significant transport of both materials occurred at a furnace temperature of just over 400°C and a pressure of about 25μm of Hg.

2.2.2 PbI_2 Purification and Stability

A charge of just over 300 gms was purified which provided ample material for all of the film deposition experiments. Following completion of transport from bulb A to bulb B, canary yellow PbI_2 filled bulb B and dirty grey residue remained in the bottom of bulb A. After sealing off bulb A, the transport process was repeated from bulb B to bulb C. A much smaller amount of grey residue remained in bulb B than in bulb A.

Spectrographic analyses were carried out with a Jarrell-Ash 3.4 meter emission spectrograph. Samples analyzed included the as-received, final product and residues in bulbs A and B. Results are presented in Table 2.2-1. Comparing the analyses of the as-received and final product, we note that Fe, Cu and Ag were removed, being concentrated in the residues. Ca was also concentrated in the residues, but a sufficient amount was carried through to be detected in the final product. Both Si and Mg showed up in slight trace amounts in the final product but were undetected in the as-received material. They may have been introduced from the pyrex glass during glass blowing or may have been concentrated in the condensing product. The other elements detected in the residues but not in the PbI_2 samples may also have been introduced from the pyrex glass or may have been concentrated in the residues. (Non-metallic constituents are not detected by this analytical technique so that iodine was not reported in the analysis results.)

The purified PbI_2 was stored in a dark dessicator and proved to be stable toward materials with which it came in contact.

2.2.3 HgI_2 Purification and Stability

A charge of just over 300 gms was purified which provided ample material for all of the film deposition experiments. The transported material was red, and residues consisted of traces of grey film on the empty bulbs.

Spectrographic analyses were carried out with a Jarrell-Ash 3.4 meter emission spectrograph on the as-received and final product. Results presented in Table 2.2-2 indicate that the purity of the as-received material

Table 2.2-1 Spectrographic Analyses of PbI_2 and Residues from Purification Process

Element	As-Received	Residue Bulb A	Residue Bulb B	Final Product Bulb C
Pb	ma	ma	ma	ma
Fe	sl tr	mi	mi	un
Cu	sl tr	tr	tr	un
Ag	sl tr	sl tr	sl tr	un
Ca	sl tr	tr	tr	sl tr
Si	un	tr	mi	sl tr
Mg	un	sl tr	sl tr	sl tr
P	un	mi	mi	un
Na	un	tr	tr	un
Al	un	sl tr	sl tr	un
B	un	sl tr	tr	un
Mn	un	sl tr	sl tr	un
Ti	un	sl tr	sl tr	un
Cr	un	sl tr	sl tr	un
Zn	un	sl tr	un	un

Legend: major 10 to 100 percent
minor 0.5 to 10 percent
trace 0.01 to 0.5 percent
slight trace <0.01 percent
undetected <0.001 percent

Table 2.2-2 Spectrographic Analyses of HgI_2

Element	As-Received	Final Product
Hg	ma	ma
Ag	sl tr	sl tr
Ca	sl tr	sl tr
Mg	sl tr	sl tr

Legend: major 10 to 100 percent
slight trace <0.01 percent

was somewhat greater than its nominal 99 percent, and that there was no noticeable change after the sublimations.

The purified HgI_2 was stored in a dark dessicator and proved to be stable in a glass container. However, several workers had reported difficulty in making electrical contacts with HgI_2 crystals due to its chemical reactivity, and since this could pose a problem in preparing HgI_2 films, a brief set of experiments was carried out to determine the extent of its reactivity with metal commonly present in a vacuum system. Samples of several metals were placed in glass vials with HgI_2 at room temperature in air for several days. No attempt was made to analyze the reaction products; however, the results were consistent with the heats of formation and free energies of the metal iodides at room temperature. The observations are summarized in Table 2.2-3.

Table 2.2-3. Action of HgI_2 on Several Metals

METAL	FORM	RESULTS
Al	foil	rapid continuous reaction, grey powder
Brass	bulk	amalgamated surface, grey scum
Ag	film	rapid reaction, silver disappeared
Cu	bulk	superficial reaction, dark brown adherent coating
Stainless Steel	bulk	superficial reaction, maroon adherent coating
Au	film	no observed change in four days

Further tests were made to determine whether anodized coatings would protect Al from HgI_2. The samples were stored in covered glass vials which were open to the atmosphere. The test materials included an Al wire whose anodizing was adequate for electrical insulation, a piece of Al foil, a piece of Al with a MIL-spec olive drab soft anodized coating, another piece of Al with a black hard anodized coating, and a length of Al wire from which the anodized coating had been removed. The samples were placed in the vials so that a portion was in contact with HgI_2 powder. After three weeks at room temperature, it was found that there was little or no reaction with the sample portion not in contact with HgI_2 powder but that any Al in contact with HgI_2 was consumed (leaving a clear viscous liquid and what appeared to be free Hg). Based on these observations, it was concluded that anodized coatings provided effective protection of Al from reaction with HgI_2 except where there were pinholes or cracks.

2.3 Substrates

2.3.1 General Considerations

The thin thermo-optic materials must be supported on substrates which have a unique combination of optical, mechanical and chemical properties. The substrate requirements are:

(a) transparency in the region of the spectrum of interest,

(b) stability under film deposition conditions,

(c) thermal expansion coefficient close to that of the thermo-optic film material,

(d) low thermal conductivity and heat diffusivity, and

(e) availability as a thin, flat sheet or film to provide a 20mm clear aperture.

Properties of substrate materials are listed in Table 2.3-1. Several materials which might otherwise have been suitable substrates were eliminated from consideration. Thus, for example, Kapton H was rejected because of its absorption edge in the spectral region of interest for PbI_2 and HgI_2. Film deposition of PbI_2 should take place at about 150°C in a vacuum so that materials which outgas or deform under these conditions were rejected. (This was one reason for not pursuing the use of nitrocellulose.)

Table 2.3-1
Properties of Substrate Materials*

Composition	Trade Name	Refractive Index (at 589.3nm)	Maximum Temperature (°C)	Thermal Expansion $(°C)^{-1}$	Thermal Conductivity $\left(\frac{Watts}{cm\text{-}C°}\right)$	Specific Heat $\left(\frac{Joules}{gm\ C°}\right)$	Density $\left(\frac{gm}{cm^3}\right)$	Thermal** Diffusivity $\left(\frac{cm^2}{sec}\right)$	Minimum Thickness (microns)
0211 Glass	Microsheet	1.523	510	7.38×10^{-6}	1.21×10^{-2}	0.753	2.57	5.0×10^{-3}	~ 40
7740 Glass	Pyrex	1.474	510	3.25	1.21×10^{-2}	0.837	2.23	5.2	~ 40
Nitrocellulose		1.50	60	130	1.67×10^{-3}	1.59	1.38	0.8	0.05
Polyxylylene	Parylene-N	1.661	200	35	1.25×10^{-3}	0.837	1.11	1.4	0.05

*Data from manufacturers' literature

**Calculated values

In one investigation of PbI_2 films, the best optical properties on a variety of substrates were obtained by deposition on NaCl substrates.[37] The thermal expansion coefficients of PbI_2 and NaCl are closely matched, suggesting that stress caused by thermal expansion mismatch between film and substrate degrades optical properties. It has also been observed that PbI_2 and HgI_2 are soft and easily form dislocations. In fact, dislocations formed by cleaving HgI_2 were followed through 500μm of material by dislocation etch pit studies.[27] Thus, in order to prepare and characterize films with low dislocation densities, all stress should be minimized, both during film growth and during subsequent handling. The thermal expansion coefficients for PbI_2 are $\alpha_a = 30 \times 10^{-6}/C°$ and $\alpha_c = 21 \times 10^{-6}/C°$[18,38,39] and for HgI_2 is $\alpha = 2.39 \times 10^{-6}/C°$.[40] As seen in Table 2.3-1, the best match of thermal expansion values for PbI_2 is parylene-N and for HgI_2 is pyrex glass.

The thermal conductivity and heat diffusivity of the substrate should be as low as possible to avoid degrading an infrared image on the thermo-optic film. As shown in Table 2.3-1, the polymers are to be preferred because they have much lower values than the glasses. The final substrate requirement is that it be available as a thin, flat sheet or film of sufficiently broad extent to provide a 20 mm clear aperture. Obviously, a relatively thick substrate, albeit one with low thermal conductivity, could permit the passage of sufficient heat along a path which parallels the surface of the thermo-optic film to mask the properties of the film. Thus organic materials, which can be deposited or cast in thicknesses of tenths of a μm or less, are preferred.

While none of the materials which were considered for use as substrates met all of the requirements, parylene N appeared to be most appropriate for use with PbI_2 and pyrex glass appeared to be most appropriate for use with HgI_2.

2.3.2 Substrate Support Rings

For convenience in handling and mounting fragile substrates, a support ring was standardized for use on this program. The configuration and dimensions are shown in Figure 2.3-1. The substrate was bonded to the flat surface of the ring using an epoxy resin (Vac-Seal from Perkin Elmer Corp., GE Vac from General Electric Co., or Epoxi-Patch from Dexter Corp.) or a silicone resin (Silastic 732 RTV from Dow Corning Corp., or Black-Silicone

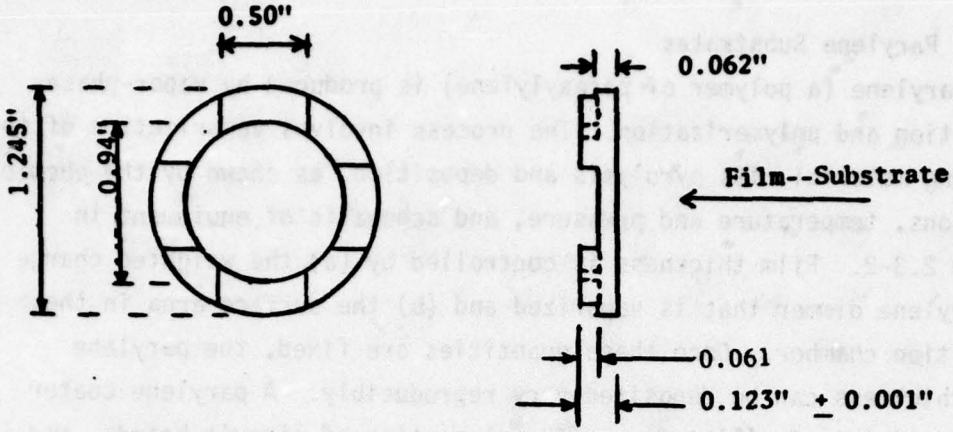

Figure 2.3-1. Substrate Support Ring

Glue and Seal from General Electric Co.). The 0.5 inch grooves on the back surface permit free gas movement from both faces of the substrate. Thus a pressure differential does not build up across a substrate foil when it is placed upon or removed from a flat surface, or when a substrate is in a chamber being evacuated.

The support ring materials were selected to match thermal expansion coefficients of the substrate materials so as not to introduce strain which could be propagated into the film. Glass support rings were made for HgI_2 depositions on glass substrates and Al support rings were made for PbI_2 depositions on parylene substrates. (The thermal expansion coefficient of Al is 23×10^{-6}/C° which is close to the thermal expansion coefficients of both PbI_2 and parylene.)

2.3.3 Glass Substrates

Glass microscope cover slips are commercially available as 25 mm diameter disks ranging in thickness from 0.10 to 0.25 mm. Unfortunately, manufacturers of this product are reluctant to disclose the type of glass or its thermal expansion coefficient. However, because of the convenience of being able to purchase glass cover slips, they were used as substrates for much of our film deposition work.

Since the thinnest slip available was about 200μm thick, a batch of 13 was optically polished down to a thickness of 46 μm. Thinner glass slips can probably be produced but the yield will be low. Work on HgI_2 was terminated before an effort was made to polish Pyrex glass for substrates.

2.3.4 Parylene Substrates

Parylene (a polymer of paraxylylene) is produced by vapor-phase deposition and polymerization. The process involves vaporization of the starting material, its pyrolysis and deposition, as shown by the chemical reactions, temperature and pressure, and schematic of equipment in Figure 2.3-2. Film thickness is controlled by (a) the weighted charge of parylene dimmer that is vaporized and (b) the surface area in the deposition chamber. Once these quantities are fixed, the parylene film thickness can be deposited very reproducibly. A parylene coater is used in this facility for conformal coating of circuit boards, and it was used to deposit parylene layers for substrates on this program.

Preparation of thin parylene substrates consists of several steps:

(a) selecting a suitably smooth surface on which the parylene is to be deposited,

(b) applying a cleaning/release agent to this surface,

(c) depositing the parylene,

(d) bonding a support ring to the parylene, and

(e) demounting the support ring with its attached parylene foil.

Initial parylene substrate preparation was based on information from a representative of Union Carbide and in-house work on demounting parylene films. The first parylene depositions were made on polished silicon wafers

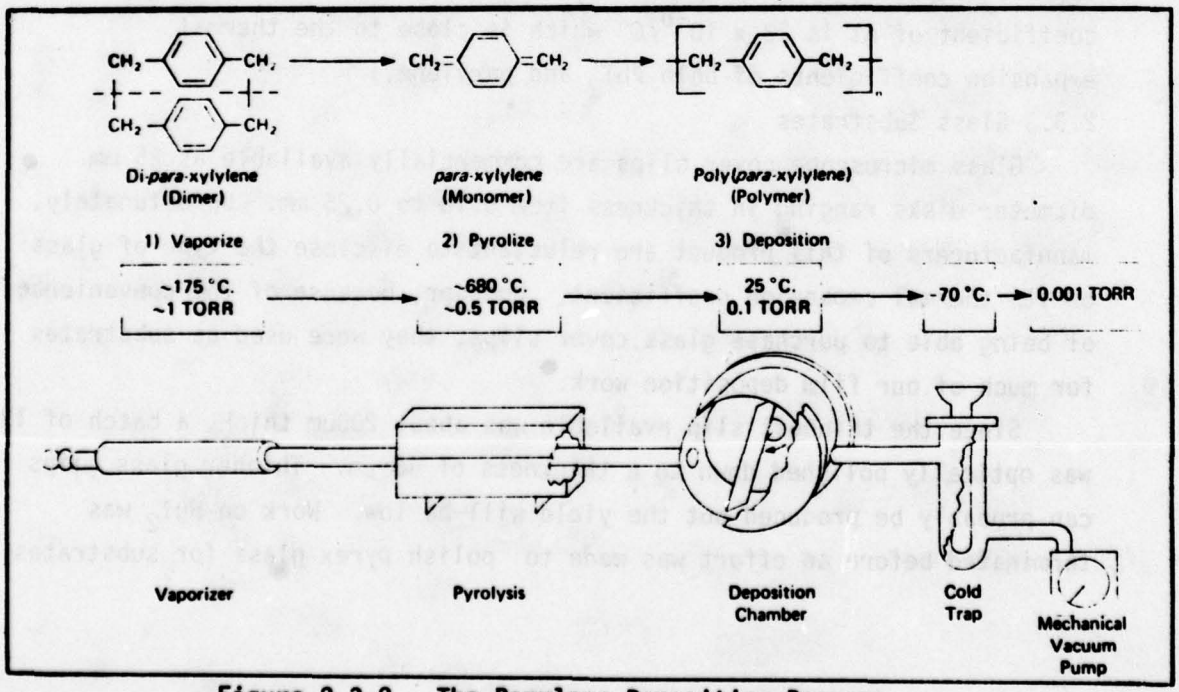

Figure 2.3-2. The Parylene Deposition Process

which had been dipped in concentrated ammoniacal Alconox solution. Smooth substrate foils were not produced and further discussions with a Union Carbide representative revealed that several improvements had been incorporated into their procedures. Use of picture-frame glass for the smooth surface was recommended. The glass was first washed with an ammoniacal solution of Alconox and then rinsed free of excess detergent. These steps yielded improved parylene films; however, the demounted foils (which had been bonded with epoxy resin to support rings) were very wrinkled. These foils were quite strong and could be stretched by supporting the weight of a second ring within the first. The procedure was thus modified to first demount the film onto an oversize ring (40 mm O.D.) and then use the smaller correct-size support ring (32 mm O.D.) to stretch the foil while its bonding silicone resin set up.

All of the foils produced contained stress lines, which upon microscopic examination,were found to be associated with dust particles. The dust may have been incorporated during many stages in the film preparation: inadequate cleaning of the glass plates, loading of the cleaned glass plates into the parylene deposition chamber, during parylene deposition, or handling of the plates and films thereafter. (These defects would have caused excessive scattering of light if the films were used as substrates for PbI_2.) In a discussion of this problem with the representative of Union Carbide, it was learned that a very low dust count room (Class 100) is used in preparing thin parylene films at Union Carbide. Since the parylene deposition equipment used for preparing our films was not in a low dust environment, it was decided to purchase parylene films for this program. An order was placed for 2000Å parylene N films transferred onto our 1.25 O.D Al support rings.

The 2000Å parylene films from Union Carbide showed some non-uniformity in the mounting procedure. Some foils were evenly taut while others appeared to be stressed in a way that produced ridges. Several films were subjected to spectroscopic scanning from 300 nm in the UV to 3000 nm in the IR. These results showed that the films measured 2054 $\pm$ 47Å in thickness.

2.4 Film Deposition

The films for this program were to be polycrystalline and ordered with the <001> or ĉ axis perpendicular to the plane of the film, in order to obtain uniform optical properties. Both PbI_2 and HgI_2 exist in more than one crystallographic form. For good thermo-optic properties, the crystallites should not have passed through a polytype or a phase transition. Therefore, the strategy was to deposit the films at temperatures which assure the formation of the crystalline structure which is stable at room temperature. For PbI_2 that is the 2H poly type, and for HgI_2 that is the α form. Physical vapor deposition by vacuum evaporation was used to meet these goals.

2.4.1 Deposition Equipment

An Ultek rapid-cycle, contaminant-free, high vacuum system with cryosorption forepumps, differential ion pumps, and titanium sublimation pump was made available to this program. It was installed in a class 100,000 clean room facility and was pumped to pressures of 10^{-9} torr during these procedures. The vacuum evaporator was outfitted with the necessary feedthroughs and electro-mechanical devices, including an automated system for supplying liquid nitrogen.

Figure 2.4-1 shows the vacuum station installation. On the left are the cryosorption forepump stand and recharging controls; in the center is the vacuum chamber, with differential ion pumps and titanium sublimation pumps in the cabinet below; and on the right are the control and monitoring panels.

Figure 2.4-2 shows the components within the bell jar. Centered at the bottom is a shiny cylindrical resistance - heated evaporator. Above that is the shutter. Next above is a square, six-position substrate holder mounted to the substrate heating chamber. The evaporator-to-substrate distance is 28 cm. Just to the right is the holder for the resonant quartz crystal of the deposition monitor. The shutter, substrate holder and substrate heater were designed and built at Rockwell International.

Components of the resistance-heated Radak evaporator, produced by the Luxel Corp., are shown in Figure 2.4-3. On the right is the tungsten wire heating element and its supporting structure on the heater base. The alumina tubing in the center of this heating element contains a chromel-

Figure 2.4-1. Ultek rapid cycle high vacuum system and control panel.

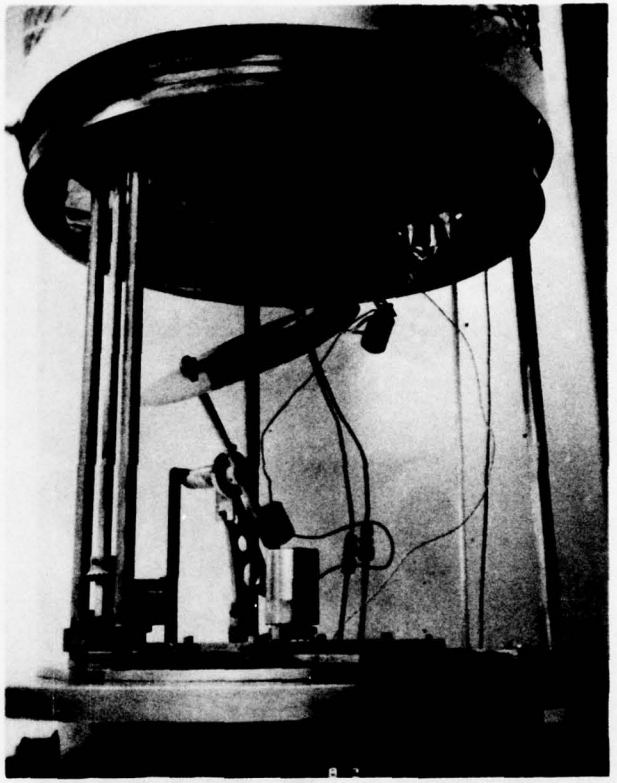

Figure 2.4.2. Components within bell jar of vacuum station.

Figure 2.4-3. Disassembled Rodak Evaporator

Figure 2.4-4. Substrate holder and substrate support ring.

alumel thermocouple for monitoring the temperature at the base of the crucible. When the evaporator is assembled, a crucible presses down on the spring-loaded thermocouple, assuring an accurate temperature measurement. In the foreground are 2 cc crucibles of fused silica and crystallized alumina. Behind the crucibles is a tantalum and molybdenum radiation baffle. On the left is the stainless steel cover which locks to the base. Due to its design, this evaporator permits attainment of high vapor flux at a low temperature, which results in a minimum of thermal decomposition of the evaporant. Power for this evaporator was provided by a voltage divider which gave precise control of the low power requirement (less than 100 watts).

Figure 2.4-4 shows the copper substrate holder from above, demounted from the substrate heating chamber. On the left is a substrate support ring which is being placed in one of the six cavities. The slots in the substrate holder are for thermocouple monitoring of the support ring's temperature.

For film characterization and retrieval, a film coding system was instituted so that each film had a unique identity. The designation included the date of the deposition (month and day), which evaporation on that date (A,B,C...), and the position in the substrate holder (1,3,5,7,9, or 11 numbered clockwise). Thus, film No. 0105C7 means that the film was deposited on January 5, during the third evaporation of that day and it was in the 7 o'clock position.

The deposition monitor was a Deposition Control Master, Model Omni II, produced by the Sloan Technology Corporation. This equipment measured the rate of film deposition by the frequency shift of a resonant quartz crystal held in the vapor stream. A Hewlett-Packard #5381A 80 MHz frequency counter was used with the deposition monitor to provide a digital readout for improved sensitivity.

2.4.2 PbI_2 Film Depositions

An initial series of PbI_2 depositions was carried out to explore deposition parameters and select preferred ones for control of polytype, crystallite axis orientation and crystalline size. In carrying out these depositions, the evaporator temperature, evaporator-to-substrate distance and substrate temperature were varied to control evaporation and deposition rates. To simplify bell jar cleaning, the bell jar was lined with Al foil which was replaced from time to time.

The vapor pressure curve for PbI_2 is presented in Figure 2.4-5.[41] For the exploratory study, the evaporator temperature was varied between 350 and 475°C, providing PbI_2 vapor pressures of ~8 x 10^{-3} to 1 torr. The glass substrates for these depositions were held at temperatures up to 170°C.

In a typical deposition run, after the substrate temperature had equilibrated, the evaporator was energized at a particular power setting and the deposition monitor was set at a frequency of 1 KHz. The shutter shielded the substrates, but the quartz crystal of the deposition monitor was open to the evaporator source throughout the run. (The deposition rate proved to be a more sensitive means for determining when the evaporator had equilibrated than the measured evaporator temperature.) When the monitor frequency reached a steady value, the shutter was opened between the evaporator and the substrates to start the deposition. When the frequency counter reached a pre-selected value, the deposition was ended by closing the shutter. Then the evaporator and substrate heater were turned off.

Film thicknesses of PbI_2 on glass substrates were measured with a Dektak surface profilometer, produced by the Sloan Technology Corp. Deposition rates of up to 400Å/min were deduced from thickness measurements.

At the completion of these preliminary experiments, the substrate temperature range of 140 to 155°C was selected as most likely to yield the oriented crystallites needed, and the evaporator-to-substrate distance was fixed at 28 cm.

Next, three PbI_2 depositions were made on glass substrates to establish the effects of deposition rate and growth temperature on film quality, as well as to determine the reproducibility and uniformity of depositions in the system. The parameters of these depositions, designated 0130A, 0202A and 0203A, are presented in Table 2.4-1.

Table 2.4-1. Parameters for Three PbI_2 Depositions

	Run 0203A	Run 0130A	Run 0202A
Substrate temperature (°C)	151	147	144
Average Δf/second (Hz/sec)	4	8	14
Deposition period (min)	23.7	14.8	6.7
Average film thickness (KÅ)	2.0	2.2	2.1
Average deposition rate (Å/min)	85	150	315

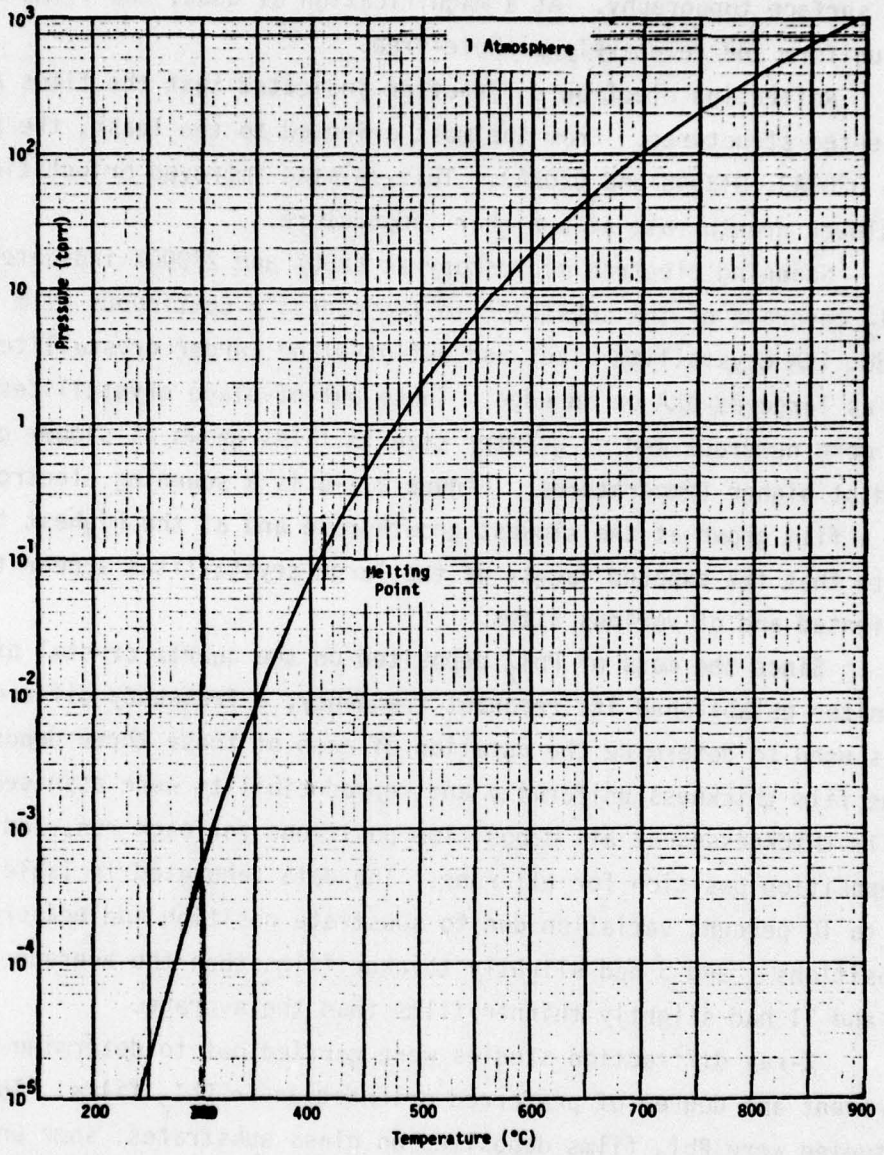

FIGURE 2.4-5. Vapor Pressure of PbI_2 as a Function of Temperature.[41]

In addition to the profilometer measurements used to obtain the film thicknesses, Nomarski interference contrast microscopy was used to evaluate the surface topography. At a magnification of 536X, the films appeared to be uniform and relatively pinhole-free.

Reflection electron diffraction indicated that the films all had oriented structures. From the most oriented to the least, the sequence was 0203A3, 0130A3 and 0202A3. This related improved orientation with a slower growth rate at a higher temperature.

Scanning electron microscopy at 6800X and 27000X indicated uniform PbI_2 coverage of the substrate in two modes: a continuous film matrix of about 1KA crystallite size, and out-of-plane larger crystallites that may be as large as 4KA on an edge. These out-of-plane crystallites appear to be more numerous and of greater size in films grown at slower growth rates and at higher temperatures. Figure 2.4-6 is a scanning electron micrograph of a film grown at the slowest growth rate and at the highest temperature. Note that the exposed facets of the large crystallites appear to be randomly oriented and of various sizes.

Since the mass of PbI_2 deposited on the quartz crystal of the Sloan monitor established its resonant frequency, a frequency difference of 5.8 KHz was used to determine the duration of each of these three deposition runs. The film thickness uniformity and reproducibility were assessed by comparing film thicknesses at all deposition positions for each run, and at each deposition position for all runs. The data tabulated in Table 2.4-2 show a 5 to 10 percent variation due to substrate position and measurement error. Positions 1 and 3 had slightly thicker films than the average and positions 9 and 11 had slightly thinner films than the average.

X-ray diffraction studies were carried out to determine the polytypes present and degree of preferred orientation in PbI_2 films. The samples studied were PbI_2 films deposited on glass substrates: some unheated during film deposition and others heated to 150°C during film deposition. For this evaluation, the relative intensities of the principal low index diffraction lines and their wavelengths were obtained with a Philips x-ray diffractometer. The intensities of the diffraction lines were then compared with:

(1) Card No. 7-235 for the 2H polytype of PbI_2 Joint Committee on Powder Diffraction Standards, International Centre for Diffraction Data, Swarthmore, Pa.,

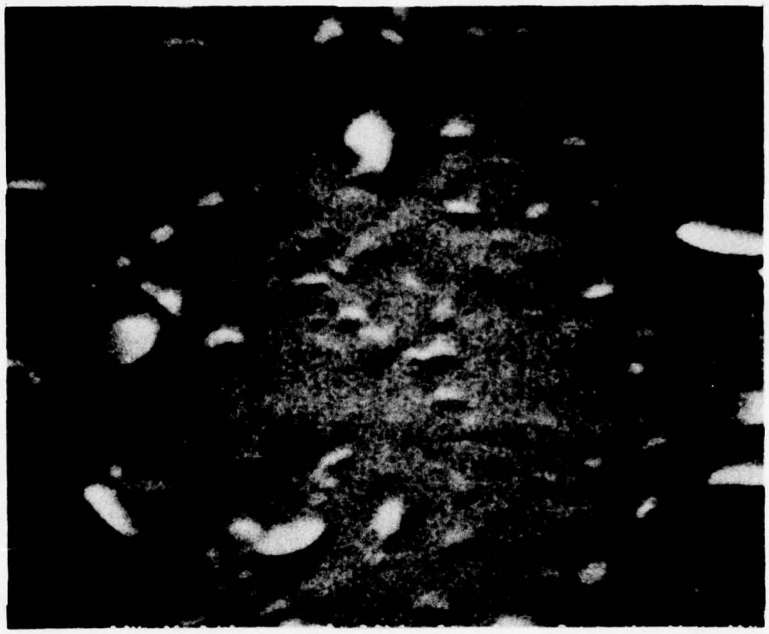

Figure 2.4-6. Scanning electron micrograph of PbI_2 film 0203A3. (2700X).

and (2) line intensities calculated for the 4H, 6H and 12H polytypes, using lattice constant data from
R. G. Wycoff, "Crystal Structure," Vol. I, and Edition, Interscience, New York, N. Y. 1963, p 276.

The X-ray diffraction patterns of all of the films matched the 2H polytype pattern; however, there were a few additional lines not shown on Card No. 7-235 which could be attributed to the 6H polytype.

It had been anticipated that film deposition at a slow rate and high temperature would favor the <00.l> direction or $\hat{c}$ axis perpendicular to the plane of the film. Surprisingly, the X-ray study showed that the degree of orientation was independent of temperature or growth rate: the films all exhibited a preferred orientation with the <00.l> direction perpendicular to the plane of the film. The degree of this orientation was about four times greater than expected for a randomly-oriented polycrystalline sample. Since the electron diffraction study indicated increasing crystallinity and the scanning electron microscope showed larger platelets in films deposited at higher temperatures and slower rates, electron diffraction must have been more sensitive to the presence of the larger, randomly-oriented crystallites than X-ray diffraction.

A series of PbI_2 depositions was planned for the parylene foils purchased from Union Carbide. In each deposition, one parylene substrate was used with five glass substrates in the substrate holder. Unfortunately, of the 12 parylene foils received, five ruptured before film deposition for no apparent reason (presumably due to high tensile stress in the foils). Two of the foils ruptured following PbI_2 deposition. The remaining five parylene foils survived PbI_2 deposition and were subsequently characterized. Table 2.4-3 lists the deposition conditions used for these films. Deposition rates were obtained from profilometer measurements of PbI_2 film thicknesses on adjacent glass substrates. Several of the foils appeared wrinkled after film deposition but became taut upon dry storage. It should be noted that the PbI_2 adhered well to the parylene. Thermo-optic properties of these films are described in subsequent sections.

In summary, the PbI_2 depositions by vacuum evaporation satisfactorily met the goals of producing polycrystalline films which were predominantly the 2H polytype and oriented with the <00.l> direction perpendicular to the plane of the film.

Table 2.4-2. Film Thickness at Each Substrate Position for Three PbI_2 Depositions

	Film Thickness in KÅ						
	Position 1	Position 3	Position 5	Position 7	Position 9	Position 11	Average
Run 0130A	2.3	2.3	2.3	2.2	2.0	2.1	2.2
Run 0202A	2.3	2.3	1.9	2.3	1.9	2.0	2.1
Run 0203A	2.0	2.0	2.0	2.0	2.1	1.9	2.0
Average	2.2	2.2	2.1	2.2	2.0	2.0	2.1

Table 2.4-3. Deposition Conditions for PbI_2 Films on Parylene Substrates

Film	Substrate Temperature °C	Growth Rate Å/min
0628A11	23	70
0705A2	52	170
0707A2	41	70
0808B2	147	70
0809A2	147	50

2.4.3 HgI_2 Film Depositions

As a consequence of the tests on the reactivity of HgI_2 with several metals (see Table 2.2-3), the Al foil liner for the vacuum system's bell jar was replaced with mylar foil and the Ag electrodes of the quartz resonant crystal (for the rate monitor) were coated with Au. It was assumed that the presence of the other metals in the vacuum chamber would not degrade the quality of the HgI_2 films.

The vapor pressure curve for HgI_2 is presented in Figure 2.4-7.[41] Note that HgI_2 has a much higher vapor pressure than PbI_2. For example, to reach a vapor pressure of 0.1 torr, HgI_2 is at 120°C and PbI_2 is at 407°C, while to reach a vapor pressure of 10^{-5} torr, HgI_2 is at 22°C and PbI_2 is at 242°C. The high vapor pressure of HgI_2 at room temperature proved to be a major problem.

Initial evaporations of HgI_2 did not produce measurable HgI_2 films on the glass substrates. There were signs of evaporation,such as a loss of weight from the evaporator crucible between the beginning and end of a run, and discoloration of the substrate holder, but no red film was found on the substrates or vacuum chamber furniture. In one experiment, a two liter beaker was placed over the evaporator source. (A two liter beaker is about 14 cm in diameter and 18 cm tall.) The first coloration of the beaker occurred when the source temperature reached 86°C. At the completion of the run, the inside of the beaker was red, orange, orange-yellow and yellow, which demonstrated that HgI_2 had been evaporated and had deposited. Other experiments without a confining beaker resulted in selective deposition of HgI_2 on the system walls but not on the substrates.

In the first evaporation run to produce HgI_2 films on substrates, the system pressure was permitted to rise to 3×10^{-2} torr with the evaporator temperature at 285°C and the substrates at room temperature. The reactant films were relatively soft so that profilometer measurements of film thickness were unsuccessful (because the stylus cut into the films). Several more HgI_2 depositions followed using elevated pressures and/or high evaporation rates in an effort to establish conditions for the reproducible growth of good quality, uniform thin films.

Since the rate of film growth is the difference between the rate of deposition and the rate of re-evaporation, high deposition rates were found to be necessary to produce HgI_2 films on room temperature glass

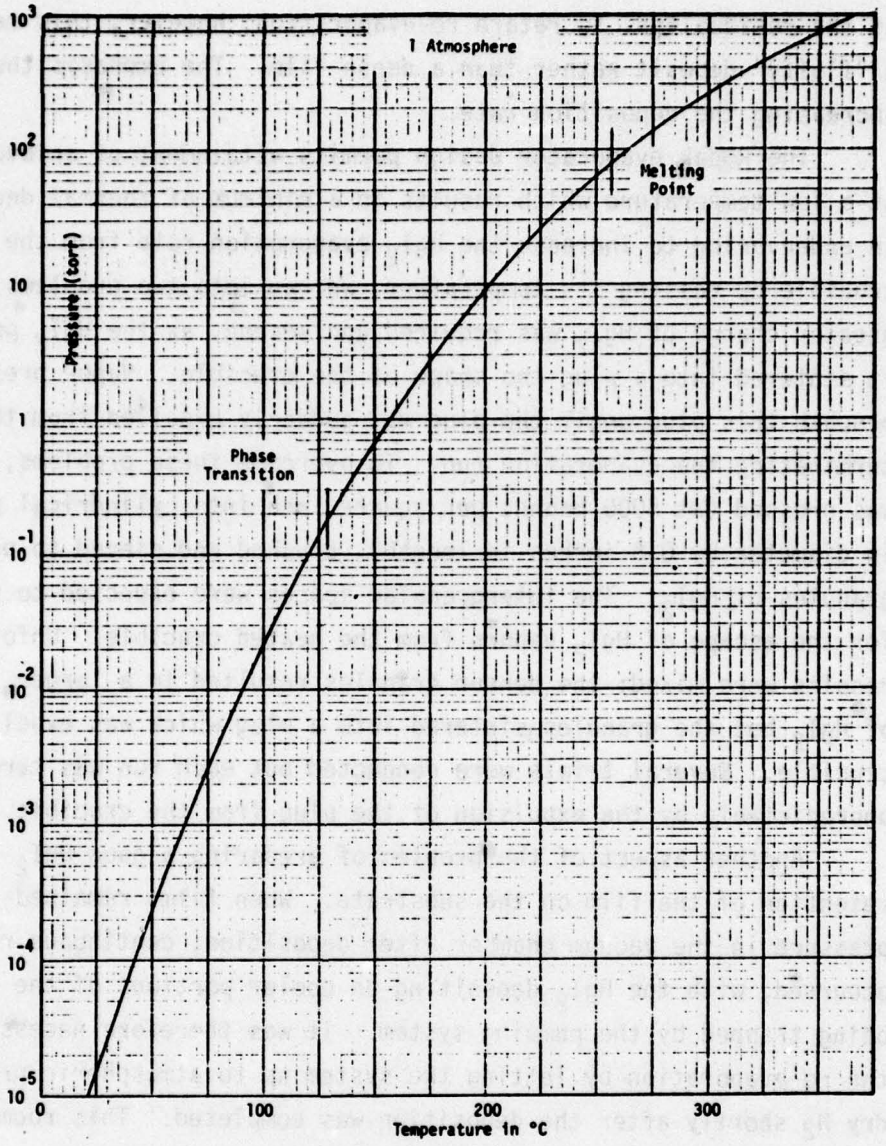

FIGURE 2.4-7. Vapor Pressure of HgI_2 as a Function of Temperature.[41]

substrates. The films deposited under poor vacuum made use of the presence of the residual gas to retard re-evaporation; however, this method produced a "fluffy" deposit rather than a dense film. The emphasis thus turned to increasing the deposition rate.

The Rodak evaporator design permits attainment of an evaporant flux at a low temperature which results in a minimum of thermal decomposition. In endeavoring to increase the HgI_2 evaporation rate from the cylindrical crucible by raising its temperature, we ran into two problems: First, a greater charge of HgI_2 was required and second, as the HgI_2 powder was heated, it sintered into a plug the shape of the crucible. Vapor pressure built up beneath this plug until the plug was suddenly expelled from the crucible, terminating the evaporation run. To overcome these problems, HgI_2 powder was pressed (at 5000 pounds per square inch into cylindrical pellets 0.5 inches in diameter by 0.5 inches in length), crushed and sieved to produce dense granules of HgI_2. The intergranular spaces were expected to provide a path for the escape of HgI_2 vapors from the heated crucible. Unfortunately, the results were mixed: the denser granules resulted in a larger initial charge of HgI_2 but the granules sintered into a plug which was expelled from the crucible. Several trials were conducted but each run was terminated unpredictably by the expulsion of the plug from the crucible.

Another aspect of the problem of preparing a good HgI_2 film is the retention of the film on the substrate. When films remained under reduced pressure in the vacuum chamber after deposition, continuous re-evaporation occurred, with the HgI_2 depositing on cooler portions of the bell jar or being trapped by the pumping system. It was therefore necessary to quench the re-evaporation by letting the system up to atmospheric pressure with dry N_2 shortly after the deposition was completed. This room temperature re-evaporation under reduced pressure also posed a problem in the characterization of films, and several attempts were made to encapsulate HgI_2 films by coating with SiO_x films by sputtering or evaporation. Neither encapsulation method was successful because no HgI_2 remained after the SiO_x depositions.

To confirm that the HgI_2 film had evaporated during the SiO_x deposition processes, an experiment was conducted in which an HgI_2 film was exposed to the same pressures that had been used during the SiO_x depositions. The

vacuum system containing the film at room temperature was pumped down to 50 microns over a three minute period, then pumped down to 4×10^{-4} torr for two minutes and held for an additional minute before opening the system to the atmosphere. At the end of this period, the HgI_2 film had disappeared. The evaporation of HgI_2 at these moderate pressures confirmed the need for an encapsulation technique.

In a paper by R. S. Scott and G. E. Fredericks[32], the authors considered the reported instability of unprotected (bulk) crystal) HgI_2 X-ray detectors in vacuum in contrast with the apparent stability of similar detectors in air. Their calculations, based on the assumed dissociation of HgI_2 and the high vapor pressure of I_2, predict that the degradation due to evaporation of I_2 would occur in one hour under high vacuum but would require about a year under atmospheric pressure. Whether or not there is significant decomposition of HgI_2 at room temperature, the high vapor pressure of HgI_2 must be solved before this material can be characterized and utilized.

In summary, HgI_2 presented two serious obstacles associated with its high vapor pressure: first, the difficulty of controlled deposition on an uncooled substrate, and, second, the need to encapsulate a deposited film. Neither of these problems was satisfactorily solved.

2.4.4. Summary of Deposition Trials

A few of the best quality films were selected for optical transmission and thermal measurements. Most of the remaining uncharacterized films are listed in Table 2.4-4, along with the relevant deposition parameters. Typically, three to six samples were produced during each deposition. The left column indicates whether samples from each run remain at the end of this program. Each deposition onto parylene was done simultaneously with five glass substrates, most of which remain. Therefore, the deposition parameters for characterized films such as PbI_2-parylene No. 628A11A or PbI_2-glass No. 210A9 may be obtained from the corresponding rows of this table.

TABLE 2.4-4 Summary of Uncharacterized PbI_2 and HgI_2 Film Depositions

Samples Available	Deposition Group	Film Material	Substrate Material	Maximum Substrate Temp: °C	Thickness Å	Average Deposition Rate: Å/min	Comments
✔	1214	PbI_2	glass	23	1000		Rapid growth, transparent, uniform (A1,3,5,7,9,11 on glass rings)
✔	1215A	"	"	23	7500	1550	Translucent, nonuniform, (A1,3,5,7,9,11 on glass rings)
✔	1216A	"	"	98	7500	400	Opaque (A1,5,7,9,11 on glass rings)
	0111A	"	"	22			
✔	0118A	"	"	23			Translucent, nonuniform (A1,3,5,7,9,11)
✔	0126A	"	"	148	2000	227	Uniform, transparent (A1,3,5,7,9,11)
✔	0130A	"	"	147	2200	150	Uniform, transparent (A5,7,9,11)
✔	0202A	"	"	144	2100	315	Uniform, transparent (A1,5,7,9,11)
✔	0203A	"	"	153	2000	85	" " (A5,7,9,11, A1 sectioned)
✔	0201A	"	"	153	2000	165	" " (A3,7,11; A1 and 9 on glass rings)
	0222A	HgI_2	"	87	no		No deposit on the substrates
	0224A	"	Pyrex beaker	23	reliable		HgI_2 deposited on pyrex beaker
	0227A	"	glass	23	thickness		No deposit on the substrates
✔	0303A	"	"	23	measurements		No films remain on substrates
	0322A	"	"	23	for		" " " " "
	0323A	"	"	23	HgI_2		" " " " "
✔	0323B	"	"	23	films		Translucent, non-reflective, nonuniform (B1,9)
✔	0323C	"	"	23			Partially uniform, non-reflective, transparent (C1,3,5,7,11)
	0324A	"	"	23			Poor quality films
	0329A	"	"	23			A5 good deposit, rest non-uniform and poor
✔	0329B	"	"	23			Fair uniformity, transparent (B1,3,7,9,11)
	0403A	"	"	23			No film
	0404A	"	"	23			Use pelletized source material, no observable improvement
✔	0405A	"	"	23			Poor quality, translucent, non-reflective, nonuniform (A1,3,5,7,9,11)
	0405B	"	"	23			Vacuum system would not pump down to hard vacuum
✔	0412A	PbI_2	"	158			Good, uniform, transparent, (A1,3,5,11)
✔	0413A	"	0018" glass parylene	156			Wrinkled, parylene torn before deposition 0413A11 (A1,3,5,7,9)
✔	0627A	"	parylene	150	5200	1350	Parylene wrinkled, broken 0627A11 (A1,3,5,7,9)
✔	0628A	"	"	23	2000	70	Good film on parylene (A3,5,9 - sectioned A1,7)
✔	0703A	"	"	50	4400	250	Wrinkled, torn (A4,8,12)
✔	0705A	"	"	53	3000	170	Wrinkled film, tautened with storage (A4,6,8,10,12)
✔	0707A	"	"	42	3000	75	Wrinkled, some wrinkles disappeared with time (A4,6,8,10,12)
✔	0803A	"	"	153	2100	50	Wrinkled, torn, sagged after deposition (A4,6,8,10,12)
✔	0808A	"	"	61	2000	70	Torn before deposition, sagged and wrinkled after (A4,6,8,10,12)
✔	0808B	"	"	150	2000	70	Wrinkled, sagged; some improvement after deposition (B4,6,8,10,12) No film remains
✔	0809A	"	"	149	2000	50	Wrinkled, sagged (A6,8,10 - sectioned A4,12)
✔	1005AI	PbI_2	nitrocellulose	92	2100	40	" " (A1,2,3)
✔	1005BII	"	"	51	2000	50	" " (A1,2,3)
✔	1006AIII	"	"	23	2100	60	" " (A1,2,3)
✔	1009AV	"	"	24	2000	70	Nitrocellulose film torn. There was a pinhole near edge (A1,2,3)
✔	1010AVI	"	"	24	2100	85	Section missing, wrinkled, sagging (A1,2,3)
✔	1011AIV	"	"	110	2000	110	Pinholes, wrinkled, sagging 1010AVI (A1,2,3)

2.5 Measurement of Optical Properties

Optical transmission measurements were made of parylene and glass substrates and metal halide film-substrate composites at visible and near-infrared wavelengths, using a Beckman Acta M-IV spectrophotometer. Temperature dependent transmission measurements were made using a cryogenic dewar equipped with fused-silica windows. The temperature of the sample compartment in the evacuated portion of the dewar was controlled automatically by a cyclic temperature control unit, using a thermocouple and resistive heater elements. The optical windows were maintained free of moisture at cold temperatures by means of heater elements. The temperature of the samples was variable between 80°K and 420°K, with temperature stability at a given setting of 0.1°C.

The samples were cemented onto support rings. Glass support rings were used with glass substrates and aluminum support rings with parylene substrates. Slots were milled into the back faces of the support rings so the thin parylene samples would not be subjected to a differential surface pressure when placed upon a flat surface. Each support ring could be fitted into a cylindrical groove in the end face of a cylindrical brass mount, as illustrated in Figure 2.5-1, and locked in place with a set-screw. The brass mount provided thermal mass in contact with the support ring. A portion of the flat end face of the cylindrical brass support extended beneath each sample, inside the support ring's circumference. Because of the fragile nature of the parylene films, a clearance of 0.005 inches was maintained between the bottom surface of each substrate and the underlying end face of the brass mount. This was accomplished by making the depth of the cylindrical groove 0.005 inches less than the thickness of the support ring. This area in near-contact with the bottom surface of the sample was intended to give more uniform heat transfer, and thus guarantee a constant temperature profile across the sample.

A hole along the axis of the cylindrical brass mount provided a clear aperture of one-half inch diameter for each sample. The brass mount was inserted into a brass housing which was attached to the bottom of the cryogenic well. Two resistive heaters and a thermocouple for temperature control were located in the brass housing.

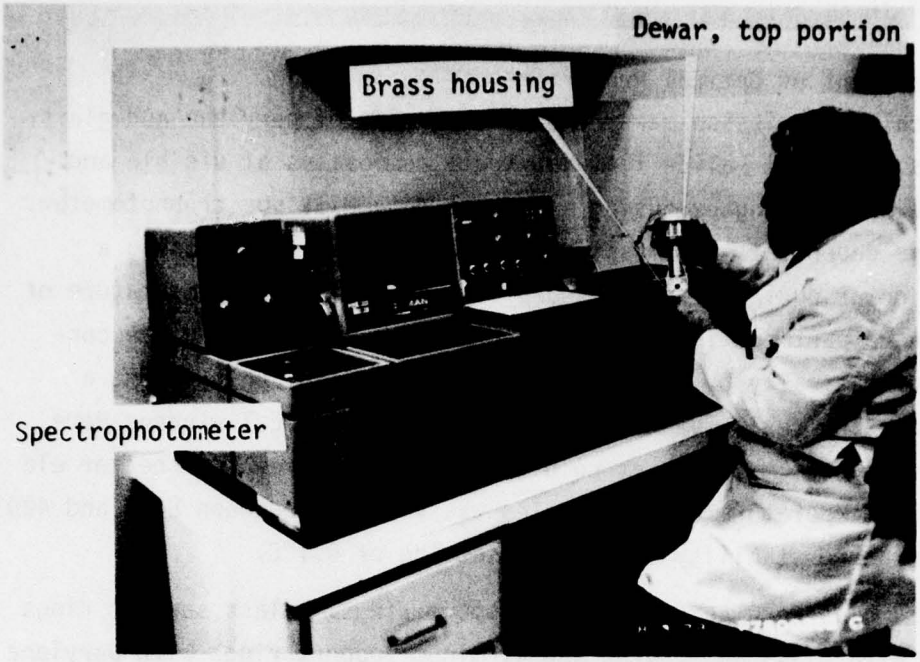

Figure 2.5-1a. Top portion of cryogenic dewar, showing brass housing at bottom of cold finger, containing brass sample mount.

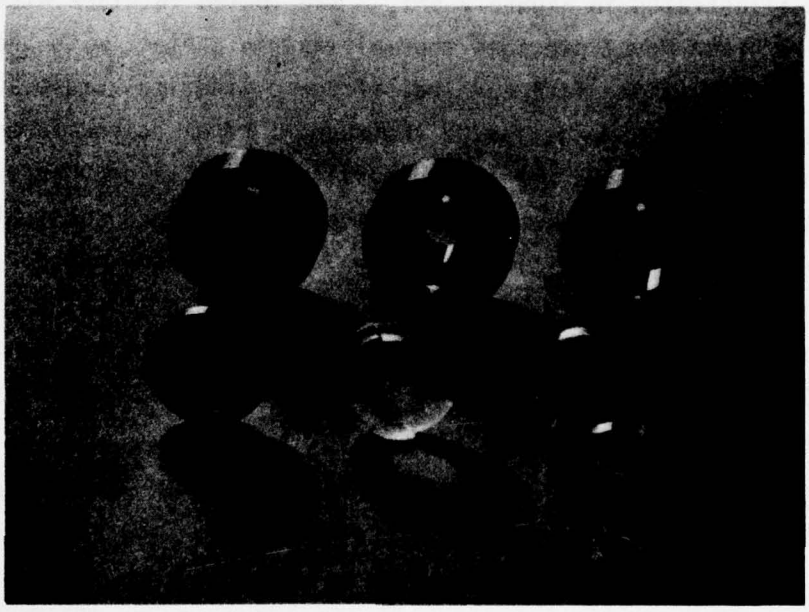

Figure 2.5-1b. Front row from left: (aluminum ring with PbI_2-glass sample, (2) back surface of glass ring, (3) back surface of aluminum ring; Back row from left: (4) PbI_2-glass sample on aluminum ring inserted in brass mount, (5) brass mount for optical transmission measurements, (6) brass mount for thermal measurements.

Figure 2.5-1. Support rings, cylindrical brass mount, and brass housing on cold finger of optical dewar.

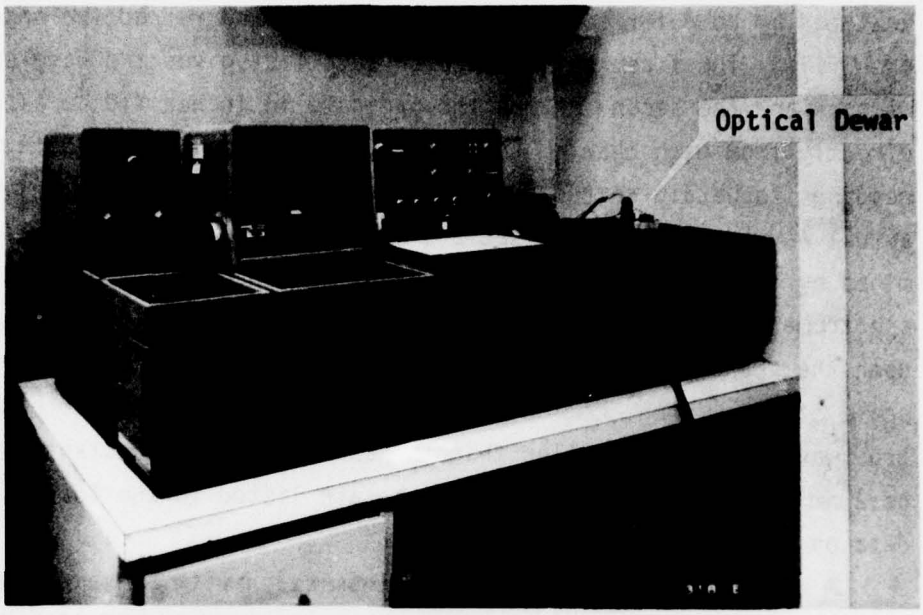

Figure 2.5-2. Beckman Acta M-IV spectrophotometer and optical dewar for temperature controlled transmission measurements.

Experimental values of transmission and wavelength are listed on each transmission curve. Corrected values of these data points are analyzed by computer to obtain the thickness and refractive index of each film. The first column of each data list gives the wavelengths in microns and the second column the ordinate in inches $X10^{-1}$, as read directly from each chart. Corrections must be applied to both these readings to obtain correct values of wavelength and transmittivity. The actual wavelengths are off-set a small amount from chart values as determined by comparing chart abscissa values to readings from the dial of the spectrometer section. The magnitude of this wavelength off-set depends upon the scan speed used. For a scan speed of one nm/second with a chart scale of 50 nm/inch, commonly used with the scans from 900 to 350 nm, the true wavelength was smaller than the chart value by constant difference of 2 nm. Corrected wavelength values are listed in the fourth column of data on each chart.

A calibration curve for 100% transmission with no sample was taken a minimum of every four hours and at the beginning and end of each series of measurements, to check for drift in the system's response and to allow corrections for spectral sensitivity. Each calibration curve was made with the one-half-inch-i.d. brass mount in place, so the aperture was the same as for the samples. This 100% calibration data is listed in the third data column on each transmission curve. Zero transmission corresponds to the lowest coarse horizontal grid on the chart, unless otherwise indicated. The correct values of transmittivity, listed in the fifth data column, are given by the following procedure. The samples are known to be non-absorbing at wavelengths around 800 nm, so the transmission peak at the wavelength λ_{max} closest to 800 nm, was taken to be $T(\lambda_{max})$ in true value. The transmission values at other wavelengths were normalized to this reference value, by dividing each experimental $T_{exp}(\lambda)$ by $T_{exp}(\lambda_{max})$, with both in units of 10 inches of vertical chart amplitude. The spectral response of the instrument was taken into account by further multiplying this result by the ratio $T_{cal}(\lambda_{max})/T_{cal}(\lambda)$. The true transmission $T(\lambda)$ at wavelength λ is then

$$T(\lambda) = \frac{T_{exp}(\lambda)\ T_{cal}(\lambda_{max})}{T_{cal}(\lambda)\ T_{exp}(\lambda_{max})} \qquad (2.5.0\text{-}1)$$

These corrected values of transmission are listed in the fifth data column on each transmission curve.

2.5.1 Optical Properties of Parylene-N Substrates

N-type parylene was selected as the thin substrate for PbI_2 films because of the close match of linear thermal expansion for these two materials. The parylene membranes were purchased from Union Carbide Corporation. Taut membranes were mounted onto aluminum support rings supplied by the Rockwell Electronics Research Center. Slots had been milled into the back surfaces of the support rings to prevent development of differential pressure on the surface of the membrane when samples are placed on a flat surface or in their containers. Holes were drilled into the plastic storage containers to prevent differential surface pressure when the containers are opened or closed. Table 2.5-1 lists some relevant physical properties of N-type parylene, along with those of aluminum and PbI_2.

The thicknesses of the twelve parylene samples procured were about 2000 Å. Table 2.5-2 lists a brief history of each sample, labeled X, A B, ... through L, during the deposition and characterization phases of the experiments. The samples were stored in individual protective plastic containers and handling was confined as much as feasible within a dust-free hood.

The optical transmission of each parylene sample was measured prior to any further treatment or handling. These transmission characteristics were then analyzed to obtain the thickness and the refractive index, including dispersion, of each sample over the wavelength range 800 nm to 350 nm. All the samples were thus characterized at 25°C. Sample K was also characterized over a range of temperatures from 0°C to 100°C in order to check the temperature dependence of the refractive index and the influence of thermal cycling on the physical properties of parylene films.

The transmission characteristics are shown in Figures 2.5-3 through 2.5-16. Wavelengths longer than 800 nm and shorter than 350 nm are ignored in the analysis of these data. The photomultiplier's spectral sensitivity drops rapidly at the longer wavelengths and the light intensity from the tungsten source drops rapidly at the shorter wavelengths, so that reliable data is limited to the range 800 - 350 nm. (The spectrophotometer can be used at shorter wavelengths by engaging a deuterium light source and at longer

wavelengths by engaging a PbS photodetector. Since these other ranges required removing samples and re-calibrating the instrument, and the 800 - 350 nm range contained sufficient information, measurements were restricted to these wavelengths.)

PHYSICAL PROPERTY	PARYLENE-N	PbI_2	ALUMINUM
Thermal Conductivity k (watt/cm-°C)	1.255×10^{-3}	2.4×10^{-3} pressed(40)	0.5
Coefficient of Linear Thermal Expansion $(°C)^{-1}$	6.9×10^{-5}	3×10^{-5} average(40)	2.5×10^{-5}
Specific Heat	0.20 to 0.21	0.174 (40)	0.22
Density (gm/cm^3)	1.12	5.625	
Optical Transparency Wavelength Range (μm)	0.28 to 3.3	0.52 to	
Refractive Index n_D (Na)	1.661	2.84 (13)	
Glass Transition Temperature for Creep (°C)	67 to 77		
Melting Temperature (°C)	405		

TABLE 2.5-1 Physical Properties of Parylene-N in Comparison to PbI_2 and Aluminum (Ref. 42).

TABLE 2.5-2

PARYLENE-N FILMS PROCURED AND THEIR DISPOSITIONS DURING CHARACTERIZATION STUDIES.

	FILM	SUBSTRATE TEMP. (°C) DURING PbI_2 DEPOSITIONS	AVERAGE PbI_2 GROWTH RATE Å/MIN.	HISTORY
(1)	0627A11X	144	1350	Ruptured after PbI_2 deposition.
(2)	0628A11A	23	70	Characterized with PbI_2 film. Ruptured during thermal tests.
(3)	0703A2B	50	250	Wrinkled, torn after PbI_2 deposition. Touched with T.C. before growth.
(4)	0705A2C*	52	170	Ruptured during thermal tests.
(5)	0707A2D*	41	70	Ruptured during thermal tests.
(6)	E			"Burst" during handling.
(7)	F			"Burst" during handling.
(8)	0803A2G	150	50	Torn before characterization - too much tension.
(9)	H			"Burst" during handling.
(10)	0808A2I	57	70	Torn before characterization - too much tension.
(11)	0808B2J*	147	70	Wrinkled as received - characterized with PbI_2 film. Ruptured during thermal cycling.
(12)	0809A2K*	147	50	Wrinkled as received - characterized. Ruptured during thermal tests,

NOTE: Letter suffix X, A, B.....K indicates the series of parylene films purchased from Union Carbide Corp. Some of them "burst" for no obvious reason while others survived much handling, in and out of holders for optical characterization and PbI_2 depositions. The stress, as noted by the increase or addition of wrinkles in some of the films, changed while they were in storage.

*Film became more taut following PbI_2 deposition after exposure to air.

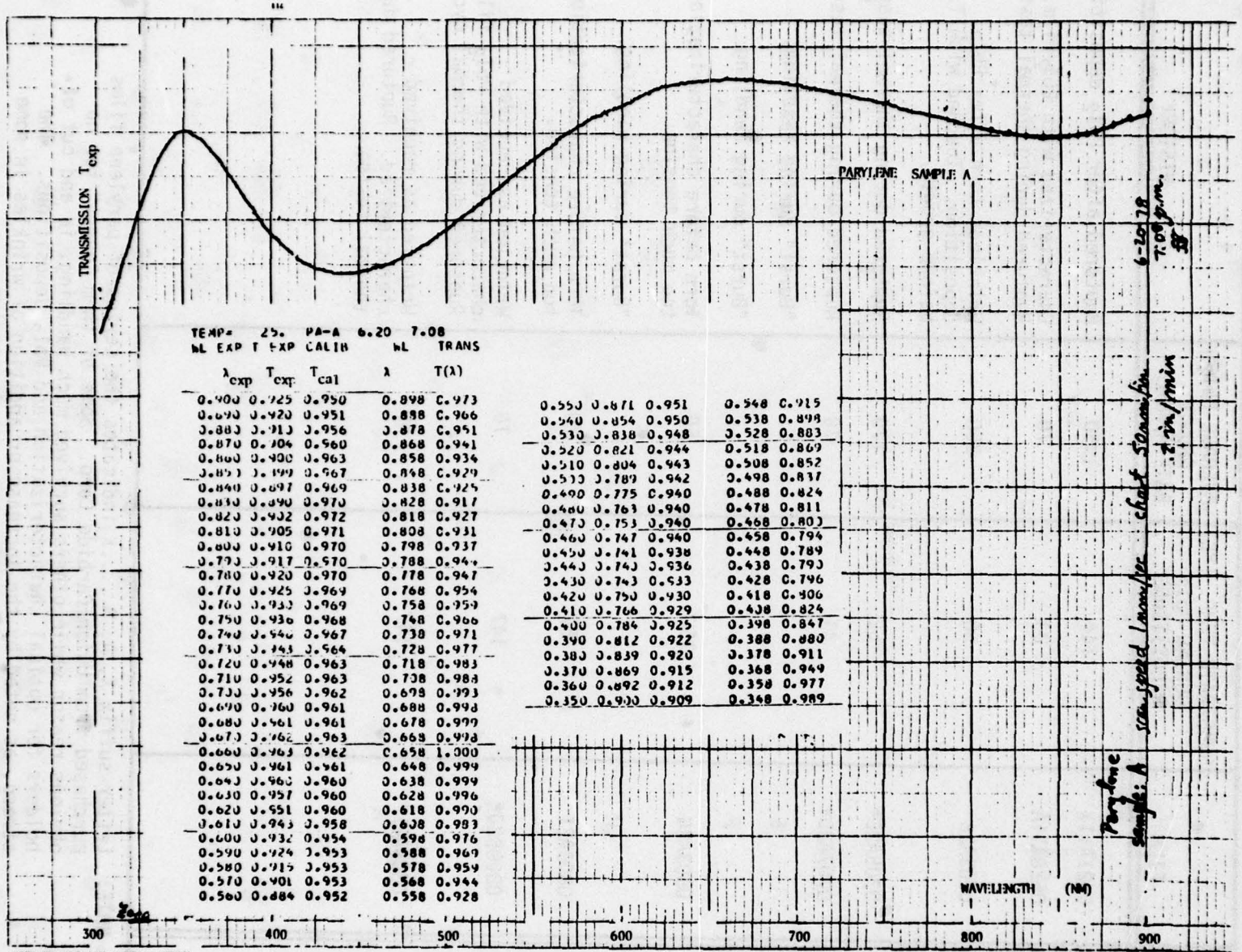

TEMP= 25. PA-A 6.20 7.08

hL EXP λ_{exp}	T EXP T_{exp}	CALIB T_{cal}	hL λ	TRANS $T(\lambda)$
0.900	0.925	0.950	0.898	0.973
0.890	0.920	0.951	0.888	0.966
0.880	0.910	0.956	0.878	0.951
0.870	0.904	0.960	0.868	0.941
0.860	0.900	0.963	0.858	0.934
0.850	0.899	0.967	0.848	0.929
0.840	0.897	0.969	0.838	0.925
0.830	0.890	0.970	0.828	0.917
0.820	0.902	0.972	0.818	0.927
0.810	0.905	0.971	0.808	0.931
0.800	0.910	0.970	0.798	0.937
0.790	0.917	0.970	0.788	0.944
0.780	0.920	0.970	0.778	0.947
0.770	0.925	0.969	0.768	0.954
0.760	0.930	0.969	0.758	0.959
0.750	0.936	0.968	0.748	0.966
0.740	0.940	0.967	0.738	0.971
0.730	0.943	0.964	0.728	0.977
0.720	0.948	0.963	0.718	0.983
0.710	0.952	0.963	0.708	0.988
0.700	0.956	0.962	0.698	0.993
0.690	0.960	0.961	0.688	0.998
0.680	0.961	0.961	0.678	0.999
0.670	0.962	0.963	0.668	0.998
0.660	0.963	0.962	0.658	1.000
0.650	0.961	0.961	0.648	0.999
0.640	0.960	0.960	0.638	0.999
0.630	0.957	0.960	0.628	0.996
0.620	0.951	0.960	0.618	0.990
0.610	0.943	0.958	0.608	0.983
0.600	0.932	0.954	0.598	0.976
0.590	0.924	0.953	0.588	0.969
0.580	0.915	0.953	0.578	0.959
0.570	0.901	0.953	0.568	0.944
0.560	0.884	0.952	0.558	0.928
0.550	0.871	0.951	0.548	0.915
0.540	0.854	0.950	0.538	0.898
0.530	0.838	0.948	0.528	0.883
0.520	0.821	0.944	0.518	0.869
0.510	0.804	0.943	0.508	0.852
0.500	0.789	0.942	0.498	0.837
0.490	0.775	0.940	0.488	0.824
0.480	0.763	0.940	0.478	0.811
0.470	0.753	0.940	0.468	0.803
0.460	0.747	0.940	0.458	0.794
0.450	0.741	0.938	0.448	0.789
0.440	0.740	0.936	0.438	0.790
0.430	0.743	0.933	0.428	0.796
0.420	0.750	0.930	0.418	0.806
0.410	0.766	0.929	0.408	0.824
0.400	0.784	0.925	0.398	0.847
0.390	0.812	0.922	0.388	0.880
0.380	0.839	0.920	0.378	0.911
0.370	0.869	0.915	0.368	0.949
0.360	0.892	0.912	0.358	0.977
0.350	0.900	0.909	0.348	0.989

FIGURE 2.5-3. Transmission of Parylene Film A.

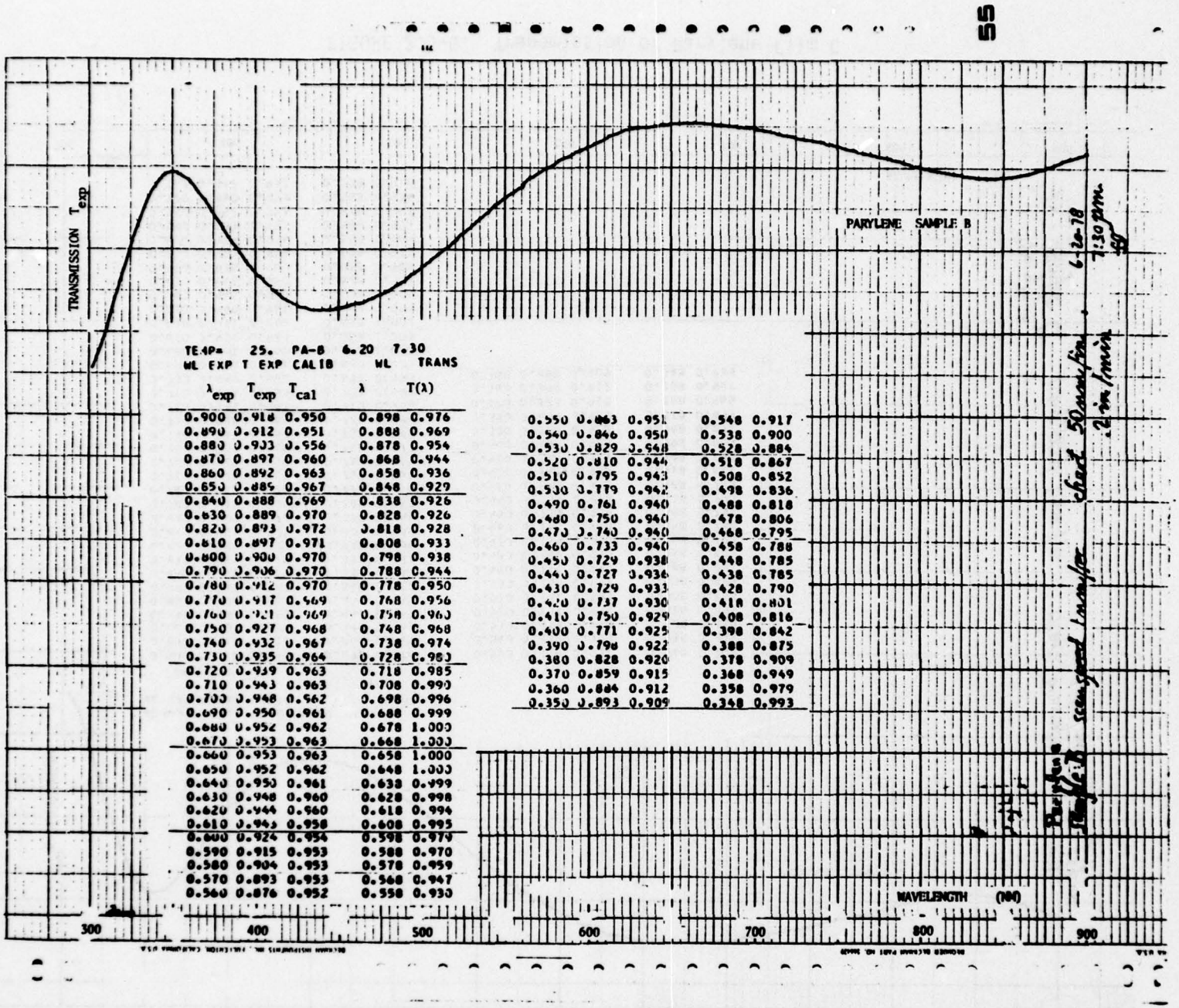

TEMP= 25. PA-B 6.20 7.30

WL EXP λ_{exp}	T EXP T_{exp}	CALIB T_{cal}	WL λ	TRANS $T(\lambda)$
0.900	0.918	0.950	0.898	0.976
0.890	0.912	0.951	0.888	0.969
0.880	0.903	0.956	0.878	0.954
0.870	0.897	0.960	0.868	0.944
0.860	0.892	0.963	0.858	0.936
0.850	0.885	0.967	0.848	0.929
0.840	0.888	0.969	0.838	0.926
0.830	0.889	0.970	0.828	0.926
0.820	0.893	0.972	0.818	0.928
0.810	0.897	0.971	0.808	0.933
0.800	0.900	0.970	0.798	0.938
0.790	0.906	0.970	0.788	0.944
0.780	0.912	0.970	0.778	0.950
0.770	0.917	0.969	0.768	0.956
0.760	0.921	0.969	0.758	0.960
0.750	0.927	0.968	0.748	0.968
0.740	0.932	0.967	0.738	0.974
0.730	0.935	0.964	0.728	0.980
0.720	0.939	0.963	0.718	0.985
0.710	0.943	0.963	0.708	0.990
0.700	0.948	0.962	0.698	0.996
0.690	0.950	0.961	0.688	0.999
0.680	0.952	0.962	0.678	1.000
0.670	0.953	0.963	0.668	1.000
0.660	0.953	0.963	0.658	1.000
0.650	0.952	0.962	0.648	1.000
0.640	0.950	0.961	0.638	0.999
0.630	0.948	0.960	0.628	0.998
0.620	0.944	0.960	0.618	0.994
0.610	0.943	0.958	0.608	0.995
0.600	0.924	0.954	0.598	0.979
0.590	0.915	0.953	0.588	0.970
0.580	0.904	0.953	0.578	0.959
0.570	0.893	0.953	0.568	0.947
0.560	0.876	0.952	0.558	0.930
0.550	0.863	0.951	0.548	0.917
0.540	0.846	0.950	0.538	0.900
0.530	0.829	0.948	0.528	0.884
0.520	0.810	0.944	0.518	0.867
0.510	0.795	0.943	0.508	0.852
0.500	0.779	0.942	0.498	0.836
0.490	0.761	0.940	0.488	0.818
0.480	0.750	0.940	0.478	0.806
0.470	0.740	0.940	0.468	0.795
0.460	0.733	0.940	0.458	0.788
0.450	0.729	0.938	0.448	0.785
0.440	0.727	0.936	0.438	0.785
0.430	0.729	0.933	0.428	0.790
0.420	0.737	0.930	0.418	0.801
0.410	0.750	0.929	0.408	0.816
0.400	0.771	0.925	0.398	0.842
0.390	0.798	0.922	0.388	0.875
0.380	0.828	0.920	0.378	0.909
0.370	0.859	0.915	0.368	0.949
0.360	0.884	0.912	0.358	0.979
0.350	0.893	0.909	0.348	0.993

FIGURE 2.5-4. Transmission of Parylene Film B

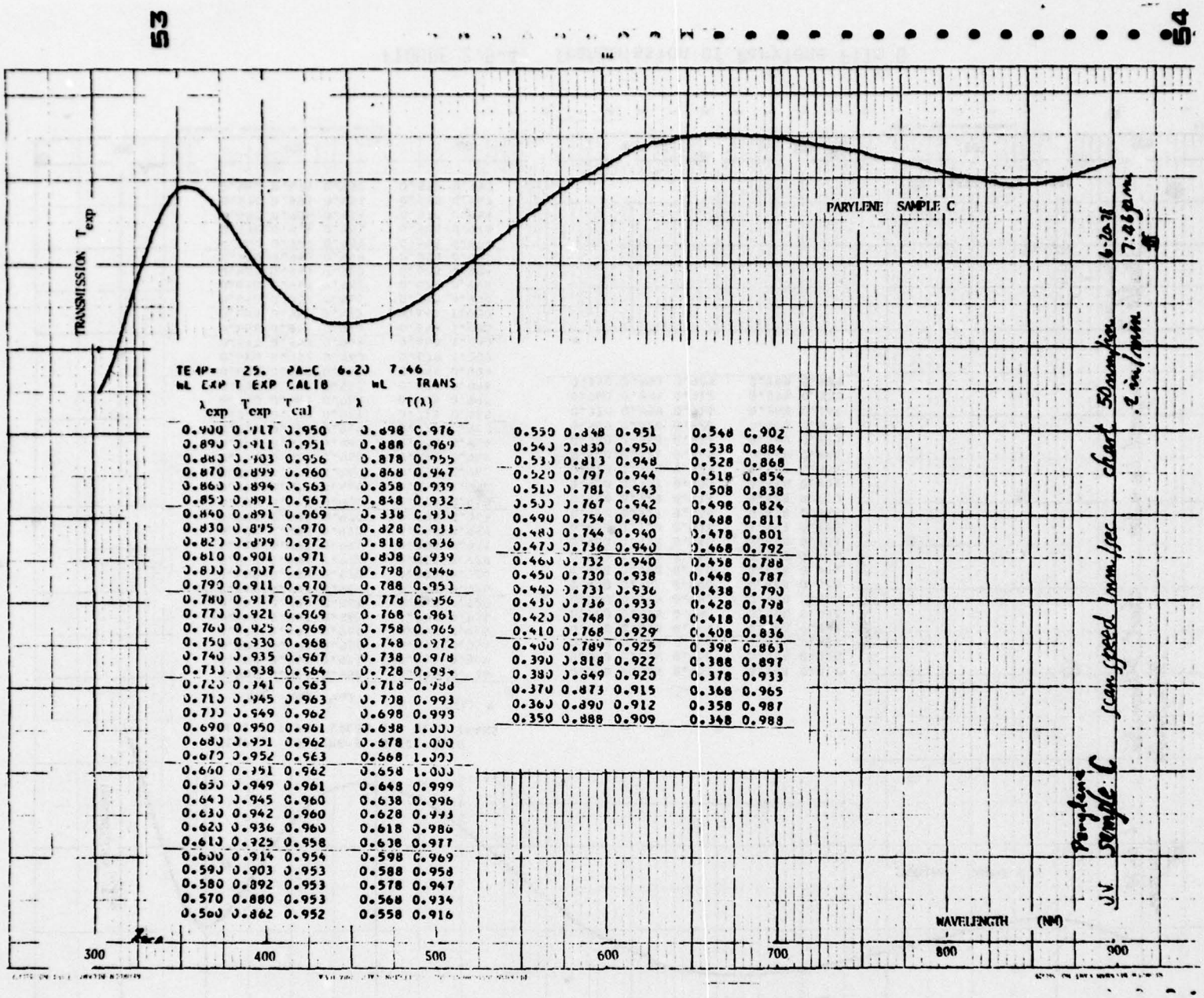

FIGURE 2.5-5. Transmission of Parylene Film C

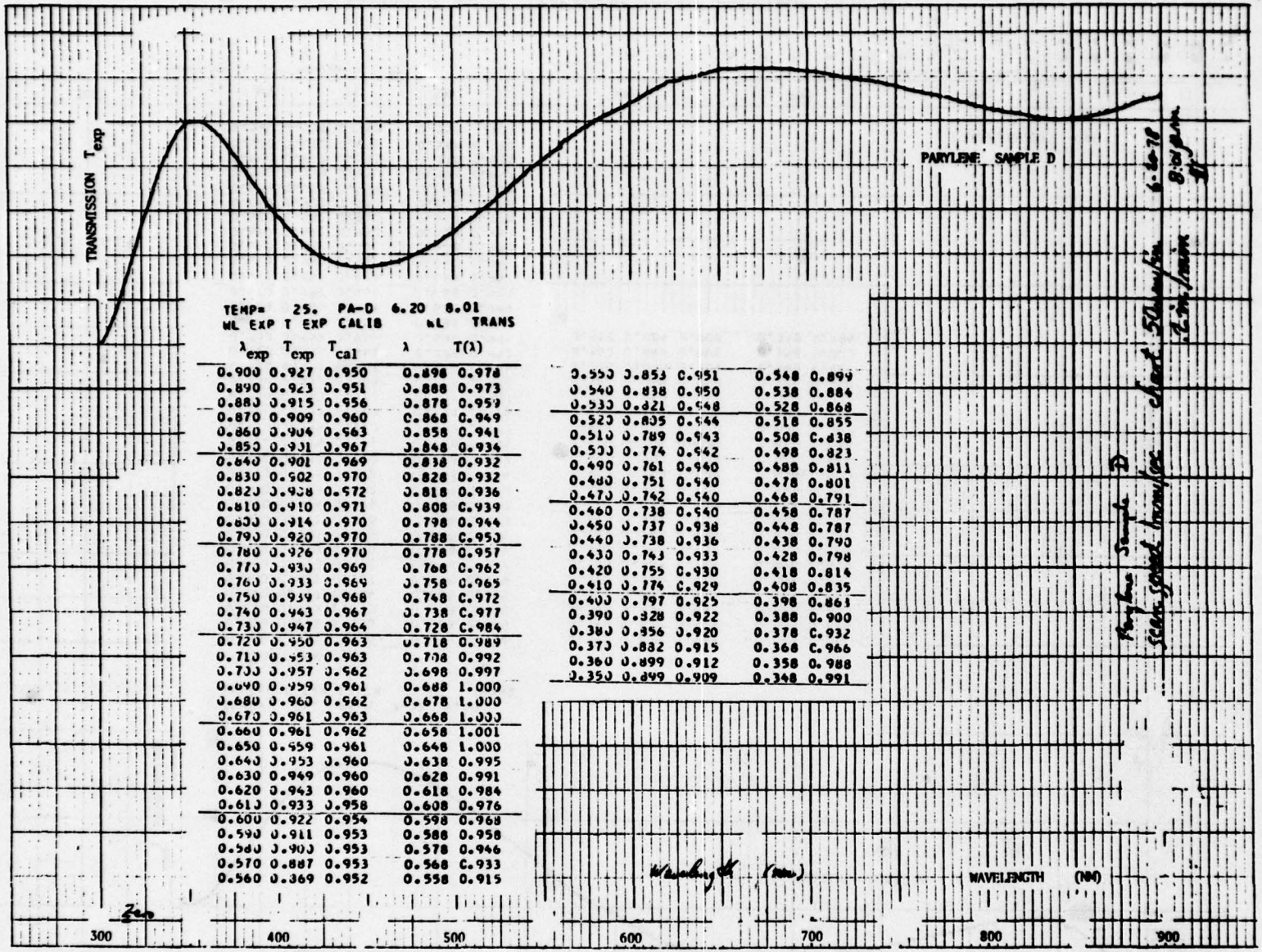

TEMP= 25. PA-D 6.20 8.01

WL EXP T EXP CALIB			WL	TRANS
λ_{exp}	T_{exp}	T_{cal}	λ	$T(\lambda)$
0.900	0.927	0.950	0.898	0.978
0.890	0.923	0.951	0.888	0.973
0.880	0.915	0.956	0.878	0.959
0.870	0.909	0.960	0.868	0.949
0.860	0.904	0.963	0.858	0.941
0.850	0.901	0.967	0.848	0.934
0.840	0.901	0.969	0.838	0.932
0.830	0.902	0.970	0.828	0.932
0.820	0.908	0.972	0.818	0.936
0.810	0.910	0.971	0.808	0.939
0.800	0.914	0.970	0.798	0.944
0.790	0.920	0.970	0.788	0.950
0.780	0.926	0.970	0.778	0.957
0.770	0.930	0.969	0.768	0.962
0.760	0.933	0.969	0.758	0.965
0.750	0.939	0.968	0.748	0.972
0.740	0.943	0.967	0.738	0.977
0.730	0.947	0.964	0.728	0.984
0.720	0.950	0.963	0.718	0.989
0.710	0.953	0.963	0.708	0.992
0.700	0.957	0.962	0.698	0.997
0.690	0.959	0.961	0.688	1.000
0.680	0.960	0.962	0.678	1.000
0.670	0.961	0.963	0.668	1.000
0.660	0.961	0.962	0.658	1.001
0.650	0.959	0.961	0.648	1.000
0.640	0.953	0.960	0.638	0.995
0.630	0.949	0.960	0.628	0.991
0.620	0.943	0.960	0.618	0.984
0.610	0.933	0.958	0.608	0.976
0.600	0.922	0.954	0.598	0.968
0.590	0.911	0.953	0.588	0.958
0.580	0.900	0.953	0.578	0.946
0.570	0.887	0.953	0.568	0.933
0.560	0.869	0.952	0.558	0.915
0.550	0.853	0.951	0.548	0.899
0.540	0.838	0.950	0.538	0.884
0.530	0.821	0.948	0.528	0.868
0.520	0.805	0.944	0.518	0.855
0.510	0.789	0.943	0.508	0.838
0.500	0.774	0.942	0.498	0.823
0.490	0.761	0.940	0.488	0.811
0.480	0.751	0.940	0.478	0.801
0.470	0.742	0.940	0.468	0.791
0.460	0.738	0.940	0.458	0.787
0.450	0.737	0.938	0.448	0.787
0.440	0.738	0.936	0.438	0.790
0.430	0.743	0.933	0.428	0.798
0.420	0.755	0.930	0.418	0.814
0.410	0.774	0.929	0.408	0.835
0.400	0.797	0.925	0.398	0.861
0.390	0.828	0.922	0.388	0.900
0.380	0.856	0.920	0.378	0.932
0.370	0.882	0.915	0.368	0.966
0.360	0.899	0.912	0.358	0.988
0.350	0.899	0.909	0.348	0.991

FIGURE 2.5-6. Transmission of Parylene Film D

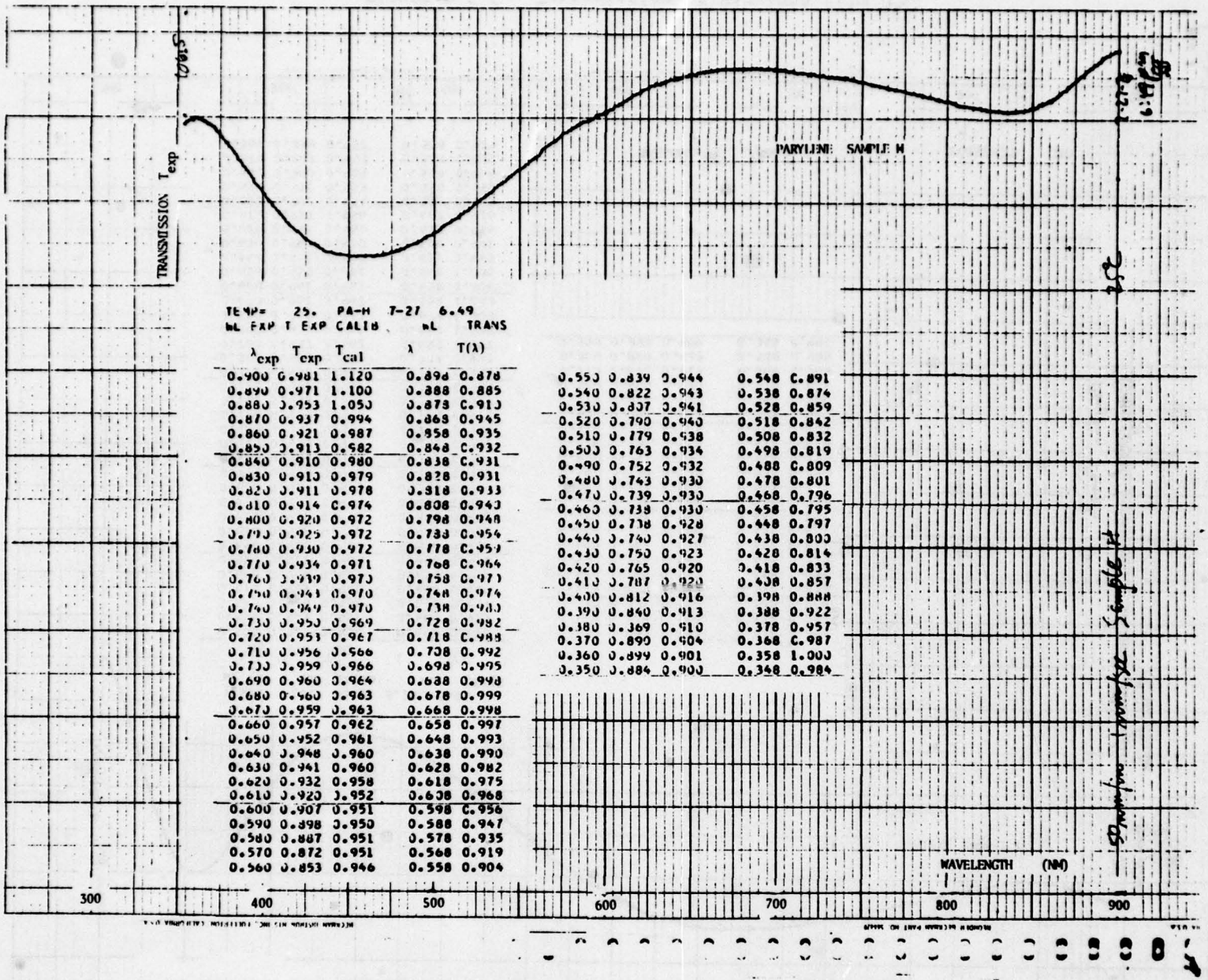

TEMP= 25. PA-H 7-27 6.49

nL EXP T EXP CALIB			nL	TRANS
λ_{exp}	T_{exp}	T_{cal}	λ	$T(\lambda)$
0.900	0.981	1.120	0.898	0.878
0.890	0.971	1.100	0.888	0.885
0.880	0.953	1.050	0.878	0.910
0.870	0.937	0.994	0.868	0.945
0.860	0.921	0.987	0.858	0.935
0.850	0.913	0.982	0.848	0.932
0.840	0.910	0.980	0.838	0.931
0.830	0.910	0.979	0.828	0.931
0.820	0.911	0.978	0.818	0.933
0.810	0.914	0.974	0.808	0.940
0.800	0.920	0.972	0.798	0.948
0.790	0.925	0.972	0.788	0.954
0.780	0.930	0.972	0.778	0.959
0.770	0.934	0.971	0.768	0.964
0.760	0.939	0.970	0.758	0.971
0.750	0.943	0.970	0.748	0.974
0.740	0.949	0.970	0.738	0.980
0.730	0.950	0.969	0.728	0.982
0.720	0.953	0.967	0.718	0.988
0.710	0.956	0.966	0.708	0.992
0.700	0.959	0.966	0.698	0.995
0.690	0.960	0.964	0.688	0.998
0.680	0.960	0.963	0.678	0.999
0.670	0.959	0.963	0.668	0.998
0.660	0.957	0.962	0.658	0.997
0.650	0.952	0.961	0.648	0.993
0.640	0.948	0.960	0.638	0.990
0.630	0.941	0.960	0.628	0.982
0.620	0.932	0.958	0.618	0.975
0.610	0.920	0.952	0.608	0.968
0.600	0.907	0.951	0.598	0.956
0.590	0.898	0.950	0.588	0.947
0.580	0.887	0.951	0.578	0.935
0.570	0.872	0.951	0.568	0.919
0.560	0.853	0.946	0.558	0.904
0.550	0.839	0.944	0.548	0.891
0.540	0.822	0.943	0.538	0.874
0.530	0.807	0.941	0.528	0.859
0.520	0.790	0.940	0.518	0.842
0.510	0.779	0.938	0.508	0.832
0.500	0.763	0.934	0.498	0.819
0.490	0.752	0.932	0.488	0.809
0.480	0.743	0.930	0.478	0.801
0.470	0.739	0.930	0.468	0.796
0.460	0.738	0.930	0.458	0.795
0.450	0.738	0.928	0.448	0.797
0.440	0.740	0.927	0.438	0.800
0.430	0.750	0.923	0.428	0.814
0.420	0.765	0.920	0.418	0.833
0.410	0.787	0.920	0.408	0.857
0.400	0.812	0.916	0.398	0.888
0.390	0.840	0.913	0.388	0.922
0.380	0.869	0.910	0.378	0.957
0.370	0.890	0.904	0.368	0.987
0.360	0.899	0.901	0.358	1.000
0.350	0.884	0.900	0.348	0.984

FIGURE 2.5-7. Transmission of Parylene Film H

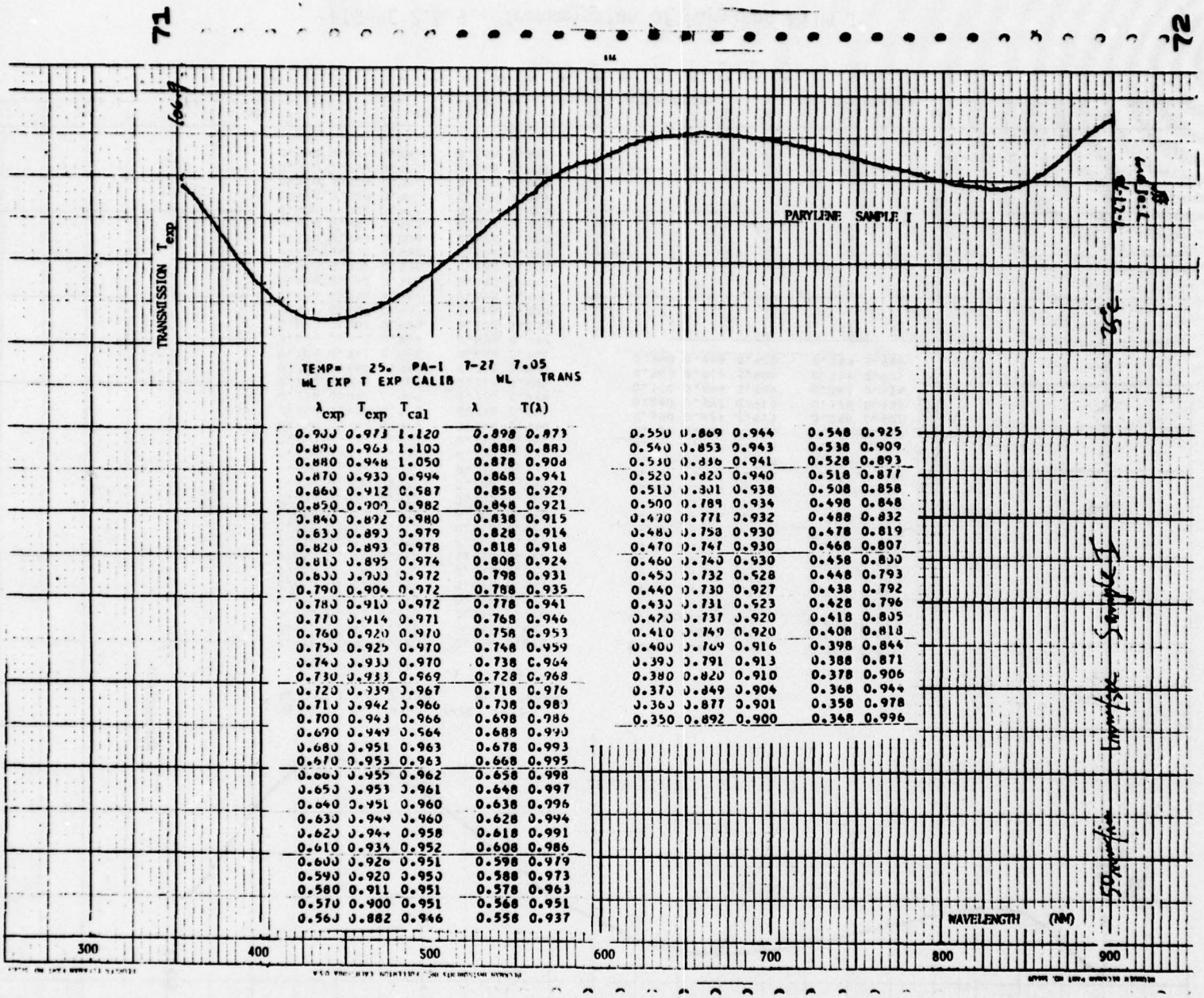

TEMP= 25. PA-I 7-27 7.05

WL EXP λexp	T EXP Texp	CALIB Tcal	WL λ	TRANS T(λ)
0.900	0.973	1.120	0.898	0.873
0.890	0.963	1.100	0.888	0.883
0.880	0.948	1.050	0.878	0.908
0.870	0.930	0.994	0.868	0.941
0.860	0.912	0.987	0.858	0.929
0.850	0.900	0.982	0.848	0.921
0.840	0.892	0.980	0.838	0.915
0.830	0.893	0.979	0.828	0.914
0.820	0.893	0.978	0.818	0.918
0.810	0.895	0.974	0.808	0.924
0.800	0.900	0.972	0.798	0.931
0.790	0.906	0.972	0.788	0.935
0.780	0.910	0.972	0.778	0.941
0.770	0.914	0.971	0.768	0.946
0.760	0.920	0.970	0.758	0.953
0.750	0.925	0.970	0.748	0.959
0.740	0.930	0.970	0.738	0.964
0.730	0.933	0.969	0.728	0.968
0.720	0.939	0.967	0.718	0.976
0.710	0.942	0.966	0.708	0.980
0.700	0.943	0.966	0.698	0.986
0.690	0.949	0.964	0.688	0.990
0.680	0.951	0.963	0.678	0.993
0.670	0.953	0.963	0.668	0.995
0.660	0.955	0.962	0.658	0.998
0.650	0.953	0.961	0.648	0.997
0.640	0.951	0.960	0.638	0.996
0.630	0.949	0.960	0.628	0.994
0.620	0.944	0.958	0.618	0.991
0.610	0.934	0.952	0.608	0.986
0.600	0.926	0.951	0.598	0.979
0.590	0.920	0.950	0.588	0.973
0.580	0.911	0.951	0.578	0.963
0.570	0.900	0.951	0.568	0.951
0.560	0.882	0.946	0.558	0.937
0.550	0.869	0.944	0.548	0.925
0.540	0.853	0.943	0.538	0.909
0.530	0.836	0.941	0.528	0.893
0.520	0.820	0.940	0.518	0.877
0.510	0.801	0.938	0.508	0.858
0.500	0.789	0.934	0.498	0.848
0.490	0.771	0.932	0.488	0.832
0.480	0.758	0.930	0.478	0.819
0.470	0.747	0.930	0.468	0.807
0.460	0.740	0.930	0.458	0.800
0.450	0.732	0.928	0.448	0.793
0.440	0.730	0.927	0.438	0.792
0.430	0.731	0.923	0.428	0.796
0.420	0.737	0.920	0.418	0.805
0.410	0.749	0.920	0.408	0.818
0.400	0.769	0.916	0.398	0.844
0.390	0.791	0.913	0.388	0.871
0.380	0.820	0.910	0.378	0.906
0.370	0.849	0.904	0.368	0.944
0.360	0.877	0.901	0.358	0.978
0.350	0.892	0.900	0.348	0.996

FIGURE 2.5-8. Transmission of Parylene Film I

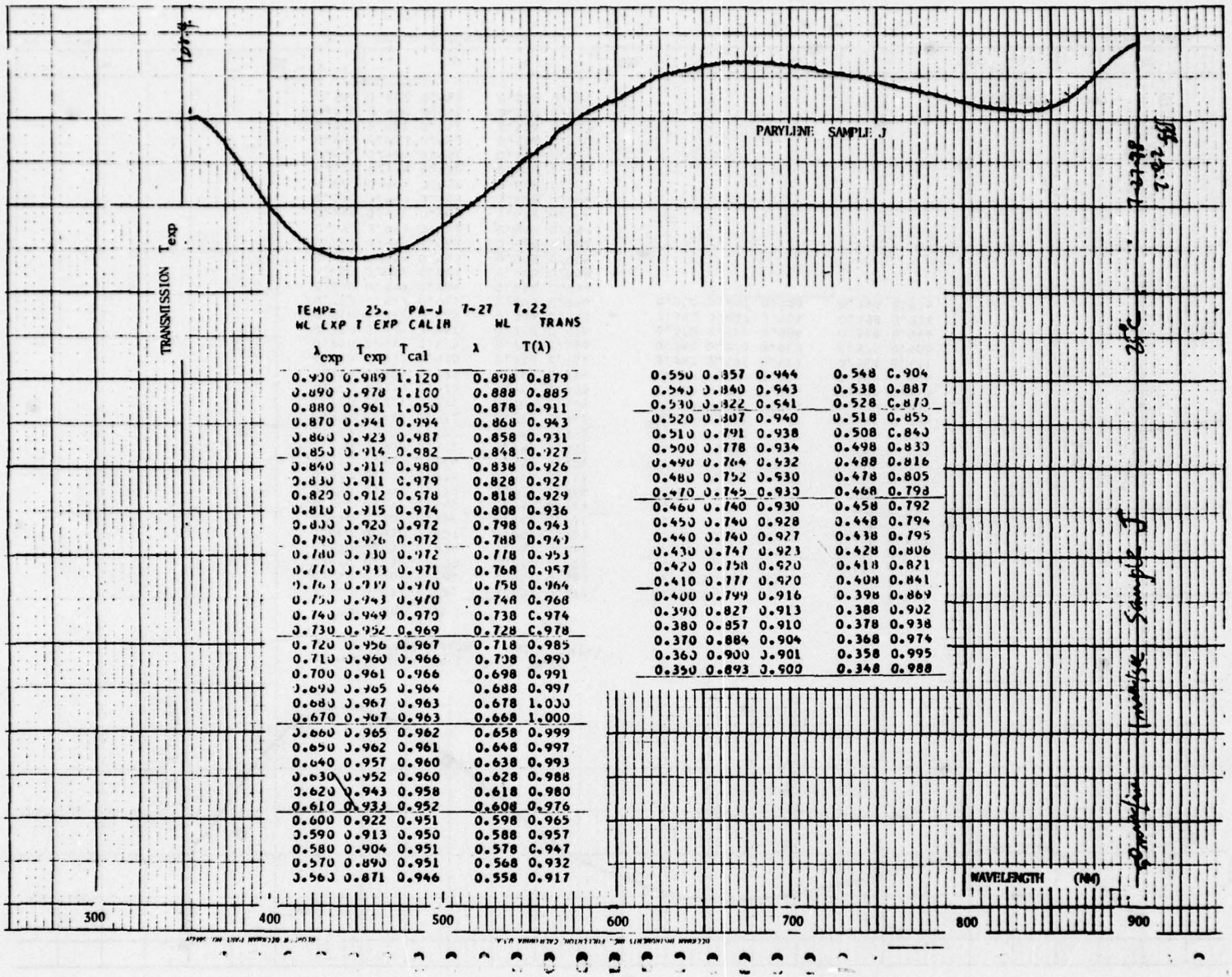

TEMP= 25. PA-J 7-27 7.22
WL EXP T EXP CALIB WL TRANS

λ_{exp}	T_{exp}	T_{cal}	λ	$T(\lambda)$
0.900	0.989	1.120	0.898	0.879
0.890	0.978	1.100	0.888	0.885
0.880	0.961	1.050	0.878	0.911
0.870	0.941	0.994	0.868	0.943
0.860	0.923	0.987	0.858	0.931
0.850	0.914	0.982	0.848	0.927
0.840	0.911	0.980	0.838	0.926
0.830	0.911	0.979	0.828	0.927
0.820	0.912	0.978	0.818	0.929
0.810	0.915	0.974	0.808	0.936
0.800	0.920	0.972	0.798	0.943
0.790	0.926	0.972	0.788	0.949
0.780	0.930	0.972	0.778	0.953
0.770	0.933	0.971	0.768	0.957
0.760	0.939	0.970	0.758	0.964
0.750	0.943	0.970	0.748	0.968
0.740	0.949	0.970	0.738	0.974
0.730	0.952	0.969	0.728	0.978
0.720	0.956	0.967	0.718	0.985
0.710	0.960	0.966	0.708	0.990
0.700	0.961	0.966	0.698	0.991
0.690	0.965	0.964	0.688	0.997
0.680	0.967	0.963	0.678	1.000
0.670	0.967	0.963	0.668	1.000
0.660	0.965	0.962	0.658	0.999
0.650	0.962	0.961	0.648	0.997
0.640	0.957	0.960	0.638	0.993
0.630	0.952	0.960	0.628	0.988
0.620	0.943	0.958	0.618	0.980
0.610	0.933	0.952	0.608	0.976
0.600	0.922	0.951	0.598	0.965
0.590	0.913	0.950	0.588	0.957
0.580	0.904	0.951	0.578	0.947
0.570	0.890	0.951	0.568	0.932
0.560	0.871	0.946	0.558	0.917
0.550	0.857	0.944	0.548	0.904
0.540	0.840	0.943	0.538	0.887
0.530	0.822	0.941	0.528	0.873
0.520	0.807	0.940	0.518	0.855
0.510	0.791	0.938	0.508	0.840
0.500	0.778	0.934	0.498	0.833
0.490	0.764	0.932	0.488	0.816
0.480	0.752	0.930	0.478	0.805
0.470	0.745	0.930	0.468	0.798
0.460	0.740	0.930	0.458	0.792
0.450	0.740	0.928	0.448	0.794
0.440	0.740	0.927	0.438	0.795
0.430	0.747	0.923	0.428	0.806
0.420	0.758	0.920	0.418	0.821
0.410	0.777	0.920	0.408	0.841
0.400	0.799	0.916	0.398	0.869
0.390	0.827	0.913	0.388	0.902
0.380	0.857	0.910	0.378	0.938
0.370	0.884	0.904	0.368	0.974
0.360	0.900	0.901	0.358	0.995
0.350	0.893	0.900	0.348	0.988

FIGURE 2.5-9. Transmission of Parylene Film J

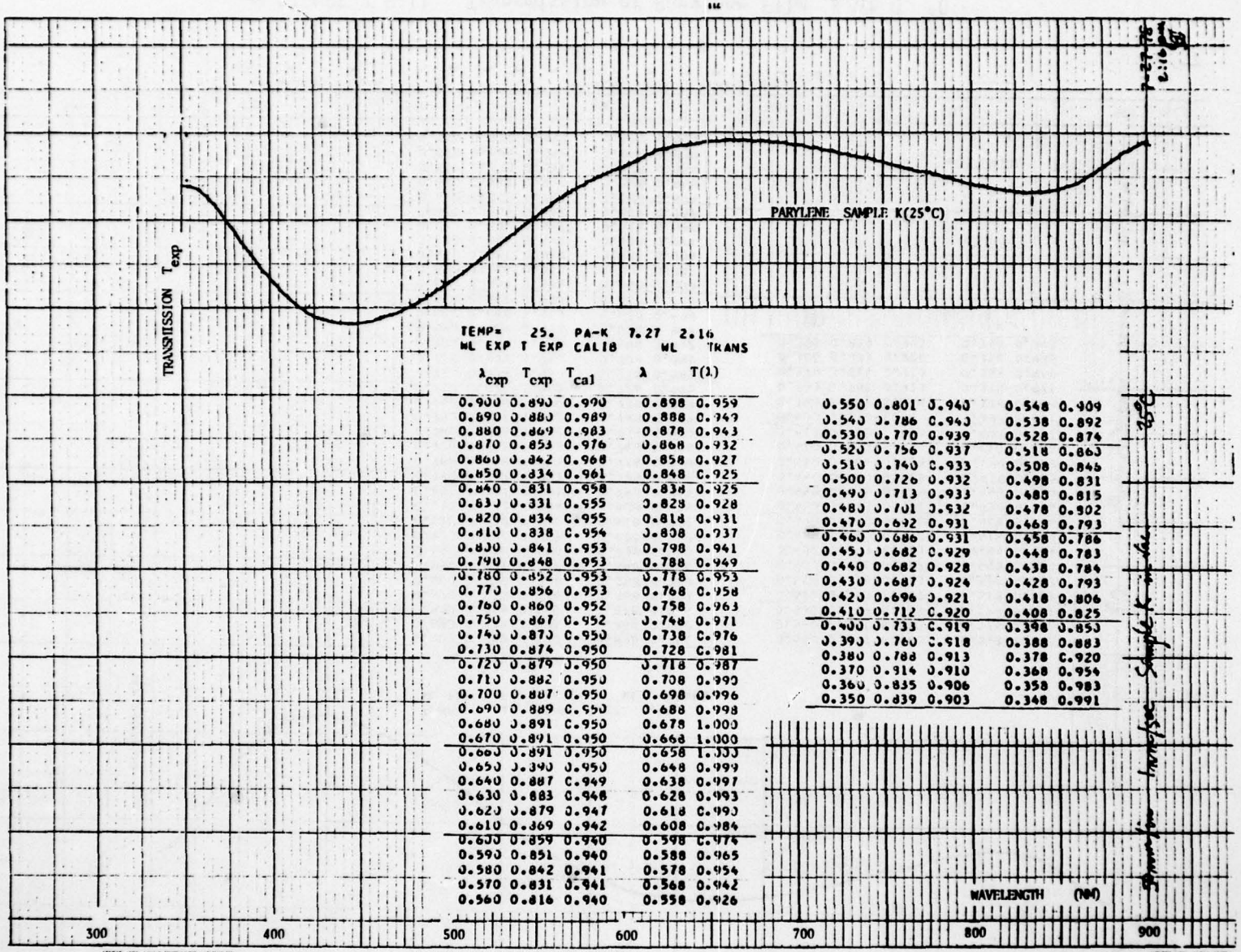

TEMP= 25. PA-K 7.27 2.16

WL EXP T EXP CALIB			WL TRANS	
λ_{exp}	T_{exp}	T_{cal}	λ	T(λ)
0.900	0.890	0.990	0.898	0.959
0.890	0.880	0.989	0.888	0.949
0.880	0.869	0.983	0.878	0.943
0.870	0.853	0.976	0.868	0.932
0.860	0.842	0.968	0.858	0.927
0.850	0.834	0.961	0.848	0.925
0.840	0.831	0.958	0.838	0.925
0.830	0.831	0.955	0.828	0.928
0.820	0.834	0.955	0.818	0.931
0.810	0.838	0.954	0.808	0.937
0.800	0.841	0.953	0.798	0.941
0.790	0.848	0.953	0.788	0.949
0.780	0.852	0.953	0.778	0.953
0.770	0.856	0.953	0.768	0.958
0.760	0.860	0.952	0.758	0.963
0.750	0.867	0.952	0.748	0.971
0.740	0.870	0.950	0.738	0.976
0.730	0.874	0.950	0.728	0.981
0.720	0.879	0.950	0.718	0.987
0.710	0.882	0.950	0.708	0.990
0.700	0.887	0.950	0.698	0.996
0.690	0.889	0.950	0.688	0.998
0.680	0.891	0.950	0.678	1.000
0.670	0.891	0.950	0.668	1.000
0.660	0.891	0.950	0.658	1.000
0.650	0.890	0.950	0.648	0.999
0.640	0.887	0.949	0.638	0.997
0.630	0.883	0.948	0.628	0.993
0.620	0.879	0.947	0.618	0.990
0.610	0.869	0.942	0.608	0.984
0.600	0.859	0.940	0.598	0.976
0.590	0.851	0.940	0.588	0.965
0.580	0.842	0.941	0.578	0.956
0.570	0.831	0.941	0.568	0.942
0.560	0.816	0.940	0.558	0.926
0.550	0.801	0.940	0.548	0.909
0.540	0.786	0.940	0.538	0.892
0.530	0.770	0.939	0.528	0.874
0.520	0.756	0.937	0.518	0.863
0.510	0.740	0.933	0.508	0.846
0.500	0.726	0.932	0.498	0.831
0.490	0.713	0.933	0.488	0.815
0.480	0.701	0.932	0.478	0.802
0.470	0.692	0.931	0.468	0.793
0.460	0.686	0.931	0.458	0.786
0.450	0.682	0.929	0.448	0.783
0.440	0.682	0.928	0.438	0.784
0.430	0.687	0.924	0.428	0.793
0.420	0.696	0.921	0.418	0.806
0.410	0.712	0.920	0.408	0.825
0.400	0.733	0.919	0.398	0.853
0.390	0.760	0.918	0.388	0.883
0.380	0.788	0.913	0.378	0.920
0.370	0.914	0.910	0.368	0.954
0.360	0.835	0.906	0.358	0.983
0.350	0.839	0.903	0.348	0.991

FIGURE 2.5-10. Transmission of Parylene Film K at 25°C

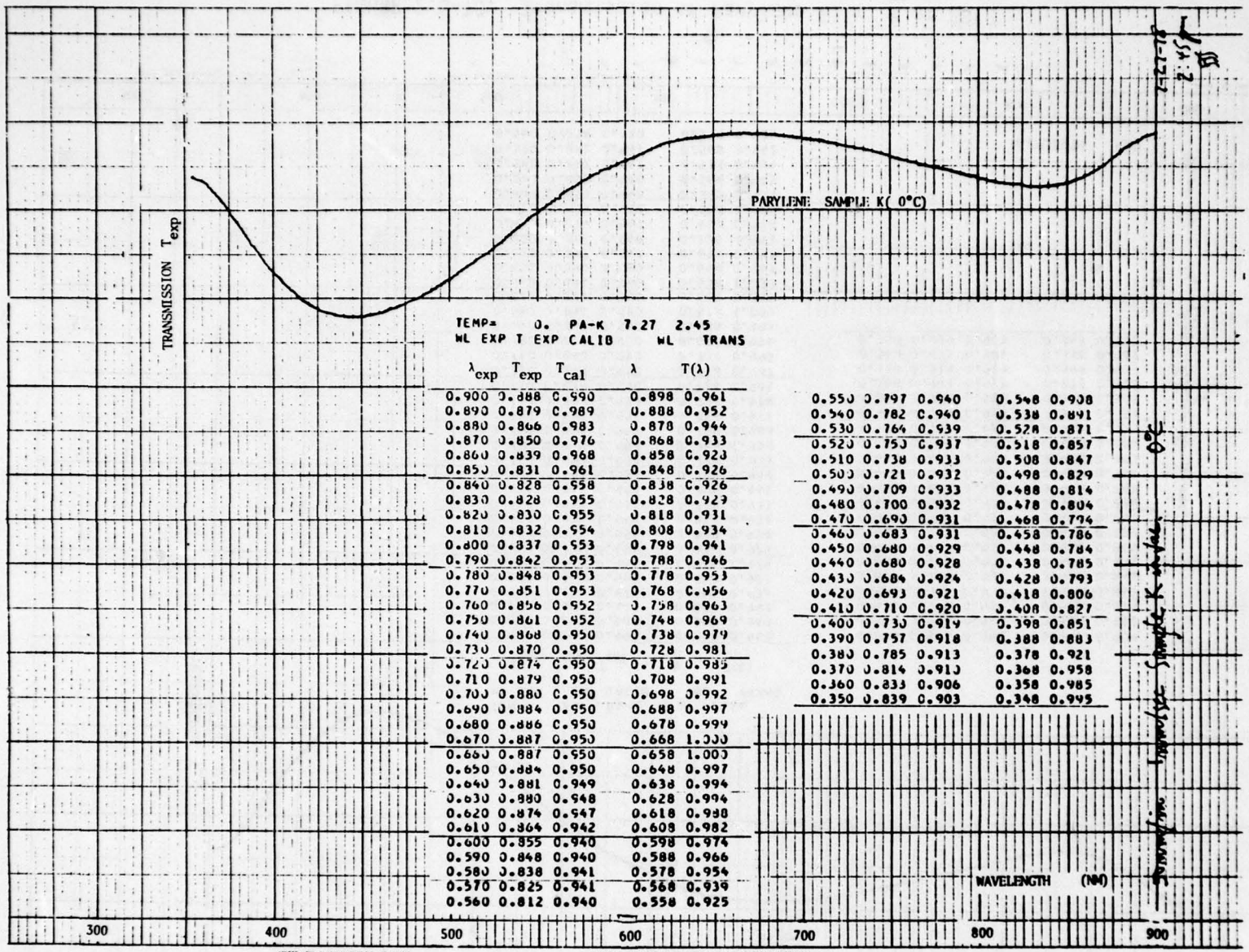

TEMP= 0. PA-K 7.27 2.45

WL EXP λ_{exp}	T EXP T_{exp}	CALIB T_{cal}	WL TRANS λ	TRANS $T(\lambda)$
0.900	0.888	0.990	0.898	0.961
0.890	0.879	0.989	0.888	0.952
0.880	0.866	0.983	0.878	0.944
0.870	0.850	0.976	0.868	0.933
0.860	0.839	0.968	0.858	0.923
0.850	0.831	0.961	0.848	0.926
0.840	0.828	0.958	0.838	0.926
0.830	0.828	0.955	0.828	0.929
0.820	0.830	0.955	0.818	0.931
0.810	0.832	0.954	0.808	0.934
0.800	0.837	0.953	0.798	0.941
0.790	0.842	0.953	0.788	0.946
0.780	0.848	0.953	0.778	0.953
0.770	0.851	0.953	0.768	0.956
0.760	0.856	0.952	0.758	0.963
0.750	0.861	0.952	0.748	0.969
0.740	0.868	0.950	0.738	0.979
0.730	0.870	0.950	0.728	0.981
0.720	0.874	0.950	0.718	0.985
0.710	0.879	0.950	0.708	0.991
0.700	0.880	0.950	0.698	0.992
0.690	0.884	0.950	0.688	0.997
0.680	0.886	0.950	0.678	0.999
0.670	0.887	0.950	0.668	1.000
0.660	0.887	0.950	0.658	1.000
0.650	0.884	0.950	0.648	0.997
0.640	0.881	0.949	0.638	0.994
0.630	0.880	0.948	0.628	0.994
0.620	0.874	0.947	0.618	0.988
0.610	0.864	0.942	0.608	0.982
0.600	0.855	0.940	0.598	0.974
0.590	0.848	0.940	0.588	0.966
0.580	0.838	0.941	0.578	0.954
0.570	0.825	0.941	0.568	0.939
0.560	0.812	0.940	0.558	0.925
0.550	0.797	0.940	0.548	0.908
0.540	0.782	0.940	0.538	0.891
0.530	0.764	0.939	0.528	0.871
0.520	0.750	0.937	0.518	0.857
0.510	0.738	0.933	0.508	0.847
0.500	0.721	0.932	0.498	0.829
0.490	0.709	0.933	0.488	0.814
0.480	0.700	0.932	0.478	0.804
0.470	0.690	0.931	0.468	0.794
0.460	0.683	0.931	0.458	0.786
0.450	0.680	0.929	0.448	0.784
0.440	0.680	0.928	0.438	0.785
0.430	0.684	0.924	0.428	0.793
0.420	0.693	0.921	0.418	0.806
0.410	0.710	0.920	0.408	0.827
0.400	0.730	0.919	0.398	0.851
0.390	0.757	0.918	0.388	0.883
0.380	0.785	0.913	0.378	0.921
0.370	0.814	0.910	0.368	0.958
0.360	0.833	0.906	0.358	0.985
0.350	0.839	0.903	0.348	0.995

FIGURE 2.5-11. Transmission of Parylene Film K at 0. °C

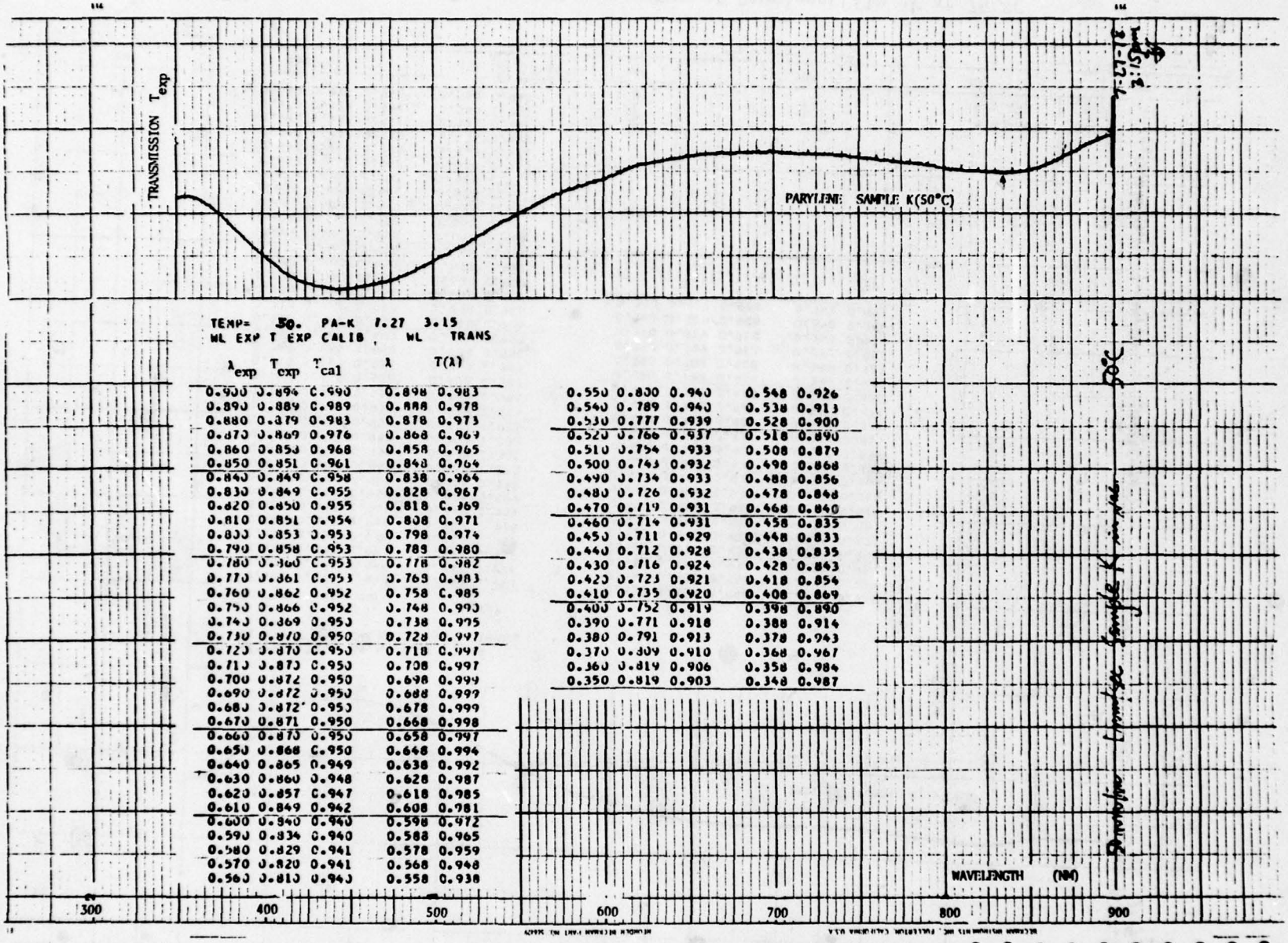

TEMP= 50. PA-K 1.27 3.15

WL EXP λ_{exp}	T EXP T_{exp}	CALIB T_{cal}	WL λ	TRANS T(λ)
0.900	0.894	0.990	0.898	0.983
0.890	0.884	0.989	0.888	0.978
0.880	0.879	0.983	0.878	0.973
0.870	0.869	0.976	0.868	0.969
0.860	0.859	0.968	0.858	0.965
0.850	0.851	0.961	0.848	0.964
0.840	0.849	0.958	0.838	0.964
0.830	0.849	0.955	0.828	0.967
0.820	0.850	0.955	0.818	0.969
0.810	0.851	0.954	0.808	0.971
0.800	0.853	0.953	0.798	0.974
0.790	0.858	0.953	0.788	0.980
0.780	0.860	0.953	0.778	0.982
0.770	0.861	0.953	0.768	0.983
0.760	0.862	0.952	0.758	0.985
0.750	0.866	0.952	0.748	0.990
0.740	0.869	0.953	0.738	0.995
0.730	0.870	0.950	0.728	0.997
0.720	0.870	0.950	0.718	0.997
0.710	0.870	0.950	0.708	0.997
0.700	0.872	0.950	0.698	0.999
0.690	0.872	0.950	0.688	0.999
0.680	0.872	0.950	0.678	0.999
0.670	0.871	0.950	0.668	0.998
0.660	0.870	0.950	0.658	0.997
0.650	0.868	0.950	0.648	0.994
0.640	0.865	0.949	0.638	0.992
0.630	0.860	0.948	0.628	0.987
0.620	0.857	0.947	0.618	0.985
0.610	0.849	0.942	0.608	0.981
0.600	0.840	0.940	0.598	0.972
0.590	0.834	0.940	0.588	0.965
0.580	0.829	0.941	0.578	0.959
0.570	0.820	0.941	0.568	0.948
0.560	0.810	0.940	0.558	0.938
0.550	0.800	0.940	0.548	0.926
0.540	0.789	0.940	0.538	0.913
0.530	0.777	0.939	0.528	0.900
0.520	0.766	0.937	0.518	0.890
0.510	0.754	0.933	0.508	0.879
0.500	0.743	0.932	0.498	0.868
0.490	0.734	0.933	0.488	0.856
0.480	0.726	0.932	0.478	0.848
0.470	0.719	0.931	0.468	0.840
0.460	0.714	0.931	0.458	0.835
0.450	0.711	0.929	0.448	0.833
0.440	0.712	0.928	0.438	0.835
0.430	0.716	0.924	0.428	0.843
0.420	0.723	0.921	0.418	0.854
0.410	0.735	0.920	0.408	0.869
0.400	0.752	0.919	0.398	0.890
0.390	0.771	0.918	0.388	0.914
0.380	0.791	0.913	0.378	0.943
0.370	0.809	0.910	0.368	0.967
0.360	0.819	0.906	0.358	0.984
0.350	0.819	0.903	0.348	0.987

FIGURE 2.5-12. Transmission of Perylene Film K at 50 °C

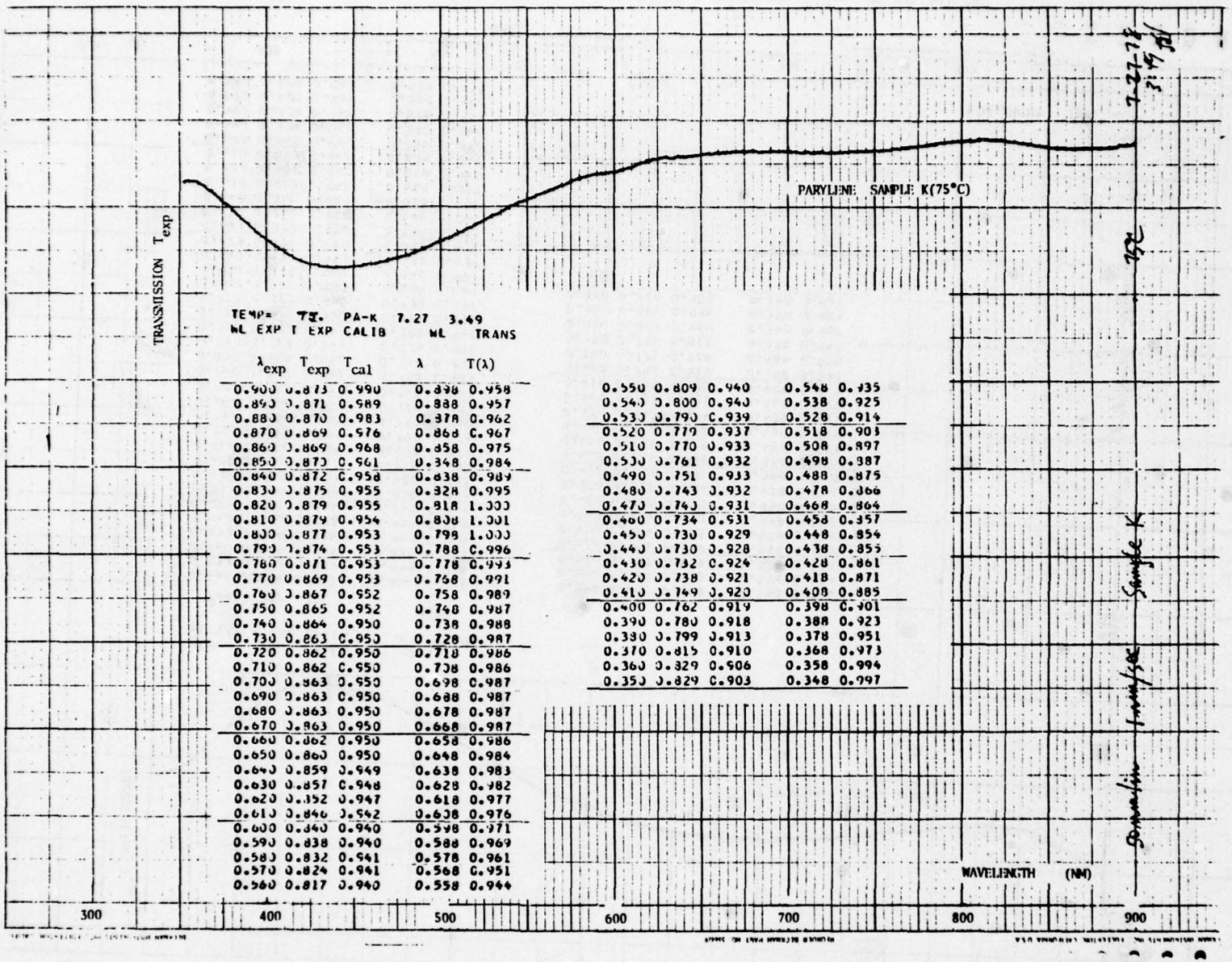

TEMP= 75. PA-K 7.27 3.49

WL EXP	T EXP	CALIB	WL	TRANS
λ_{exp}	T_{exp}	T_{cal}	λ	$T(\lambda)$
0.900	0.873	0.990	0.898	0.958
0.890	0.871	0.989	0.888	0.957
0.880	0.870	0.983	0.878	0.962
0.870	0.869	0.976	0.868	0.967
0.860	0.869	0.968	0.858	0.975
0.850	0.870	0.961	0.848	0.984
0.840	0.872	0.958	0.838	0.989
0.830	0.875	0.955	0.828	0.995
0.820	0.879	0.955	0.818	1.000
0.810	0.879	0.954	0.808	1.001
0.800	0.877	0.953	0.798	1.000
0.790	0.874	0.953	0.788	0.996
0.780	0.871	0.953	0.778	0.993
0.770	0.869	0.953	0.768	0.991
0.760	0.867	0.952	0.758	0.989
0.750	0.865	0.952	0.748	0.987
0.740	0.864	0.950	0.738	0.988
0.730	0.863	0.950	0.728	0.987
0.720	0.862	0.950	0.718	0.986
0.710	0.862	0.950	0.708	0.986
0.700	0.863	0.950	0.698	0.987
0.690	0.863	0.950	0.688	0.987
0.680	0.863	0.950	0.678	0.987
0.670	0.863	0.950	0.668	0.987
0.660	0.862	0.950	0.658	0.986
0.650	0.860	0.950	0.648	0.984
0.640	0.859	0.949	0.638	0.983
0.630	0.857	0.948	0.628	0.982
0.620	0.852	0.947	0.618	0.977
0.610	0.846	0.942	0.608	0.976
0.600	0.840	0.940	0.598	0.971
0.590	0.838	0.940	0.588	0.969
0.580	0.832	0.941	0.578	0.961
0.570	0.824	0.941	0.568	0.951
0.560	0.817	0.940	0.558	0.944
0.550	0.809	0.940	0.548	0.935
0.540	0.800	0.940	0.538	0.925
0.530	0.790	0.939	0.528	0.914
0.520	0.779	0.937	0.518	0.903
0.510	0.770	0.933	0.508	0.897
0.500	0.761	0.932	0.498	0.887
0.490	0.751	0.933	0.488	0.875
0.480	0.743	0.932	0.478	0.866
0.470	0.740	0.931	0.468	0.864
0.460	0.734	0.931	0.458	0.857
0.450	0.730	0.929	0.448	0.854
0.440	0.730	0.928	0.438	0.855
0.430	0.732	0.924	0.428	0.861
0.420	0.738	0.921	0.418	0.871
0.410	0.749	0.920	0.408	0.885
0.400	0.762	0.919	0.398	0.901
0.390	0.780	0.918	0.388	0.923
0.380	0.799	0.913	0.378	0.951
0.370	0.815	0.910	0.368	0.973
0.360	0.829	0.906	0.358	0.994
0.350	0.829	0.903	0.348	0.997

FIGURE 2.5-13. Transmission of Parylene Film K at 75 °C

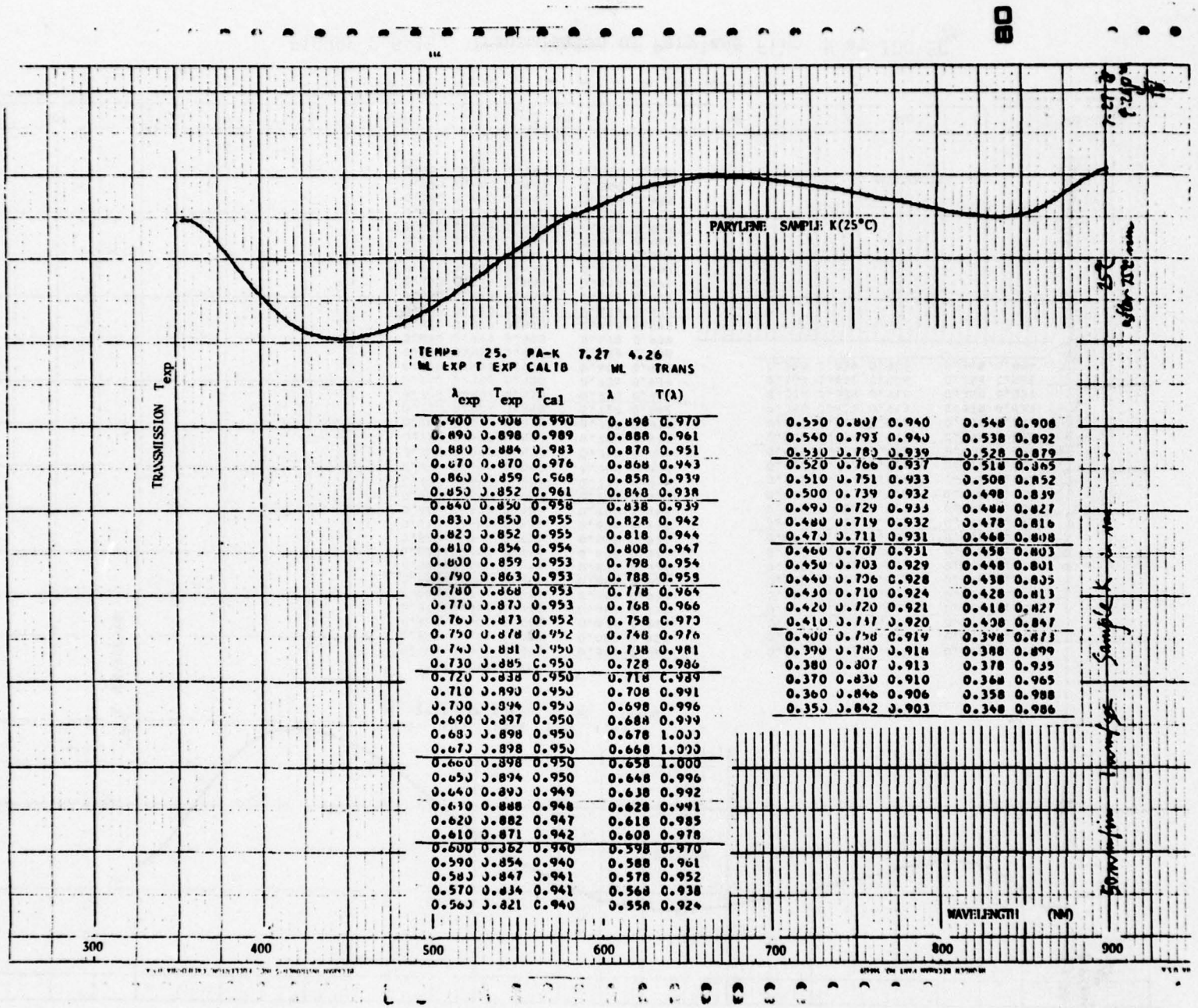

TEMP= 25. PA-K 7.27 4.26

WL EXP T EXP CALIB			WL	TRANS
λ_{exp}	T_{exp}	T_{cal}	λ	$T(\lambda)$
0.900	0.906	0.990	0.898	0.970
0.890	0.898	0.989	0.888	0.961
0.880	0.884	0.983	0.878	0.951
0.870	0.870	0.976	0.868	0.943
0.860	0.859	0.968	0.858	0.939
0.850	0.852	0.961	0.848	0.938
0.840	0.850	0.958	0.838	0.939
0.830	0.850	0.955	0.828	0.942
0.820	0.852	0.955	0.818	0.944
0.810	0.854	0.954	0.808	0.947
0.800	0.859	0.953	0.798	0.954
0.790	0.863	0.953	0.788	0.959
0.780	0.868	0.953	0.778	0.964
0.770	0.870	0.953	0.768	0.966
0.760	0.873	0.952	0.758	0.970
0.750	0.878	0.952	0.748	0.976
0.740	0.881	0.950	0.738	0.981
0.730	0.885	0.950	0.728	0.986
0.720	0.888	0.950	0.718	0.989
0.710	0.890	0.950	0.708	0.991
0.700	0.894	0.950	0.698	0.996
0.690	0.897	0.950	0.688	0.999
0.680	0.898	0.950	0.678	1.000
0.670	0.898	0.950	0.668	1.000
0.660	0.898	0.950	0.658	1.000
0.650	0.894	0.950	0.648	0.996
0.640	0.890	0.949	0.638	0.992
0.630	0.888	0.948	0.628	0.991
0.620	0.882	0.947	0.618	0.985
0.610	0.871	0.942	0.608	0.978
0.600	0.862	0.940	0.598	0.970
0.590	0.854	0.940	0.588	0.961
0.580	0.847	0.941	0.578	0.952
0.570	0.834	0.941	0.568	0.938
0.560	0.821	0.940	0.558	0.924
0.550	0.807	0.940	0.548	0.908
0.540	0.793	0.940	0.538	0.892
0.530	0.780	0.939	0.528	0.879
0.520	0.766	0.937	0.518	0.865
0.510	0.751	0.933	0.508	0.852
0.500	0.739	0.932	0.498	0.839
0.490	0.729	0.933	0.488	0.827
0.480	0.719	0.932	0.478	0.816
0.470	0.711	0.931	0.468	0.808
0.460	0.707	0.931	0.458	0.803
0.450	0.703	0.929	0.448	0.801
0.440	0.706	0.928	0.438	0.805
0.430	0.710	0.924	0.428	0.813
0.420	0.720	0.921	0.418	0.827
0.410	0.737	0.920	0.408	0.847
0.400	0.758	0.919	0.398	0.873
0.390	0.780	0.918	0.388	0.899
0.380	0.807	0.913	0.378	0.935
0.370	0.830	0.910	0.368	0.965
0.360	0.846	0.906	0.358	0.988
0.350	0.862	0.903	0.348	0.986

FIGURE 2.5-14. Transmission of Parylene Film K at 25 °C

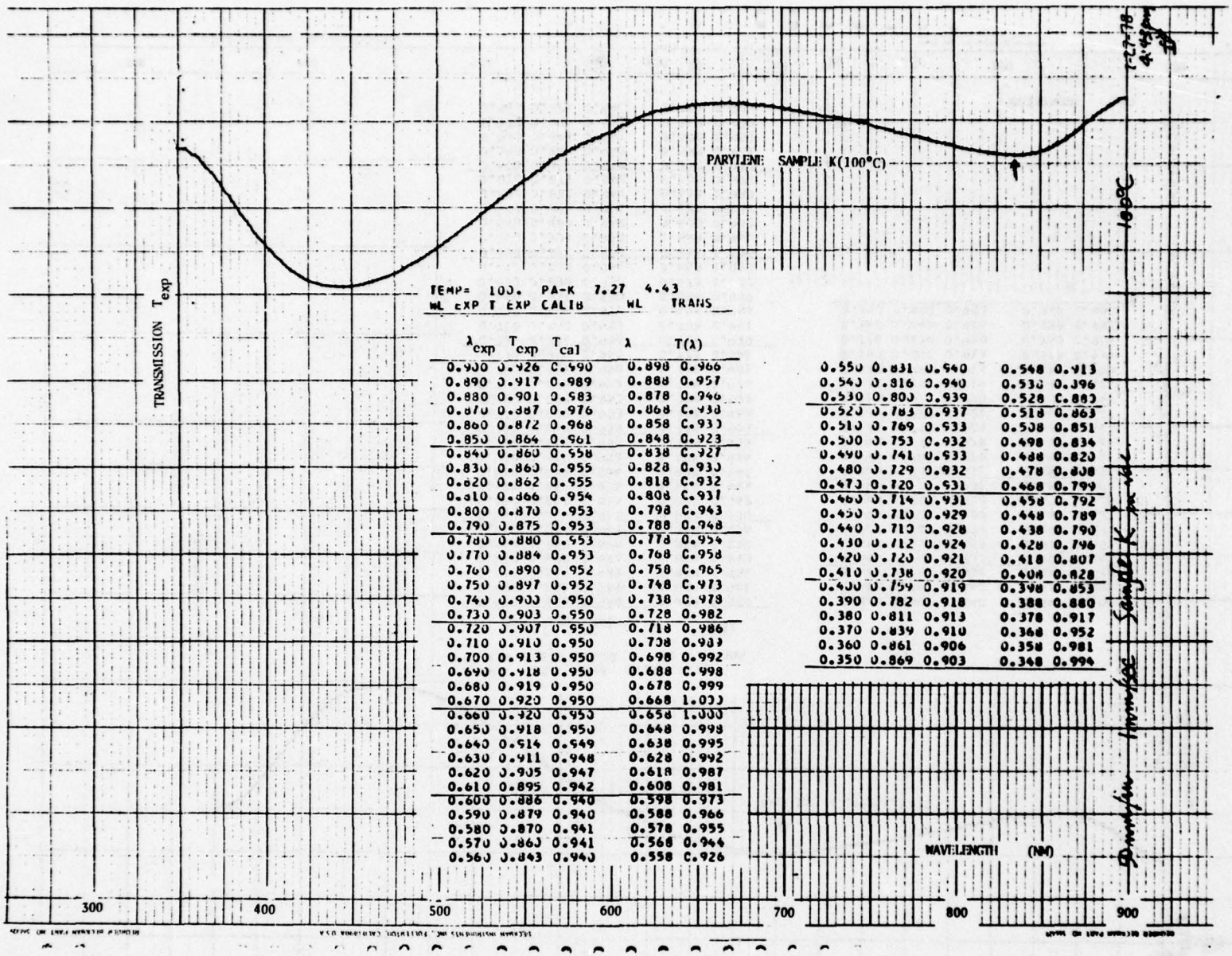

TEMP= 100. PA-K 7.27 4.43

WL EXP λ_{exp}	T EXP T_{exp}	CALIB T_{cal}	WL λ	TRANS $T(\lambda)$
0.900	0.926	0.990	0.898	0.966
0.890	0.917	0.989	0.888	0.957
0.880	0.901	0.983	0.878	0.946
0.870	0.887	0.976	0.868	0.938
0.860	0.872	0.968	0.858	0.930
0.850	0.864	0.961	0.848	0.923
0.840	0.860	0.958	0.838	0.927
0.830	0.860	0.955	0.828	0.930
0.820	0.862	0.955	0.818	0.932
0.810	0.866	0.954	0.808	0.931
0.800	0.870	0.953	0.798	0.943
0.790	0.875	0.953	0.788	0.948
0.780	0.880	0.953	0.778	0.954
0.770	0.884	0.953	0.768	0.958
0.760	0.890	0.952	0.758	0.965
0.750	0.897	0.952	0.748	0.973
0.740	0.900	0.950	0.738	0.978
0.730	0.903	0.950	0.728	0.982
0.720	0.907	0.950	0.718	0.986
0.710	0.910	0.950	0.708	0.989
0.700	0.913	0.950	0.698	0.992
0.690	0.918	0.950	0.688	0.998
0.680	0.919	0.950	0.678	0.999
0.670	0.920	0.950	0.668	1.000
0.660	0.920	0.950	0.658	1.000
0.650	0.918	0.950	0.648	0.998
0.640	0.914	0.949	0.638	0.995
0.630	0.911	0.948	0.628	0.992
0.620	0.905	0.947	0.618	0.987
0.610	0.895	0.942	0.608	0.981
0.600	0.886	0.940	0.598	0.973
0.590	0.879	0.940	0.588	0.966
0.580	0.870	0.941	0.578	0.955
0.570	0.863	0.941	0.568	0.944
0.560	0.843	0.940	0.558	0.926
0.550	0.831	0.940	0.548	0.913
0.540	0.816	0.940	0.538	0.896
0.530	0.800	0.939	0.528	0.883
0.520	0.785	0.937	0.518	0.863
0.510	0.769	0.933	0.508	0.851
0.500	0.753	0.932	0.498	0.834
0.490	0.741	0.933	0.488	0.820
0.480	0.729	0.932	0.478	0.808
0.470	0.720	0.931	0.468	0.799
0.460	0.714	0.931	0.458	0.792
0.450	0.710	0.929	0.448	0.789
0.440	0.710	0.928	0.438	0.790
0.430	0.712	0.924	0.428	0.796
0.420	0.720	0.921	0.418	0.807
0.410	0.738	0.920	0.408	0.828
0.400	0.759	0.919	0.398	0.853
0.390	0.782	0.918	0.388	0.880
0.380	0.811	0.913	0.378	0.917
0.370	0.839	0.910	0.368	0.952
0.360	0.861	0.906	0.358	0.981
0.350	0.869	0.903	0.348	0.994

FIGURE 2.5-15. Transmission of Parylene Film K at 100 °C

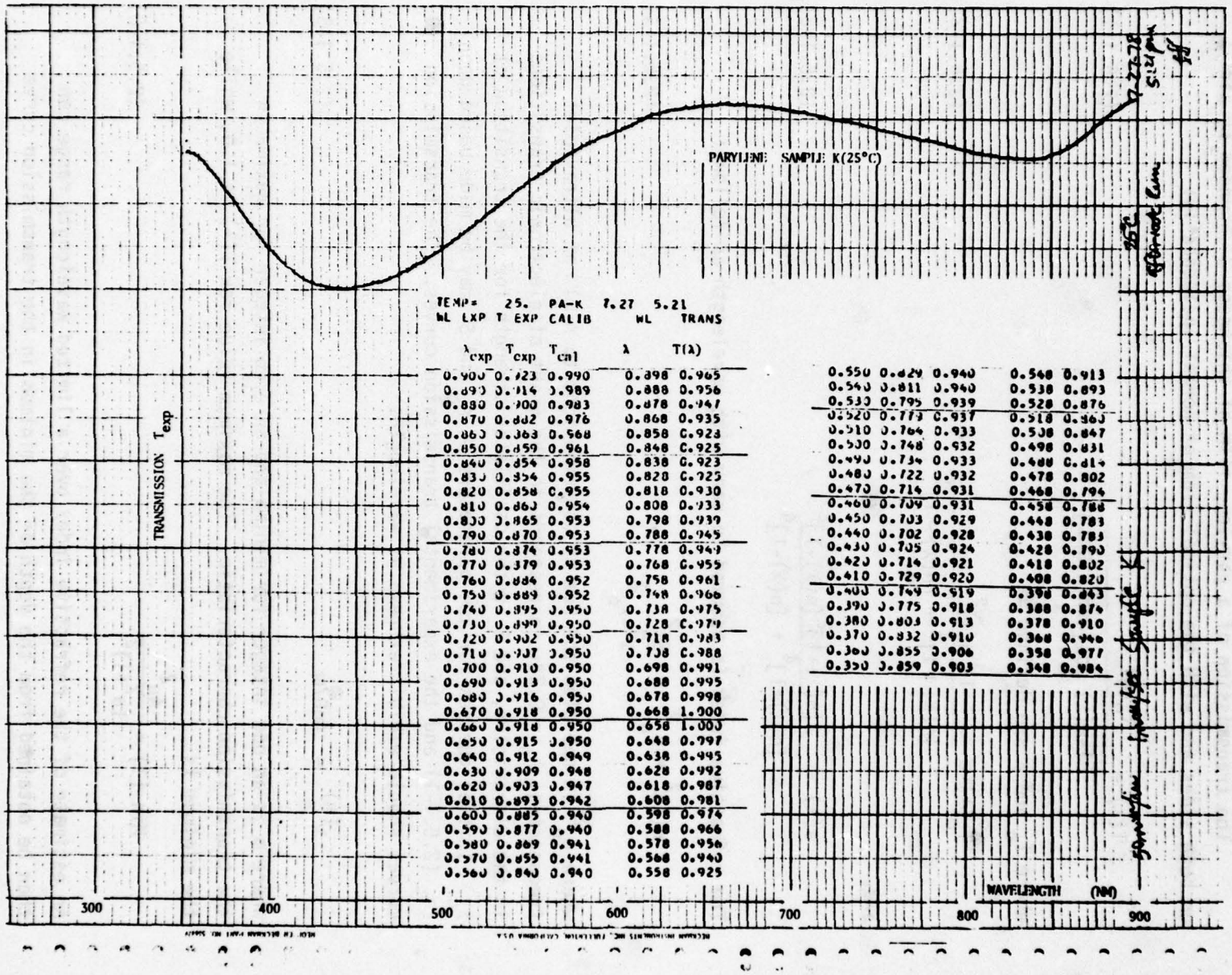

TEMP= 25. PA-K 7.27 5.21
WL EXP T EXP CALIB WL TRANS

λ_{exp}	T_{exp}	T_{cal}	λ	$T(\lambda)$
0.900	0.923	0.990	0.898	0.965
0.890	0.914	0.989	0.888	0.956
0.880	0.900	0.983	0.878	0.947
0.870	0.902	0.976	0.868	0.935
0.860	0.883	0.968	0.858	0.923
0.850	0.859	0.961	0.848	0.925
0.840	0.854	0.958	0.838	0.923
0.830	0.854	0.955	0.828	0.925
0.820	0.858	0.955	0.818	0.930
0.810	0.860	0.954	0.808	0.933
0.800	0.865	0.953	0.798	0.939
0.790	0.870	0.953	0.788	0.945
0.780	0.874	0.953	0.778	0.949
0.770	0.879	0.953	0.768	0.955
0.760	0.884	0.952	0.758	0.961
0.750	0.889	0.952	0.748	0.966
0.740	0.895	0.950	0.738	0.975
0.730	0.899	0.950	0.728	0.979
0.720	0.902	0.950	0.718	0.983
0.710	0.907	0.950	0.708	0.988
0.700	0.910	0.950	0.698	0.991
0.690	0.913	0.950	0.688	0.995
0.680	0.916	0.950	0.678	0.998
0.670	0.918	0.950	0.668	1.000
0.660	0.918	0.950	0.658	1.000
0.650	0.915	0.950	0.648	0.997
0.640	0.912	0.949	0.638	0.995
0.630	0.909	0.948	0.628	0.992
0.620	0.903	0.947	0.618	0.987
0.610	0.893	0.942	0.608	0.981
0.600	0.885	0.940	0.598	0.974
0.590	0.877	0.940	0.588	0.966
0.580	0.869	0.941	0.578	0.956
0.570	0.855	0.941	0.568	0.940
0.560	0.840	0.940	0.558	0.925
0.550	0.829	0.940	0.548	0.913
0.540	0.811	0.940	0.538	0.893
0.530	0.795	0.939	0.528	0.876
0.520	0.773	0.937	0.518	0.853
0.510	0.764	0.933	0.508	0.847
0.500	0.748	0.932	0.498	0.831
0.490	0.734	0.933	0.488	0.814
0.480	0.722	0.932	0.478	0.802
0.470	0.714	0.931	0.468	0.794
0.460	0.709	0.931	0.458	0.786
0.450	0.703	0.929	0.448	0.783
0.440	0.702	0.928	0.438	0.783
0.430	0.705	0.924	0.428	0.790
0.420	0.714	0.921	0.418	0.802
0.410	0.729	0.920	0.408	0.820
0.400	0.749	0.919	0.398	0.843
0.390	0.775	0.918	0.388	0.874
0.380	0.803	0.913	0.378	0.910
0.370	0.832	0.910	0.368	0.946
0.360	0.855	0.906	0.358	0.977
0.350	0.859	0.903	0.348	0.984

FIGURE 2.5-16. Transmission of Parylene Film K at 25 °C

The transmission of a parylene film of thickness D bounded by air on both sides and with the optical beam at normal incidence is:

$$T(\lambda) = \frac{T_o(\lambda)}{1-a(\lambda)\cos[4\pi n(\lambda)D/\lambda]} \qquad (2.5.1\text{-}1)$$

where T_o and a are defined as

$$T_o(\lambda) \equiv \frac{16\, n(\lambda)^2}{[n(\lambda)+1]^4 + [n(\lambda)-1]^4} \quad , \qquad (2.5.1\text{-}2)$$

and

$$a(\lambda) \equiv \frac{2[n(\lambda)+1]^2[n(\lambda)-1]^2}{[n(\lambda)+1]^4 + [n(\lambda)-1]^4} \quad . \qquad (2.5.1\text{-}3)$$

The refractive index is assumed to vary with wavelength as follows:

$$n(\lambda)^2 = n_o^2 + \frac{S\lambda^2}{\lambda^2-\lambda_o^2} \quad , \qquad (2.5.1\text{-}4)$$

where n_o^2 is one plus the sum of contributions to $n(\omega)^2$ at ultraviolet frequencies, $\lambda_o = 0.28\mu$ corresponds to the onset of electronic transitions in the ultraviolet, and S is the oscillator strength for the transition at λ_o. Initial guesses for the parameters D, n_o and S may be made based upon Eq. (2.5.1-1) and the experimental transmission curves. The transmission curves should exhibit extrema at wavelengths

$$\lambda^{(m)} = 4nD/m \qquad (2.5.1\text{-}5)$$

where m is an odd integer for minima and an even integer for maxima in the transmission characteristic. The maximum value for $T(\lambda)$ is 1.0, while the minimum is

$$\text{Min } (T) = \frac{4n^2}{(n^2+1)^2} \quad . \qquad (2.5.1\text{-}6)$$

An estimate of the refractive index over a limited wavelength range can then be obtained from the depth of the minimum in the transmission curve as follows:

$$n \simeq \left\{ \frac{2}{\mathrm{Min}(T)} - 1 + \left[\left(\frac{2}{\mathrm{Min}(T)} - 1 \right)^2 - 1 \right]^{1/2} \right\}^{1/2} . \qquad (2.5.1\text{-}7)$$

With the refractive index calculated from the minimum transmission value, the thickness D can then be calculated using the wavelength $\lambda^{(m)}$ at which the minimum occurs, provided the order m can be accurately specified. The values of $n(\lambda)$ at the wavelengths of the other transmission extrema are calculated using this value of D. The results of these approximations are listed for the parylene samples in Table 2.5-3.

Table 2.5-4 lists the values of D, n_o and S which give the best fit of Eq. 2.5.1-1 to the experimental transmission curves. The transmission data was digitized and analyzed by computer at wavelengths between 800 nm and 350 nm. The three parameters D, n_o and S were varied systematically until a least-squared-deviation analysis indicated "best-fit values." The normalization $T(\lambda_{max}) = 1.0$ was used for $\lambda_{max} \simeq 650$ nm in each transmission curve.

The uncertainties in Table 2.5-4 represent one-half the smallest increment used in varying the associated parameter in order to fit the data to theory. The magnitude of the sum of squared deviations is also listed and may be loosely interpreted as a measure of the quality of the curve fitting. The thicknesses of the parylene samples averaged 2054 Å, with the thinnest sample at 2020 Å, and the thickest 2115 Å. This range of thicknesses is not surprising in view of the varying degrees of tautness and "wrinkling" among different samples.

As a final check on the accuracy of our values of n_o and S, transmission curves for 0.51 μ thick parylene-N films published in the supplier's literature were analyzed. The more detailed transmission fringes of this thicker sample should provide more precise refractive index values than for our 0.2 μ thick samples, for which only three extrema are observable at visible wavelengths. The extrema and corresponding values of $n(\lambda)$ calculated from Eq. (2.5.1-5) are listed in Table 2.5-5.

It is noted that the refractive indices of Table 2.5-5 calculated from transmission extrema are consistently higher than the value $n(.5893\ \mu) = 1.661$ reported in the supplier's literature. However, this may be due to the uncertainty of one percent in the 0.51 μ thickness specified for the sample.

Parylene Samples	Extrema m	$\lambda^{(m)}$ (nm)	Corrected $T(\lambda^{(m)})$	$n(\lambda^{(m)})$ from Min(T)	D(μ)
A (25°C)	2	662	1.000	1.638	
	3	442	0.790	1.641	0.2021
	4	348	0.989	1.722	
B (25°C)	2	665	1.0	1.657	
	3	442	0.785	1.652	0.2007
	4	347	0.993	1.231	
C (25°C)	2	668	1.000	1.641	
	3	447	0.787	1.648	0.2035
	4	354	0.988	1.740	
D (25°C)	2	670	1.000	1.646	
	3	447	0.787	1.648	0.2035
	4	354	0.991	1.740	
H (25°C)	2	686	0.999	1.634	
	3	456	0.795	1.629	0.2099
	4	360	1.000	1.715	
I (25°C)	2	668	0.998	1.675	
	3	435	0.792	1.636	0.1994
	4	348	0.996	1.745	
J (25°C)	2	673	1.000	1.639	
	3	448	0.792	1.636	0.2054
	4	356	0.995	1.734	
K (25°C)	2	663	1.000	1.647	
	3	444	0.784	1.654	0.2013
	4	352	0.992	1.749	
K (0°C)	2	668	1.000	1.647	
	3	443	0.784	1.638	0.2028
	4	351	0.995	1.731	± 0.0052
K (50°C)	2	688	0.999	1.696	
	3	443	0.833	1.638	0.2028
	4	355	0.987	1.750	± 0.0052
K (75°C)	2	693	0.999	(1.709?)	
	3	443	0.864	1.638	0.2028
	4	353	1.000	1.741	± 0.0052
K (25°C)	2	672	1.000	1.623	
	3	446	0.801	1.616	0.2070
	4	355	0.988	1.715	
K (100°C)	2	666	1.000	1.642	
	3	443	0.789	1.638	.2028
	4	352	0.994	1.736	± 0.0052
K (25°C)	2	664	1.000	1.659	
	3	442	0.783	1.657	0.2001
	4	353	0.984	1.764	

TABLE 2.5-3 Refractive Indices and Thicknesses of Parylene Films Calculated From Transmission Extrema.

PARYLENE SAMPLE	THICKNESS D (μ)	DISPERSION PARAMETERS n_o	DISPERSION PARAMETERS S	SUM OF SQUARED DEVIATIONS	n(λ) at Extrema λ's
A	0.2040 ± 0.0003	1.547 ± 0.0005	0.176 ± 0.001	0.1532×10^{-3}	Sample A:
B	0.2020 0.0003	1.543 0.0005	0.210 ± 0.001	0.3697×10^{-3}	n(.662μ) = 1.615 (1.4%)
C	0.2060 0.0003	1.544 0.0005	0.202 ± 0.001	0.2244×10^{-3}	n(.442μ) = 1.639 (.12%)
D	0.2060 0.0003	1.545 0.0005	0.202 ± 0.001	0.1994×10^{-3}	n(.348μ) = 1.701 (2.1%)
H	0.2115 0.0005	1.523 0.0005	0.2190± 0.0005	0.2386×10^{-3}	Sample J:
I	0.2025 0.0005	1.519 0.0005	0.2240± 0.0005	0.2810×10^{-3}	n(.673μ) = 1.609 (1.8%)
J	0.2080 0.0003	1.529 0.0005	0.208 ± 0.001	0.2320×10^{-3}	n(.448μ) = 1.637 (.06%)
K (25°C)	0.2035 0.0003	1.5492 0.00025	0.1995± 0.0005	0.2485×10^{-3}	n(.356μ) = 1.698 (2.1%)
K (0°C)	0.2040 0.0003	1.546 0.0005	0.2030± 0.0005	0.2237×10^{-3}	Sample K at 25°C:
K (50°C)	no reasonable fit of data to theory				n(.663μ) = 1.626 (1.3%)
K (75°C)	no reasonable fit of data to theory				n(.444μ) = 1.653 (.06%)
K (25°C)	0.2100 0.0005	1.518 0.001	0.184 ± 0.001	0.1560×10^{-3}	n(.352μ) = 1.715 (1.9%)
K (100°C)	0.2045 0.0003	1.5500 0.0005	0.176 ± 0.001	0.1669×10^{-3}	
K (25°C)	0.2025 0.0003	1.5685 0.0005	0.165 ± 0.001	0.1637×10^{-3}	

TABLE 2.5-4 Thickness and Refractive Index Dispersion of Parylene Films Determined by Computer Analysis of Optical Transmission Curves.

TABLE 2.5-5

Transmission extrema for 0.51 μ thick parylene film, taken from Figure 5 of reference 42. Refractive index is calculated for each extremum wavelength.

$\lambda^{(m)}_{(\mu)}$	m	$n(\lambda^{(m)})$	
.8706	4	1.684	
.5701	6	1.677	
.4881	7	1.675	
.4297	8	1.685	
.3853	9	1.700	
.3531	10	1.731	

The parylene films were to be heated to temperatures as high as 150°C during PbI_2 depositions and 50°C during characterization of PbI_2 overlayers. Therefore, it was of interest to determine beforehand the influence of temperature cycling upon the optical properties of parylene. Sample K was cycled through temperatures between 0°C and 100°C, and the transmission measured at temperatures shown in Figures 2.5-10 through 2.5-16 and listed in Table 2.5-4. Both the figures and the data in the Table follow the chronological order of the temperature cycling. Note that the transmission peak at 663 nm disappeared at 75°C, then re-appeared subsequently at temperatures of 25°C and 100°C. This behavior may be related to the glass transition temperature for the onset of creep, which is between 67°C and 77°C for N-parylene. Although the sample could not be directly observed during the transmission scan at 75°C, it is presumed that the film either sagged or became wrinkled, therefore producing the "peculiar" transmission curve of Figure 2.5-13.

In order to make a direct comparison between refractive indices obtained from transmission extrema and those calculated from the dispersion analysis, the data in Table 2.5-4 were used to calculate $n(\lambda)$ from Eq. 2.5.1-4 at the extrema wavelengths $\lambda^{(m)}$ (m = 2,3 and 4) given in Table 2.5-3 for Samples A, J and K. These calculated refractive indices are listed in the

right-most column of Table 2.5-4. After each calculated refractive index is listed the percentage difference with the value obtained from the depth of the transmission fringe listed in Table 2.5-3 for the same wavelength.

The refractive indices obtained by the two methods, transmission fringe analysis and computerized curve fitting, agree within 0.06 percent to 2 percent. This agreement is unexpectedly close, considering that the transmission fringe analysis actually gives an average refractive index over a range of wavelengths between successive maxima and minima. For the sake of further comparison, Figure 2.5-17 shows the theoretical transmission curve for parylene Sample A, using the dispersion parameters and thickness given in Table 2.5-4. Direct comparison with Figure 2.5-3 shows the two curves are essentially identical.

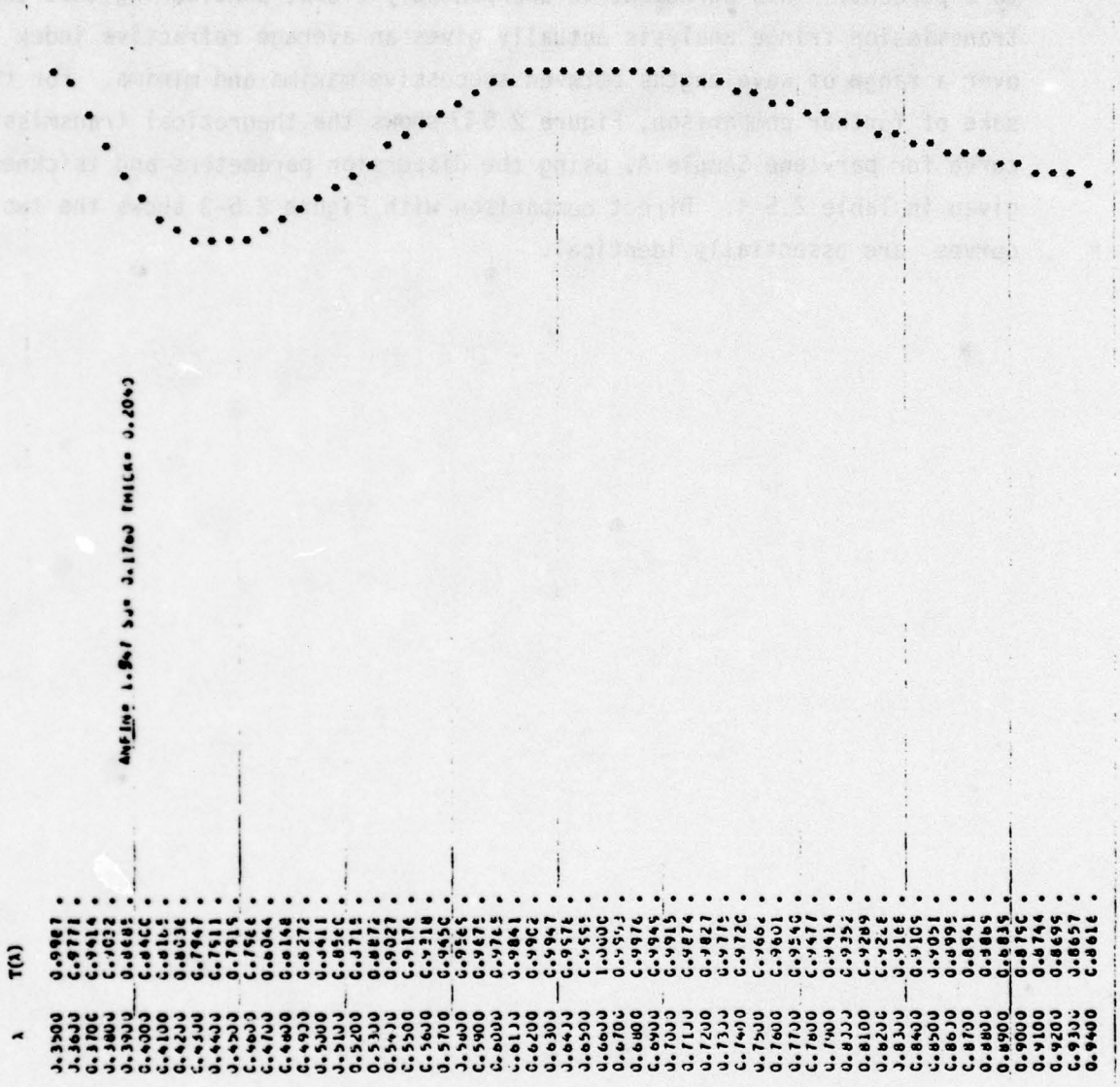

Figure 2.5-17. Theoretical Transmission Curve for Parylene Sample A With Best-Fit Values of D, n_o and S from Table 2.5-4.

2.5.2 Optical Properties of Glass Substrates

The substrates used for HgI_2 films and for trial depositions of PbI_2 films are borosilicate microscope cover glass, No. 12-546-2, purchased from Fisher Scientific. The thicknesses of the glass samples are 200 ± 6 microns, as determined by microcaliper measurements of twenty selected at random. Thirteen of these slides were lapped and polished chemo-abrasively to a thickness of 18 ± 1 microns to be used as HgI_2 substrates.

The refractive index and its dispersion were determined by analyzing the transmission curve of Figure 2.5-18. The average transmission for a thick sample is

$$T = \frac{16\, n^2}{(n+1)^2} \quad . \qquad (2.5.2\text{-}1)$$

It is assumed that the sample is sufficiently thick that interference effects are not observable, and only reflection at the two surfaces accounts for the transmission loss through the sample.

Refractive index values calculated from the corrected transmission values T_{corr} and Eq. (2.5.2-1), are plotted as dotted data in Figure 2.5-19. These experimentally determined values of n are analyzed using the dispersion equation 2.5.1-4 and the method of least squared deviations to obtain the dispersion parameters n_o and S. The wavelength for the high-frequency resonance for glass was taken to be 0.168μ, consistent with the ultraviolet absorption edge of borosilicate glass. The refractive index of the glass substrate is then given by the positive square

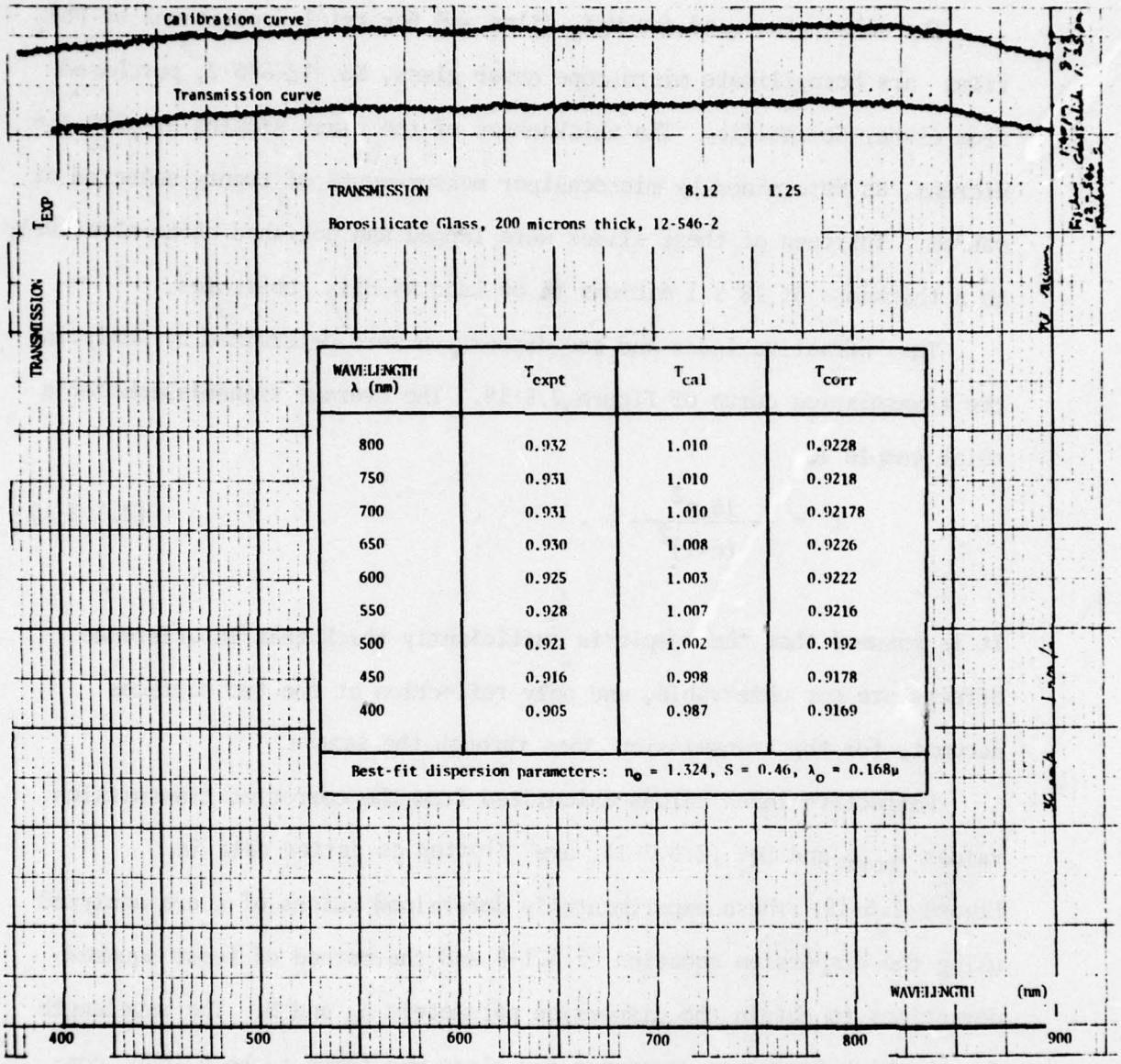

WAVELENGTH λ (nm)	T_{expt}	T_{cal}	T_{corr}
800	0.932	1.010	0.9228
750	0.931	1.010	0.9218
700	0.931	1.010	0.92178
650	0.930	1.008	0.9226
600	0.925	1.003	0.9222
550	0.928	1.007	0.9216
500	0.921	1.002	0.9192
450	0.916	0.998	0.9178
400	0.905	0.987	0.9169

Best-fit dispersion parameters: $n_o = 1.324$, $S = 0.46$, $\lambda_o = 0.168\mu$

Figure 2.5-18. Transmission of 200μ thick borosilicate glass sample

root of

$$n(\lambda)^2 = 1.324^2 + \frac{0.46\ \lambda^2}{\lambda^2 - (0.168\mu)^2} , \qquad (2.5.2\text{-}2)$$

which is plotted as the solid curve in Figure 2.5-19. This expression is used to characterize the glass substrate when analyzing optical properties of metal halide films on glass substrates in the following sections.

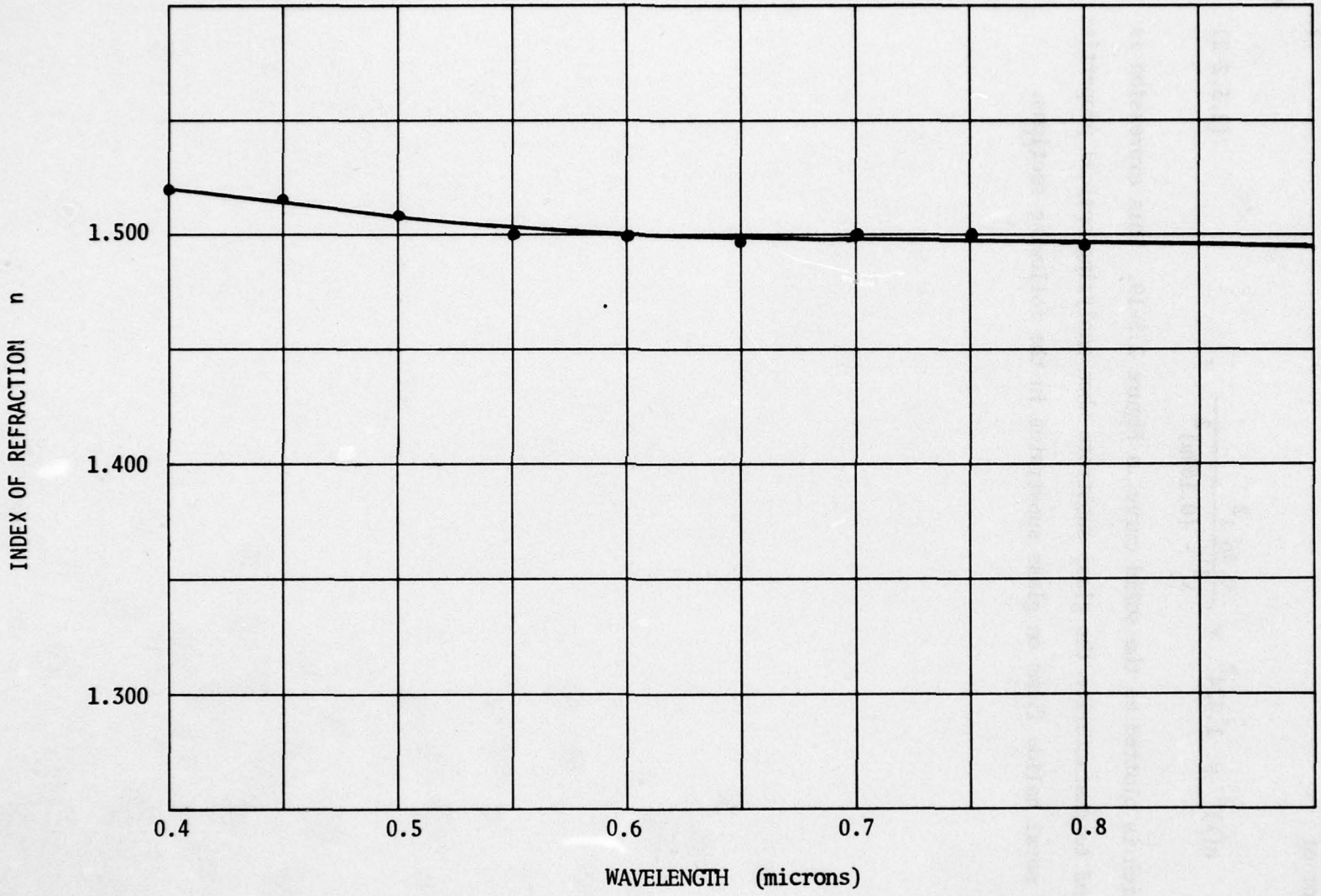

Figure 2.5-19. Refractive Index of Borosilicate Glass Substrate as a Function of Wavelength.

2.5.3 Optical Properties of PbI_2 Films on Glass

Although parylene-N was intended as the thin substrate for PbI_2 films, a number of PbI_2 depositions were made on glass substrates in order to optimize deposition parameters such as rate of growth, substrate temperature, and the amount of source material required to produce a given film thickness. These optimization experiments were more conveniently performed on glass substrates because of the fragility and higher cost of parylene membranes. Initially, optical characterization was performed on these PbI_2 on glass samples, including measurement of the temperature dependence of the absorption edge. The most significant differences anticipated between these samples and the PbI_2 films on parylene would be caused by stresses arising from the different coefficients of linear thermal expansion of PbI_2 and glass. The influence of stress is an important consideration in selection of substrate materials, and complete characterization of PbI_2 on glass samples should provide useful information about the consequences of using other thin polymer substrates such as nitrocellulose which are also not well matched in thermal expansion to the PbI_2 film.

The transmission spectrum of PbI_2 on glass samples was measured at temperatures between -196°C and 50°C. The PbI_2 film thicknesses were approximately 0.2μ, as verified by profilometer measurements. The substrates were 200μ thick borosilicate glass microsheets, circular in cross section, with a one inch diameter. The optical properties of the glass at 25°C are reported in the previous section.

The configuration under consideration is illustrated in Figure 2.5-20. The transmission of a thin film on a thick substrate is given by

$$T = \frac{T_{123}}{[1 - a_{13} \cos (4\pi n_2 D/\lambda)]} \quad T_{31}, \qquad (2.5.3\text{-}1)$$

where

$$T_{123} \equiv \frac{16\, n_2^2}{[\,(n_2 + 1)^2(n_2 + n_3)^2 + (n_2 - 1)^2(n_2 - n_3)^2\,]}, \qquad (2.5.3\text{-}2)$$

$$a_{13} \equiv \frac{2(n_2+1)(n_2-1)(n_2+n_3)(n_2-n_3)}{[\,(n_2 + 1)^2(n_2 + n_3)^2 + (n_2 - 1)^2(n_2 - n_3)^2\,]}, \qquad (2.5.3\text{-}3)$$

and

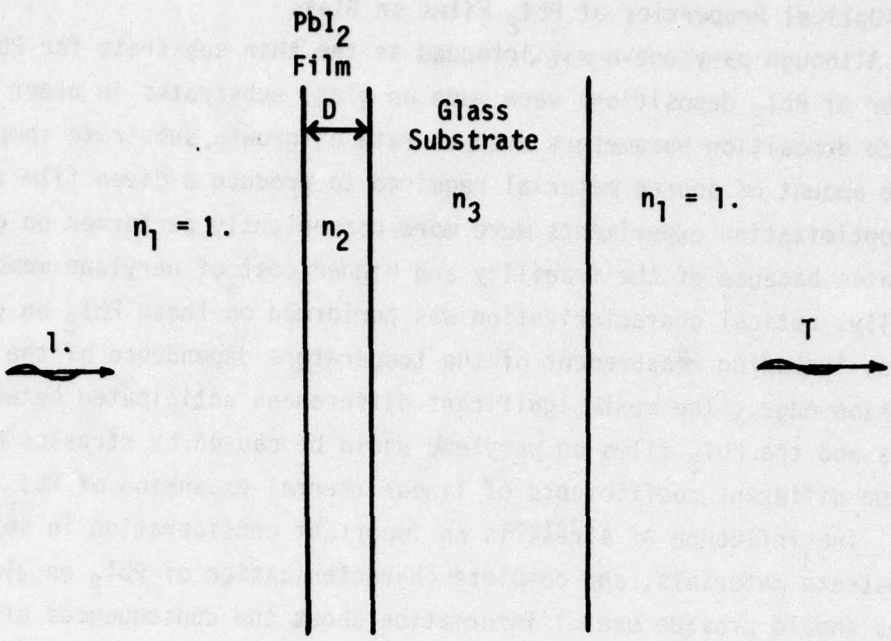

Figure 2.5-20. Configuration for optical transmission of a thin (D = 0.2μ) metal halide film on a thick (200μ) glass substrate.

$$T_{31} = \frac{4\, n_3^2}{(1 + n_3)^2} \qquad (2.5.3\text{-}4)$$

The refractive indices are n_2 for the PbI_2 film of thickness D and n_3 for the glass substrate. T_{31} is the transmission factor for the glass to air surface. Interference effects from multiple reflections are considered only in the thin PbI_2 film. Nonuniformities in thickness and a minute amount of curvature in the sample diminish the amplitude of any interference structure due to multiple reflections within the thick glass substrates. Interference structure from the substrate actually is observed in high-resolution scans, with peaks separated by $\Delta\lambda \simeq 7$Å corresponding to $n_2 D \simeq 300\mu$, but the peak-to-peak amplitude of this transmission structure

is smaller than one percent. Therefore, for faster scans with lower resolution, interference structure arising from the thick substrate is missing altogether, and the transmission formula is corrected only for the reflection loss at the glass to air surface.

For wavelengths at which absorption is negligible and n_2 is pure real, extrema in the transmission spectrum occur at wavelengths given by

$$\lambda^{(m)} = 4n_2 D/m \ , \qquad (2.5.3\text{-}5)$$

where m = 0, 2, 4, 6, ... for maxima and m = 1, 3, 5, 7 ..... for minima. The maximum possible transmission is given by

$$\text{Max } (T) = \frac{16\ n_3^{\,2}}{(n_3 + 1)^4} \ , \qquad (2.5.3\text{-}6)$$

independent of the value of n_2. The minimum transmission values are given by

$$\text{Min } (T) = \frac{16\ n_2^{\,2}\ n_3^{\,2}}{(n_2^{\,2} + n_3)^2\ (n_3 + 1)^2} \ . \qquad (2.5.3\text{-}7)$$

Just as for the case of the single slab, the difference between maximum and minimum values of T depends upon n_2, independent of D, as given by the following equation

$$n_2 = \frac{2\ n_3(n_3 + 1) + \left\{4\ n_3^{\,2}(n_3 - 1)^2 + n_3(n_3 + 1)^4\ \Delta T\right\}^{1/2}}{\left\{16\ n_3^{\,2} - (n_3 + 1)^4\ \Delta T\right\}^{1/2}} \ , \qquad (2.5.3\text{-}8)$$

where ΔT is defined as Max(T) - Min(T). Therefore, n_2 is calculated from Max(T) - Min(T), and D then can be found from the transmission extrema and Eq. 2.5.3-5.

Consider the transmission curve for PbI_2 on glass sample No. 210A9 in Figure 2.5-21. The peak transmission at 632 nm wavelength is theoretically 92.18 percent, calculated from Eq. 2.5.3-6, using n_3 = 1.499 calculated from Eq. 2.5.2-2 of the previous section. This value is $T_{theory}\ (\lambda_{max})$ for this particular transmission curve. This compares to an experimental peak at that wavelength of $T_{exp}(\lambda_{max})$=0.919. In order to correct for systematic errors in the absolute transmission values, the experimental transmission value is renormalized by the ratios of theoretical to experimental transmittivities at λ_{max} and the change in spectral sensitivity indicated by the 100 percent transmission calibration curve.

$$T(\lambda) = T_{exp}(\lambda) \cdot \frac{T_{theory}(\lambda_{max})}{T_{exp}(\lambda_{max})} \cdot \frac{T_{cal}(\lambda_{max})}{T_{cal}(\lambda)} \qquad (2.5.3\text{-}9)$$

The corrected wavelengths and transmission values are listed on each transmission spectrum, just as previously in Section 2.5.1 for parylene membranes.

The refractive index n_2 of PbI_2 is calculated from corrected values of transmission $T(\lambda)$ at the wavelengths for maxima and minima indicated in Table 2.5-6. The order's m are determined from the frequency intervals

Extrema		Corrected	$n(\lambda^{(m)})$ from	Thickness D(μ)
m	$\lambda^{(m)}$(nm)	$T(\lambda^{(m)})$	Eq. (2.5.3-8)	from Eq. (2.5.3-5)
3	783.	0.5693	2.604	0.22
4	630.	0.9218		
5	542.	0.4757	2.975	0.23

Computer	D =	0.2220	+ 0.0010 μ
Best-Fit	n_o =	2.698	± 0.001
Parameters	S =	0.265	± 0.002
for PbI_2	λ_{o_2} =	0.5120 μ	

Table 2.5-6 Thickness, refractive index and its dispersion for PbI_2 on glass film No. 210A9 at 30°C, by analysis of transmission extrema and by computerized curve fitting over the wavelength range 800 nm to 540 nm.

(ratios) of adjacent extrema. Refractive indices calculated from Eq. 2.5.3-8 are average values for each of the two wavelength ranges indicated. The PbI_2 film thickness is calculated from Eq. 2.5.3-5 using the two longer-wavelength extrema for which absorption should be negligible. Independent thickness measurements using a profilometer indicate a thickness of the order of 0.2μ, in rough agreement with these optical measurements. The refractive indices in Table 2.5-6 are somewhat lower than the values 3.6 to 6.7 reported by Tubbs, or 2.8 to 3.7 reported by Imai, or 3.1 to 3.6 reported by Buckman and Hong for the same range of wavelengths.[10,13,20]

The complex refractive index $n + i\kappa$ of PbI_2 is given by the square root of the complex dielectric constant $\varepsilon_r + i\varepsilon_i$ which satisfies

$$\varepsilon_r = n_o^2 + \sum_{m=1}^{N} \frac{S_m \lambda^2 (\lambda^2 - \lambda_{om}^2)}{(\lambda^2 - \lambda_{om}^2)^2 + (\lambda_{om}^2 \lambda/\lambda_{Gm})^2} \qquad (2.5.3\text{-}10)$$

and

$$\varepsilon_i = \sum_{m=1}^{N} \frac{S_m \lambda^2 \lambda_{om}^2 \lambda/\lambda_{Gm}}{(\lambda^2 - \lambda_{om}^2)^2 + (\lambda_{om}^2 \lambda/\lambda_{Gm})^2} , \qquad (2.5.3\text{-}11)$$

where n_o was previously defined, S_m is the oscillator strength for the m'th electric dipole resonance at free-space wavelength λ_{om}, and λ_{Gm} is a damping parameter defined such that $2\pi c/\lambda_{Gm}$ is the damping rate for the m'th resonance. At wavelengths much larger than fundamental absorption edge values, damping is assumed to be very small and $\varepsilon_i \simeq 0$. Therefore, at wavelengths between 0.8μ and 0.54μ, well beyond the fundamental absorption edge just below 0.52μ, experimental transmission curves of PbI_2 are analyzed using Eqs. 2.5.3-1, -10, and -11 with the PbI_2 film thickness D and the parameters n_o and S varied to give best agreement between theory and experiment. λ_G is set equal to infinity and λ_o = 0.5120μ for this long-wavelength analysis, and pure real values are obtained for the refractive index and its dispersion. The value of λ_o cannot be identified precisely by inspection of the transmission curves. However, a small error in assignment of λ_o does not introduce significant error in analysis of long-wavelength data to obtain D, n_o and S. For the purpose of comparison, the fundamental absorption edge of PbI_2 at 25°C has been previously reported to be 0.4919μ by Imai, 0.5120μ for the ordinary ray and 0.4920μ for the extraordinary ray by Tubbs, and 0.510μ for oriented polycrystalline films by Tubbs.[13,10,9] Best-fit values are calculated for D, n_o and S by performing a least-squared-deviation analysis of the long-wavelength transmission data by computer. For example, for the curve at 30°C in Figure 2.5.3-29 the best-fit values are D = 0.2220μ, n_o = 2.698. and S = 0.265, calculated by analyzing the transmission data between 0.540μ and 0.800μ with λ_o = 0.5120μ. A theoretical transmission curve based upon these values is shown in Figure 2.5.3-30 to illustrate the agreement between experiment and theory at long wavelengths. The dispersion formula Eq. 2.5.2-2 is used for the refractive index of the glass substrate.

For wavelengths covering the absorption edge, two terms (N=2) must be included in Eqs. 2.5.3-10 and -11 to describe the observed transmission characteristics. There is a transmission minimum at about 0.498μ wavelength, in addition to the short-wavelength cut-off of the absorption edge where the transmission becomes zero at 0.435μ for 30°C temperature. The minimum at 0.498μ has been previously identified as an exciton transition.[9-19] This exciton is neither tightly nor loosely bound, but is of an intermediate type, and is believed to be associated with defect structures in PbI_2. The strength of this absorption feature increases very sharply as the temperature decreases from 0°C to -175°C, and the wavelength at which the minimum occurs appears to shift to smaller values at the lower temperatures. These results are in agreement with the transmission data reported by Imai for temperatures over the the same range.[13] Again, for the sake of comparison between experiment and theory, Figure 2.5-30 shows the theoretical transmission calculated for absorption edge wavelengths between .5500μ and 0.4000μ using the best-fit parameters D = 0.2220μ, n_o = 2.698, S_1 = 0.04, λ_{G1} = 35. μ, S_2 = 1.2, and λ_{G2} = 16. μ from Table 2.5-7, with λ_{o1} = 0.4980μ and λ_{o2} = 0.4430μ as taken from the experimental transmission curve.

The procedure for analyzing the absorption edge is to first fit the transmission values to theory using only the fundamental edge parameters S_2, λ_{G2} and λ_{o2} = 0.435μ, with S_1 set equal to zero. Then S_1 and λ_{G1} are systematically varied along with S_2 and λ_{G2}, using λ_{o1} = 0.498μ, until the best fit is obtained which includes the exciton transition. It should be noted that even without the exciton feature a small peak is calculated between 0.5μ and 0.435μ because of interference effects in the film. An interference peak may occur at these wavelengths because the real part of the refractive index of PbI_2 varies rapidly with wavelength. This interference peak complicates the data analysis somewhat, and makes necessary the low-temperature transmission data. At low temperatures, the smaller damping rate for the exciton line causes it to clearly dominate the short-wavelength portion of the absorption edge.

Sample No. 210A9 was also characterized at other temperatures ranging from -175°C to 50°C. The data between 0°C and 50°C were taken for increments of 10°C, because this is the range of primary interest for the intended thermo-optic imaging application. These transmission curves are shown in Figures 2.5.3-21 through 2.5.3-33. The date and chronological order of each transmission curve (month . day No. XX) are included in the heading

TEMP= 0. PBI2 GLAS 1.09 NO.1

WL EXP	T EXP	CALIB	WL	TRANS
0.800	0.560	0.998	0.798	0.559
0.795	0.559	0.998	0.793	0.558
0.790	0.559	0.998	0.788	0.558
0.785	0.559	0.998	0.783	0.558
0.780	0.560	0.998	0.778	0.559
0.775	0.561	0.999	0.773	0.559
0.770	0.562	0.999	0.768	0.560
0.765	0.565	0.999	0.763	0.564
0.760	0.569	0.999	0.758	0.568
0.755	0.572	1.000	0.753	0.572
0.750	0.579	1.000	0.748	0.579
0.745	0.583	1.000	0.743	0.584
0.740	0.591	1.000	0.738	0.592
0.735	0.599	1.000	0.733	0.599
0.730	0.608	0.999	0.728	0.608
0.725	0.617	0.998	0.723	0.616
0.720	0.629	0.999	0.718	0.627
0.715	0.636	0.999	0.713	0.634
0.710	0.645	0.999	0.708	0.644
0.705	0.650	0.999	0.703	0.649
0.700	0.668	0.999	0.698	0.667
0.695	0.685	0.999	0.693	0.684
0.690	0.705	0.999	0.688	0.704
0.685	0.724	0.999	0.683	0.723
0.680	0.746	0.999	0.678	0.745
0.675	0.768	0.999	0.673	0.766
0.670	0.792	0.999	0.668	0.790
0.665	0.815	0.999	0.663	0.813
0.660	0.840	0.999	0.658	0.838
0.655	0.859	0.999	0.653	0.857
0.650	0.877	0.999	0.648	0.875
0.645	0.890	0.998	0.643	0.888
0.640	0.899	0.998	0.638	0.897
0.635	0.902	0.998	0.633	0.900
0.630	0.900	0.999	0.628	0.898
0.625	0.890	0.998	0.623	0.888
0.620	0.872	0.999	0.618	0.870
0.615	0.847	0.999	0.613	0.845
0.610	0.863	0.999	0.608	0.861
0.605	0.780	0.998	0.603	0.797
0.600	0.737	0.997	0.598	0.754
0.595	0.700	0.995	0.593	0.719
0.590	0.657	0.994	0.588	0.674
0.585	0.618	0.993	0.583	0.635
0.580	0.579	0.992	0.578	0.595
0.575	0.545	0.991	0.573	0.561
0.570	0.514	0.991	0.568	0.529
0.565	0.489	0.990	0.563	0.504
0.560	0.466	0.990	0.558	0.478
0.555	0.450	0.990	0.553	0.464
0.550	0.441	0.990	0.548	0.454
0.545	0.441	0.990	0.543	0.454
0.540	0.450	0.990	0.538	0.464
0.535	0.472	0.988	0.533	0.487
0.530	0.519	0.986	0.528	0.537
0.525	0.590	0.985	0.523	0.611
0.520	0.669	0.984	0.518	0.693
0.515	0.560	0.984	0.513	0.580
0.510	0.750	0.983	0.508	0.759
0.505	0.098	0.982	0.503	0.102
0.500	0.056	0.981	0.498	0.058
0.495	0.057	0.981	0.493	0.059
0.490	0.058	0.980	0.488	0.060
0.485	0.056	0.980	0.483	0.056
0.480	0.065	0.980	0.478	0.067
0.475	0.037	0.980	0.473	0.039
0.470	0.029	0.980	0.468	0.030
0.465	0.021	0.980	0.463	0.022
0.460	0.015	0.981	0.458	0.016
0.455	0.011	0.981	0.453	0.011
0.450	0.008	0.981	0.448	0.008
0.445	0.004	0.980	0.443	0.004
0.440	0.003	0.980	0.438	0.003
0.435	0.002	0.980	0.433	0.002
0.430	0.001	0.980	0.428	0.001
0.425	0.001	0.979	0.423	0.001
0.420	0.0	0.978	0.418	0.0
0.415	0.0	0.977	0.413	0.0
0.410	0.0	0.976	0.408	0.0
0.405	0.0	0.974	0.403	0.0

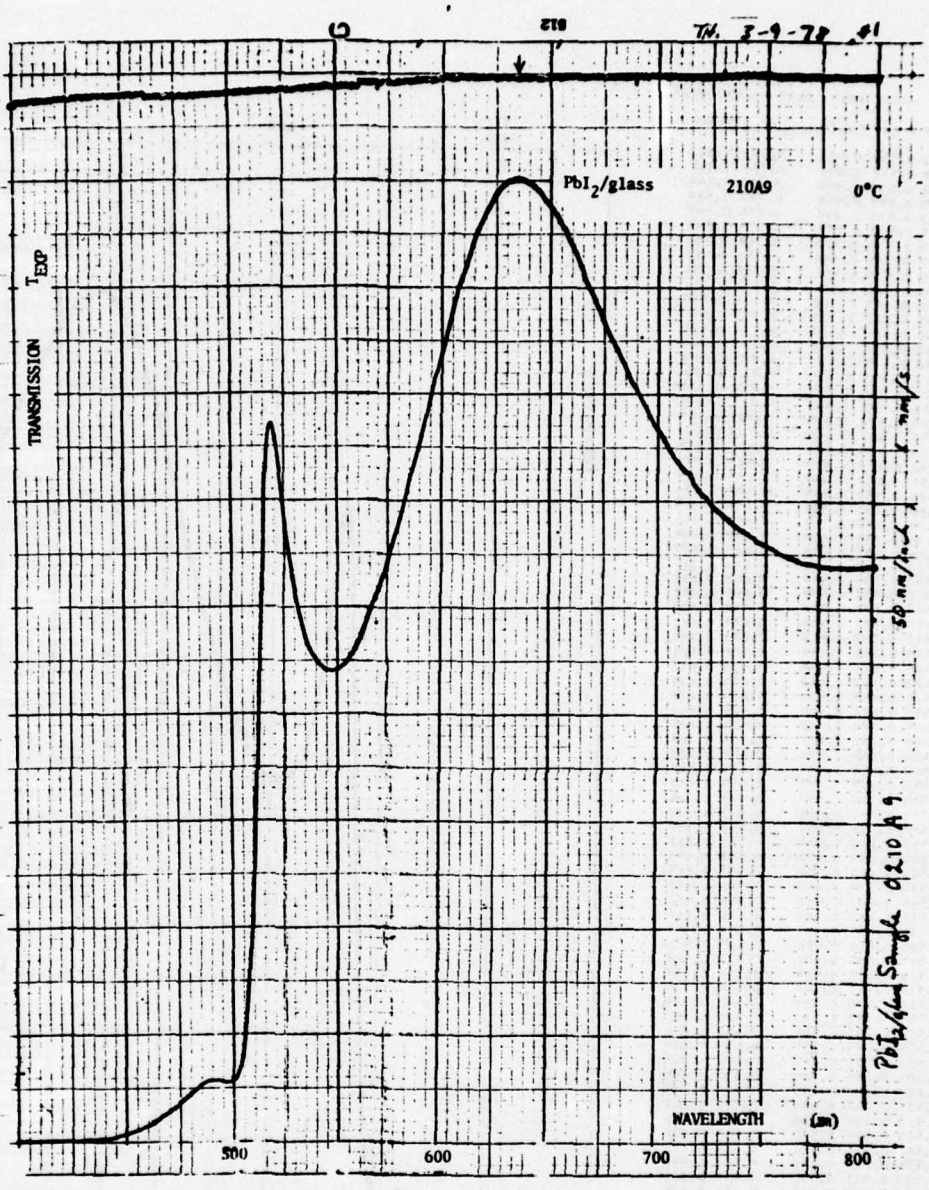

Figure 2.5-21. Transmission of PbI_2 on glass sample No. 210A9 at T = 0°C.

TEMP: -30. PBI2 GLAS 3.09 NO.2

WL	EXP T	EXP CALIB	WL	TRANS
0.800	0.533	0.998	0.798	0.552
0.795	0.531	0.998	0.793	0.550
0.790	0.530	0.998	0.788	0.549
0.785	0.530	0.998	0.783	0.549
0.780	0.530	0.999	0.778	0.549
0.775	0.531	0.999	0.773	0.549
0.770	0.533	0.999	0.768	0.551
0.765	0.535	0.999	0.763	0.554
0.760	0.539	0.999	0.758	0.558
0.755	0.541	1.000	0.753	0.559
0.750	0.549	1.000	0.748	0.567
0.745	0.552	1.000	0.743	0.571
0.740	0.560	1.000	0.738	0.579
0.735	0.568	1.000	0.733	0.587
0.730	0.575	0.999	0.728	0.595
0.725	0.583	0.998	0.723	0.604
0.720	0.598	0.999	0.718	0.619
0.715	0.608	0.999	0.713	0.629
0.710	0.621	0.999	0.708	0.643
0.705	0.635	0.999	0.703	0.657
0.700	0.655	0.999	0.698	0.678
0.695	0.669	0.999	0.693	0.692
0.690	0.690	0.999	0.688	0.714
0.685	0.708	0.999	0.683	0.733
0.680	0.730	0.999	0.678	0.755
0.675	0.750	0.999	0.673	0.776
0.670	0.772	0.999	0.668	0.799
0.665	0.797	0.999	0.663	0.825
0.660	0.819	0.999	0.658	0.847
0.655	0.838	0.999	0.653	0.867
0.650	0.857	0.999	0.648	0.887
0.645	0.870	0.998	0.643	0.901
0.640	0.881	0.998	0.638	0.912
0.635	0.889	0.998	0.633	0.921
0.630	0.890	0.999	0.628	0.921
0.625	0.881	0.998	0.623	0.912
0.620	0.867	0.999	0.618	0.897
0.615	0.845	0.999	0.613	0.874
0.610	0.814	0.999	0.608	0.842
0.605	0.779	0.998	0.603	0.807
0.600	0.739	0.997	0.598	0.766
0.595	0.700	0.995	0.593	0.727
0.590	0.658	0.994	0.588	0.686
0.585	0.620	0.993	0.583	0.645
0.580	0.580	0.992	0.578	0.606
0.575	0.547	0.991	0.573	0.571
0.570	0.515	0.991	0.568	0.537
0.565	0.490	0.990	0.563	0.512
0.560	0.463	0.990	0.558	0.483
0.555	0.440	0.990	0.553	0.459
0.550	0.439	0.990	0.548	0.458
0.545	0.437	0.990	0.543	0.456
0.540	0.443	0.990	0.538	0.463
0.535	0.460	0.988	0.533	0.481
0.530	0.500	0.986	0.528	0.524
0.525	0.560	0.985	0.523	0.588
0.520	0.655	0.984	0.518	0.688
0.515	0.677	0.984	0.513	0.706
0.510	0.370	0.983	0.508	0.389
0.505	0.125	0.982	0.503	0.132
0.500	0.051	0.981	0.498	0.054
0.495	0.040	0.981	0.493	0.041
0.490	0.036	0.980	0.488	0.037
0.485	0.046	0.980	0.483	0.047
0.480	0.050	0.980	0.478	0.051
0.475	0.041	0.980	0.473	0.041
0.470	0.032	0.980	0.468	0.033
0.465	0.026	0.980	0.463	0.027
0.460	0.020	0.981	0.458	0.021
0.455	0.015	0.981	0.453	0.016
0.450	0.011	0.981	0.448	0.012
0.445	0.009	0.980	0.443	0.009
0.440	0.005	0.980	0.438	0.005
0.435	0.003	0.980	0.433	0.003
0.430	0.002	0.980	0.428	0.002
0.425	0.001	0.979	0.423	0.001
0.420	0.0	0.978	0.418	0.0
0.415	0.0	0.977	0.413	0.0
0.410	0.0	0.976	0.408	0.0
0.405	0.0	0.974	0.403	0.0

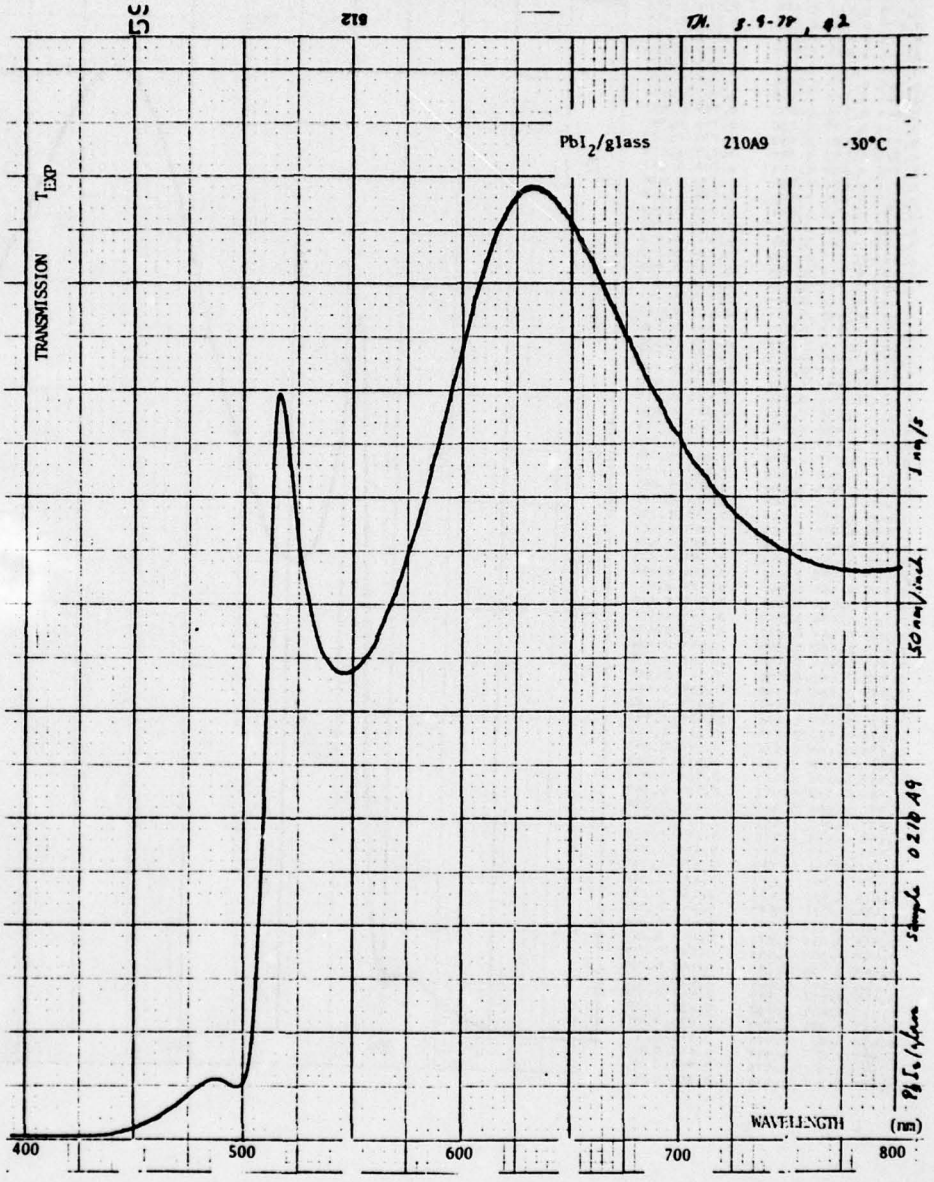

Figure 2.5-22. Transmission of PbI_2 on glass sample No. 210A9 at T = -30°C.

TEMP= -155 PBI2 GLAS 3.09 NO.1

WL	EXP T	EXP CALIB	WL	TRANS
0.800	0.531	0.991	0.798	0.563
0.795	0.530	0.993	0.793	0.562
0.790	0.529	0.998	0.788	0.560
0.785	0.529	0.998	0.783	0.560
0.780	0.528	0.998	0.778	0.559
0.775	0.530	0.999	0.773	0.561
0.770	0.530	0.999	0.768	0.561
0.765	0.535	0.999	0.763	0.566
0.760	0.539	0.999	0.758	0.571
0.755	0.543	1.000	0.753	0.574
0.750	0.548	1.000	0.748	0.579
0.745	0.554	1.000	0.743	0.586
0.740	0.560	1.000	0.738	0.592
0.735	0.567	1.000	0.733	0.600
0.730	0.577	0.999	0.728	0.611
0.725	0.586	0.998	0.723	0.621
0.720	0.596	0.999	0.718	0.631
0.715	0.608	0.999	0.713	0.644
0.710	0.622	0.999	0.708	0.658
0.705	0.637	0.999	0.703	0.674
0.700	0.656	0.999	0.698	0.696
0.695	0.668	0.999	0.693	0.707
0.690	0.687	0.999	0.688	0.727
0.685	0.703	0.999	0.683	0.744
0.680	0.725	0.999	0.678	0.767
0.675	0.745	0.999	0.673	0.789
0.670	0.767	0.999	0.668	0.812
0.665	0.787	0.999	0.663	0.833
0.660	0.809	0.999	0.658	0.856
0.655	0.826	0.999	0.653	0.874
0.650	0.843	0.999	0.648	0.892
0.645	0.857	0.998	0.643	0.908
0.640	0.865	0.998	0.638	0.917
0.635	0.870	0.998	0.633	0.922
0.630	0.870	0.999	0.628	0.921
0.625	0.862	0.998	0.623	0.913
0.620	0.848	0.999	0.618	0.898
0.615	0.828	0.999	0.613	0.876
0.610	0.799	0.999	0.608	0.846
0.605	0.768	0.998	0.603	0.814
0.600	0.729	0.997	0.598	0.773
0.595	0.695	0.995	0.593	0.739
0.590	0.651	0.994	0.588	0.693
0.585	0.625	0.993	0.583	0.666
0.580	0.576	0.992	0.578	0.614
0.575	0.548	0.991	0.573	0.585
0.570	0.514	0.991	0.568	0.548
0.565	0.490	0.990	0.563	0.523
0.560	0.465	0.990	0.558	0.497
0.555	0.450	0.990	0.553	0.481
0.550	0.440	0.990	0.548	0.470
0.545	0.438	0.990	0.543	0.468
0.540	0.443	0.990	0.538	0.473
0.535	0.459	0.988	0.533	0.491
0.530	0.495	0.986	0.528	0.531
0.525	0.550	0.985	0.523	0.590
0.520	0.640	0.984	0.518	0.688
0.515	0.760	0.984	0.513	0.817
0.510	0.795	0.983	0.508	0.855
0.505	0.440	0.982	0.503	0.474
0.500	0.029	0.981	0.498	0.031
0.495	0.013	0.981	0.493	0.014
0.490	0.041	0.980	0.488	0.044
0.485	0.053	0.980	0.483	0.057
0.480	0.051	0.980	0.478	0.055
0.475	0.045	0.980	0.473	0.049
0.470	0.037	0.980	0.468	0.040
0.465	0.030	0.980	0.463	0.032
0.460	0.023	0.981	0.458	0.025
0.455	0.019	0.981	0.453	0.020
0.450	0.012	0.981	0.448	0.013
0.445	0.009	0.980	0.443	0.010
0.440	0.008	0.980	0.438	0.009
0.435	0.004	0.980	0.433	0.004
0.430	0.003	0.980	0.428	0.003
0.425	0.001	0.979	0.423	0.001
0.420	0.0	0.978	0.418	0.0
0.415	0.0	0.977	0.413	0.0
0.410	0.0	0.976	0.408	0.0
0.405	0.0	0.974	0.403	0.0

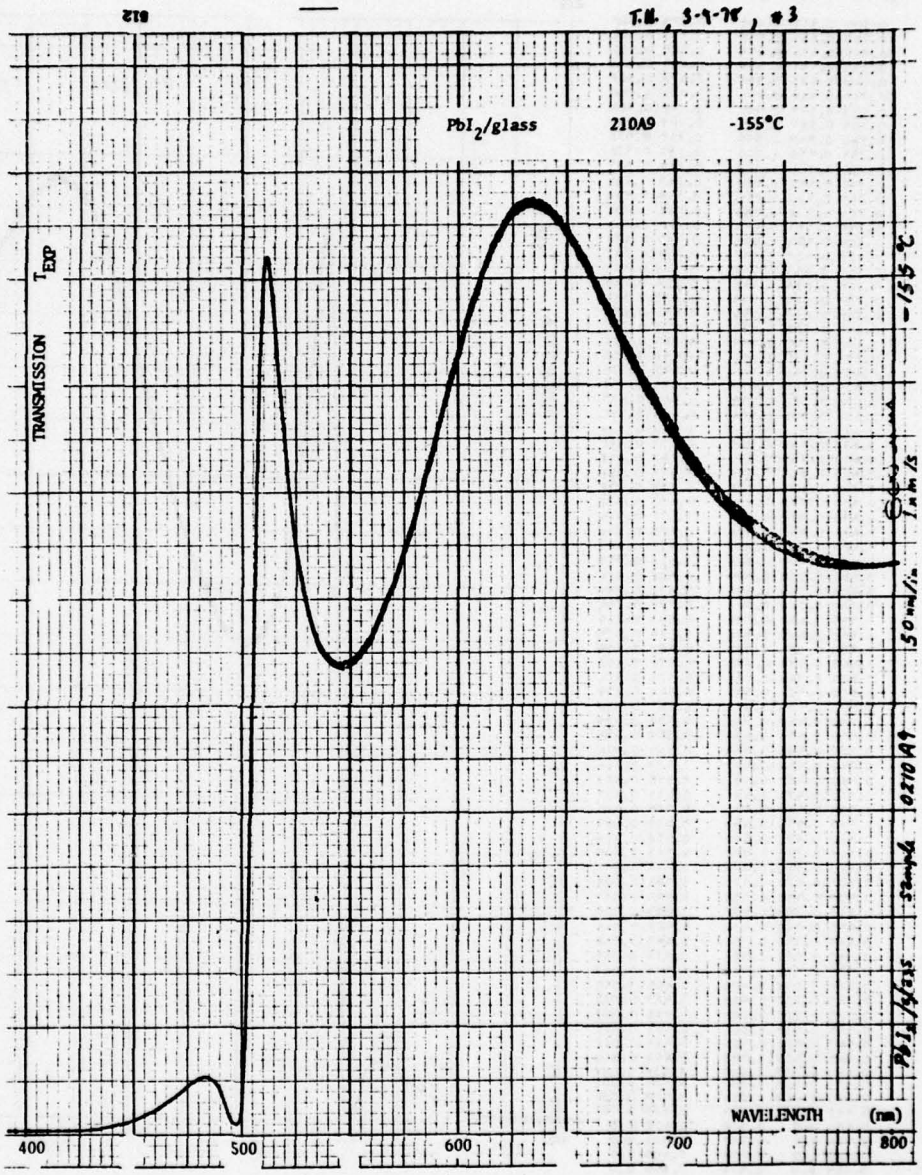

Figure 2.5-23. Transmission of PbI_2 on glass sample No. 210A9 at T = -155°C.

TEMP= -175 PBI2 GLAS 3.09 NO.4

WL	EXP T	EXP CALIB	WL	TRANS
0.800	0.535	0.998	0.798	0.962
0.795	0.534	0.998	0.793	0.961
0.790	0.534	0.998	0.788	0.961
0.785	0.535	0.998	0.783	0.962
0.780	0.535	0.998	0.778	0.962
0.775	0.538	0.999	0.773	0.964
0.770	0.539	0.999	0.768	0.965
0.765	0.540	0.999	0.763	0.966
0.760	0.545	0.999	0.758	0.972
0.755	0.550	1.000	0.753	0.976
0.750	0.556	1.000	0.748	0.981
0.745	0.562	1.000	0.743	0.989
0.740	0.570	1.000	0.738	0.997
0.735	0.578	1.000	0.733	0.606
0.730	0.585	0.999	0.728	0.614
0.725	0.595	0.998	0.723	0.625
0.720	0.607	0.999	0.718	0.637
0.715	0.619	0.999	0.713	0.649
0.710	0.634	0.999	0.708	0.665
0.705	0.649	0.999	0.703	0.681
0.700	0.665	0.999	0.698	0.697
0.695	0.683	0.999	0.693	0.716
0.690	0.700	0.999	0.688	0.734
0.685	0.720	0.998	0.683	0.755
0.680	0.740	0.998	0.678	0.776
0.675	0.760	0.999	0.673	0.797
0.670	0.782	0.999	0.668	0.820
0.665	0.807	0.999	0.663	0.841
0.660	0.822	0.999	0.658	0.862
0.655	0.840	0.999	0.653	0.881
0.650	0.855	0.999	0.648	0.897
0.645	0.868	0.998	0.643	0.911
0.640	0.874	0.998	0.638	0.918
0.635	0.877	0.998	0.633	0.921
0.630	0.872	0.999	0.628	0.915
0.625	0.861	0.998	0.623	0.904
0.620	0.842	0.999	0.618	0.883
0.615	0.819	0.999	0.613	0.859
0.610	0.789	0.999	0.608	0.828
0.605	0.756	0.998	0.603	0.794
0.600	0.719	0.997	0.598	0.756
0.595	0.682	0.995	0.593	0.718
0.590	0.640	0.994	0.588	0.675
0.585	0.606	0.993	0.583	0.639
0.580	0.570	0.992	0.578	0.602
0.575	0.540	0.991	0.573	0.571
0.570	0.510	0.991	0.568	0.539
0.565	0.488	0.990	0.563	0.516
0.560	0.465	0.990	0.558	0.497
0.555	0.453	0.990	0.553	0.484
0.550	0.445	0.990	0.548	0.476
0.545	0.445	0.990	0.543	0.476
0.540	0.457	0.991	0.538	0.483
0.535	0.471	0.991	0.533	0.503
0.530	0.510	0.991	0.528	0.545
0.525	0.570	0.990	0.523	0.609
0.520	0.670	0.990	0.518	0.716
0.515	0.785	0.990	0.513	0.839
0.510	0.810	0.990	0.508	0.866
0.505	0.475	0.979	0.503	0.508
0.500	0.030	0.978	0.498	0.032
0.495	0.008	0.977	0.493	0.009
0.490	0.043	0.976	0.488	0.046
0.485	0.054	0.976	0.483	0.058
0.480	0.051	0.980	0.478	0.055
0.475	0.044	0.980	0.473	0.047
0.470	0.037	0.980	0.468	0.040
0.465	0.030	0.980	0.463	0.032
0.460	0.022	0.981	0.458	0.023
0.455	0.018	0.981	0.453	0.019
0.450	0.011	0.981	0.448	0.012
0.445	0.009	0.980	0.443	0.010
0.440	0.007	0.980	0.438	0.007
0.435	0.006	0.980	0.433	0.006
0.430	0.002	0.980	0.428	0.002
0.425	0.001	0.979	0.423	0.001
0.420	0.0	0.978	0.418	0.0
0.415	0.0	0.977	0.413	0.0
0.410	0.0	0.976	0.408	0.0
0.405	0.0	0.974	0.403	0.0

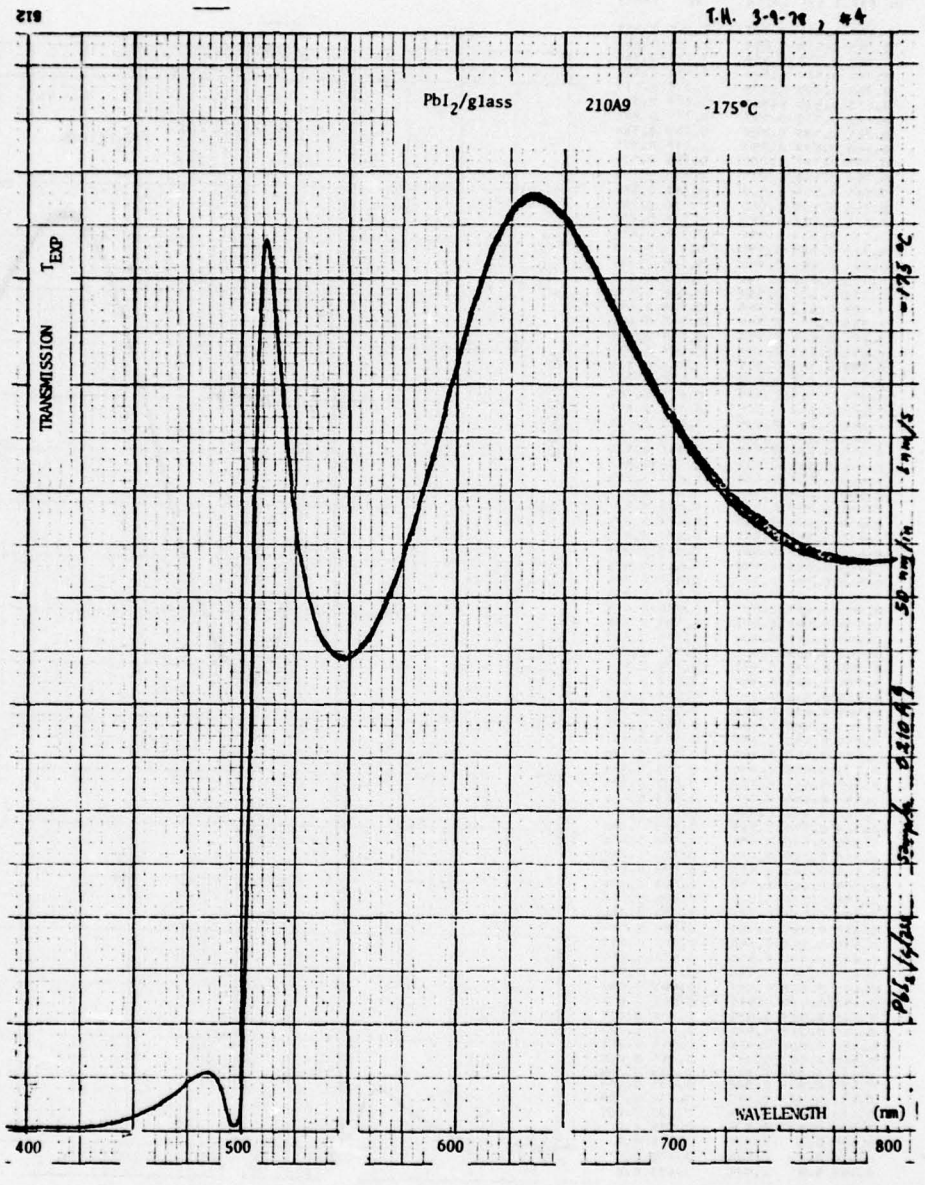

Figure 2.5-24. Transmission of PbI_2 on glass sample No. 210A9 at T = -175°C.

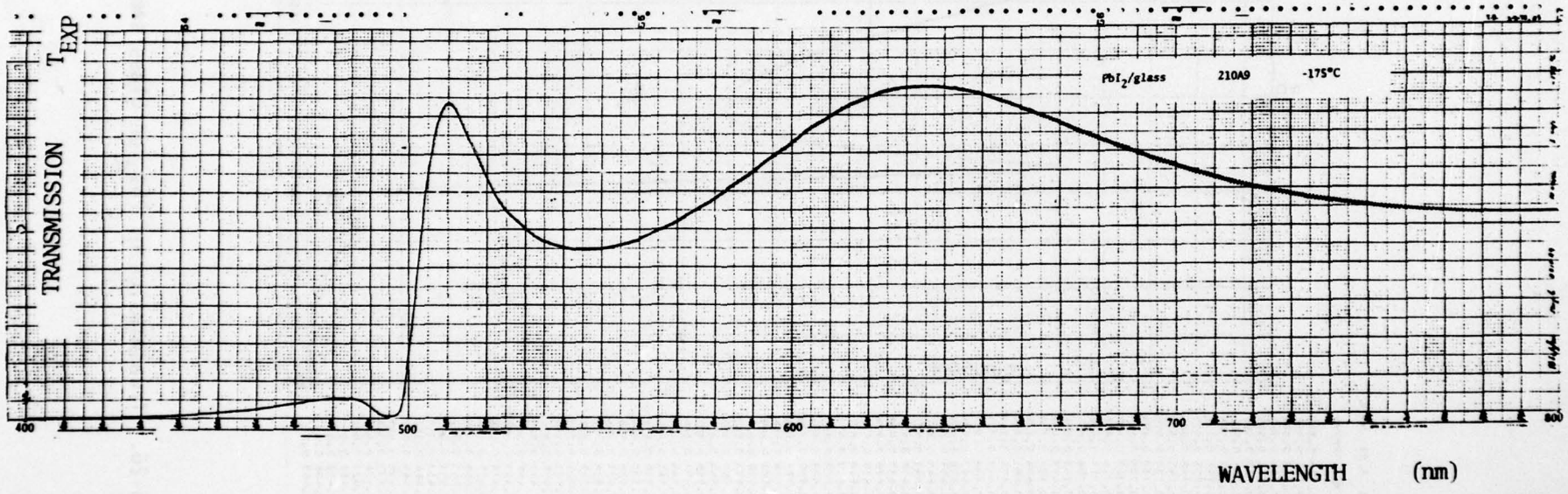

Figure 2.5-25. Transmission of PbI_2 on glass sample No. 210A9 at T = -175°C. High resolution scan.

AD-A069 537 ROCKWELL INTERNATIONAL ANAHEIM CA ELECTRONICS RESEAR--ETC F/G 11/6
TEMPERATURE SENSITIVE OPTICAL PHENOMENA IN HEAVY METAL HALIDE F--ETC(U)
JAN 79 J D MCMULLEN, D M HEINZ, F S STEARNS DAAK70-77-C-0165

UNCLASSIFIED C79-8-501 NL

2 OF 4
AD
A069537

TEMP= -100 PBI2 GLAS 1.09 NO.6

WL	EXP T	EXP CALIB	WL	TRANS
0.800	0.541	0.998	0.798	0.565
0.795	0.540	0.998	0.793	0.564
0.790	0.540	0.998	0.788	0.564
0.785	0.540	0.998	0.783	0.564
0.780	0.541	0.998	0.778	0.565
0.775	0.541	0.999	0.773	0.565
0.770	0.542	0.999	0.768	0.566
0.765	0.544	0.999	0.763	0.568
0.760	0.548	0.999	0.758	0.572
0.755	0.551	1.000	0.753	0.575
0.750	0.559	1.000	0.748	0.583
0.745	0.562	1.000	0.743	0.586
0.740	0.570	1.000	0.738	0.595
0.735	0.578	1.000	0.733	0.603
0.730	0.587	0.999	0.728	0.613
0.725	0.595	0.998	0.723	0.622
0.720	0.606	0.999	0.718	0.633
0.715	0.619	0.999	0.713	0.646
0.710	0.631	0.999	0.708	0.659
0.705	0.646	0.999	0.703	0.674
0.700	0.662	0.999	0.698	0.691
0.695	0.679	0.999	0.693	0.709
0.690	0.698	0.999	0.688	0.729
0.685	0.719	0.999	0.683	0.747
0.680	0.737	0.999	0.678	0.769
0.675	0.755	0.999	0.673	0.788
0.670	0.778	0.999	0.668	0.812
0.665	0.799	0.999	0.663	0.834
0.660	0.819	0.999	0.658	0.855
0.655	0.836	0.999	0.653	0.873
0.650	0.851	0.999	0.648	0.891
0.645	0.868	0.998	0.643	0.907
0.640	0.878	0.998	0.638	0.918
0.635	0.880	0.998	0.633	0.920
0.630	0.880	0.999	0.628	0.919
0.625	0.871	0.998	0.623	0.912
0.620	0.859	0.999	0.618	0.897
0.615	0.839	0.999	0.613	0.876
0.610	0.809	0.999	0.608	0.845
0.605	0.776	0.998	0.603	0.811
0.600	0.736	0.997	0.598	0.770
0.595	0.702	0.995	0.593	0.736
0.590	0.661	0.994	0.588	0.694
0.585	0.627	0.993	0.583	0.659
0.580	0.587	0.992	0.578	0.617
0.575	0.554	0.991	0.573	0.583
0.570	0.523	0.991	0.568	0.550
0.565	0.500	0.990	0.563	0.527
0.560	0.476	0.990	0.558	0.501
0.555	0.459	0.990	0.553	0.484
0.550	0.449	0.990	0.548	0.473
0.545	0.447	0.990	0.543	0.471
0.540	0.450	0.990	0.538	0.474
0.535	0.468	0.988	0.533	0.496
0.530	0.500	0.986	0.528	0.529
0.525	0.553	0.985	0.523	0.586
0.520	0.662	0.986	0.518	0.707
0.515	0.775	0.986	0.513	0.821
0.510	0.710	0.983	0.508	0.753
0.505	0.300	0.992	0.503	0.319
0.500	0.030	0.991	0.498	0.032
0.495	0.021	0.991	0.493	0.022
0.490	0.045	0.990	0.488	0.048
0.485	0.052	0.990	0.483	0.055
0.480	0.051	0.990	0.478	0.054
0.475	0.045	0.990	0.473	0.048
0.470	0.037	0.990	0.468	0.039
0.465	0.030	0.990	0.463	0.032
0.460	0.021	0.991	0.458	0.022
0.455	0.018	0.991	0.453	0.019
0.450	0.011	0.991	0.448	0.012
0.445	0.009	0.990	0.443	0.010
0.440	0.007	0.990	0.438	0.007
0.435	0.004	0.989	0.433	0.004
0.430	0.002	0.990	0.428	0.002
0.425	0.001	0.979	0.423	0.001
0.420	0.0	0.978	0.418	0.0
0.415	0.0	0.977	0.413	0.0
0.410	0.0	0.976	0.408	0.0
0.405	0.0	0.974	0.403	0.0

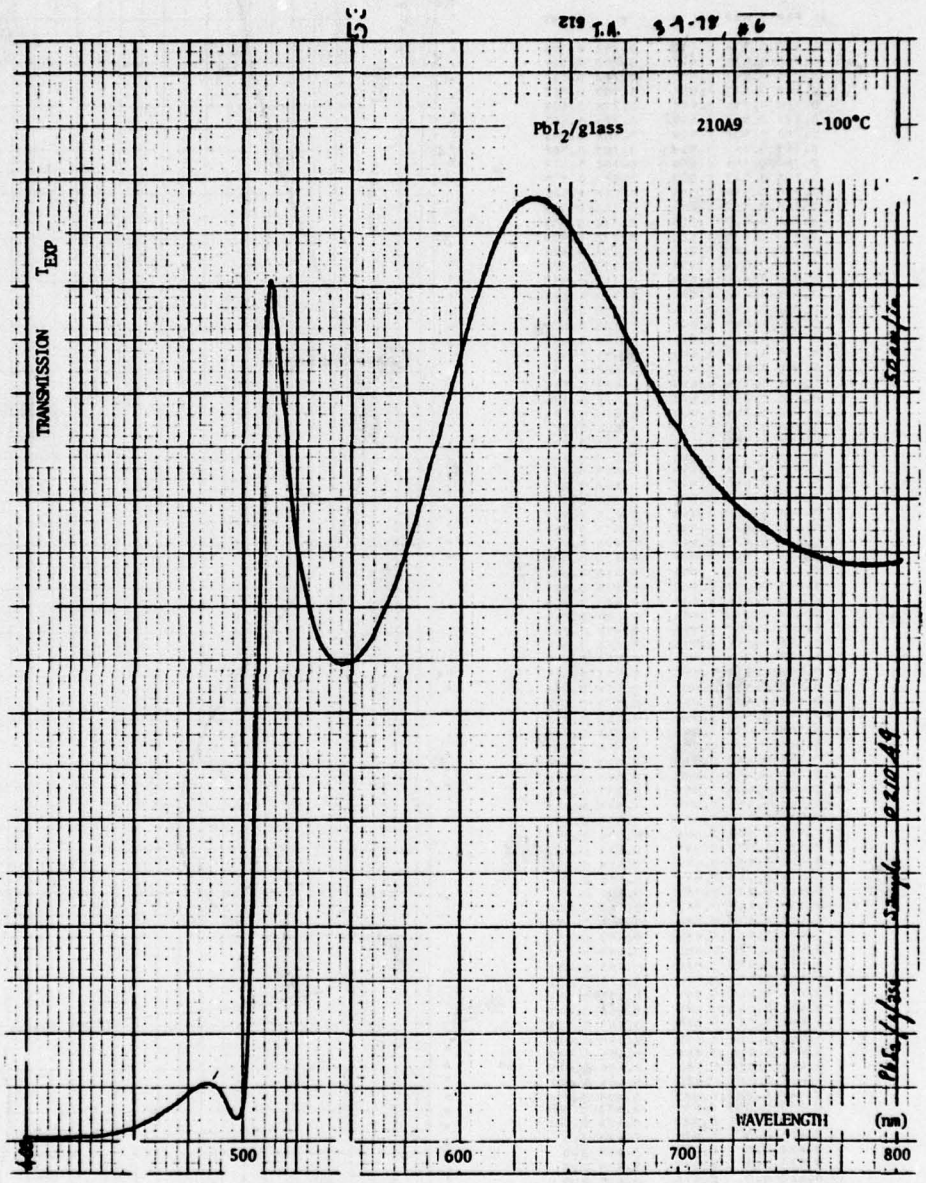

Figure 2.5-26. Transmission of PbI_2 on glass sample No. 210A9 at T = -100°C.

TEMP= 10. PBI2 GLAS 3.14 NO.2

WL	EXP T	EXP CALIB	WL	TRANS
0.800	0.568	0.997	0.798	0.572
0.795	0.567	0.998	0.793	0.571
0.790	0.566	0.999	0.788	0.569
0.785	0.566	0.999	0.783	0.569
0.780	0.567	0.999	0.778	0.570
0.775	0.568	0.999	0.773	0.571
0.770	0.569	1.000	0.768	0.571
0.765	0.570	1.000	0.763	0.572
0.760	0.573	1.000	0.758	0.575
0.755	0.579	1.000	0.753	0.581
0.750	0.583	1.000	0.748	0.585
0.745	0.589	1.000	0.743	0.591
0.740	0.595	1.000	0.738	0.598
0.735	0.602	1.000	0.733	0.605
0.730	0.611	1.000	0.728	0.614
0.725	0.621	1.000	0.723	0.624
0.720	0.632	1.000	0.718	0.635
0.715	0.645	1.000	0.713	0.648
0.710	0.659	1.000	0.708	0.662
0.705	0.671	1.000	0.703	0.674
0.700	0.689	1.000	0.698	0.692
0.695	0.706	1.000	0.693	0.709
0.690	0.722	1.000	0.688	0.725
0.685	0.740	1.000	0.683	0.743
0.680	0.761	1.000	0.678	0.764
0.675	0.783	1.000	0.673	0.786
0.670	0.806	1.000	0.668	0.809
0.665	0.827	1.000	0.663	0.830
0.660	0.849	1.000	0.658	0.853
0.655	0.869	1.000	0.653	0.873
0.650	0.886	0.999	0.648	0.891
0.645	0.900	0.999	0.643	0.905
0.640	0.910	0.999	0.638	0.915
0.635	0.916	0.999	0.633	0.921
0.630	0.915	0.999	0.628	0.920
0.625	0.909	0.999	0.623	0.914
0.620	0.891	0.999	0.618	0.896
0.615	0.871	0.999	0.613	0.876
0.610	0.841	0.999	0.608	0.845
0.605	0.809	0.999	0.603	0.813
0.600	0.770	0.998	0.598	0.775
0.595	0.730	0.998	0.593	0.735
0.590	0.690	0.997	0.588	0.695
0.585	0.650	0.997	0.583	0.655
0.580	0.610	0.996	0.578	0.615
0.575	0.576	0.996	0.573	0.581
0.570	0.545	0.996	0.568	0.550
0.565	0.520	0.996	0.563	0.524
0.560	0.495	0.995	0.558	0.501
0.555	0.480	0.992	0.553	0.486
0.550	0.470	0.991	0.548	0.476
0.545	0.469	0.990	0.543	0.476
0.540	0.477	0.990	0.538	0.484
0.535	0.499	0.990	0.533	0.506
0.530	0.540	0.990	0.528	0.548
0.525	0.610	0.989	0.523	0.619
0.520	0.671	0.989	0.518	0.681
0.515	0.535	0.988	0.513	0.544
0.510	0.225	0.987	0.508	0.229
0.505	0.090	0.987	0.503	0.092
0.500	0.058	0.986	0.498	0.059
0.495	0.059	0.986	0.493	0.060
0.490	0.058	0.985	0.488	0.059
0.485	0.043	0.984	0.483	0.044
0.480	0.044	0.984	0.478	0.045
0.475	0.035	0.984	0.473	0.036
0.470	0.027	0.983	0.468	0.028
0.465	0.020	0.984	0.463	0.020
0.460	0.013	0.986	0.458	0.013
0.455	0.009	0.986	0.453	0.009
0.450	0.004	0.985	0.448	0.004
0.445	0.001	0.984	0.443	0.001
0.440	0.0	0.984	0.438	0.0
0.435	0.0	0.983	0.433	0.0
0.430	0.0	0.983	0.428	0.0
0.425	0.0	0.982	0.423	0.0
0.420	0.0	0.981	0.418	0.0
0.415	0.0	0.980	0.413	0.0
0.410	0.0	0.980	0.408	0.0
0.405	0.0	0.980	0.403	0.0

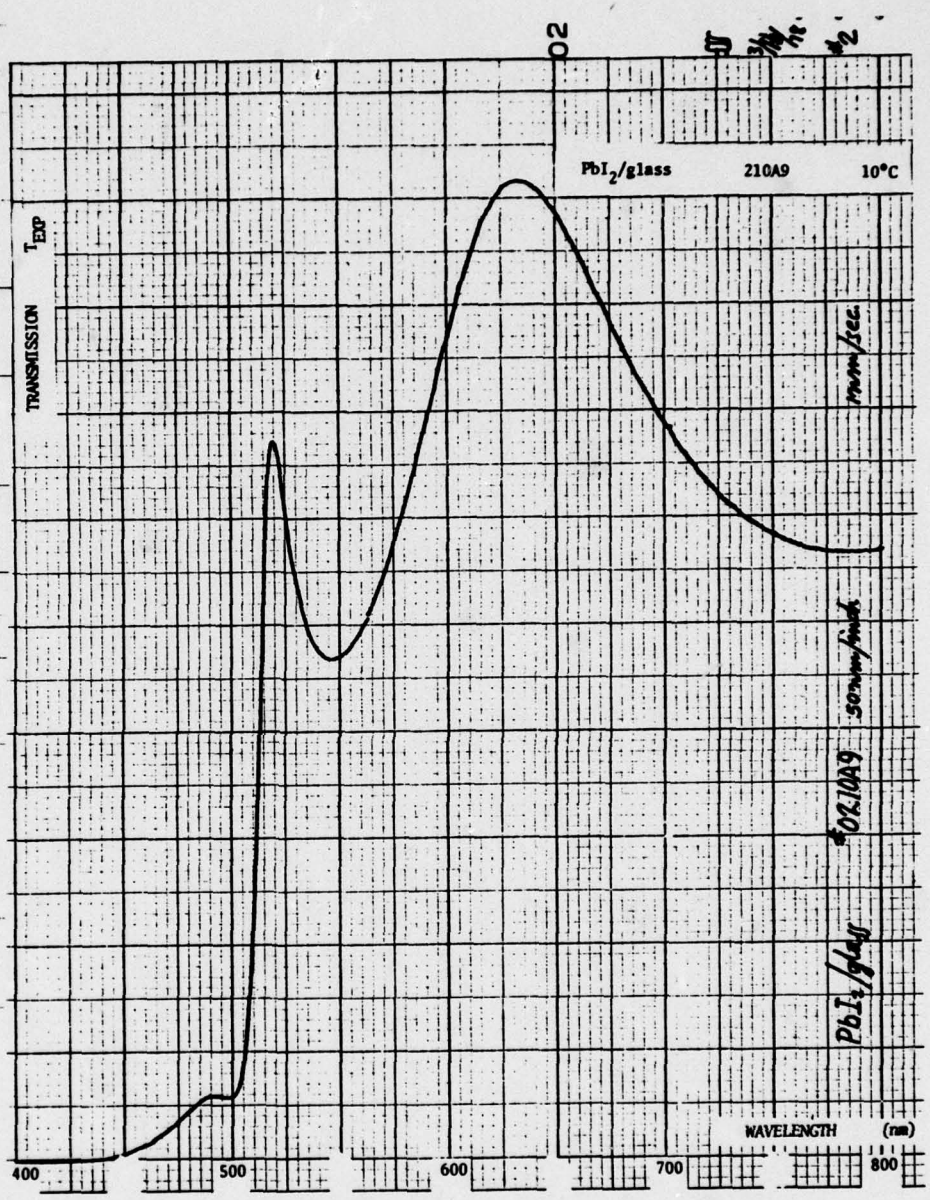

Figure 2.5-27. Transmission of PbI_2 on glass sample No. 210A9 at T = 10°C.

TEMP= 20. PBI2 GLAS 3.16 40.9

WL	EXP T	EXP CALIB	WL	TRANS
0.800	0.570	0.997	0.798	0.574
0.795	0.569	0.998	0.793	0.572
0.790	0.568	0.999	0.788	0.570
0.785	0.567	0.999	0.783	0.569
0.780	0.568	0.999	0.778	0.570
0.775	0.569	0.999	0.775	0.571
0.770	0.570	1.000	0.768	0.572
0.765	0.571	1.000	0.763	0.573
0.760	0.573	1.000	0.758	0.575
0.755	0.578	1.000	0.753	0.580
0.750	0.582	1.000	0.748	0.584
0.745	0.588	1.000	0.743	0.590
0.740	0.594	1.000	0.738	0.596
0.735	0.600	1.000	0.733	0.602
0.730	0.610	1.000	0.728	0.612
0.725	0.619	1.000	0.723	0.621
0.720	0.630	1.000	0.718	0.632
0.715	0.640	1.000	0.713	0.642
0.710	0.653	1.000	0.708	0.655
0.705	0.669	1.000	0.703	0.671
0.700	0.684	1.000	0.698	0.686
0.695	0.700	1.000	0.693	0.702
0.690	0.719	1.000	0.688	0.721
0.685	0.736	1.000	0.683	0.738
0.680	0.759	1.000	0.678	0.761
0.675	0.779	1.000	0.673	0.781
0.670	0.800	1.000	0.668	0.803
0.665	0.820	1.000	0.663	0.823
0.660	0.844	1.000	0.658	0.847
0.655	0.863	1.000	0.653	0.866
0.650	0.883	0.999	0.648	0.887
0.645	0.898	0.999	0.643	0.902
0.640	0.910	0.999	0.638	0.914
0.635	0.917	0.999	0.633	0.921
0.630	0.917	0.999	0.628	0.921
0.625	0.910	0.999	0.623	0.914
0.620	0.893	0.999	0.618	0.897
0.615	0.873	0.998	0.613	0.877
0.610	0.844	0.999	0.608	0.847
0.605	0.810	0.999	0.603	0.813
0.600	0.771	0.998	0.598	0.775
0.595	0.732	0.998	0.593	0.736
0.590	0.691	0.997	0.588	0.695
0.585	0.652	0.997	0.583	0.656
0.580	0.612	0.996	0.578	0.614
0.575	0.579	0.996	0.573	0.583
0.570	0.547	0.996	0.568	0.551
0.565	0.521	0.996	0.563	0.525
0.560	0.498	0.995	0.558	0.503
0.555	0.481	0.995	0.553	0.486
0.550	0.471	0.995	0.548	0.477
0.545	0.469	0.995	0.543	0.475
0.540	0.478	0.995	0.538	0.484
0.535	0.498	0.995	0.533	0.505
0.530	0.539	0.995	0.528	0.546
0.525	0.600	0.994	0.523	0.609
0.520	0.661	0.989	0.518	0.670
0.515	0.530	0.988	0.513	0.538
0.510	0.725	0.987	0.508	0.729
0.505	0.096	0.987	0.503	0.096
0.500	0.061	0.986	0.498	0.062
0.495	0.060	0.986	0.493	0.061
0.490	0.060	0.985	0.488	0.061
0.485	0.046	0.984	0.483	0.047
0.480	0.045	0.984	0.478	0.046
0.475	0.035	0.984	0.473	0.036
0.470	0.027	0.983	0.468	0.028
0.465	0.020	0.984	0.463	0.020
0.460	0.013	0.984	0.458	0.013
0.455	0.009	0.986	0.453	0.009
0.450	0.006	0.985	0.448	0.006
0.445	0.007	0.984	0.443	0.007
0.440	0.0	0.986	0.438	0.0
0.435	0.0	0.983	0.433	0.0
0.430	0.0	0.983	0.428	0.0
0.425	0.0	0.982	0.423	0.0
0.420	0.0	0.981	0.418	0.0
0.415	0.0	0.980	0.413	0.0
0.410	0.0	0.980	0.408	0.0
0.405	0.0	0.980	0.403	0.0

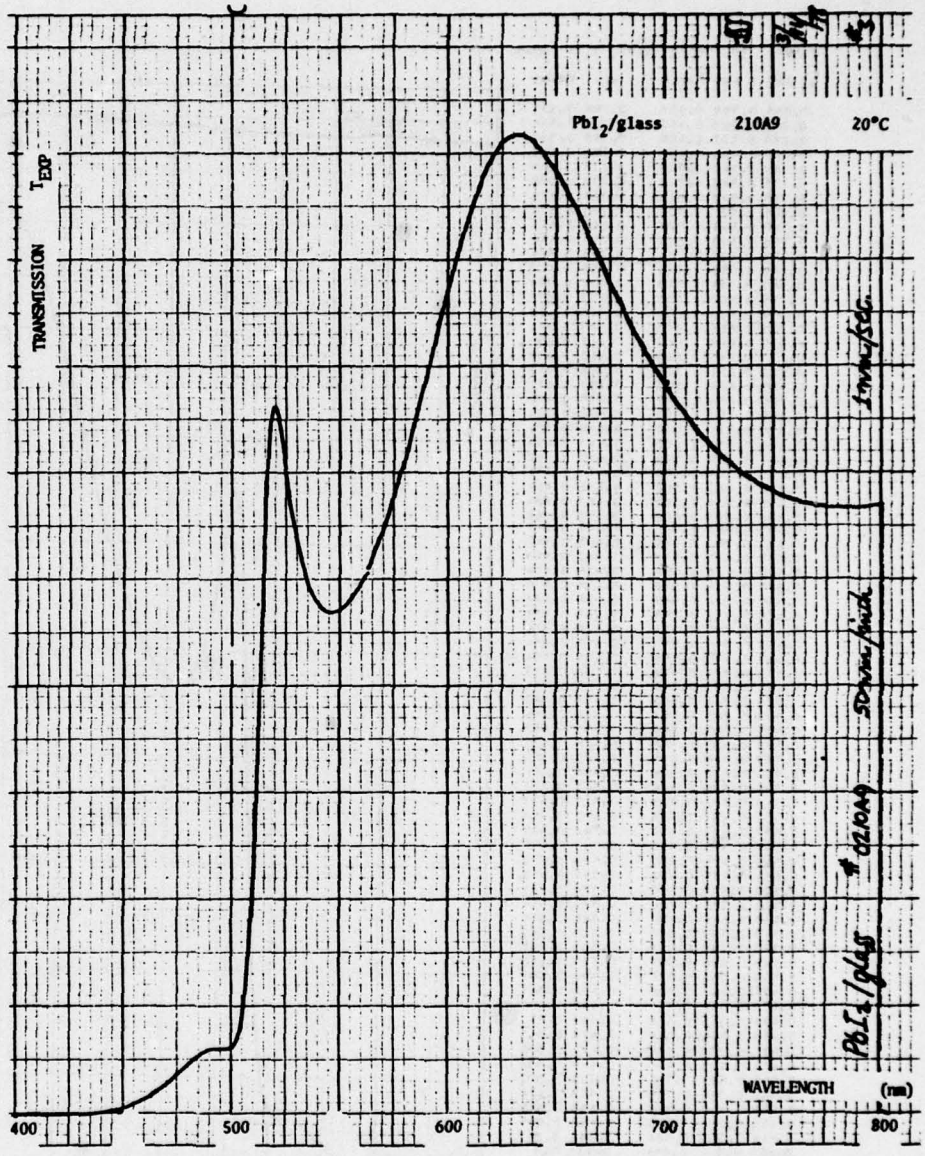

Figure 2.5-28. Transmission of PbI_2 on glass sample No. 210A9 at T = 20°C.

TEMP= 30. PBI2 GLAS 3.16 NO.4

WL EXP	T EXP	CALIB	WL	TRANS
0.800	0.569	0.957	0.798	0.571
0.795	0.568	0.998	0.793	0.571
0.790	0.567	0.999	0.788	0.569
0.785	0.566	0.999	0.783	0.568
0.780	0.567	0.999	0.778	0.569
0.775	0.568	0.999	0.773	0.570
0.770	0.570	1.000	0.768	0.572
0.765	0.571	1.000	0.763	0.573
0.760	0.573	1.000	0.758	0.575
0.755	0.578	1.000	0.753	0.580
0.750	0.582	1.000	0.748	0.584
0.745	0.588	1.000	0.743	0.590
0.740	0.594	1.000	0.738	0.596
0.735	0.600	1.000	0.733	0.602
0.730	0.610	1.000	0.728	0.612
0.725	0.619	1.000	0.723	0.621
0.720	0.629	1.000	0.718	0.631
0.715	0.640	1.000	0.713	0.642
0.710	0.654	1.000	0.708	0.656
0.705	0.669	1.000	0.703	0.671
0.700	0.686	1.000	0.698	0.689
0.695	0.700	1.000	0.693	0.702
0.690	0.719	1.000	0.688	0.721
0.685	0.738	1.000	0.683	0.740
0.680	0.759	1.000	0.678	0.761
0.675	0.779	1.000	0.673	0.781
0.670	0.801	1.000	0.668	0.804
0.665	0.821	1.000	0.663	0.824
0.660	0.845	1.000	0.658	0.848
0.655	0.864	1.000	0.653	0.867
0.650	0.883	0.999	0.648	0.887
0.645	0.899	0.999	0.643	0.903
0.640	0.910	0.999	0.638	0.914
0.635	0.916	0.999	0.633	0.920
0.630	0.918	0.999	0.628	0.922
0.625	0.911	0.999	0.623	0.917
0.620	0.900	0.999	0.618	0.904
0.615	0.880	0.999	0.613	0.884
0.610	0.850	0.999	0.608	0.854
0.605	0.820	0.999	0.603	0.823
0.600	0.780	0.998	0.598	0.784
0.595	0.743	0.998	0.593	0.747
0.590	0.700	0.997	0.588	0.704
0.585	0.663	0.997	0.583	0.667
0.580	0.623	0.996	0.578	0.627
0.575	0.589	0.996	0.573	0.593
0.570	0.554	0.996	0.568	0.558
0.565	0.529	0.996	0.563	0.533
0.560	0.502	0.995	0.558	0.507
0.555	0.487	0.995	0.553	0.492
0.550	0.473	0.995	0.548	0.479
0.545	0.469	0.995	0.543	0.475
0.540	0.474	0.995	0.538	0.480
0.535	0.489	0.995	0.533	0.495
0.530	0.526	0.995	0.528	0.533
0.525	0.580	0.995	0.523	0.588
0.520	0.645	0.995	0.518	0.654
0.515	0.580	0.995	0.513	0.589
0.510	0.290	0.987	0.508	0.295
0.505	0.120	0.987	0.503	0.122
0.500	0.066	0.986	0.498	0.067
0.495	0.062	0.986	0.493	0.063
0.490	0.060	0.985	0.488	0.061
0.485	0.096	0.984	0.483	0.097
0.480	0.048	0.986	0.478	0.049
0.475	0.039	0.986	0.473	0.040
0.470	0.029	0.983	0.468	0.030
0.465	0.021	0.984	0.463	0.021
0.460	0.014	0.986	0.458	0.014
0.455	0.010	0.986	0.453	0.010
0.450	0.009	0.985	0.448	0.009
0.445	0.002	0.986	0.443	0.002
0.440	0.0	0.986	0.438	0.0
0.435	0.0	0.983	0.433	0.0
0.430	0.0	0.983	0.428	0.0
0.425	0.0	0.982	0.423	0.0
0.420	0.0	0.981	0.418	0.0
0.415	0.0	0.980	0.413	0.0
0.410	0.0	0.980	0.408	0.0
0.405	0.0	0.980	0.403	0.0

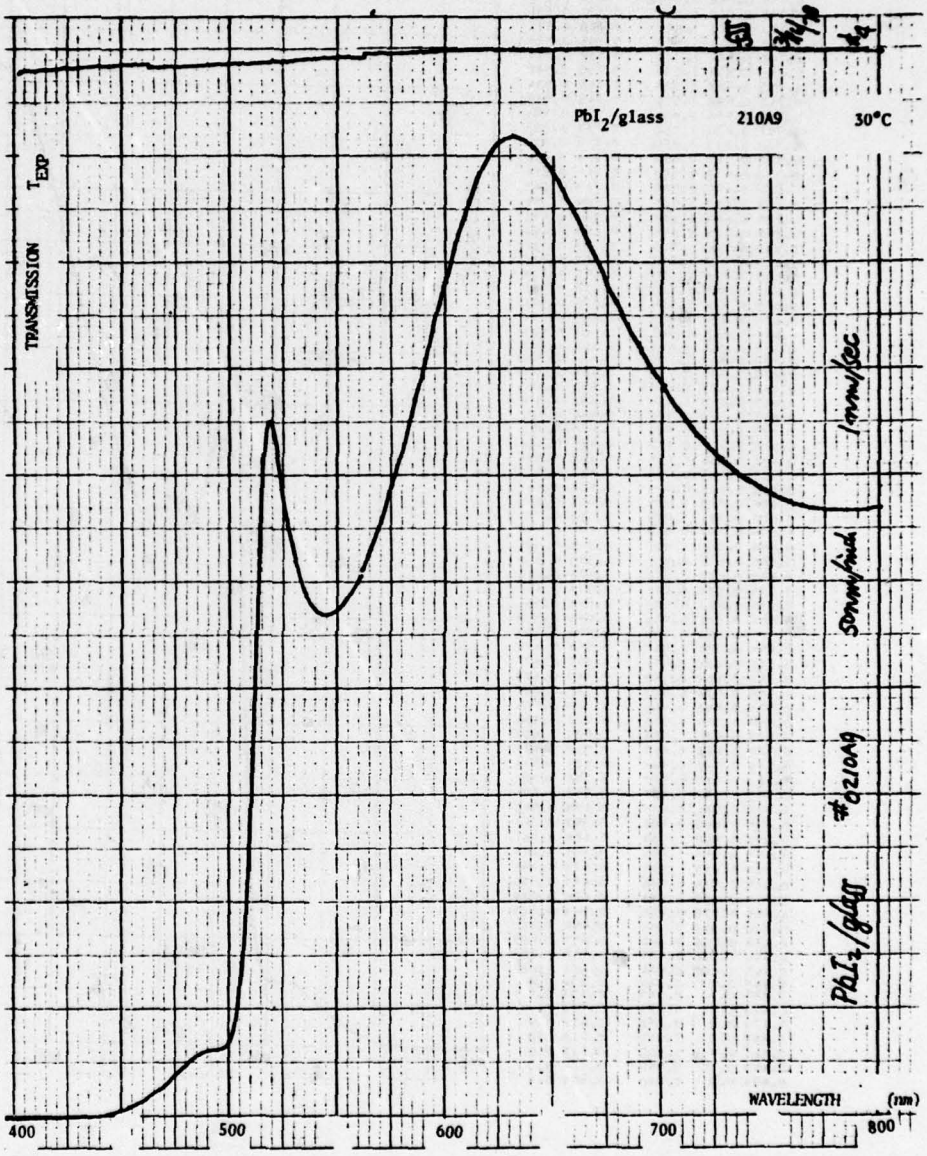

Figure 2.5-29. Transmission of PbI_2 on glass sample No. 210A9 at T = 30°C.

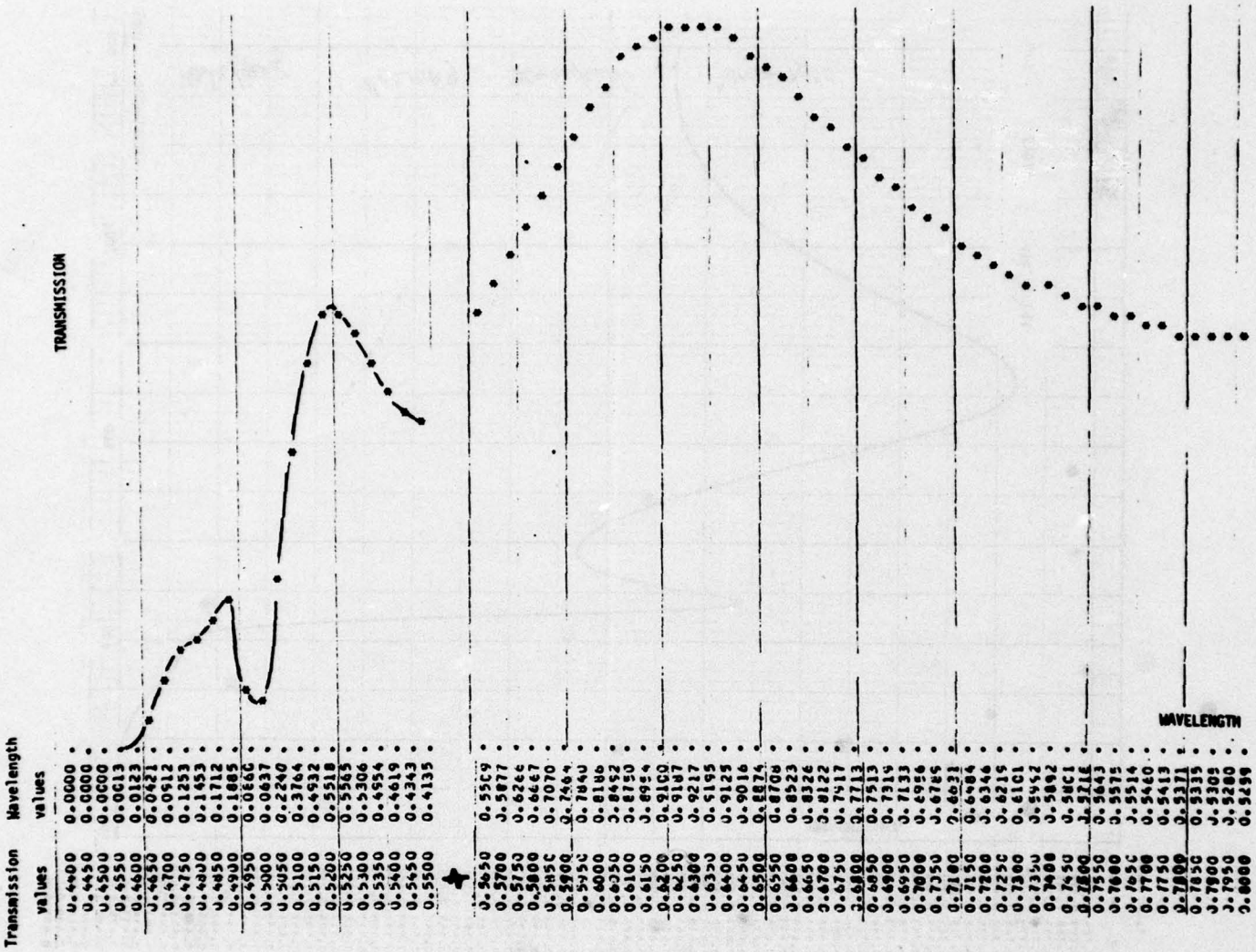

Figure 2.5-30. Theoretical transmission curve for PbI_2 film on thick glass substrate, corresponding to transmission curve at 30°C in Figure 2.5-29.
Glass substrate: $n_o = 1.324$, $S = 0.460$, $\lambda_o = 0.1680\mu$.
PbI_2 film: $n_o = 2.698$, $S = 0.265$, $\lambda_o = 0.5120\mu$, $D = 0.2220\mu$ from 0.8μ to 0.56μ.
$n_o = 2.698$, $D = 0.2220\mu$, $S_1 = 0.04$, $\lambda_{G1} = 35.\mu$, $\lambda_{01} = 0.4980\mu$, $S_2 = 1.2$, $\lambda_{G2} = 16.\mu$, $\lambda_{02} = 0.4430\mu$ from 0.55μ to 0.43μ.

TEMP= 40. PBI2 GLAS 3.16 NO.9

WL EXP	T EXP	CALIB	WL	TRANS
0.800	0.571	0.997	0.798	0.573
0.795	0.570	0.998	0.793	0.572
0.790	0.570	0.999	0.788	0.571
0.785	0.570	0.999	0.783	0.571
0.780	0.570	0.999	0.778	0.571
0.775	0.571	0.999	0.773	0.572
0.770	0.571	1.000	0.768	0.572
0.765	0.572	1.000	0.763	0.573
0.760	0.576	1.000	0.758	0.577
0.755	0.580	1.000	0.753	0.581
0.750	0.585	1.000	0.748	0.586
0.745	0.590	1.000	0.743	0.591
0.740	0.598	1.000	0.738	0.599
0.735	0.603	1.000	0.733	0.604
0.730	0.612	1.000	0.728	0.613
0.725	0.621	1.000	0.723	0.622
0.720	0.632	1.000	0.718	0.633
0.715	0.645	1.000	0.713	0.646
0.710	0.659	1.000	0.708	0.660
0.705	0.671	1.000	0.703	0.672
0.700	0.689	1.000	0.698	0.690
0.695	0.706	1.000	0.693	0.707
0.690	0.723	1.000	0.688	0.724
0.685	0.741	1.000	0.683	0.742
0.680	0.762	1.000	0.678	0.763
0.675	0.782	1.000	0.673	0.783
0.670	0.806	1.000	0.668	0.807
0.665	0.827	1.000	0.663	0.828
0.660	0.849	1.000	0.658	0.850
0.655	0.868	1.000	0.653	0.869
0.650	0.887	0.999	0.648	0.889
0.645	0.900	0.999	0.643	0.902
0.640	0.911	0.999	0.638	0.913
0.635	0.918	0.999	0.633	0.920
0.630	0.920	0.999	0.628	0.922
0.625	0.915	0.999	0.623	0.917
0.620	0.900	0.999	0.618	0.902
0.615	0.881	0.999	0.613	0.883
0.610	0.851	0.999	0.608	0.853
0.605	0.821	0.999	0.603	0.823
0.600	0.780	0.998	0.598	0.782
0.595	0.746	0.998	0.593	0.746
0.590	0.700	0.997	0.588	0.703
0.585	0.662	0.997	0.583	0.665
0.580	0.622	0.996	0.578	0.625
0.575	0.589	0.996	0.573	0.592
0.570	0.554	0.996	0.568	0.557
0.565	0.528	0.996	0.563	0.531
0.560	0.501	0.995	0.558	0.505
0.555	0.484	0.992	0.553	0.488
0.550	0.474	0.991	0.548	0.479
0.545	0.470	0.990	0.543	0.475
0.540	0.477	0.990	0.538	0.482
0.535	0.494	0.990	0.533	0.499
0.530	0.533	0.990	0.528	0.539
0.525	0.590	0.989	0.523	0.597
0.520	0.640	0.989	0.518	0.648
0.515	0.520	0.988	0.513	0.527
0.510	0.245	0.987	0.508	0.249
0.505	0.105	0.987	0.503	0.106
0.500	0.069	0.986	0.498	0.070
0.495	0.066	0.986	0.493	0.065
0.490	0.061	0.985	0.488	0.062
0.485	0.055	0.984	0.483	0.056
0.480	0.045	0.984	0.478	0.046
0.475	0.037	0.984	0.473	0.038
0.470	0.027	0.983	0.468	0.027
0.465	0.020	0.984	0.463	0.020
0.460	0.012	0.986	0.458	0.012
0.455	0.009	0.986	0.453	0.009
0.450	0.004	0.985	0.448	0.004
0.445	0.001	0.984	0.443	0.001
0.440	0.0	0.984	0.438	0.0
0.435	0.0	0.983	0.433	0.0
0.430	0.0	0.983	0.428	0.0
0.425	0.0	0.982	0.423	0.0
0.420	0.0	0.981	0.418	0.0
0.415	0.0	0.980	0.413	0.0
0.410	0.0	0.980	0.408	0.0
0.405	0.0	0.980	0.403	0.0

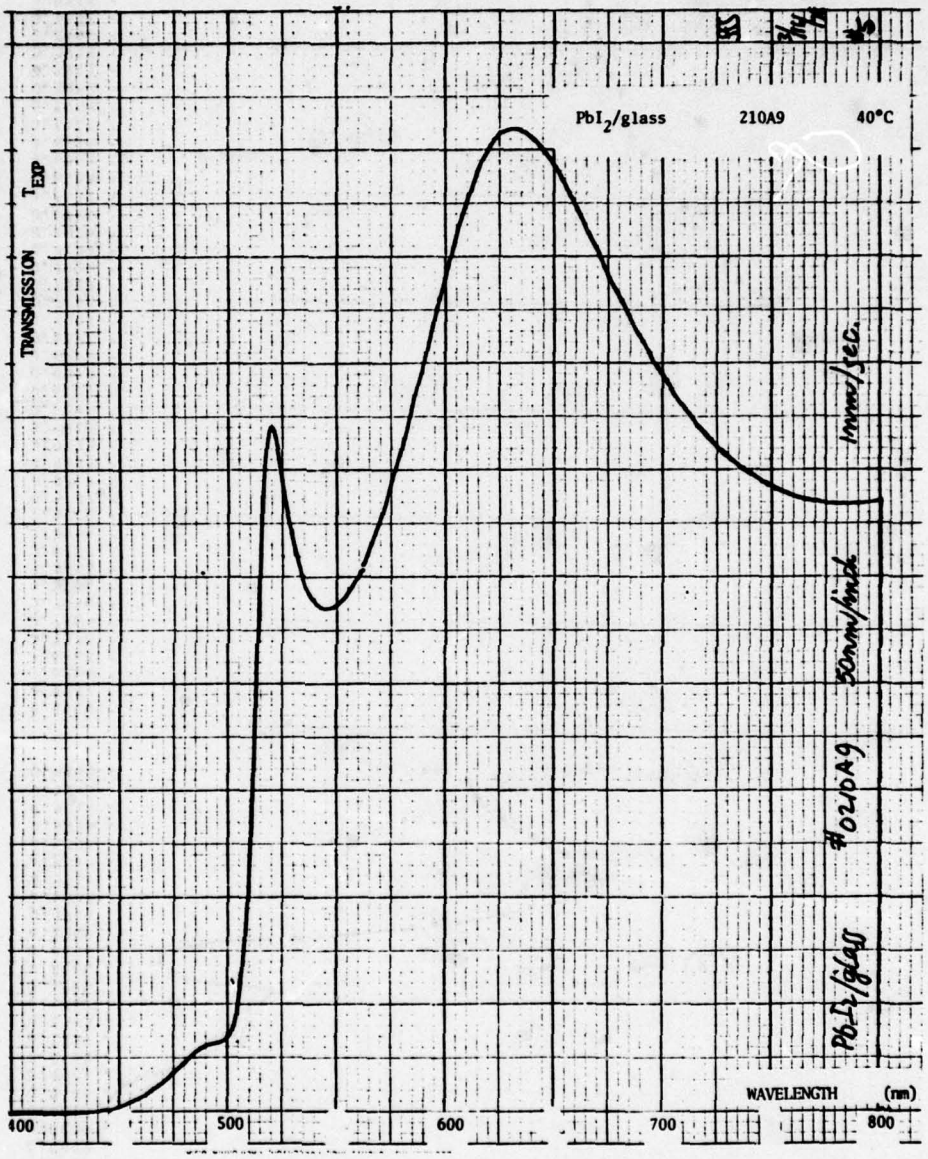

Figure 2.5-31. Transmission of PbI_2 on glass sample No. 210A9 at T = 40°C.

TEMP= 50. PBI2 GLAS 3.16 NO.6

WL	EXP T	EXP CALIB	WL	TRANS
0.800	0.575	0.997	0.798	0.577
0.795	0.574	0.998	0.793	0.571
0.790	0.572	0.999	0.788	0.568
0.785	0.571	0.999	0.783	0.567
0.780	0.572	0.999	0.778	0.569
0.775	0.573	0.999	0.773	0.569
0.770	0.575	1.000	0.768	0.571
0.765	0.578	1.000	0.763	0.574
0.760	0.580	1.000	0.758	0.576
0.755	0.585	1.000	0.753	0.581
0.750	0.590	1.000	0.748	0.585
0.745	0.596	1.000	0.743	0.591
0.740	0.601	1.000	0.738	0.596
0.735	0.610	1.000	0.733	0.605
0.730	0.619	1.000	0.728	0.614
0.725	0.629	1.000	0.723	0.624
0.720	0.639	1.000	0.718	0.634
0.715	0.651	1.000	0.713	0.646
0.710	0.665	1.000	0.708	0.660
0.705	0.679	1.000	0.703	0.674
0.700	0.696	1.000	0.698	0.691
0.695	0.712	1.000	0.693	0.707
0.690	0.730	1.000	0.688	0.724
0.685	0.750	1.000	0.683	0.744
0.680	0.772	1.000	0.678	0.766
0.675	0.793	1.000	0.673	0.787
0.670	0.816	1.000	0.668	0.810
0.665	0.838	1.000	0.663	0.832
0.660	0.859	1.000	0.658	0.852
0.655	0.880	1.000	0.653	0.873
0.650	0.898	0.999	0.648	0.892
0.645	0.910	0.999	0.643	0.904
0.640	0.922	0.999	0.638	0.916
0.635	0.927	0.999	0.633	0.921
0.630	0.927	0.999	0.628	0.921
0.625	0.920	0.999	0.623	0.914
0.620	0.903	0.999	0.618	0.897
0.615	0.883	0.999	0.613	0.877
0.610	0.852	0.999	0.608	0.846
0.605	0.821	0.999	0.603	0.816
0.600	0.780	0.998	0.598	0.776
0.595	0.744	0.998	0.593	0.740
0.590	0.699	0.997	0.588	0.696
0.585	0.660	0.997	0.583	0.657
0.580	0.620	0.996	0.578	0.618
0.575	0.585	0.996	0.573	0.583
0.570	0.553	0.996	0.568	0.551
0.565	0.526	0.996	0.563	0.524
0.560	0.501	0.995	0.558	0.501
0.555	0.488	0.997	0.553	0.488
0.550	0.477	0.991	0.548	0.478
0.545	0.475	0.990	0.543	0.476
0.540	0.481	0.990	0.538	0.482
0.535	0.501	0.990	0.533	0.504
0.530	0.545	0.990	0.528	0.546
0.525	0.600	0.990	0.523	0.602
0.520	0.626	0.990	0.518	0.628
0.515	0.455	0.988	0.513	0.457
0.510	0.215	0.987	0.508	0.216
0.505	0.104	0.987	0.503	0.105
0.500	0.070	0.986	0.498	0.070
0.495	0.065	0.986	0.493	0.065
0.490	0.061	0.985	0.488	0.061
0.485	0.053	0.986	0.483	0.053
0.480	0.043	0.986	0.478	0.043
0.475	0.033	0.984	0.473	0.033
0.470	0.024	0.983	0.468	0.024
0.465	0.018	0.984	0.463	0.018
0.460	0.011	0.984	0.458	0.011
0.455	0.007	0.986	0.453	0.007
0.450	0.003	0.985	0.448	0.003
0.445	0.001	0.984	0.443	0.001
0.440	0.0	0.984	0.438	0.0
0.435	0.0	0.983	0.433	0.0
0.430	0.0	0.983	0.428	0.0
0.425	0.0	0.982	0.423	0.0
0.420	0.0	0.981	0.418	0.0
0.415	0.0	0.980	0.413	0.0
0.410	0.0	0.980	0.408	0.0
0.405	0.0	0.980	0.403	0.0

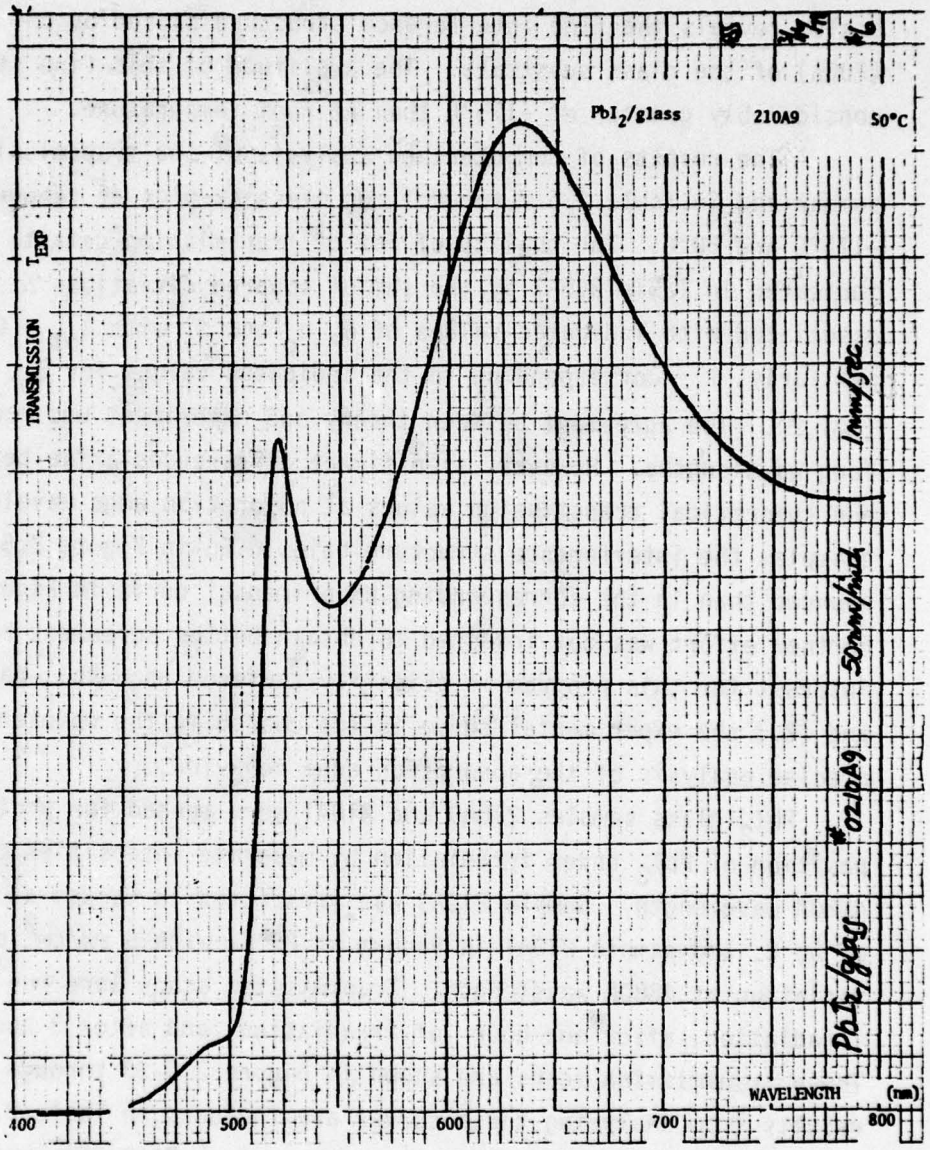

Figure 2.5-32. Transmission of PbI_2 on glass sample No. 210A9 at T = 50°C.

for the data listing on each figure, just in case it becomes necessary to know the thermal cycling history of the sample. The transmission curve of Figure 2.5.3-25, recorded using a slow scan speed and an expanded wavelength scale, reveals the fine interference structure caused by the finite thickness (200μ) of the glass substrate. The amplitude of this fine structure is considerably greater at -175°C than at room temperature.

The results of computerized analysis of the transmission curves are summarized in Table 2.5-7 for PbI_2 on glass samples at temperatures between -175°C and 50°C. The quality of fit of transmission data to theory is indicated in Table 2.5-7 by the sum of squared deviations Σ which is associated with indicated values of D, n_o and S_1 with $\lambda_{o1} = 0.5120$; and, similarly, Σ corresponding to the indicated values for S_m, λ_{Gm} and λ_{om} (m=1,2). The agreement between theory and experiment was reasonably good at long wavelengths. However, significant differences arise between experimental and theoretical transmission values at absorption edge wavelengths. For example, the interference structure below 0.5μ in Figure 2.5-30 is more pronounced than in the corresponding experimental curve in Figure 2.5-29. Further effort was not invested to obtain better agreement because (1.) interest for this program is primarily centered upon PbI_2-parylene samples, and (2.) the experimental curve is too coarse in the wavelength scale for precise analysis of the absorption edge behavior.

PbI_2-glass samples 210A9 and 210A1 were tested for photolytic decomposition of PbI_2 under irradiation by moderate intensities of light at 4880Å wavelength. Sample 210A9 was irradiated in vacuum at a temperature of 50°C, and sample 210A1 in vacuum at 25°C, with 5 mW/cm^2 of argon laser radiation at 4880Å wavelength. Transmission scans were run before irradiation, after one hour of irradiation, and after 3 hours of irradiation. These transmission scans are shown in Figure 2.5-33 through 2.5-38, and the results from analyzing these curves are included in Table 2.5-7. Photolysis is expected to give increased absorption at about 0.55μ, which would in turn cause the peak-to-peak amplitude in the transmission curve to diminish in this wavelength regime. No pronounced changes were noted in the transmission curves, and we conclude that no significant photolysis occurs at this intensity level for 3 hours irradiation at temperatures up to 50°C. In view of this apparent stability and large amount of published data on the photolysis of PbI_2 films, experimental emphasis was placed upon measurement of thermal properties of the films rather than extensive photolysis testing. Our results, insofar as they extend, agree with results reported in the literature.[9, 19-23, 33]

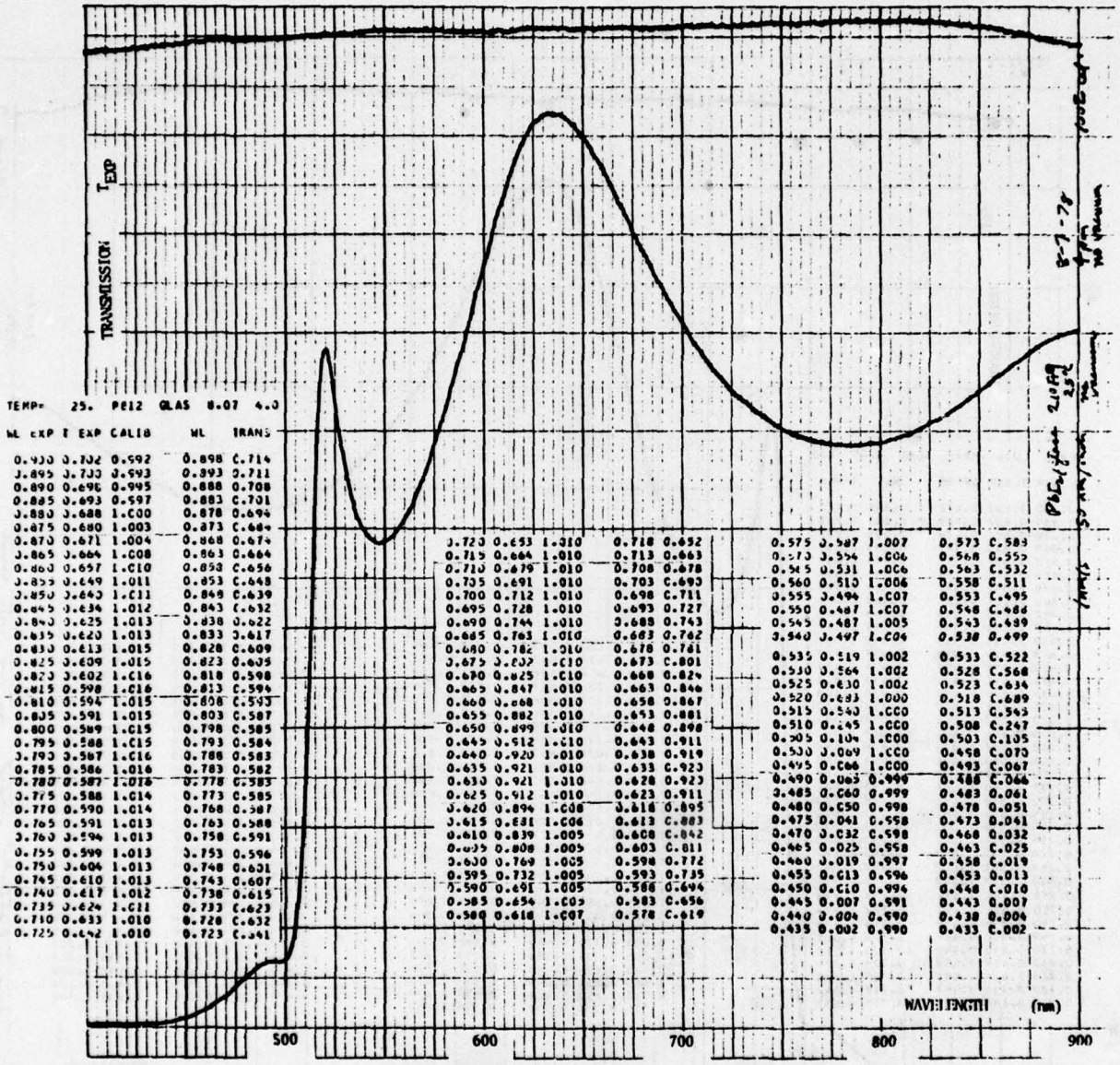

TEMP= 25. PBI2 GLAS 0.07 4.0

WL	EXP T	EXP	CALIB	WL	TRANS
0.900	0.702	0.992		0.898	0.714
0.895	0.703	0.993		0.893	0.711
0.890	0.698	0.995		0.888	0.708
0.885	0.693	0.997		0.883	0.701
0.880	0.688	1.000		0.878	0.694
0.875	0.680	1.003		0.873	0.684
0.870	0.671	1.004		0.868	0.674
0.865	0.664	1.008		0.863	0.664
0.860	0.657	1.010		0.858	0.656
0.855	0.649	1.011		0.853	0.648
0.850	0.640	1.011		0.848	0.639
0.845	0.634	1.012		0.843	0.632
0.840	0.625	1.013		0.838	0.622
0.835	0.620	1.013		0.833	0.617
0.830	0.613	1.015		0.828	0.609
0.825	0.609	1.015		0.823	0.605
0.820	0.602	1.016		0.818	0.598
0.815	0.598	1.016		0.813	0.594
0.810	0.594	1.015		0.808	0.593
0.805	0.591	1.015		0.803	0.587
0.800	0.589	1.015		0.798	0.585
0.795	0.588	1.015		0.793	0.584
0.790	0.587	1.016		0.788	0.583
0.785	0.586	1.016		0.783	0.582
0.780	0.587	1.018		0.778	0.583
0.775	0.588	1.014		0.773	0.585
0.770	0.590	1.014		0.768	0.587
0.765	0.591	1.013		0.763	0.588
0.760	0.594	1.013		0.758	0.591
0.755	0.599	1.013		0.753	0.596
0.750	0.604	1.013		0.748	0.601
0.745	0.610	1.013		0.743	0.607
0.740	0.617	1.012		0.738	0.615
0.735	0.624	1.011		0.733	0.623
0.730	0.633	1.010		0.728	0.632
0.725	0.642	1.010		0.723	0.641
0.720	0.653	1.010		0.718	0.652
0.715	0.664	1.010		0.713	0.663
0.710	0.679	1.010		0.708	0.678
0.705	0.691	1.010		0.703	0.690
0.700	0.712	1.010		0.698	0.711
0.695	0.728	1.010		0.693	0.727
0.690	0.744	1.010		0.688	0.743
0.685	0.763	1.010		0.683	0.762
0.680	0.782	1.010		0.678	0.781
0.675	0.802	1.010		0.673	0.801
0.670	0.825	1.010		0.668	0.824
0.665	0.847	1.010		0.663	0.846
0.660	0.868	1.010		0.658	0.867
0.655	0.892	1.010		0.653	0.881
0.650	0.899	1.010		0.648	0.898
0.645	0.912	1.010		0.643	0.911
0.640	0.920	1.010		0.638	0.919
0.635	0.921	1.010		0.633	0.923
0.630	0.921	1.010		0.628	0.923
0.625	0.912	1.010		0.623	0.911
0.620	0.894	1.008		0.618	0.895
0.615	0.881	1.006		0.613	0.883
0.610	0.839	1.005		0.608	0.842
0.605	0.808	1.005		0.603	0.811
0.600	0.769	1.005		0.598	0.772
0.595	0.732	1.005		0.593	0.735
0.590	0.691	1.005		0.588	0.694
0.585	0.654	1.005		0.583	0.656
0.580	0.618	1.007		0.578	0.619
0.575	0.587	1.007		0.573	0.589
0.570	0.554	1.006		0.568	0.557
0.565	0.531	1.006		0.563	0.532
0.560	0.510	1.006		0.558	0.511
0.555	0.494	1.007		0.553	0.495
0.550	0.487	1.007		0.548	0.488
0.545	0.487	1.005		0.543	0.489
0.540	0.497	1.004		0.538	0.499
0.535	0.519	1.002		0.533	0.522
0.530	0.564	1.002		0.528	0.568
0.525	0.630	1.002		0.523	0.634
0.520	0.683	1.000		0.518	0.689
0.515	0.540	1.000		0.513	0.545
0.510	0.245	1.000		0.508	0.247
0.505	0.104	1.000		0.503	0.105
0.500	0.069	1.000		0.498	0.070
0.495	0.066	1.000		0.493	0.067
0.490	0.063	0.999		0.488	0.064
0.485	0.060	0.999		0.483	0.061
0.480	0.050	0.998		0.478	0.051
0.475	0.041	0.998		0.473	0.041
0.470	0.032	0.998		0.468	0.032
0.465	0.025	0.998		0.463	0.025
0.460	0.019	0.997		0.458	0.019
0.455	0.013	0.996		0.453	0.013
0.450	0.010	0.994		0.448	0.010
0.445	0.007	0.991		0.443	0.007
0.440	0.004	0.990		0.438	0.004
0.435	0.002	0.990		0.433	0.002

Figure 2.5-33. Transmission of PbI_2 on glass sample No. 210A9 at T = 25°C, before photolysis.

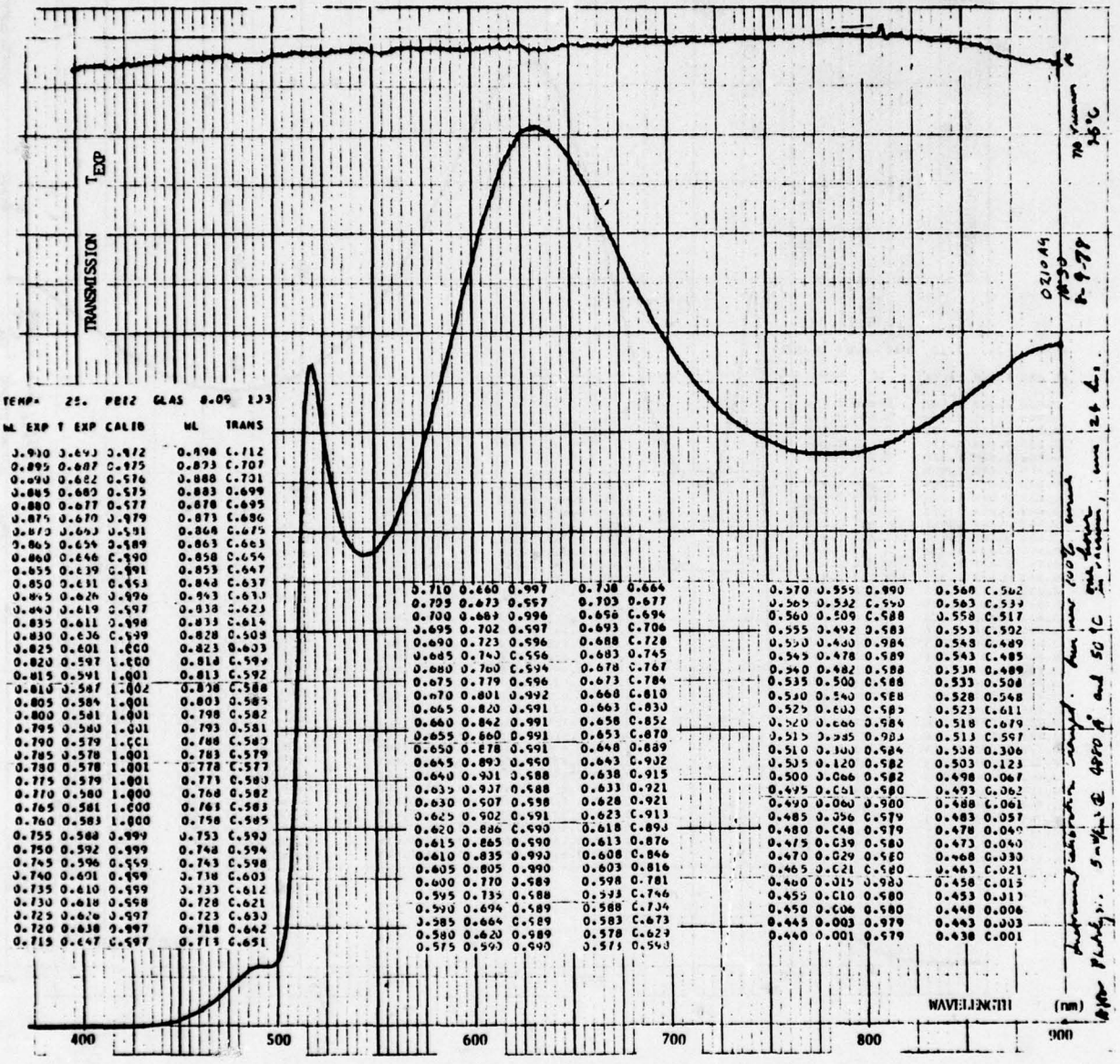

Figure 2.5-34. Transmission of PbI_2 on glass sample No. 210A9 at T = 25°C, after exposure in vacuum to 5 mW/cm^2 laser radiation at 4880A wavelength for one hour at 50°C.

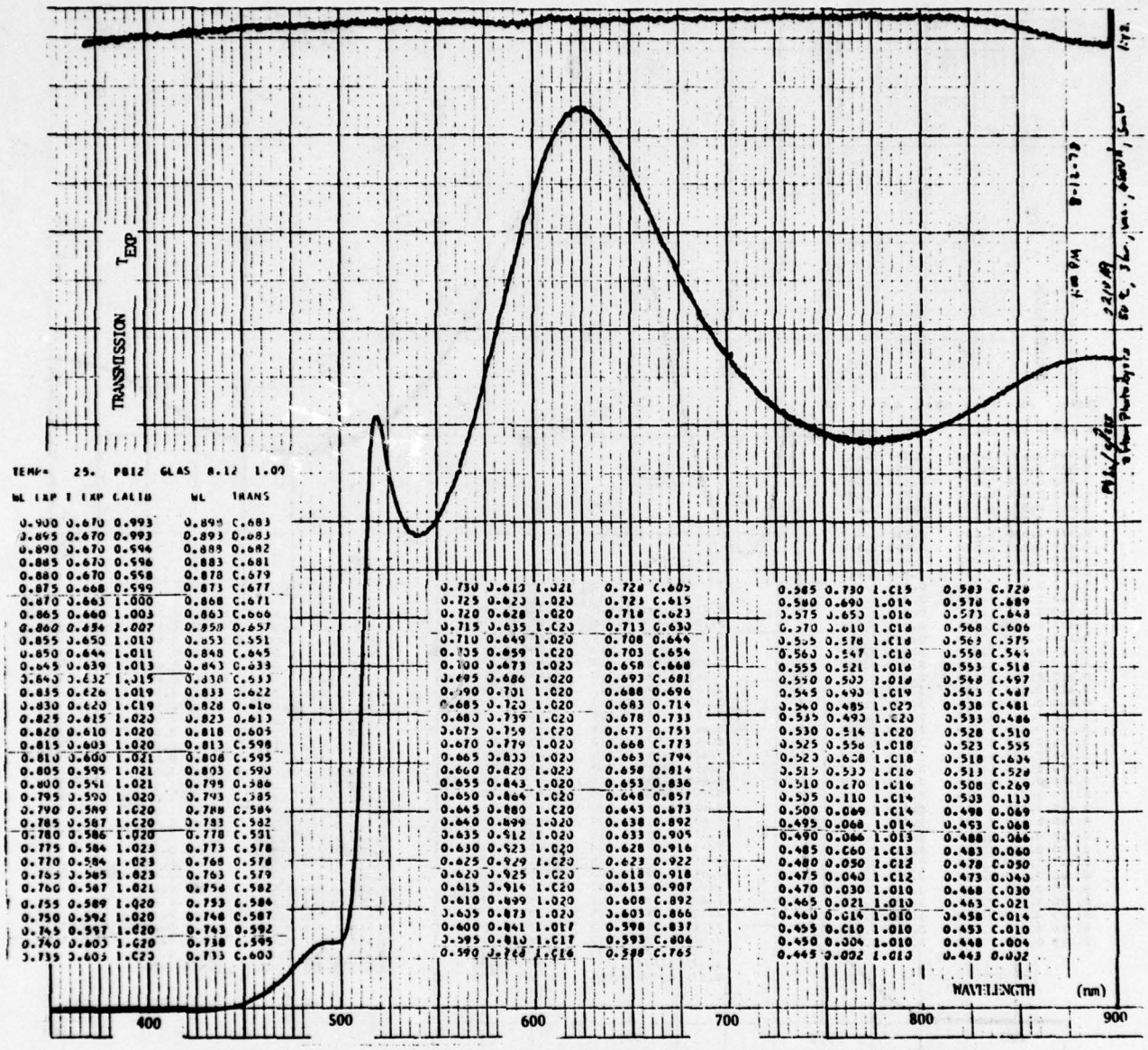

Figure 2.5-35. Transmission of PbI_2 on glass sample No. 210A9 at T = 25°C, after exposure in vacuum to 5 mW/cm^2 laser radiation at 4880Å wavelength for 3 hours at 50°C.

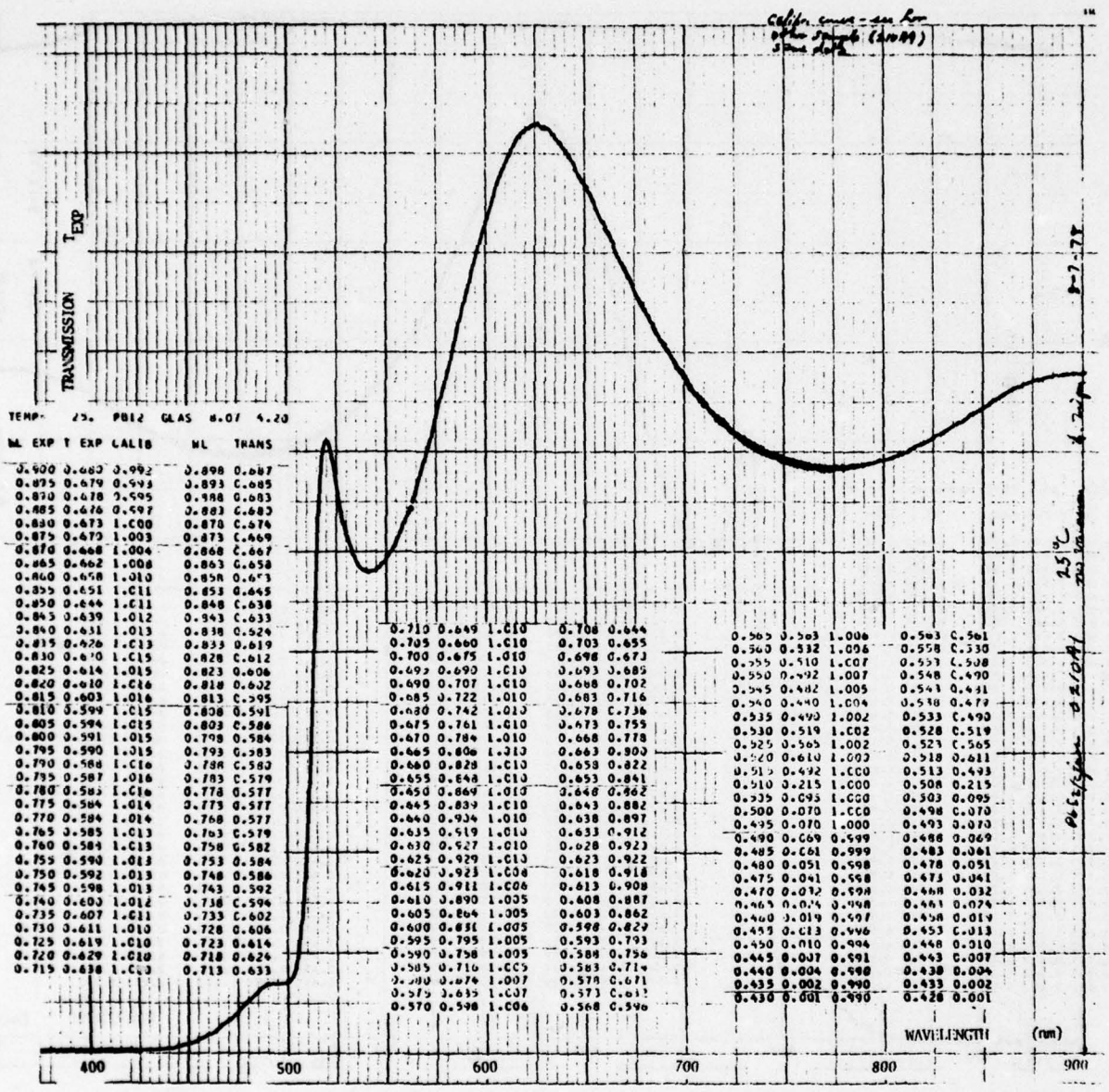

Figure 2.5-36. Transmission of PbI_2 on glass sample No. 210A1 at T = 25°C, before photolysis.

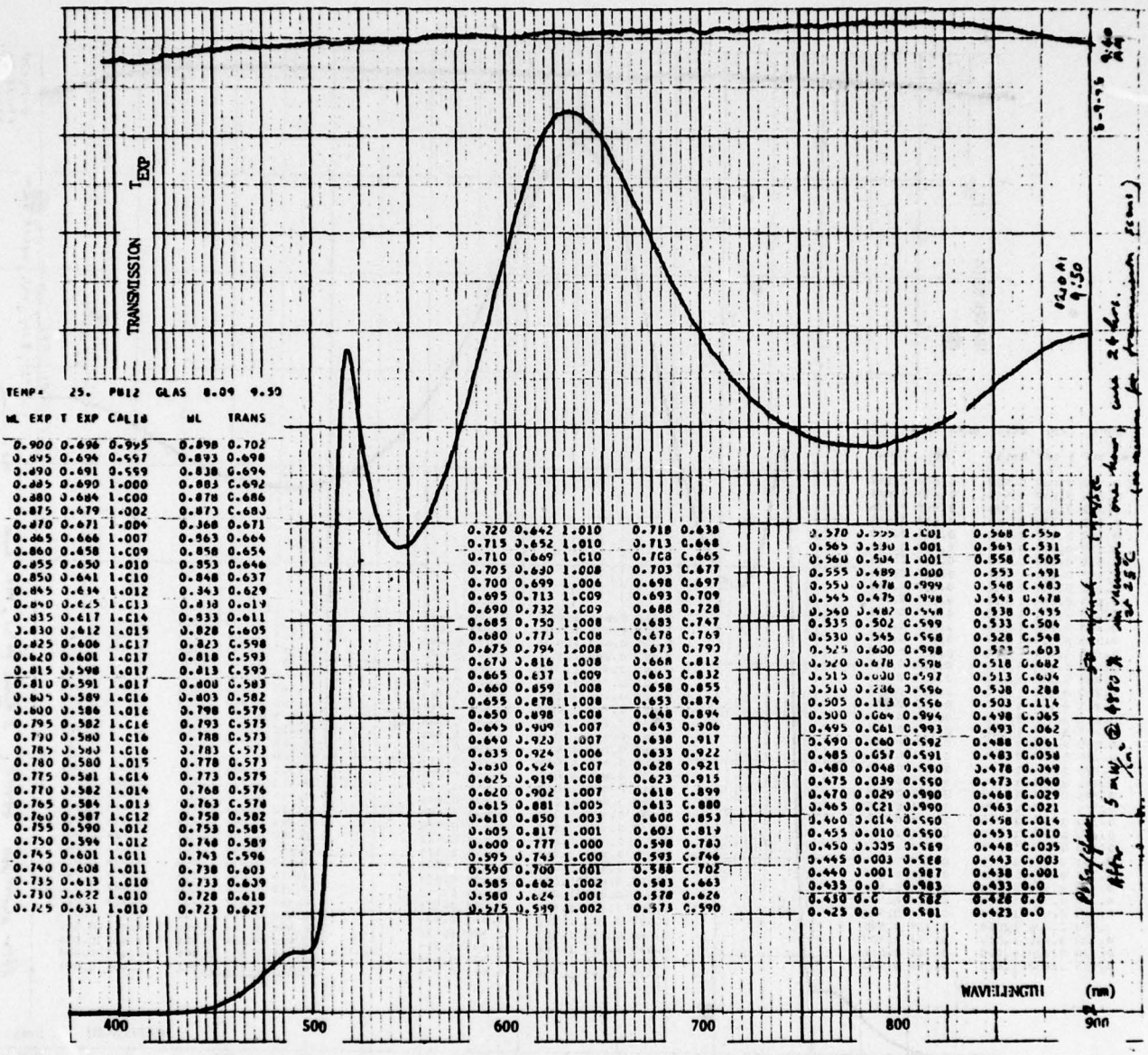

TEMP= 25. PBI2 GLAS 8.09 9.50

WL	EXP T	EXP CALIB	WL	TRANS
0.900	0.696	0.995	0.898	0.702
0.895	0.694	0.997	0.893	0.698
0.890	0.691	0.999	0.888	0.694
0.885	0.690	1.000	0.883	0.692
0.880	0.684	1.000	0.878	0.686
0.875	0.679	1.002	0.873	0.680
0.870	0.671	1.004	0.868	0.671
0.865	0.666	1.007	0.863	0.664
0.860	0.658	1.009	0.858	0.654
0.855	0.650	1.010	0.853	0.646
0.850	0.641	1.010	0.848	0.637
0.845	0.634	1.012	0.843	0.629
0.840	0.625	1.013	0.838	0.619
0.835	0.617	1.014	0.833	0.611
0.830	0.612	1.015	0.828	0.605
0.825	0.606	1.017	0.823	0.598
0.820	0.601	1.017	0.818	0.593
0.815	0.598	1.017	0.813	0.590
0.810	0.591	1.017	0.808	0.583
0.805	0.589	1.016	0.803	0.582
0.800	0.586	1.016	0.798	0.579
0.795	0.582	1.016	0.793	0.575
0.790	0.580	1.016	0.788	0.573
0.785	0.580	1.016	0.783	0.573
0.780	0.580	1.015	0.778	0.573
0.775	0.581	1.014	0.773	0.575
0.770	0.582	1.014	0.768	0.576
0.765	0.584	1.013	0.763	0.578
0.760	0.587	1.012	0.758	0.582
0.755	0.590	1.012	0.753	0.585
0.750	0.594	1.012	0.748	0.589
0.745	0.601	1.011	0.743	0.596
0.740	0.608	1.011	0.738	0.603
0.735	0.613	1.010	0.733	0.619
0.730	0.622	1.010	0.728	0.618
0.725	0.631	1.010	0.723	0.627

0.720	0.642	1.010	0.718	0.638
0.715	0.652	1.010	0.713	0.648
0.710	0.669	1.010	0.708	0.665
0.705	0.680	1.008	0.703	0.677
0.700	0.699	1.006	0.698	0.697
0.695	0.713	1.009	0.693	0.709
0.690	0.732	1.009	0.688	0.728
0.685	0.750	1.008	0.683	0.747
0.680	0.773	1.008	0.678	0.769
0.675	0.794	1.008	0.673	0.790
0.670	0.816	1.008	0.668	0.812
0.665	0.837	1.009	0.663	0.832
0.660	0.859	1.008	0.658	0.855
0.655	0.878	1.008	0.653	0.874
0.650	0.898	1.008	0.648	0.894
0.645	0.909	1.007	0.643	0.906
0.640	0.920	1.007	0.638	0.917
0.635	0.924	1.006	0.633	0.922
0.630	0.924	1.007	0.628	0.921
0.625	0.919	1.008	0.623	0.915
0.620	0.902	1.007	0.618	0.899
0.615	0.881	1.005	0.613	0.880
0.610	0.850	1.003	0.608	0.853
0.605	0.817	1.001	0.603	0.819
0.600	0.777	1.000	0.598	0.780
0.595	0.743	1.000	0.593	0.746
0.590	0.700	1.001	0.588	0.702
0.585	0.662	1.002	0.583	0.663
0.580	0.624	1.001	0.578	0.626
0.575	0.599	1.002	0.573	0.590

0.570	0.555	1.001	0.568	0.556
0.565	0.530	1.001	0.563	0.531
0.560	0.504	1.001	0.558	0.505
0.555	0.489	1.000	0.553	0.491
0.550	0.478	0.999	0.548	0.483
0.545	0.475	0.998	0.543	0.478
0.540	0.487	0.998	0.538	0.435
0.535	0.502	0.999	0.533	0.504
0.530	0.545	0.998	0.528	0.548
0.525	0.600	0.998	0.523	0.603
0.520	0.678	0.998	0.518	0.682
0.515	0.690	0.997	0.513	0.694
0.510	0.286	0.996	0.508	0.288
0.505	0.113	0.996	0.503	0.114
0.500	0.064	0.994	0.498	0.065
0.495	0.061	0.993	0.493	0.062
0.490	0.060	0.992	0.488	0.061
0.485	0.057	0.991	0.483	0.058
0.480	0.048	0.990	0.478	0.049
0.475	0.039	0.990	0.473	0.040
0.470	0.029	0.990	0.468	0.029
0.465	0.021	0.990	0.463	0.021
0.460	0.014	0.990	0.458	0.014
0.455	0.010	0.990	0.453	0.010
0.450	0.005	0.989	0.448	0.005
0.445	0.003	0.988	0.443	0.003
0.440	0.001	0.987	0.438	0.001
0.435	0.0	0.985	0.433	0.0
0.430	0.0	0.982	0.428	0.0
0.425	0.0	0.981	0.423	0.0

Figure 2.5-37. Transmission of PbI_2 on glass sample No. 210A1 at T = 25°C, after exposure in vacuum to 5 mW/cm^2 laser radiation at 4880Å wavelength for one hour at 25°C.

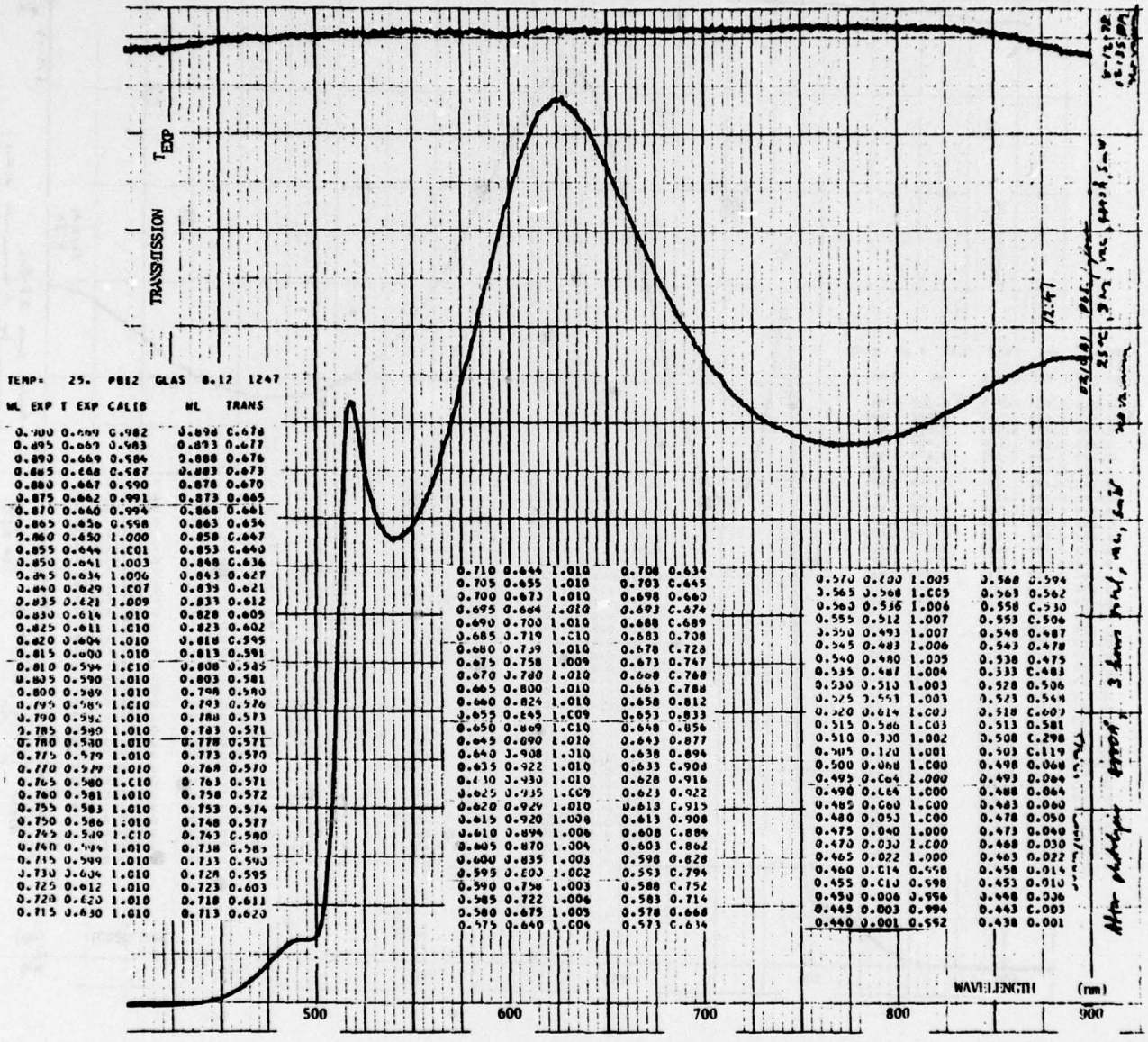

Figure 2.5-38. Transmission of PbI_2 on glass sample No. 210A1 at T = 25°C, after exposure in vacuum to 5 mW/cm^2 laser radiation at 4880A wavelength for three hours at 25°C.

TABLE 2.5-7. Thickness, Refractive Index, and Dispersion Parameters for PbI_2 Films on Glass Substrates, Obtained by Computerized Least-Squared-Deviation Analysis of Transmission Curves.

SCAN NO.	TEMPERATURE °C	PbI_2 THICKNESS D (μ) ± 0.0010	REFRACTIVE INDEX DISPERSION PARAMETERS										
			n_o ± 0.001	S ± 0.002	Σ DEV.^{2}'s	S_1 ± 0.01	λ_{G1} (μ) ±1.0	λ_{01} (μ)	S_2 ± 0.10	λ_{G2} (μ) ±1.	λ_{02} (μ)	Σ Dev.^{2}'s, Absorption Edge
SAMPLE NO. 210A9												
3.9.1	0	0.2220	2.705	0.275	.02891	.04	35.	.4980	1.2	16.	.4430	.1067
3.9.2	-30	0.2220	2.694	0.280	.02869	.04	43.	.4960	1.2	15.	.4400	.1339
3.9.3	-155	0.2220	2.705	0.265	.01635	.02	68.	.4950	1.2	19.	.4390	.3310
3.9.4	-175	0.2220	2.724	0.260	.01961	.02	70.	.4950	1.2	19.	.4380	.3674
3.9.5	-175	0.2220	2.733	0.260	.03453	.02	82.	.4950	1.1	19.	.4380	.4006
3.9.6	-100	0.2220	2.711	0.260	.01785	.02	57.	.4960	1.2	17.	.4390	.2853
3.16.2	10	0.2220	2.704	0.270	.02092	.06	39.	.4970	1.2	16.	.4420	.1022
3.16.3	20	0.2220	2.696	0.275	.02364	.04	37.	.4980	1.3	15.	.4420	.1011
3.16.4	30	0.2220	2.698	0.265	.02007	.04	35.	.4980	1.2	16.	.4430	.09751
3.16.5	40	0.2220	2.700	0.265	.02001	.05	39.	.4980	1.2	15.	.4430	.08592
3.16.6	50	0.2220	2.702	0.270	.02011	.03	33.	.4990	1.3	15.	.4440	.07480
PHOTOLYSIS MEASUREMENTS, SAMPLE NO. 210A9												
(a) 8.7.1	25	0.2220	2.713	0.265	.05672	.05	36.	.4970	1.3	15.	.4380	.1063
(b) 8.9.1	25	0.2220	2.691	0.273	.05161	.04	36.	.4960	1.3	15.	.4390	.1009
(c) 8.12.1	25	0.2220	2.623	0.290	.04121	.03	33.	.4980	1.5	14.	.4380	.07881
PHOTOLYSIS MEASUREMENTS, SAMPLE NO. 210A1												
(A) 8.7.1	25	0.2280	2.561	0.285	.02864	.04	33.	.4990	1.4	13.	.4360	.08380
(B) 8.9.1	25	0.2280	2.615	0.270	.03390	.04	37.	.4970	1.2	15.	.4410	.1023
(C) 8.12.1	25	0.2260	2.577	0.290	.03111	.03	37.	.4970	1.4	13.	.4380	.08479

Data analyzed .800μ to 540μ to yield D, n_o S using λ_e = .5120μ, λ_G = ∞ for fundamental edge.

Data analyzed .555μ to .425μ, including exciton absorption at λ_{01} and funaamental edge at λ_{02}, using D and n_o from columns 3 and 4.

FOOTNOTES:

(a), (A) Before photolysis.
(b) After 1 hr. exposure in vacuum at 50°C to 5mW/cm^2 at 4880Å.
(c) After 3 hr. exposure in vacuum at 50°C to 5mW/cm^2 at 4880Å.
(B) After 1 hr. exposure in vacuum at 25°C to 5mW/cm^2 at 4880Å.
(C) After 3 hr. exposure in vacuum at 25°C to 5mW/cm^2 at 4880Å.

The real and imaginary parts n and κ of the refractive index are plotted in Figures 2.5-39 and 2.5-40 as functions of wavelength for several temperatures, as calculated from Eqs. 2.5.3-10 and -11 and the best-fit parameters listed in Table 2.5-7. The real and imaginary components of $n+i\kappa$ are calculated from $\varepsilon_r + \varepsilon_i$ according to the following equations:

$$n = \left\{ \frac{\varepsilon_r}{2} + \frac{1}{2} \sqrt{\varepsilon_r^2 + \varepsilon_i^2} \right\}^{1/2} \qquad (2.5.3\text{-}12)$$

and

$$\kappa = \left\{ \frac{-\varepsilon_r}{2} + \frac{1}{2}\sqrt{\varepsilon_r^2 + \varepsilon_i^2} \right\}^{1/2} \qquad (2.5.3.13)$$

The complex refractive index $n + i\kappa$ is thus obtained for wavelengths across the absorption edge. The absorption coefficient $\alpha(\lambda)$ for each wavelength is obtained from κ using the equation

$$\alpha \equiv 4\pi\kappa/\lambda \ . \qquad (2.5.3\text{-}14)$$

In the long-wavelength tail of the absorption edge the absorption coefficient should obey Urbach's exponential rule given by[43,44]

$$\alpha = \alpha_0 \ \exp\left[- \sigma \frac{hc}{kT} \left(\frac{1}{\lambda} - \frac{1}{\lambda_0} \right) \right] \qquad (2.5.3\text{-}15)$$

where h is Planck's constant, c is the phase velocity of light in vacuum, k is Boltzmann's constant, $\alpha_0 \equiv \alpha\ (\lambda_0)$ at the fundamental absorption edge frequency $2\pi c/\lambda_0$, and α is a phenomenological parameter previously reported to be about 1.3 for PbI_2. A semilogarithmic plot of α versus $1/\lambda$, such as shown for sample 21A9 at 0°C in Figure 2.5-41, should be a straight line in the long-wavelength edge. The slope of this curve yields the steepness parameter σ. However, the presence of the exciton absorption at 0.5μ wavelength complicates the interpretation of an "absorption edge wavelength λ_0", as is apparent in Figure 2.5-41. Because of this exciton structure, it does not seem physically meaningful to attach a specific value to λ_0, or to specify a quantitative value for its temperature dependence $d\lambda_0/dT$. Instead, the meaningful data is the change in transmission with temperature at a specific wavelength.

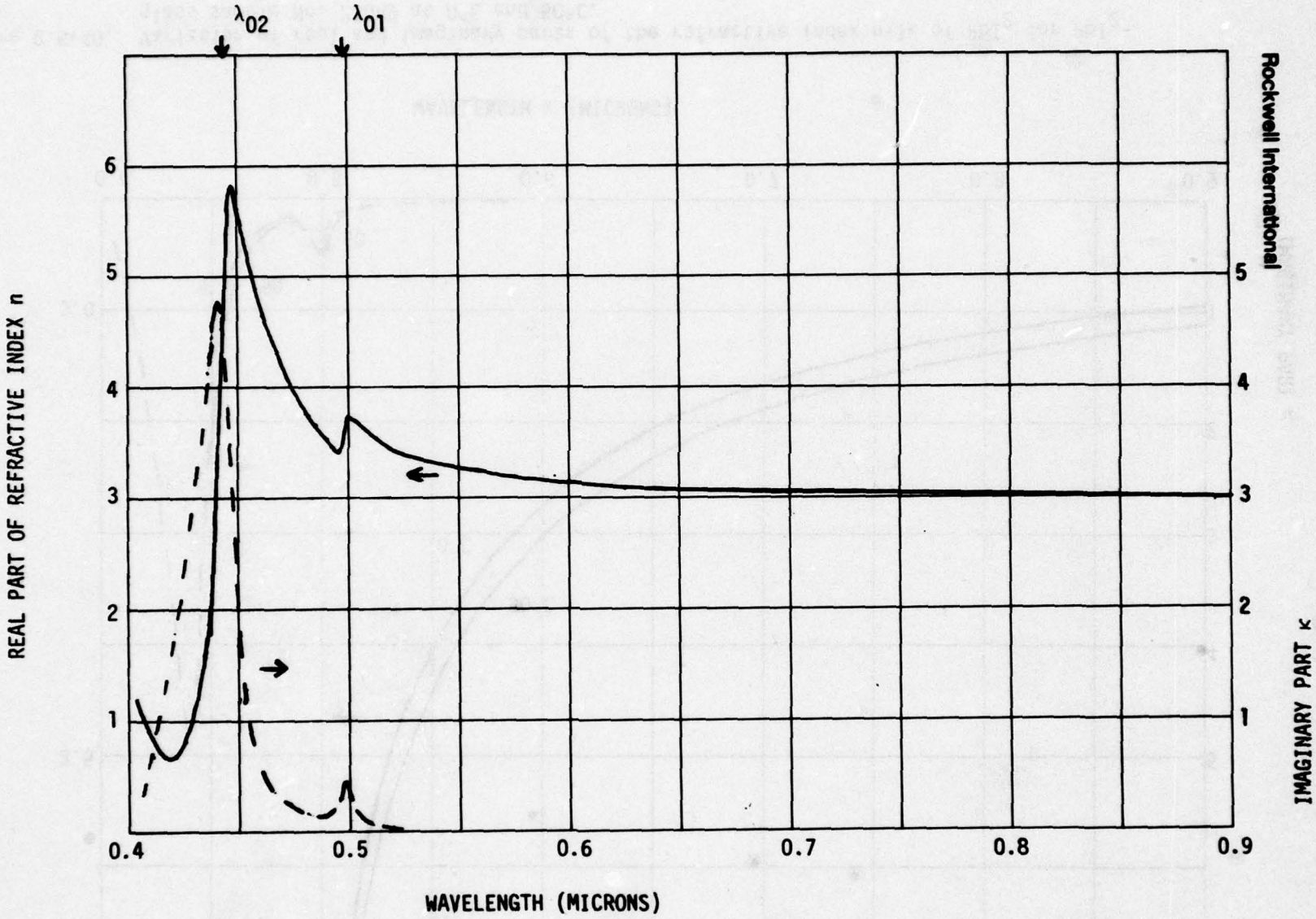

Figure 2.5-39. Variation of real part n and imagninary part κ of the refractive index of the PbI_2 film for PbI_2-glass sample 210A9 at 30°C.

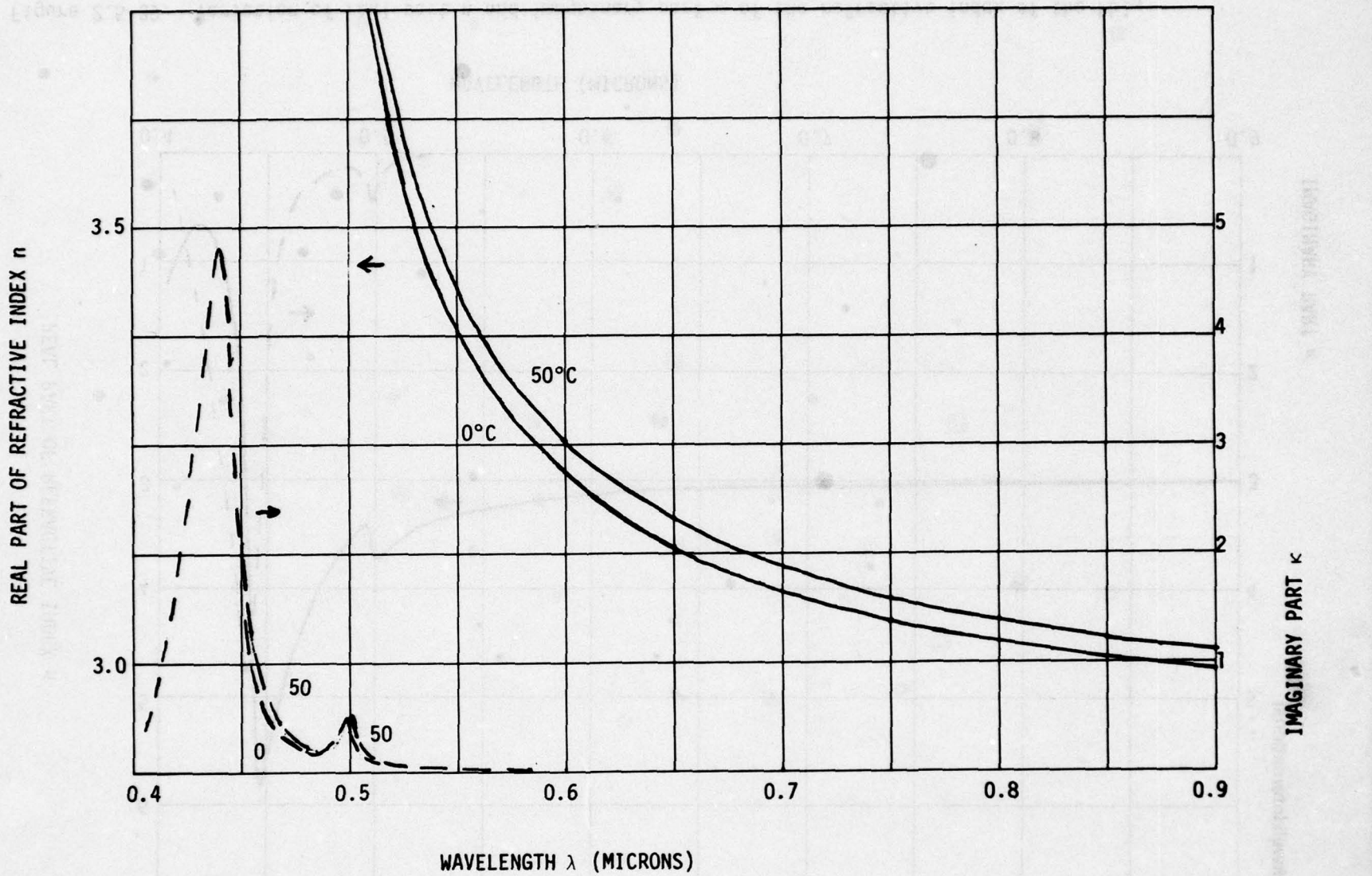

Figure 2.5-40. Variation of real and imaginary parts of the refractive index n+iκ of PbI_2 for PbI_2-glass sample No. 210A9 at 0°C and 50°C.

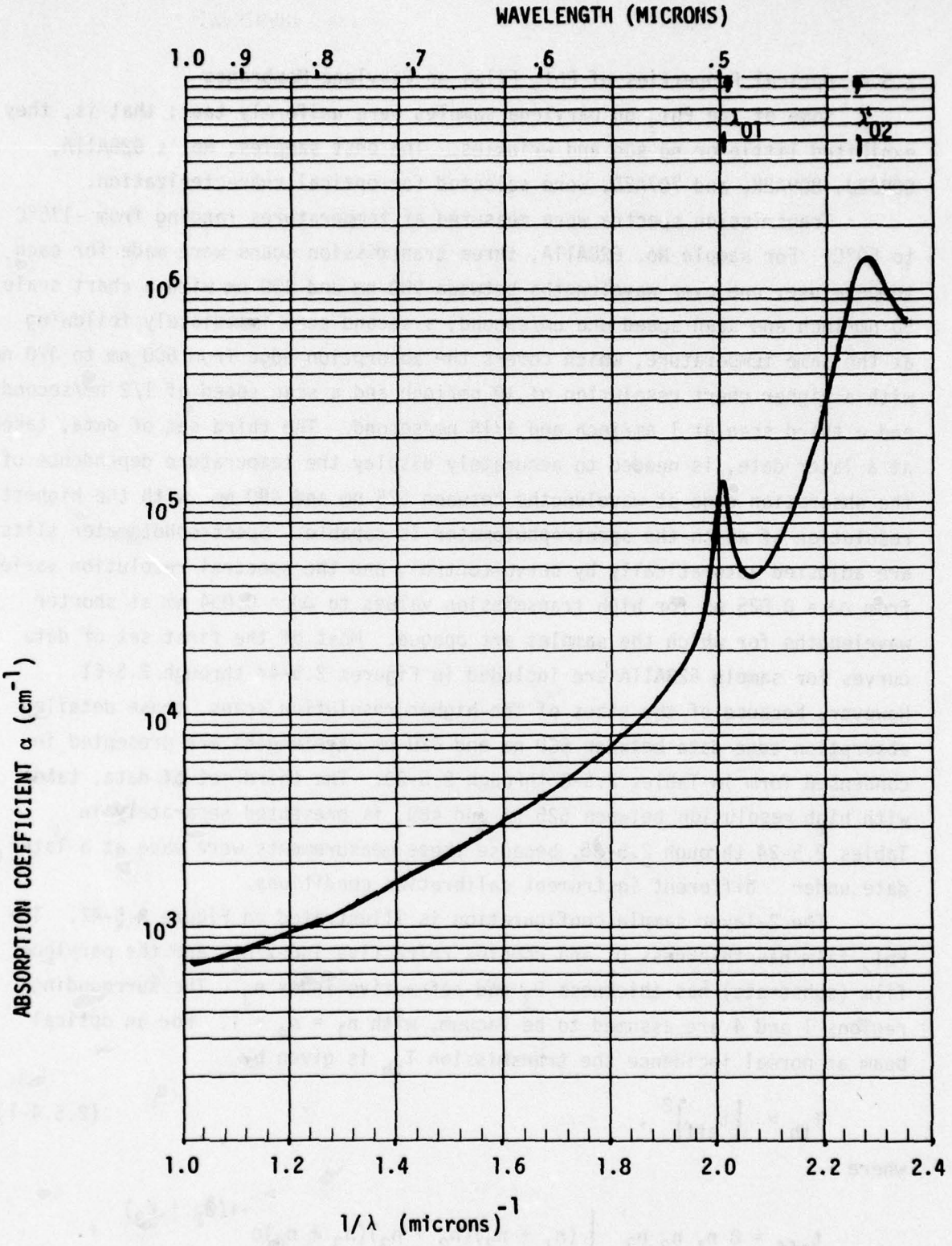

Figure 2.5-41. Frequency dependence of the absorption coefficient of PbI_2, for sample 210A9 at 0°C.

2.5.4 Optical Properties of PbI_2 Films on Parylene Membranes

Some of the PbI_2 on parylene samples were uniformly taut; that is, they exhibited little or no sag and wrinkles. The best samples, No.'s 628A11A, 808B2J, 809A2K, and 707A2D, were selected for optical characterization.

Transmission spectra were measured at temperatures ranging from -175°C to 50°C. For sample No. 628A11A, three transmission scans were made for each temperature; one over wavelengths between 900 nm and 400 nm with a chart scale 50 nm/inch and scan speed one nm/second; a second scan immediately following at the same temperature, which covers the absorption edge from 600 nm to 420 nm with a higher chart resolution of 10 nm/inch and a scan speed of 1/2 nm/second; and a third scan at 1 nm/inch and 1/16 nm/second. The third set of data, taken at a later date, is needed to accurately display the temperature dependence of the absorption edge at wavelengths between 525 nm and 480 nm with the highest resolution of which the spectrophotometer is capable. Spectrophotometer slits are adjusted automatically by servo-control, and the spectral resolution varies from $\Delta\lambda = 0.025$ nm for high transmission values to $\Delta\lambda = 0.034$ nm at shorter wavelengths for which the samples are opaque. Most of the first set of data curves for sample 628A11A are included in Figures 2.5-44 through 2.5-61. However, because of the sizes of the higher resolution scans, those detailed absorption edge data between 600 nm and 420 nm wavelengths are presented in condensed form in Tables 2.5-8 through 2.5-23. The third set of data, taken with high resolution between 525 nm and 480, is presented separately in Tables 2.5-24 through 2.5-35, because these measurements were made at a later date under different instrument calibration conditions.

The 2-layer sample configuration is illustrated in Figure 2.5-42. The PbI_2 film has thickness D_2 and complex refractive index n_2, and the parylene film (substrate) has thickness D_3 and refractive index n_3. The surrounding regions 1 and 4 are assumed to be vacuum, with $n_1 = n_4 = 1$. For an optical beam at normal incidence the transmission T_{th} is given by

$$T_{th} = \left| t_{eff} \right|^2 , \qquad (2.5.4\text{-}1)$$

where

$$t_{eff} = 8\, n_1\, n_2\, n_3 \left\{ (n_1 + n_2)(n_2 + n_3)(n_3 + n_4)e^{-i(\phi_2 + \phi_3)} + \right.$$

$$\left. (n_1 - n_2)(n_2 - n_3)(n_3 + n_4)e^{i(\phi_2 - \phi_3)} + \right.$$

$$(n_1 + n_2)(n_2 - n_3)(n_3 - n_4)e^{-i(\phi_2 - \phi_3)} + (n_1 - n_2)(n_2 + n_3)(n_3 - n_4)e^{i(\phi_2 + \phi_3)}\Big|^{-1}, \quad (2.5.4\text{-}2)$$

with ϕ_1 and ϕ_2 defined by

$$\phi_2 = 2\pi n_2 D_2/\lambda , \quad (2.5.4\text{-}3)$$

and

$$\phi_3 = 2\pi n_3 D_3/\lambda . \quad (2.5.4\text{-}4)$$

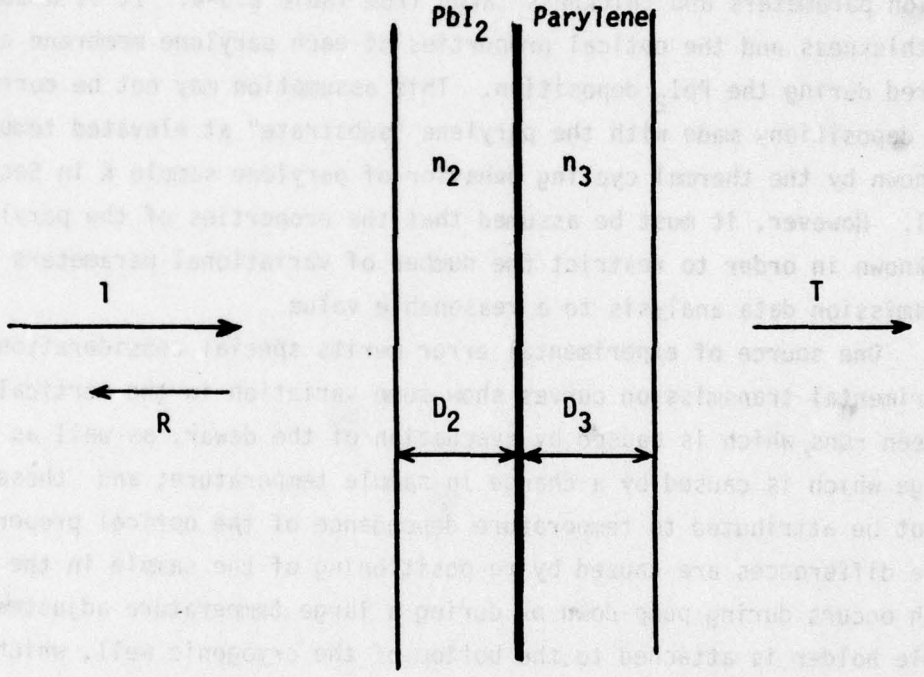

Figure 2.5-42. PbI_2-parylene sample in cross-section, showing incident and transmitted beams.

The refractive index n_2 is complex, with $Im(n_2)>0$. The theoretical transmission curve $T_{th}(\lambda)$ is calculated by computer, using complex variables. It is not convenient to analyze transmission extrema to estimate thickness and refractive index, as was done previously for films on thick substrates, because of the complexity of the transmission formula. However, a typical

theoretical transmission curve is illustrated in Figure 2.5-43 for the parameters which were obtained by computer analysis of the experimental transmission curve of Figure 2.5-44. The theoretical transmission maxima may be close to 1.0, but they may also be somewhat less. However, the interference among sinusoidal terms in the denominator of Eq. 2.5.4-2 is not predictable in a simple manner. Therefore, a fully computerized analysis is required for the experimental PbI_2-on-parylene transmission curves.

The refractive index $n_3(\lambda)$ for each parylene substrate is calculated as a function of wavelength, using Eq. 2.5.1-4 with the appropriate dispersion parameters and thickness taken from Table 2.5-4. It is assumed that the thickness and the optical properties of each parylene membrane are not altered during the PbI_2 deposition. This assumption may not be correct for PbI_2 depositions made with the parylene "substrate" at elevated temperatures, as shown by the thermal cycling behavior of parylene sample K in Section 2.5.1. However, it must be assumed that the properties of the parylene are known in order to restrict the number of variational parameters for transmission data analysis to a reasonable value.

One source of experimental error merits special consideration. The experimental transmission curves show some variation in the vertical scale, between runs, which is caused by evacuation of the dewar, as well as an occasional change which is caused by a change in sample temperature; and these changes cannot be attributed to temperature dependence of the optical properties of PbI_2. These differences are caused by re-positioning of the sample in the optical beam, which occurs during pump-down or during a large temperature adjustment. The sample holder is attached to the bottom of the cryogenic well, which in turn is part of the top portion of the dewar. This top portion is vacuum-sealed to the bottom container by seating upon a rubber gasket. The optical beam is a verticle slit image at the sample's position, and its height closely matches the aperture of the sample. The compressibility of the rubber gasket allows the sample to shift downward during pump-down, so the area of overlap between the optical beam and the sample changes. The transmission at long wavelengths may increase by as much as five percent during pump-down. This influence was compensated for by running 100 percent calibration scans under the same vacuum conditions as the samples in later experiments. This influence can be eliminated altogether by modification of the dewar. However, some of the data presented here is subject to this effect, which was not fully appreciated at

the time the measurements were being made. This effect was also present in the previously reported measurements on parylene films and PbI_2-on-glass samples. However, for those samples the values of the transmission peaks at long wavelengths were predictable, and this provided a basis for renormalizing the data to remove the error caused by a shift in sample position. That renormalization procedure may not be used with the present PbI_2-parylene curves, because the peak theoretical transmission values are not necessarily known for the 2-layer structures. Instead, the following procedure is used to renormalize PbI_2-parylene data and remove the error introduced by variable overlap between optical beam and sample. A calibration curve $T_{cal}(\lambda)$ is run at 25°C, noting whether the dewar is evacuated, using an empty sample holder to provide the same aperture. Then the transmission scan is run again at 25°C with the sample in place and the dewar under the same condition of evacuation. The highest transmission peak at long wavelengths provides the reference peak $T_{EXP}(\lambda_{ref})'$ at wavelength λ_{ref}. The transmission $T(\lambda)'$ at another wavelength on the same curve is

$$T(\lambda)' = T_{EXP}(\lambda)' \cdot \frac{T_{cal}(\lambda_{ref})}{T_{cal}(\lambda)} \quad , \qquad (2.5.4\text{-}5)$$

where $T_{EXP}(\lambda)'$ is the "raw" experimental value read directly from the curve. The transmission $T(\lambda)$ for a different scan, however, is normalized by both the calibration curve $T_{cal}(\lambda)$ and the reference transmission curve $T(\lambda)'$ as follows:

$$T(\lambda) = T_{EXP}(\lambda) \cdot \frac{T_{cal}(\lambda_{ref})}{T_{cal}(\lambda)} \cdot \frac{T_{EXP}(\lambda_{ref})'}{T_{EXP}(\lambda_{ref})} \quad . \qquad (2.5.4\text{-}6)$$

The effects of beam-sample overlap are thus removed in the corrected values of $T(\lambda)$. It is assumed with this procedure that neither λ_{ref} nor $T_{EXP}(\lambda_{ref})$ changes significantly with temperature. This should be a reasonable assumption at long wavelengths and for temperatures between 0°C and 50°C, for which the refractive index of PbI_2 changes with temperature by only about $+10^{-5}$ per °C. A small error is introduced at temperatures below -100°C, as evidenced by the shift in the peak at 600 nm to about 610 nm.

The theoretical transmission $T_{th}(\lambda)$ is compared to the corrected experimental transmission values $T(\lambda)$ using Eqs. 2.5.4-1 and -2, with the complex refractive index $n_2(\lambda)$ of PbI_2 calculated from the 2-oscillator model of Eqs. 2.5.3-10 through 2.5.3-13. In the data which follows, the transmission

scans at 25°C are occasionally repeated. This repetition provides a means to check whether thermal cycling has altered the optical properties of the sample. The transmission scans are presented in the order in which they were taken, so the thermal cycling history is readily followed.

The best-fit values of refractive index parameters and thickness for sample No. 628A11A, found by computer analysis of the first two sets of transmission curves, are summarized in Table 2.5-36. The highest resolution absorption edge scans are summarized in Table 2.5-37. The most significant difference in data reduction procedures among different scans is that λ_{02} is assigned a constant value, estimated from the onset of zero transmittivity for the long-wavelength analysis; whereas λ_{02} is a variational parameter for analysis of the two sets of high-resolution transmission curves. The absorption-edge transmission curves are complicated considerably by the presence of both a multiple-reflection interference peak arising from the rapidly varying Real($n_2(\lambda)$) and a transmission "dip" caused by the exciton absorption at 0.4960μ. Above 30°C temperature, the exciton feature is strongly damped, and the interference structure dominates. Therefore, at these temperatures, "initial values" may be established for S_2 and λ_{G2} of the fundamental edge with the assumptions $S_1 = 0.$ and $\lambda_{G1} = \infty$. This procedure greatly simplifies the calculational effort to obtain best-fit values of S_1, λ_{G1}, S_2 and λ_{G2} for the high-resolution, absorption-edge curves. As the temperature decreases below 10°C, the exciton dip at 0.496μ becomes apparent, and is quite strong at temperatures approaching -175°C. (Discussion continues on page 151).

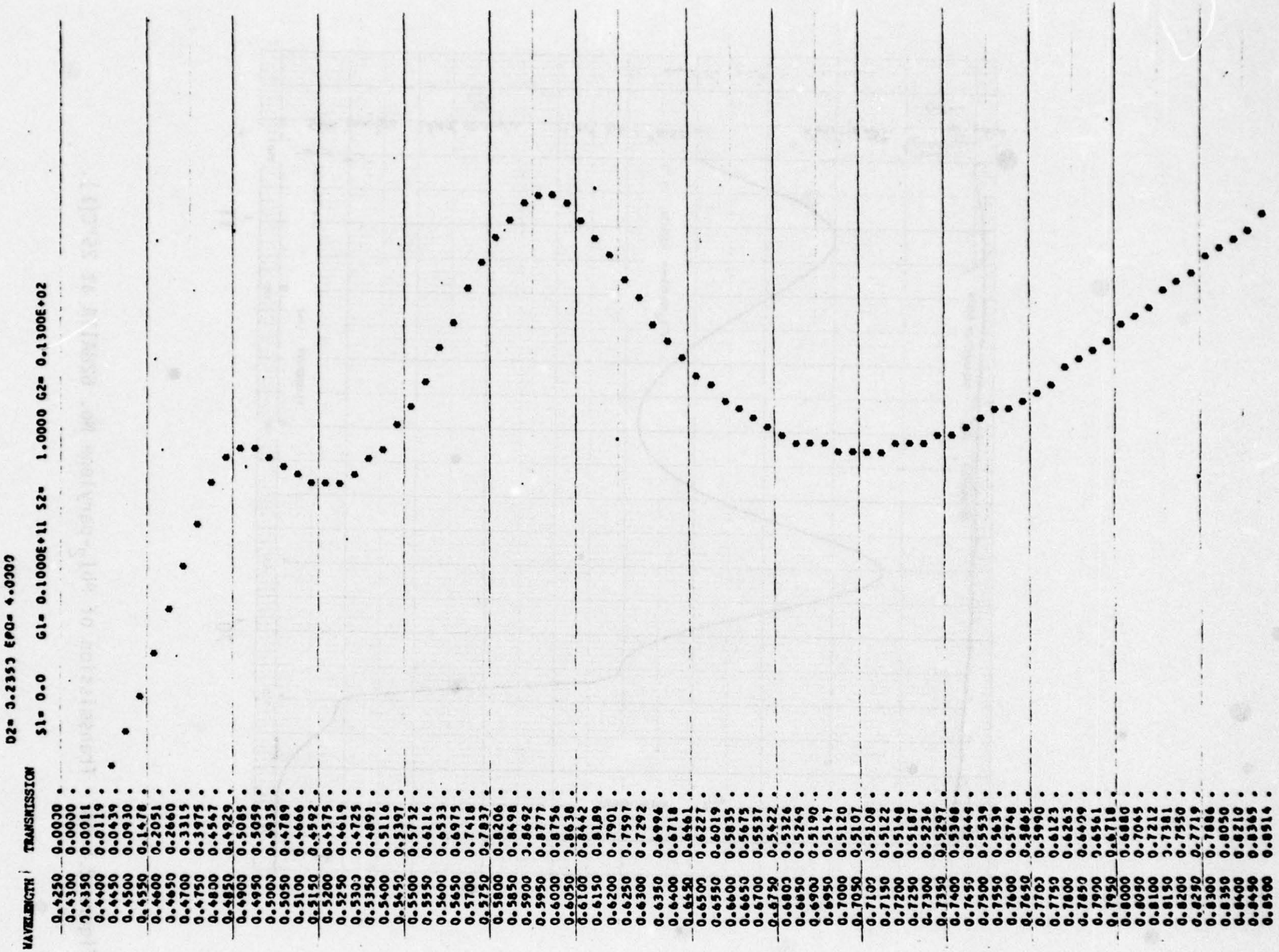

FIGURE 2.5-43. Theoretical Transmission Curve for PbI_2-Parylene Sample 628A11A at 25°C, with Dispersion Parameters Calculated from Figure 2.5-44 as Listed in the First row of Table 2.5-36.

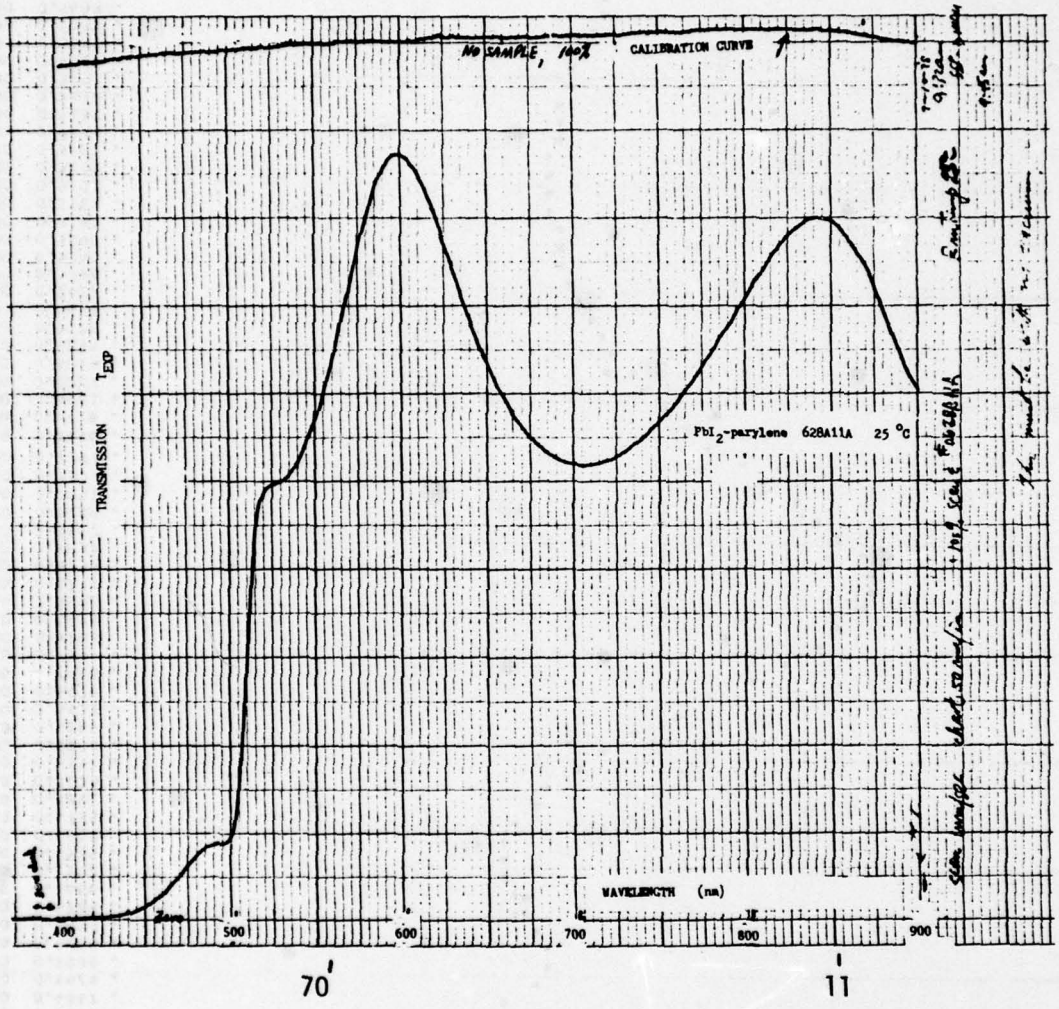

Figure 2.5-44. Transmission of PbI_2-parylene No. 628A11A at 25°C(I).

Table 2.5-8. Absorption edge transmission of PbI_2-parylene No. 628A11A at 25°C, from 600 to 420 nm.

TEMP= 25. PBI2 PARY 7-10 9.59

WL EXP	T EXP	CALIB	WL	TRANS
0.600	0.860	1.000	0.600	0.860
0.595	0.860	1.000	0.595	0.860
0.590	0.850	1.000	0.590	0.850
0.585	0.830	1.000	0.585	0.830
0.580	0.799	1.000	0.580	0.799
0.575	0.765	1.000	0.575	0.765
0.570	0.721	1.000	0.570	0.721
0.565	0.682	1.000	0.565	0.682
0.560	0.639	1.000	0.560	0.639
0.555	0.603	0.999	0.555	0.604
0.550	0.570	0.999	0.550	0.571
0.545	0.543	0.999	0.545	0.544
0.540	0.521	0.998	0.540	0.522
0.535	0.504	0.998	0.535	0.505
0.530	0.494	0.996	0.530	0.496
0.525	0.490	0.995	0.525	0.492
0.520	0.485	0.995	0.520	0.487
0.515	0.457	0.994	0.515	0.460
0.510	0.336	0.994	0.510	0.338
0.505	0.183	0.993	0.505	0.184
0.500	0.101	0.992	0.500	0.102
0.495	0.089	0.991	0.495	0.090
0.490	0.087	0.990	0.490	0.088
0.485	0.083	0.990	0.485	0.084
0.480	0.073	0.990	0.480	0.074
0.475	0.065	0.989	0.475	0.066
0.470	0.052	0.989	0.470	0.053
0.465	0.041	0.989	0.465	0.041
0.460	0.031	0.988	0.460	0.031
0.455	0.023	0.987	0.455	0.023
0.450	0.018	0.985	0.450	0.018
0.445	0.011	0.984	0.445	0.011
0.440	0.008	0.983	0.440	0.008
0.435	0.004	0.981	0.435	0.004
0.430	0.002	0.980	0.430	0.002
0.425	0.001	0.979	0.425	0.001
0.420	0.0	0.978	0.420	0.0

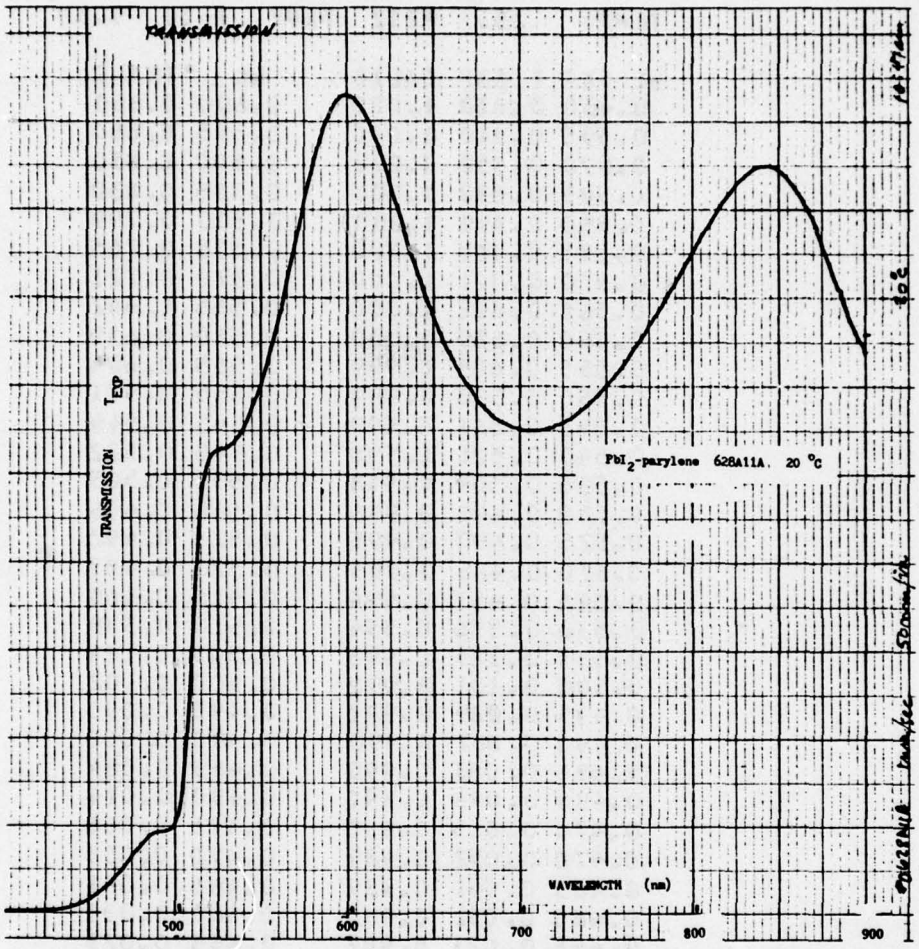

Figure 2.5-45. Transmission of PbI_2-parylene No. 628A11A at 20°C.

Table 2.5-9. Absorption edge transmission of PbI_2-parylene No. 628A11A at 20°C, from 600 to 420 nm.

TEMP= 20. PBI2 PARY 7-10 1057

WL EXP	T EXP	CALIB	WL	TRANS
0.600	0.929	1.000	0.600	0.869
0.595	0.929	1.000	0.595	0.869
0.590	0.917	1.000	0.590	0.858
0.585	0.894	1.000	0.585	0.836
0.580	0.860	1.000	0.580	0.805
0.575	0.822	1.000	0.575	0.769
0.570	0.775	1.000	0.570	0.725
0.565	0.731	1.000	0.565	0.684
0.560	0.683	1.000	0.560	0.639
0.555	0.650	0.999	0.555	0.609
0.550	0.612	0.999	0.550	0.573
0.545	0.585	0.999	0.545	0.548
0.540	0.560	0.998	0.540	0.525
0.535	0.543	0.998	0.535	0.509
0.530	0.532	0.996	0.530	0.500
0.525	0.529	0.995	0.525	0.497
0.520	0.522	0.995	0.520	0.491
0.515	0.490	0.994	0.515	0.461
0.510	0.360	0.994	0.510	0.339
0.505	0.200	0.993	0.505	0.188
0.500	0.110	0.992	0.500	0.104
0.495	0.094	0.991	0.495	0.089
0.490	0.093	0.990	0.490	0.088
0.485	0.091	0.990	0.485	0.086
0.480	0.081	0.990	0.480	0.077
0.475	0.070	0.989	0.475	0.066
0.470	0.055	0.989	0.470	0.052
0.465	0.043	0.989	0.465	0.041
0.460	0.032	0.988	0.460	0.030
0.455	0.024	0.987	0.455	0.023
0.450	0.018	0.985	0.450	0.017
0.445	0.011	0.984	0.445	0.010
0.440	0.009	0.983	0.440	0.009
0.435	0.006	0.981	0.435	0.006
0.430	0.003	0.980	0.430	0.003
0.425	0.002	0.979	0.425	0.002
0.420	0.001	0.978	0.420	0.001

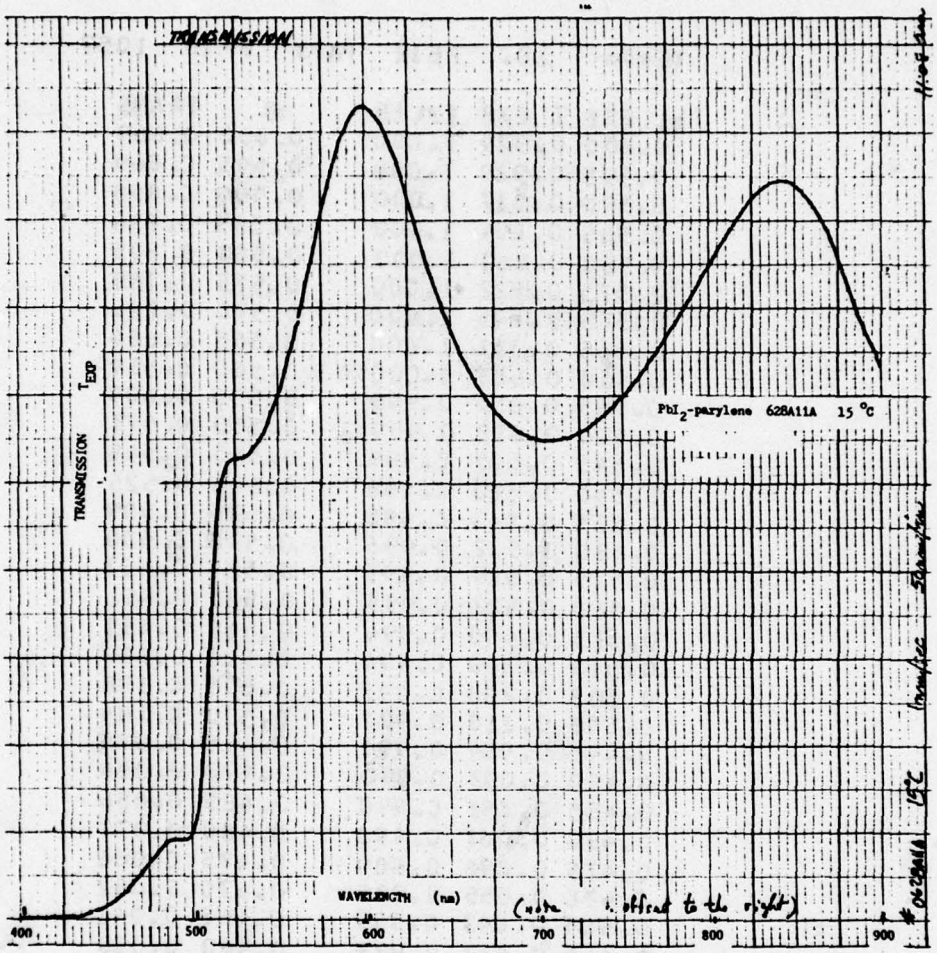

Figure 2.5-46. Transmission of PbI_2-parylene No. 628A11A at 15°C.

Table 2.5-10. Absorption edge transmission of PbI_2-parylene No. 628A11A at 15°C, from 600 to 420 nm.

TEMP= 15. PBI2 PARY 7-10 1118

WL EXP	T EXP	CALIB	WL	TRANS
0.600	0.928	1.000	0.600	0.868
0.595	0.926	1.000	0.595	0.866
0.590	0.913	1.000	0.590	0.854
0.585	0.892	1.000	0.585	0.834
0.580	0.859	1.000	0.580	0.804
0.575	0.821	1.000	0.575	0.768
0.570	0.774	1.000	0.570	0.724
0.565	0.731	1.000	0.565	0.684
0.560	0.683	1.000	0.560	0.639
0.555	0.649	0.999	0.555	0.608
0.550	0.610	0.999	0.550	0.571
0.545	0.582	0.999	0.545	0.545
0.540	0.558	0.998	0.540	0.523
0.535	0.541	0.998	0.535	0.507
0.530	0.531	0.996	0.530	0.499
0.525	0.530	0.995	0.525	0.498
0.520	0.526	0.995	0.520	0.495
0.515	0.500	0.994	0.515	0.471
0.510	0.378	0.994	0.510	0.356
0.505	0.202	0.993	0.505	0.190
0.500	0.105	0.992	0.500	0.099
0.495	0.091	0.991	0.495	0.086
0.490	0.092	0.990	0.490	0.087
0.485	0.090	0.990	0.485	0.085
0.480	0.081	0.990	0.480	0.077
0.475	0.070	0.989	0.475	0.066
0.470	0.056	0.989	0.470	0.053
0.465	0.045	0.989	0.465	0.043
0.460	0.034	0.988	0.460	0.032
0.455	0.026	0.987	0.455	0.025
0.450	0.019	0.985	0.450	0.018
0.445	0.013	0.984	0.445	0.012
0.440	0.011	0.983	0.440	0.010
0.435	0.006	0.981	0.435	0.006
0.430	0.003	0.980	0.430	0.003
0.425	0.002	0.979	0.425	0.002
0.420	0.001	0.978	0.420	0.001

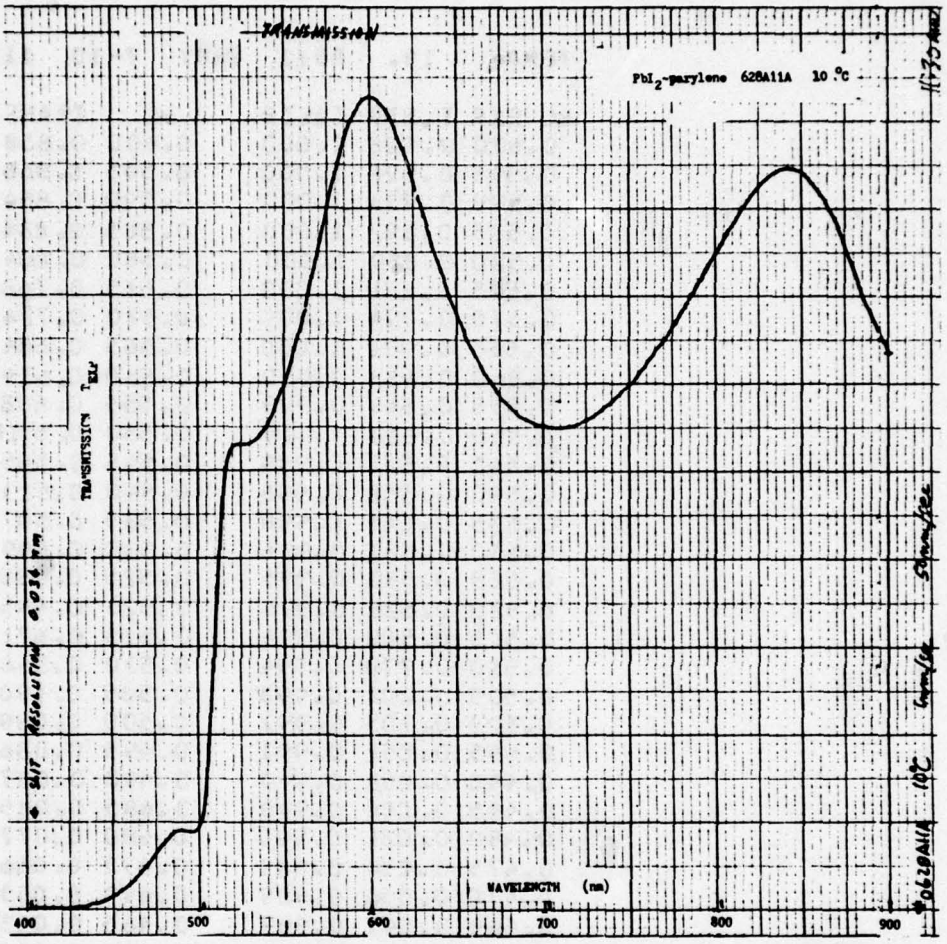

Table 2.5-47. Transmission of PbI_2 No. 628A11A at 10°C.

Table 2.5-11. Absorption edge transmission of PbI_2-parylene No. 628A11A at 10°C, from 600-420 nm.

TEMP= 10. PBI2 PARY 7-10 1140

WL EXP	T EXP	CALIB	WL	TRANS
0.600	0.928	1.000	0.600	0.870
0.595	0.926	1.000	0.595	0.868
0.590	0.913	1.000	0.590	0.856
0.585	0.892	1.000	0.585	0.836
0.580	0.860	1.000	0.580	0.806
0.575	0.821	1.000	0.575	0.770
0.570	0.775	1.000	0.570	0.727
0.565	0.732	1.000	0.565	0.686
0.560	0.685	1.000	0.560	0.642
0.555	0.649	0.999	0.555	0.609
0.550	0.611	0.999	0.550	0.573
0.545	0.583	0.999	0.545	0.547
0.540	0.560	0.998	0.540	0.526
0.535	0.542	0.998	0.535	0.509
0.530	0.533	0.996	0.530	0.502
0.525	0.530	0.995	0.525	0.499
0.520	0.530	0.995	0.520	0.499
0.515	0.510	0.994	0.515	0.481
0.510	0.396	0.994	0.510	0.373
0.505	0.213	0.993	0.505	0.201
0.500	0.105	0.992	0.500	0.099
0.495	0.090	0.991	0.495	0.085
0.490	0.091	0.990	0.490	0.086
0.485	0.090	0.990	0.485	0.085
0.480	0.091	0.990	0.480	0.086
0.475	0.071	0.989	0.475	0.067
0.470	0.057	0.989	0.470	0.054
0.465	0.047	0.989	0.465	0.045
0.460	0.033	0.988	0.460	0.031
0.455	0.025	0.987	0.455	0.024
0.450	0.019	0.985	0.450	0.018
0.445	0.013	0.984	0.445	0.012
0.440	0.009	0.983	0.440	0.009
0.435	0.005	0.981	0.435	0.005
0.430	0.003	0.980	0.430	0.003
0.425	0.002	0.979	0.425	0.002
0.420	0.001	0.978	0.420	0.001

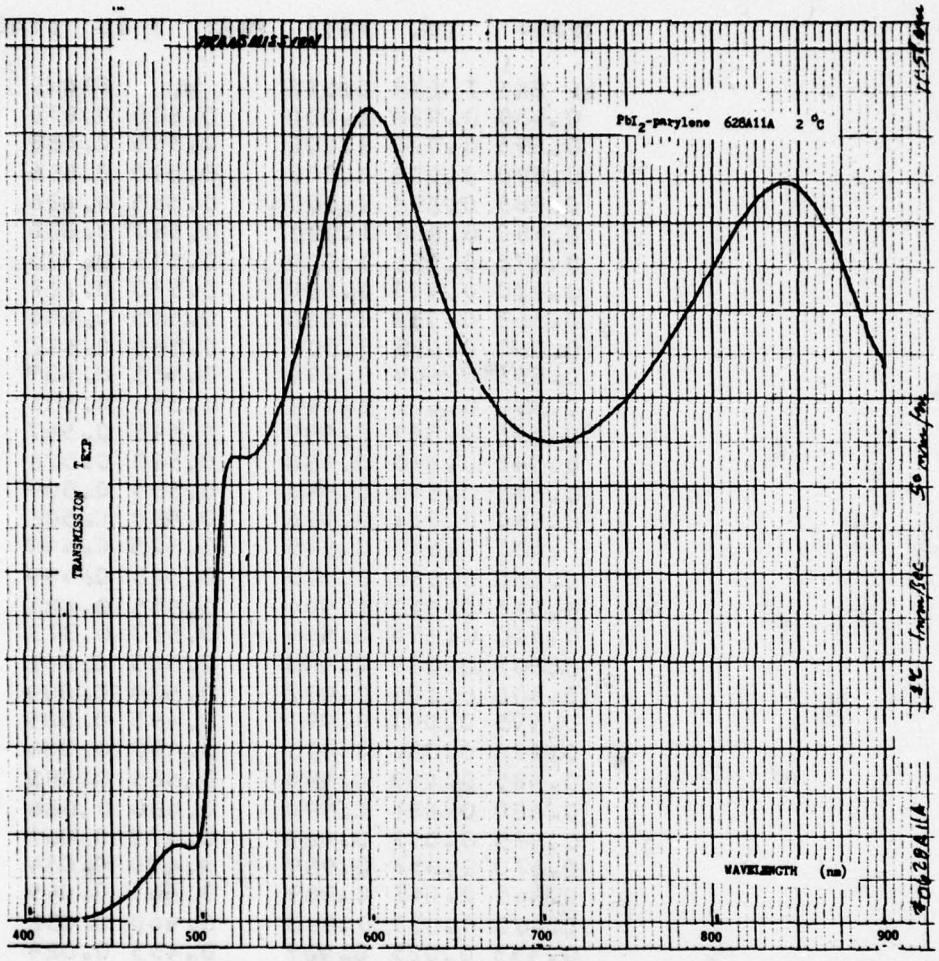

Figure 2.5-48. Transmission of PbI_2-parylene No. 628A11A at 2°C.

Table 2.5-12. Absorption edge transmission of PbI_2-parylene No. 628A11A at 2°C, from 600 to 420 nm.

TEMP= 2. PBI2 PARY 7-10 1208

WL EXP	T EXP	CALIB	WL	TRANS
0.600	0.928	1.000	0.600	0.869
0.595	0.927	1.000	0.595	0.868
0.590	0.912	1.000	0.590	0.854
0.585	0.890	1.000	0.585	0.833
0.580	0.855	1.000	0.580	0.801
0.575	0.819	1.000	0.575	0.767
0.570	0.771	1.000	0.570	0.722
0.565	0.729	1.000	0.565	0.683
0.560	0.682	1.000	0.560	0.639
0.555	0.645	0.999	0.555	0.605
0.550	0.610	0.999	0.550	0.572
0.545	0.582	0.999	0.545	0.546
0.540	0.559	0.998	0.540	0.525
0.535	0.541	0.998	0.535	0.508
0.530	0.532	0.996	0.530	0.500
0.525	0.530	0.995	0.525	0.499
0.520	0.532	0.995	0.520	0.501
0.515	0.518	0.994	0.515	0.488
0.510	0.400	0.994	0.510	0.377
0.505	0.210	0.993	0.505	0.198
0.500	0.100	0.992	0.500	0.094
0.495	0.085	0.991	0.495	0.080
0.490	0.089	0.990	0.490	0.084
0.485	0.089	0.990	0.485	0.084
0.480	0.081	0.990	0.480	0.077
0.475	0.071	0.989	0.475	0.067
0.470	0.058	0.989	0.470	0.055
0.465	0.044	0.989	0.465	0.042
0.460	0.033	0.988	0.460	0.031
0.455	0.025	0.987	0.455	0.024
0.450	0.018	0.985	0.450	0.017
0.445	0.011	0.984	0.445	0.010
0.440	0.009	0.983	0.440	0.009
0.435	0.004	0.981	0.435	0.004
0.430	0.003	0.980	0.430	0.003
0.425	0.002	0.979	0.425	0.002
0.420	0.001	0.978	0.420	0.001

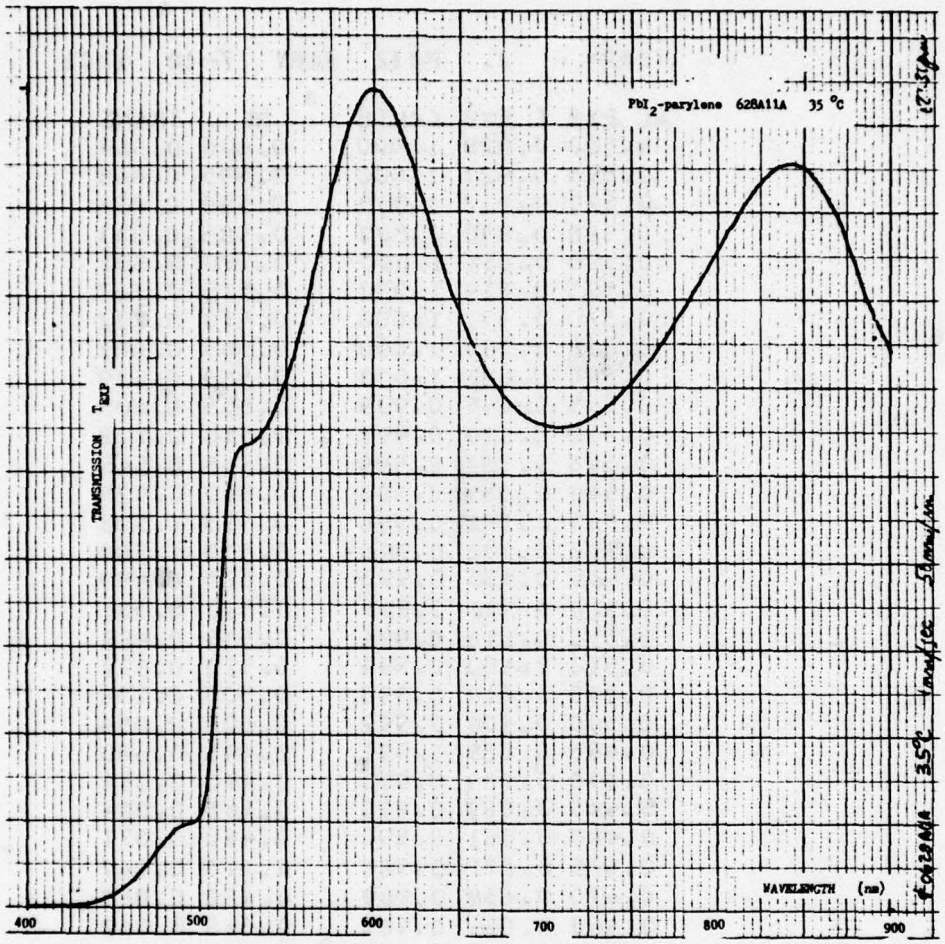

Figure 2.5-49. Transmission of PbI_2-parylene No. 628A11A at 35°C.

Table 2.5-13. Absorption edge transmission of PbI_2-parylene No. 628A11A at 35°C, from 600 to 420 nm.

TEMP= 35. PBI2 PARY 7-10 1243

WL EXP	T EXP	CALIB	WL	TRANS
0.600	0.938	1.000	0.600	0.869
0.595	0.939	1.000	0.595	0.870
0.590	0.925	1.000	0.590	0.857
0.585	0.903	1.000	0.585	0.837
0.580	0.870	1.000	0.580	0.806
0.575	0.831	1.000	0.575	0.770
0.570	0.784	1.000	0.570	0.726
0.565	0.741	1.000	0.565	0.687
0.560	0.693	1.000	0.560	0.642
0.555	0.655	0.999	0.555	0.607
0.550	0.620	0.999	0.550	0.575
0.545	0.590	0.999	0.545	0.547
0.540	0.564	0.998	0.540	0.524
0.535	0.549	0.998	0.535	0.510
0.530	0.537	0.996	0.530	0.500
0.525	0.531	0.995	0.525	0.494
0.520	0.523	0.995	0.520	0.487
0.515	0.489	0.994	0.515	0.456
0.510	0.358	0.994	0.510	0.334
0.505	0.200	0.993	0.505	0.187
0.500	0.114	0.992	0.500	0.106
0.495	0.099	0.991	0.495	0.093
0.490	0.096	0.990	0.490	0.090
0.485	0.092	0.990	0.485	0.086
0.480	0.080	0.990	0.480	0.075
0.475	0.070	0.989	0.475	0.066
0.470	0.056	0.989	0.470	0.052
0.465	0.043	0.989	0.465	0.040
0.460	0.033	0.988	0.460	0.031
0.455	0.024	0.987	0.455	0.023
0.450	0.018	0.985	0.450	0.017
0.445	0.011	0.984	0.445	0.010
0.440	0.008	0.983	0.440	0.008
0.435	0.004	0.981	0.435	0.004
0.430	0.003	0.980	0.430	0.003
0.425	0.002	0.979	0.425	0.002
0.420	0.002	0.978	0.420	0.002

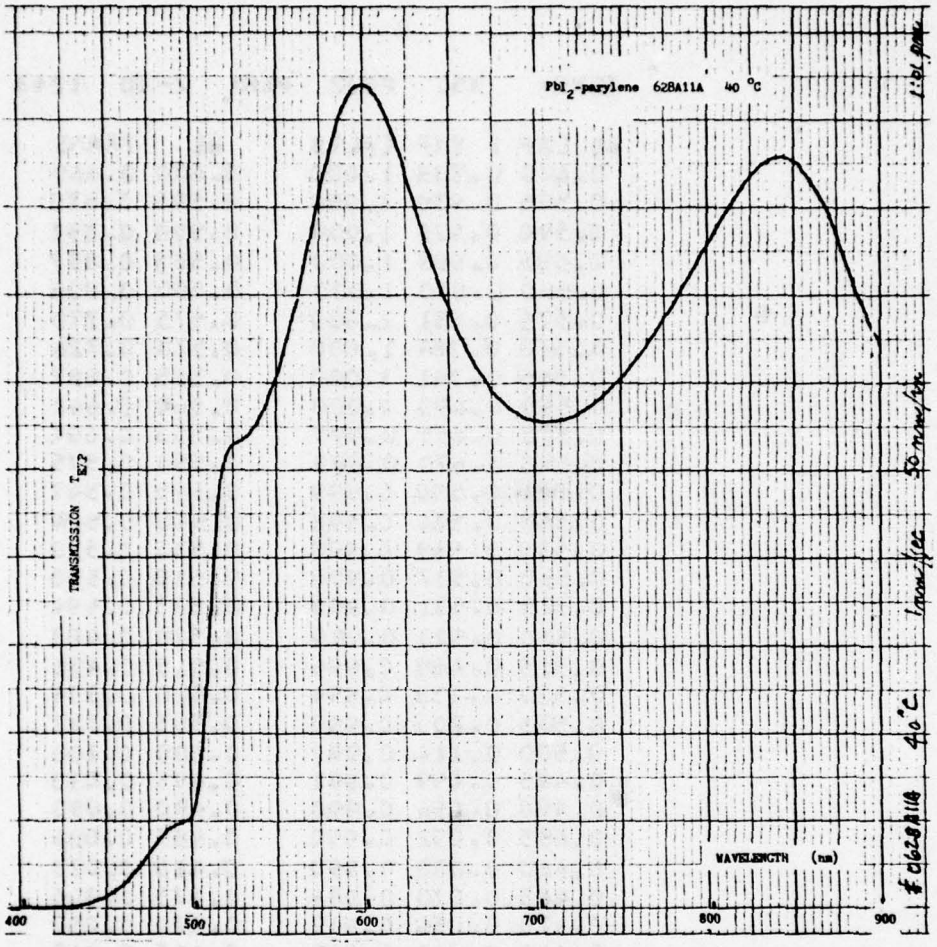

Figure 2.5-50. Transmission of PbI_2-parylene No. 628A11A at 40°C.

Table 2.5-14. Absorption edge transmission of PbI_2-parylene No. 628A11A at 40°C from 600 to 420 nm.

TEMP= 40. PBI2 PARY 7-10 1.12

WL EXP	T EXP	CALIB	WL	TRANS
0.600	0.941	1.000	0.600	0.871
0.595	0.941	1.000	0.595	0.871
0.590	0.930	1.000	0.590	0.861
0.585	0.910	1.000	0.585	0.842
0.580	0.876	1.000	0.580	0.811
0.575	0.837	1.000	0.575	0.775
0.570	0.790	1.000	0.570	0.731
0.565	0.745	1.000	0.565	0.690
0.560	0.698	1.000	0.560	0.646
0.555	0.660	0.999	0.555	0.611
0.550	0.621	0.999	0.550	0.575
0.545	0.593	0.999	0.545	0.549
0.540	0.569	0.998	0.540	0.528
0.535	0.551	0.998	0.535	0.511
0.530	0.540	0.996	0.530	0.502
0.525	0.532	0.995	0.525	0.495
0.520	0.523	0.995	0.520	0.486
0.515	0.483	0.994	0.515	0.450
0.510	0.350	0.994	0.510	0.326
0.505	0.200	0.993	0.505	0.186
0.500	0.118	0.992	0.500	0.110
0.495	0.100	0.991	0.495	0.093
0.490	0.098	0.990	0.490	0.092
0.485	0.091	0.990	0.485	0.085
0.480	0.081	0.990	0.480	0.076
0.475	0.069	0.989	0.475	0.065
0.470	0.054	0.989	0.470	0.051
0.465	0.043	0.989	0.465	0.040
0.460	0.031	0.988	0.460	0.029
0.455	0.023	0.987	0.455	0.022
0.450	0.016	0.985	0.450	0.015
0.445	0.011	0.984	0.445	0.010
0.440	0.008	0.983	0.440	0.008
0.435	0.003	0.981	0.435	0.003
0.430	0.002	0.980	0.430	0.002
0.425	0.001	0.979	0.425	0.001
0.420	0.0	0.978	0.420	0.0

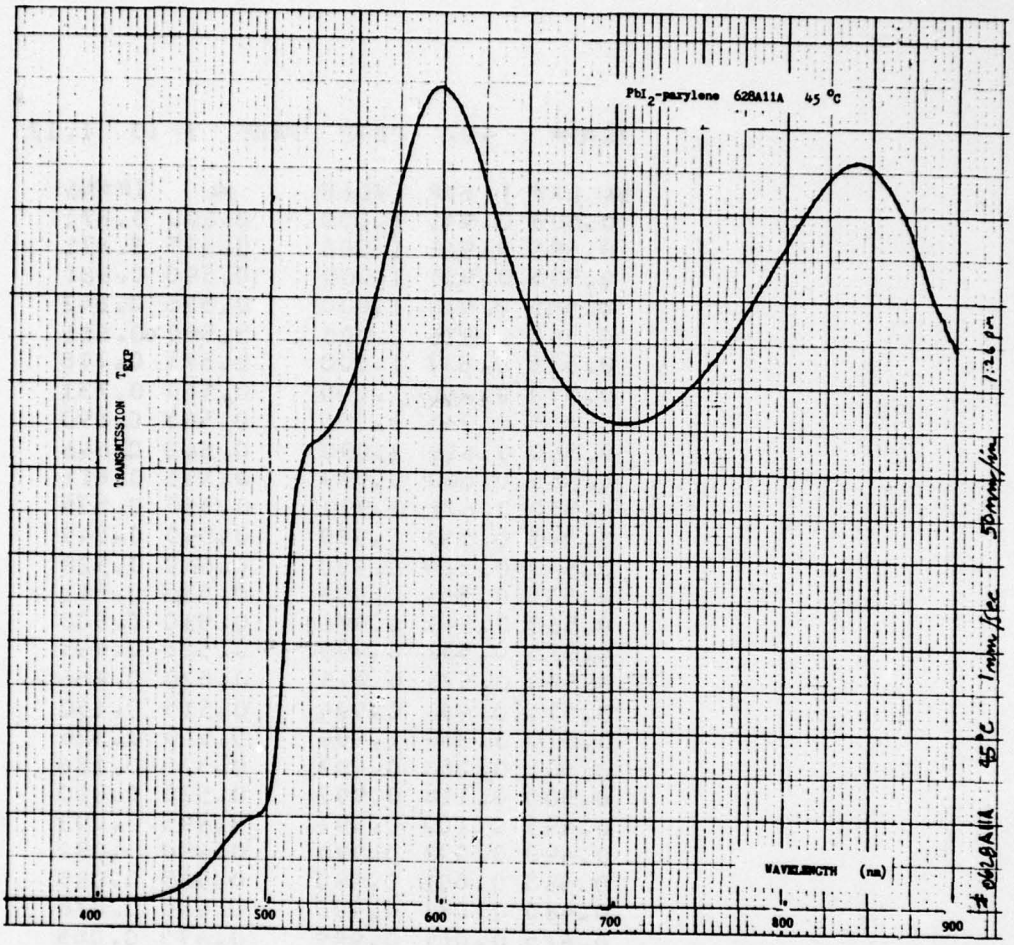

Figure 2.5-51. Transmission of PbI_2-parylene No. 628A11A at 45°C.

Table 2.5-15. Absorption edge transmission of PbI_2-parylene No. 628A11A at 45°C, from 600 to 420 nm.

TEMP= 45. PBI2 PARY 7-10 1.39

WL EXP	T EXP	CALIB	WL	TRANS
0.600	0.941	1.000	0.600	0.869
0.595	0.942	1.000	0.595	0.870
0.590	0.930	1.000	0.590	0.859
0.585	0.910	1.000	0.585	0.840
0.580	0.874	1.000	0.580	0.807
0.575	0.837	1.000	0.575	0.773
0.570	0.790	1.000	0.570	0.730
0.565	0.745	1.000	0.565	0.688
0.560	0.696	1.000	0.560	0.643
0.555	0.659	0.999	0.555	0.609
0.550	0.621	0.999	0.550	0.574
0.545	0.593	0.999	0.545	0.548
0.540	0.568	0.998	0.540	0.526
0.535	0.550	0.998	0.535	0.509
0.530	0.539	0.996	0.530	0.500
0.525	0.531	0.995	0.525	0.493
0.520	0.520	0.995	0.520	0.483
0.515	0.477	0.994	0.515	0.443
0.510	0.339	0.994	0.510	0.315
0.505	0.195	0.993	0.505	0.181
0.500	0.119	0.992	0.500	0.111
0.495	0.102	0.991	0.495	0.095
0.490	0.098	0.990	0.490	0.091
0.485	0.091	0.990	0.485	0.085
0.480	0.080	0.990	0.480	0.075
0.475	0.069	0.989	0.475	0.064
0.470	0.054	0.989	0.470	0.050
0.465	0.042	0.989	0.465	0.039
0.460	0.030	0.988	0.460	0.028
0.455	0.023	0.987	0.455	0.022
0.450	0.017	0.985	0.450	0.016
0.445	0.010	0.984	0.445	0.009
0.440	0.008	0.983	0.440	0.008
0.435	0.005	0.981	0.435	0.005
0.430	0.003	0.980	0.430	0.003
0.425	0.001	0.979	0.425	0.001
0.420	0.0	0.978	0.420	0.0

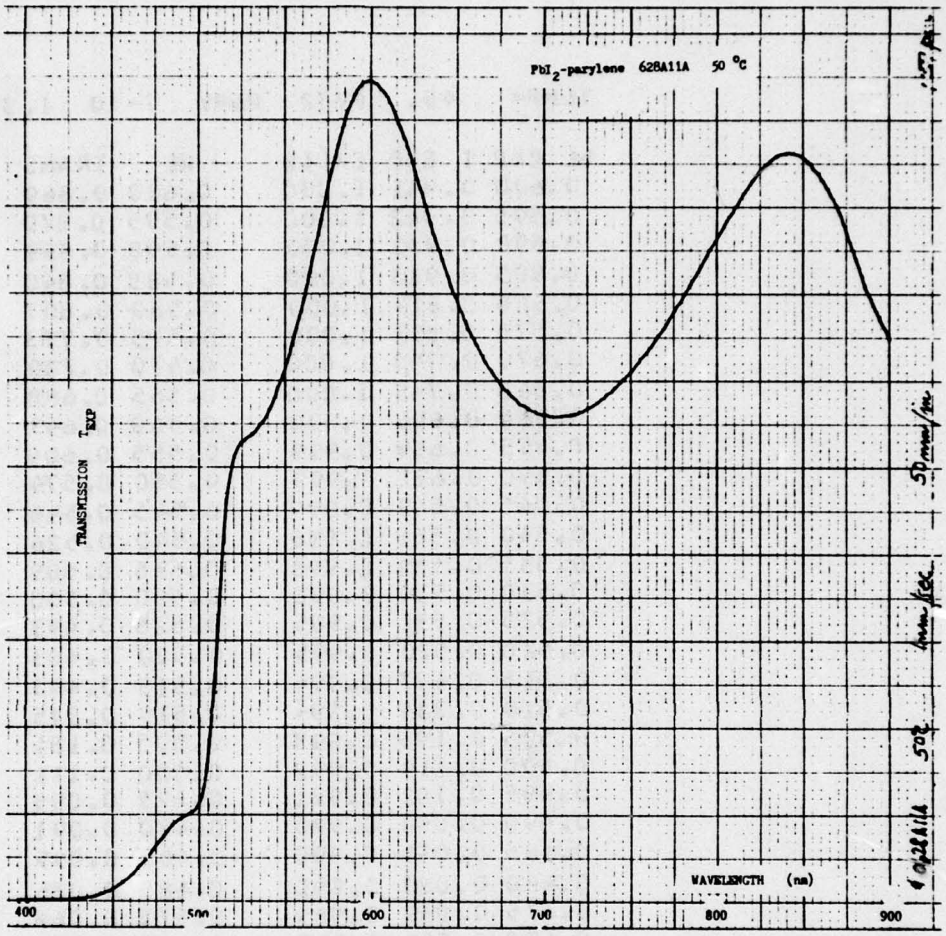

Figure 2.5-52. Transmission of PbI_2-parylene No. 628A11A at 50°C.

Table 2.5-16. Absorption edge transmission of PbI_2-parylene No. 628A11A at 50°C, from 600 to 420 nm.

TEMP= 50. PBI2 PARY 7-10 2.07

WL EXP	T EXP	CALIB	WL	TRANS
0.600	0.944	1.000	0.600	0.870
0.595	0.944	1.000	0.595	0.870
0.590	0.934	1.000	0.590	0.861
0.585	0.911	1.000	0.585	0.840
0.580	0.878	1.000	0.580	0.809
0.575	0.839	1.000	0.575	0.773
0.570	0.790	1.000	0.570	0.728
0.565	0.748	1.000	0.565	0.689
0.560	0.699	1.000	0.560	0.644
0.555	0.660	0.999	0.555	0.609
0.550	0.621	0.999	0.550	0.573
0.545	0.594	0.999	0.545	0.548
0.540	0.569	0.998	0.540	0.525
0.535	0.551	0.998	0.535	0.509
0.530	0.539	0.996	0.530	0.499
0.525	0.532	0.995	0.525	0.493
0.520	0.517	0.995	0.520	0.479
0.515	0.470	0.994	0.515	0.436
0.510	0.333	0.994	0.510	0.309
0.505	0.195	0.993	0.505	0.181
0.500	0.121	0.992	0.500	0.112
0.495	0.103	0.991	0.495	0.096
0.490	0.099	0.990	0.490	0.092
0.485	0.091	0.990	0.485	0.085
0.480	0.081	0.990	0.480	0.075
0.475	0.069	0.989	0.475	0.064
0.470	0.054	0.989	0.470	0.050
0.465	0.042	0.989	0.465	0.039
0.460	0.030	0.988	0.460	0.028
0.455	0.022	0.987	0.455	0.021
0.450	0.017	0.985	0.450	0.016
0.445	0.010	0.984	0.445	0.009
0.440	0.008	0.983	0.440	0.008
0.435	0.004	0.981	0.435	0.004
0.430	0.002	0.980	0.430	0.002
0.425	0.001	0.979	0.425	0.001
0.420	0.0	0.978	0.420	0.0

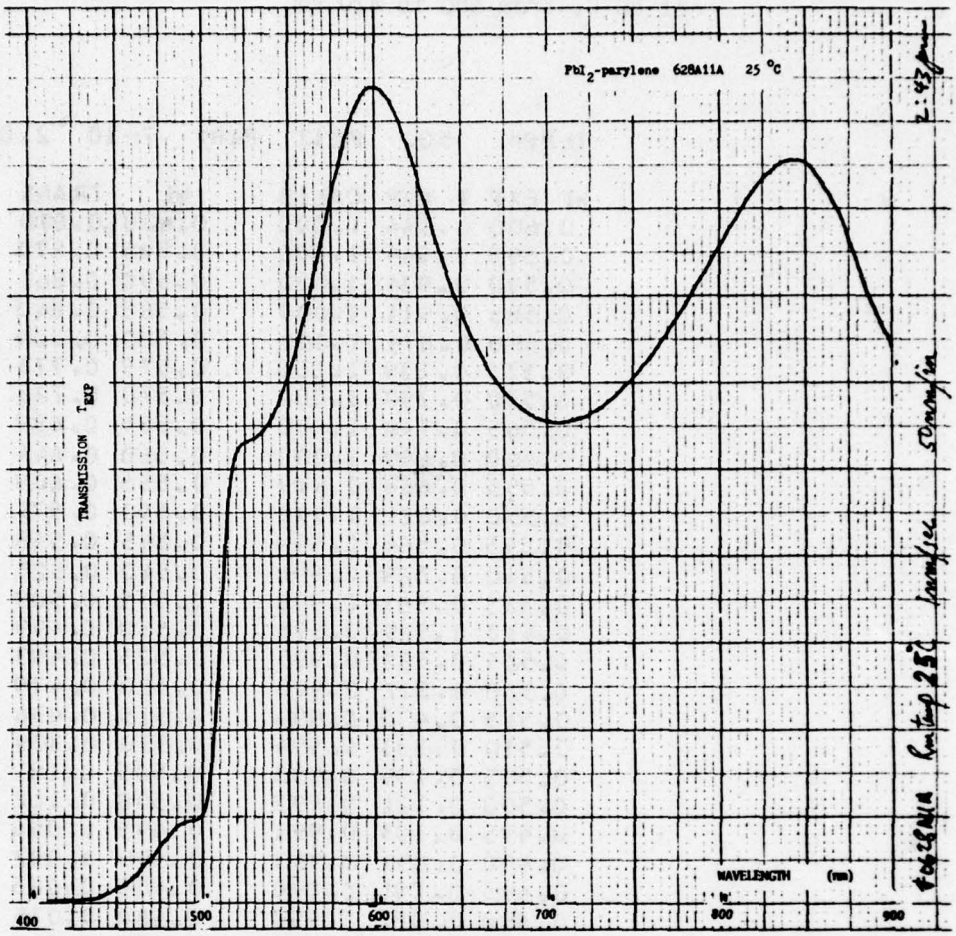

Figure 2.5-53. Transmission of PbI_2-parylene No. 628A11A at 25°C (2).

Table 2.5-17. Absorption edge transmission of PbI_2-parylene No. 628A11A at 25°C, from 600 to 420 nm (after 50°C curve).

TEMP= 25. PBI2 PARY 7-10 2.53

WL EXP	T EXP	CALIB	WL	TRANS
0.600	0.940	1.000	0.600	0.871
0.595	0.939	1.000	0.595	0.870
0.590	0.927	1.000	0.590	0.859
0.585	0.904	1.000	0.585	0.838
0.580	0.870	1.000	0.580	0.806
0.575	0.832	1.000	0.575	0.771
0.570	0.786	1.000	0.570	0.728
0.565	0.742	1.000	0.565	0.687
0.560	0.694	1.000	0.560	0.643
0.555	0.657	0.999	0.555	0.609
0.550	0.619	0.999	0.550	0.574
0.545	0.591	0.999	0.545	0.548
0.540	0.565	0.998	0.540	0.525
0.535	0.549	0.998	0.535	0.510
0.530	0.538	0.996	0.530	0.500
0.525	0.532	0.995	0.525	0.495
0.520	0.526	0.995	0.520	0.490
0.515	0.493	0.994	0.515	0.460
0.510	0.365	0.994	0.510	0.340
0.505	0.205	0.993	0.505	0.191
0.500	0.116	0.992	0.500	0.108
0.495	0.099	0.991	0.495	0.093
0.490	0.097	0.990	0.490	0.091
0.485	0.092	0.990	0.485	0.086
0.480	0.082	0.990	0.480	0.077
0.475	0.069	0.989	0.475	0.065
0.470	0.054	0.989	0.470	0.051
0.465	0.044	0.989	0.465	0.041
0.460	0.032	0.988	0.460	0.030
0.455	0.025	0.987	0.455	0.023
0.450	0.019	0.985	0.450	0.018
0.445	0.012	0.984	0.445	0.011
0.440	0.010	0.983	0.440	0.009
0.435	0.004	0.981	0.435	0.004
0.430	0.004	0.980	0.430	0.004
0.425	0.003	0.979	0.425	0.003
0.420	0.002	0.978	0.420	0.002

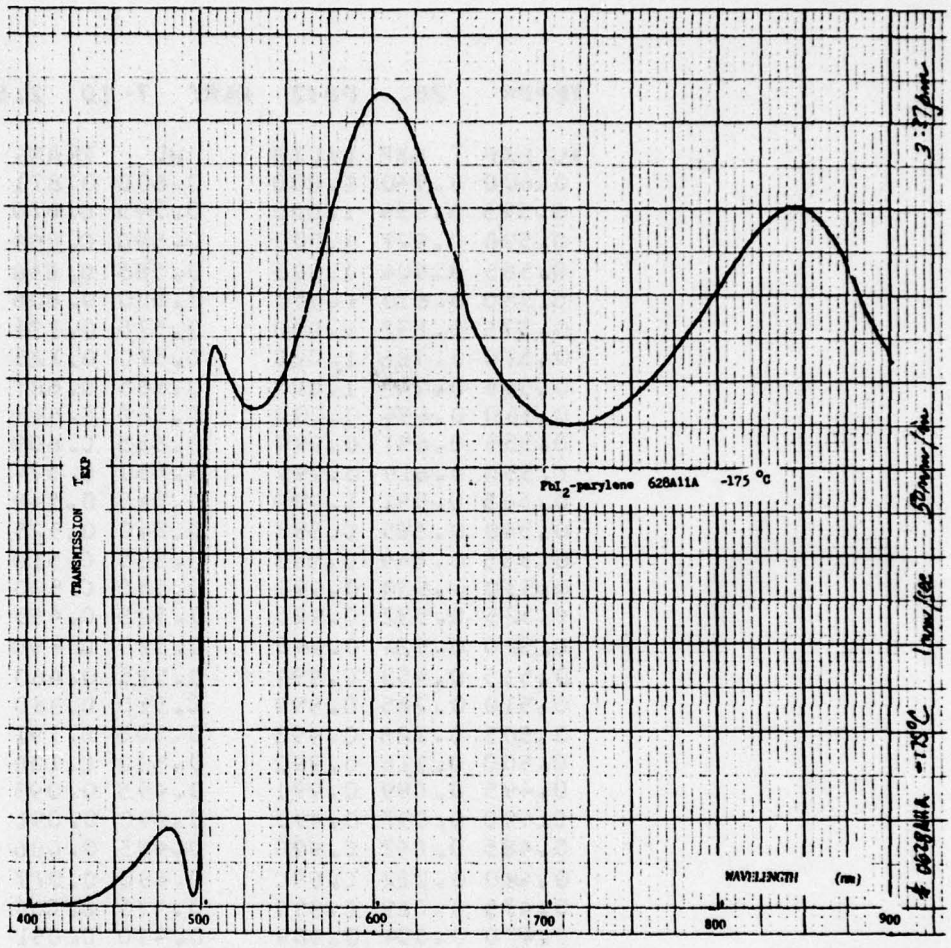

Figure 2.5-54. Transmission of PbI_2-parylene No. 62A11A at -175°C.

Table 2.5-18. Absorption edge transmission of PbI_2-parylene No. 628A11A at -175°C, from 600 to 420 nm.

TEMP= -175 PBI2 PARY 7-10 3.48

WL EXP	T EXP	CALIB	WL	TRANS
0.600	0.898	1.000	0.600	0.839
0.595	0.886	1.000	0.595	0.828
0.590	0.813	1.000	0.590	0.760
0.585	0.839	1.000	0.585	0.784
0.580	0.805	1.000	0.580	0.752
0.575	0.772	1.000	0.575	0.721
0.570	0.733	1.000	0.570	0.685
0.565	0.700	1.000	0.565	0.654
0.560	0.663	1.000	0.560	0.620
0.555	0.638	0.999	0.555	0.597
0.550	0.611	0.999	0.550	0.572
0.545	0.593	0.999	0.545	0.555
0.540	0.578	0.998	0.540	0.541
0.535	0.570	0.998	0.535	0.534
0.530	0.569	0.996	0.530	0.534
0.525	0.571	0.995	0.525	0.536
0.520	0.586	0.995	0.520	0.550
0.515	0.603	0.994	0.515	0.567
0.510	0.628	0.994	0.510	0.590
0.505	0.611	0.993	0.505	0.575
0.500	0.235	0.992	0.500	0.221
0.495	0.012	0.991	0.495	0.011
0.490	0.046	0.990	0.490	0.043
0.485	0.081	0.990	0.485	0.076
0.480	0.088	0.990	0.480	0.083
0.475	0.081	0.989	0.475	0.077
0.470	0.070	0.989	0.470	0.066
0.465	0.059	0.989	0.465	0.056
0.460	0.045	0.988	0.460	0.043
0.455	0.037	0.987	0.455	0.035
0.450	0.028	0.985	0.450	0.027
0.445	0.020	0.984	0.445	0.019
0.440	0.012	0.983	0.440	0.011
0.435	0.009	0.981	0.435	0.009
0.430	0.004	0.980	0.430	0.004
0.425	0.002	0.979	0.425	0.002
0.420	0.001	0.978	0.420	0.001

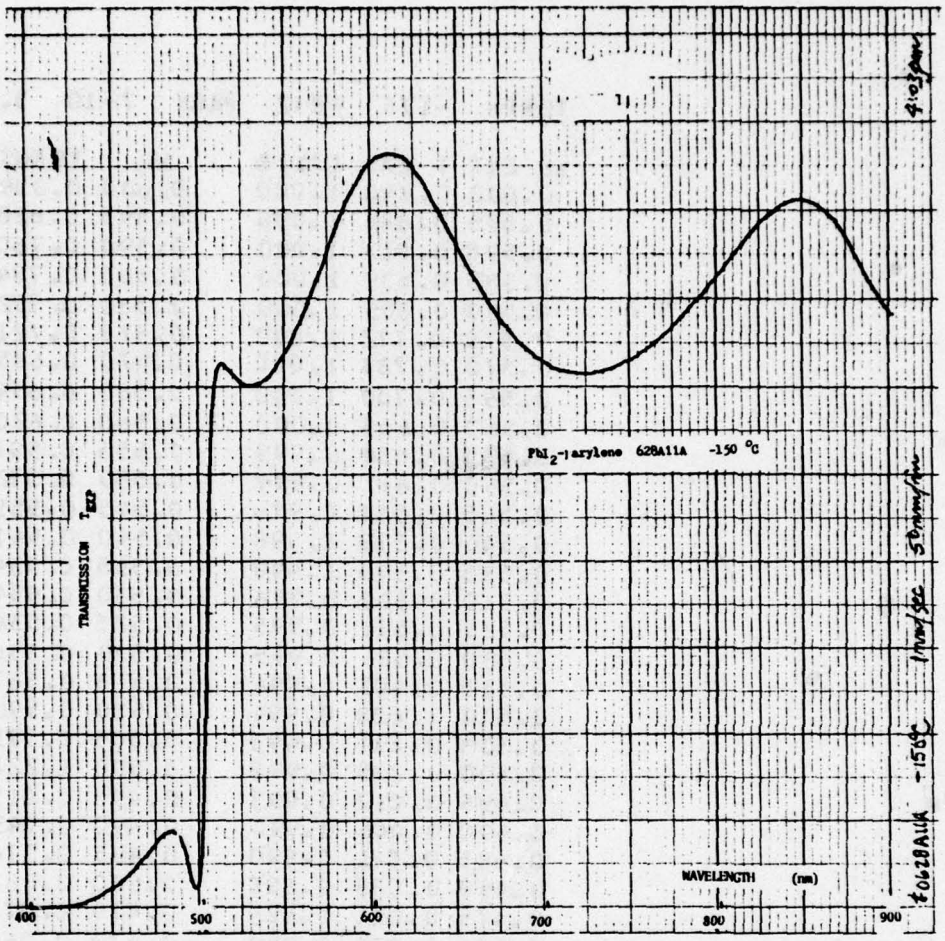

Figure 2.5-55. Transmission of PbI_2-parylene No. 628A11A at -150°C.

Table 2.5-19. Absorption edge transmission of PbI_2-parylene No. 628A11A at -150°C from 600 to 420 nm.

TEMP= -150 PBI2 PARY 7-10 4.15

WL EXP	T EXP	CALIB	WL	TRANS
0.600	0.853	1.000	0.600	0.859
0.595	0.848	1.000	0.595	0.854
0.590	0.835	1.000	0.590	0.841
0.585	0.820	1.000	0.585	0.826
0.580	0.799	1.000	0.580	0.805
0.575	0.777	1.000	0.575	0.782
0.570	0.751	1.000	0.570	0.756
0.565	0.729	1.000	0.565	0.734
0.560	0.701	1.000	0.560	0.706
0.555	0.682	0.999	0.555	0.687
0.550	0.661	0.999	0.550	0.666
0.545	0.643	0.999	0.545	0.648
0.540	0.630	0.998	0.540	0.636
0.535	0.619	0.998	0.535	0.625
0.530	0.611	0.996	0.530	0.618
0.525	0.610	0.995	0.525	0.617
0.520	0.613	0.995	0.520	0.620
0.515	0.620	0.994	0.515	0.628
0.510	0.628	0.994	0.510	0.636
0.505	0.569	0.993	0.505	0.577
0.500	0.140	0.992	0.500	0.142
0.495	0.024	0.991	0.495	0.024
0.490	0.057	0.990	0.490	0.058
0.485	0.084	0.990	0.485	0.085
0.480	0.089	0.990	0.480	0.091
0.475	0.081	0.989	0.475	0.082
0.470	0.070	0.989	0.470	0.071
0.465	0.058	0.989	0.465	0.059
0.460	0.045	0.988	0.460	0.046
0.455	0.036	0.987	0.455	0.037
0.450	0.025	0.985	0.450	0.026
0.445	0.019	0.984	0.445	0.019
0.440	0.011	0.983	0.440	0.011
0.435	0.009	0.981	0.435	0.009
0.430	0.003	0.980	0.430	0.003
0.425	0.001	0.979	0.425	0.001
0.420	0.0	0.978	0.420	0.0

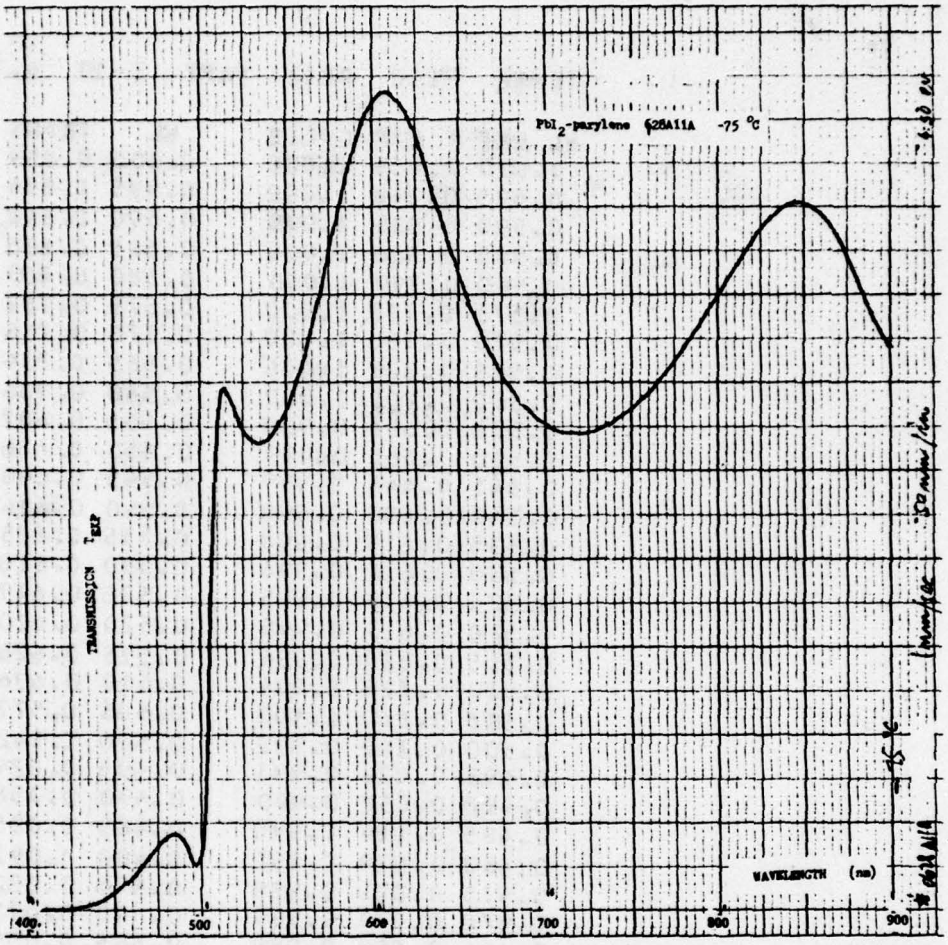

Figure 2.5-56. Transmission of PbI_2-parylene No. 628A11A at -75°C.

Table 2.5-20. Absorption edge transmission of PbI_2-parylene No. 628A11A at -75°C from 600 to 420 nm.

TEMP= -75. PBI2 PARY 7-10 5.06

WL EXP	T EXP	CALIB	WL	TRANS
0.600	0.920	1.000	0.600	0.861
0.595	0.901	1.000	0.595	0.843
0.590	0.869	1.000	0.590	0.813
0.585	0.838	1.000	0.585	0.784
0.580	0.796	1.000	0.580	0.745
0.575	0.753	1.000	0.575	0.704
0.570	0.709	1.000	0.570	0.663
0.565	0.670	1.000	0.565	0.627
0.560	0.630	1.000	0.560	0.589
0.555	0.600	0.999	0.555	0.562
0.550	0.573	0.999	0.550	0.537
0.545	0.554	0.999	0.545	0.519
0.540	0.540	0.998	0.540	0.506
0.535	0.533	0.998	0.535	0.500
0.530	0.537	0.996	0.530	0.504
0.525	0.545	0.995	0.525	0.512
0.520	0.568	0.995	0.520	0.534
0.515	0.590	0.994	0.515	0.555
0.510	0.579	0.994	0.510	0.545
0.505	0.360	0.993	0.505	0.339
0.500	0.080	0.992	0.500	0.075
0.495	0.054	0.991	0.495	0.051
0.490	0.074	0.990	0.490	0.070
0.485	0.088	0.990	0.485	0.083
0.480	0.085	0.990	0.480	0.080
0.475	0.078	0.989	0.475	0.074
0.470	0.064	0.989	0.470	0.061
0.465	0.052	0.989	0.465	0.049
0.460	0.040	0.988	0.460	0.038
0.455	0.031	0.987	0.455	0.029
0.450	0.022	0.985	0.450	0.021
0.445	0.017	0.984	0.445	0.016
0.440	0.010	0.983	0.440	0.010
0.435	0.007	0.981	0.435	0.007
0.430	0.003	0.980	0.430	0.003
0.425	0.001	0.979	0.425	0.001
0.420	0.0	0.978	0.420	0.0

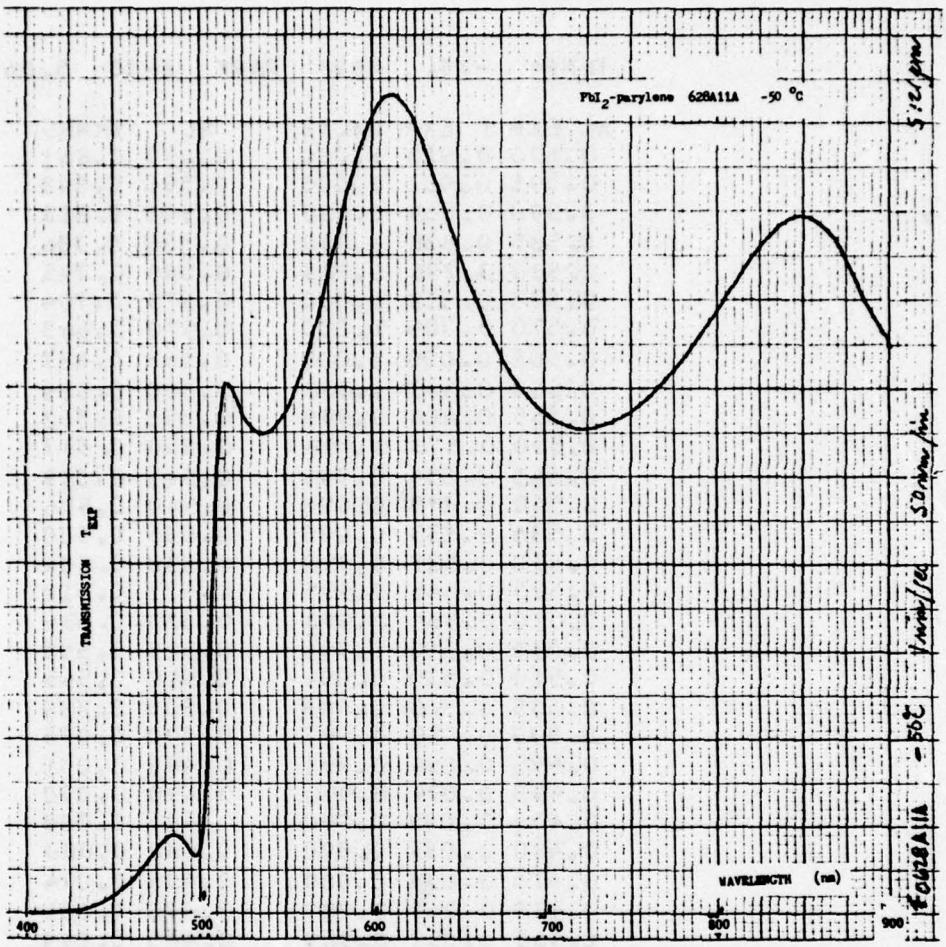

Figure 2.5-57. Transmission of PbI_2-parylene No. 628A11A at -50°C.

Table 2.5-21. Absorption edge transmission of PbI_2-parylene No. 628A11A at -50°C from 600 to 420 nm.

TEMP= -50. PBI2 PARY 7-10 5.31

WL EXP	T EXP	CALIB	WL	TRANS
0.600	0.903	1.000	0.600	0.845
0.595	0.883	1.000	0.595	0.826
0.590	0.852	1.000	0.590	0.797
0.585	0.820	1.000	0.585	0.767
0.580	0.780	1.000	0.580	0.730
0.575	0.740	1.000	0.575	0.692
0.570	0.698	1.000	0.570	0.653
0.565	0.661	1.000	0.565	0.618
0.560	0.624	1.000	0.560	0.584
0.555	0.599	0.999	0.555	0.561
0.550	0.575	0.999	0.550	0.538
0.545	0.560	0.999	0.545	0.524
0.540	0.549	0.998	0.540	0.515
0.535	0.546	0.998	0.535	0.512
0.530	0.551	0.996	0.530	0.518
0.525	0.564	0.995	0.525	0.530
0.520	0.587	0.995	0.520	0.552
0.515	0.602	0.994	0.515	0.567
0.510	0.546	0.994	0.510	0.514
0.505	0.300	0.993	0.505	0.283
0.500	0.086	0.992	0.500	0.081
0.495	0.068	0.991	0.495	0.064
0.490	0.082	0.990	0.490	0.077
0.485	0.090	0.990	0.485	0.085
0.480	0.088	0.990	0.480	0.083
0.475	0.078	0.989	0.475	0.074
0.470	0.064	0.989	0.470	0.061
0.465	0.051	0.989	0.465	0.048
0.460	0.039	0.988	0.460	0.037
0.455	0.030	0.987	0.455	0.028
0.450	0.021	0.985	0.450	0.020
0.445	0.015	0.984	0.445	0.014
0.440	0.010	0.983	0.440	0.010
0.435	0.006	0.981	0.435	0.006
0.430	0.003	0.980	0.430	0.003
0.425	0.001	0.979	0.425	0.001
0.420	0.0	0.978	0.420	0.0

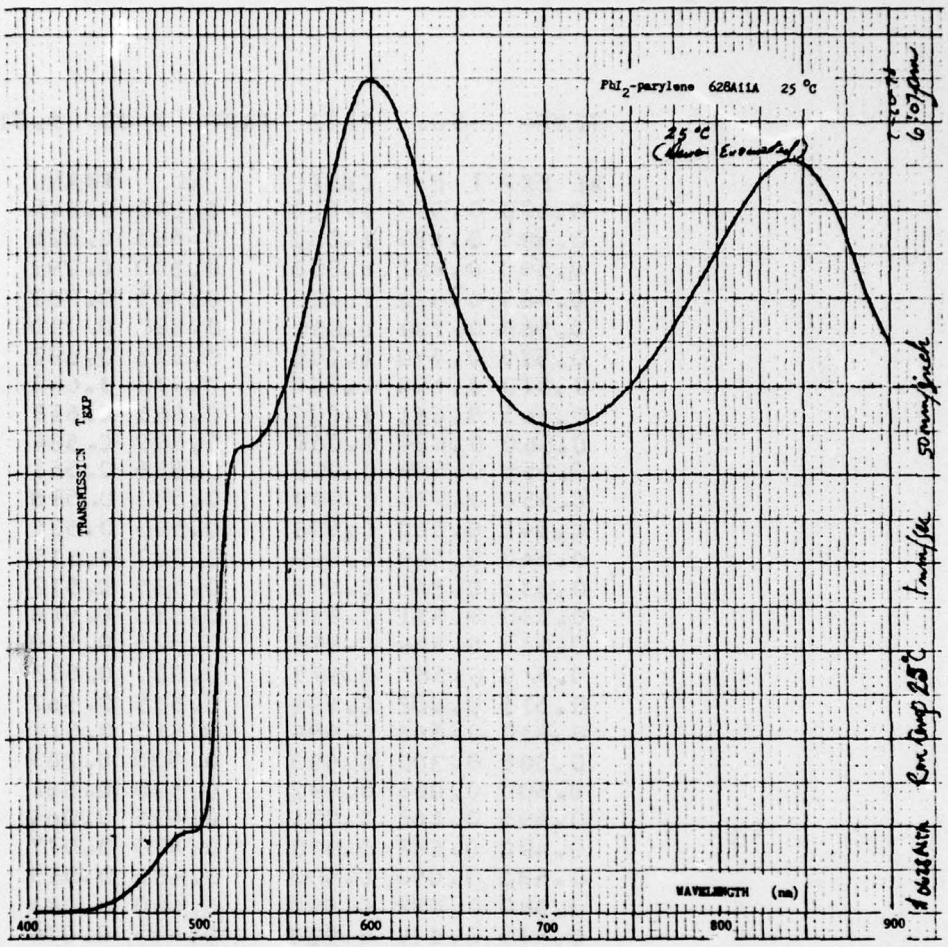

Figure 2.5-58. Transmission of PbI_2-parylene No. 628A11A at 25°C(3).

Table 2.5-22. Absorption edge transmission of PbI_2-parylene No. 628A11A at 25°C from 600 to 420 nm (after-50°C curve).

TEMP= 25. PBI2 PARY 7-10 6.18

WL EXP	T EXP	CALIB	WL	TRANS
0.600	0.947	1.000	0.600	0.870
0.595	0.947	1.000	0.595	0.870
0.590	0.931	1.000	0.590	0.855
0.585	0.910	1.000	0.585	0.836
0.580	0.872	1.000	0.580	0.801
0.575	0.831	1.000	0.575	0.763
0.570	0.783	1.000	0.570	0.719
0.565	0.740	1.000	0.565	0.680
0.560	0.691	1.000	0.560	0.635
0.555	0.652	0.999	0.555	0.600
0.550	0.615	0.999	0.550	0.566
0.545	0.588	0.999	0.545	0.541
0.540	0.562	0.998	0.540	0.517
0.535	0.548	0.998	0.535	0.504
0.530	0.538	0.996	0.530	0.496
0.525	0.532	0.995	0.525	0.491
0.520	0.530	0.995	0.520	0.489
0.515	0.498	0.994	0.515	0.460
0.510	0.360	0.994	0.510	0.333
0.505	0.200	0.993	0.505	0.185
0.500	0.112	0.992	0.500	0.104
0.495	0.098	0.991	0.495	0.091
0.490	0.094	0.990	0.490	0.087
0.485	0.091	0.990	0.485	0.084
0.480	0.081	0.990	0.480	0.075
0.475	0.069	0.989	0.475	0.064
0.470	0.055	0.989	0.470	0.051
0.465	0.043	0.989	0.465	0.040
0.460	0.032	0.988	0.460	0.030
0.455	0.023	0.987	0.455	0.021
0.450	0.017	0.985	0.450	0.016
0.445	0.011	0.984	0.445	0.010
0.440	0.008	0.983	0.440	0.007
0.435	0.004	0.981	0.435	0.004
0.430	0.002	0.980	0.430	0.002
0.425	0.001	0.979	0.425	0.001
0.420	0.0	0.978	0.420	0.0

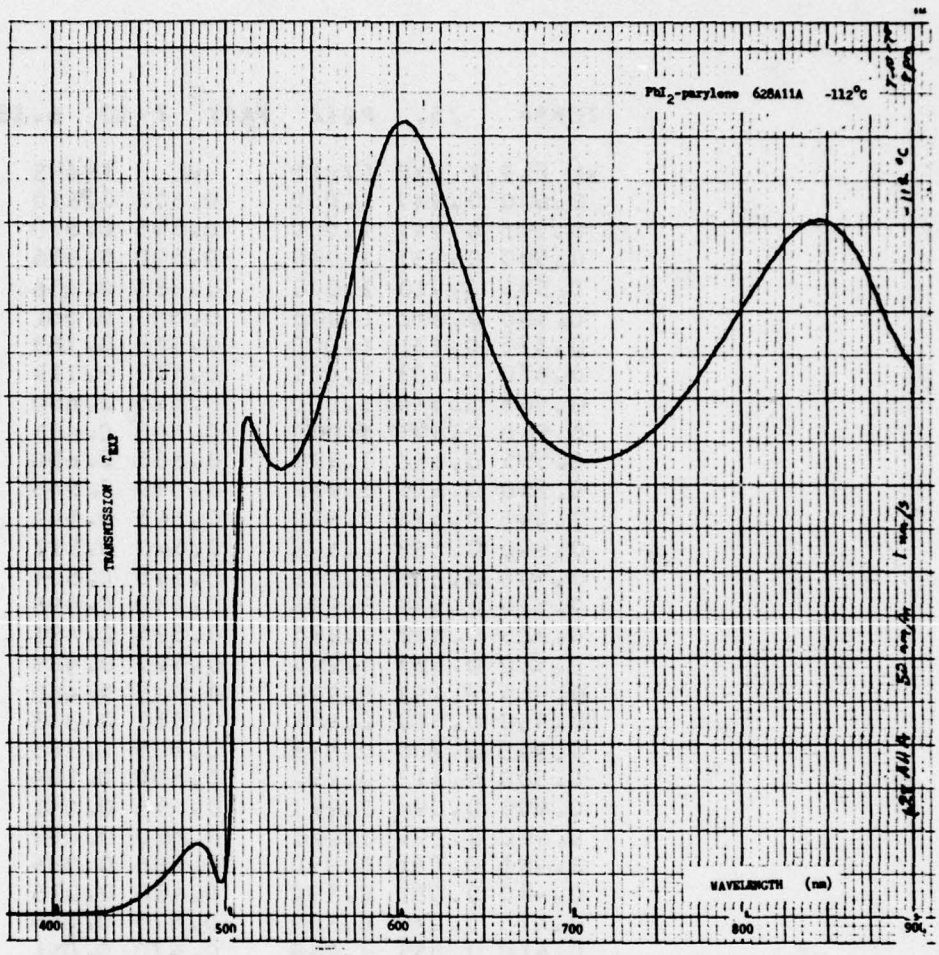

Figure 2.5-59. Transmission of PbI_2-parylene No. 628A11A at -112°C.

Table 2.5-23. Absorption edge transmission of PbI_2-parylene No. 628A11A at -112°C, from 600 to 420 nm.

TEMP= -112 PBI2 PARY 7-10 8.08

WL EXP	T EXP	CALIB	WL	TRANS
0.600	0.918	1.000	0.600	0.871
0.595	0.908	1.000	0.595	0.861
0.590	0.884	1.000	0.590	0.839
0.585	0.855	1.000	0.585	0.811
0.580	0.811	1.000	0.580	0.769
0.575	0.771	1.000	0.575	0.731
0.570	0.722	1.000	0.570	0.685
0.565	0.681	1.000	0.565	0.646
0.560	0.638	1.000	0.560	0.605
0.555	0.604	0.999	0.555	0.574
0.550	0.571	0.999	0.550	0.542
0.545	0.550	0.999	0.545	0.522
0.540	0.531	0.998	0.540	0.505
0.535	0.521	0.998	0.535	0.495
0.530	0.518	0.996	0.530	0.493
0.525	0.521	0.995	0.525	0.497
0.520	0.539	0.995	0.520	0.514
0.515	0.561	0.994	0.515	0.535
0.510	0.578	0.994	0.510	0.552
0.505	0.437	0.993	0.505	0.418
0.500	0.078	0.992	0.500	0.075
0.495	0.041	0.991	0.495	0.039
0.490	0.067	0.990	0.490	0.064
0.485	0.082	0.990	0.485	0.079
0.480	0.084	0.990	0.480	0.080
0.475	0.077	0.989	0.475	0.074
0.470	0.063	0.989	0.470	0.060
0.465	0.052	0.989	0.465	0.050
0.460	0.040	0.988	0.460	0.038
0.455	0.031	0.987	0.455	0.030
0.450	0.023	0.985	0.450	0.022
0.445	0.018	0.984	0.445	0.017
0.440	0.011	0.983	0.440	0.011
0.435	0.009	0.981	0.435	0.009
0.430	0.004	0.980	0.430	0.004
0.425	0.003	0.979	0.425	0.003
0.420	0.002	0.978	0.420	0.002

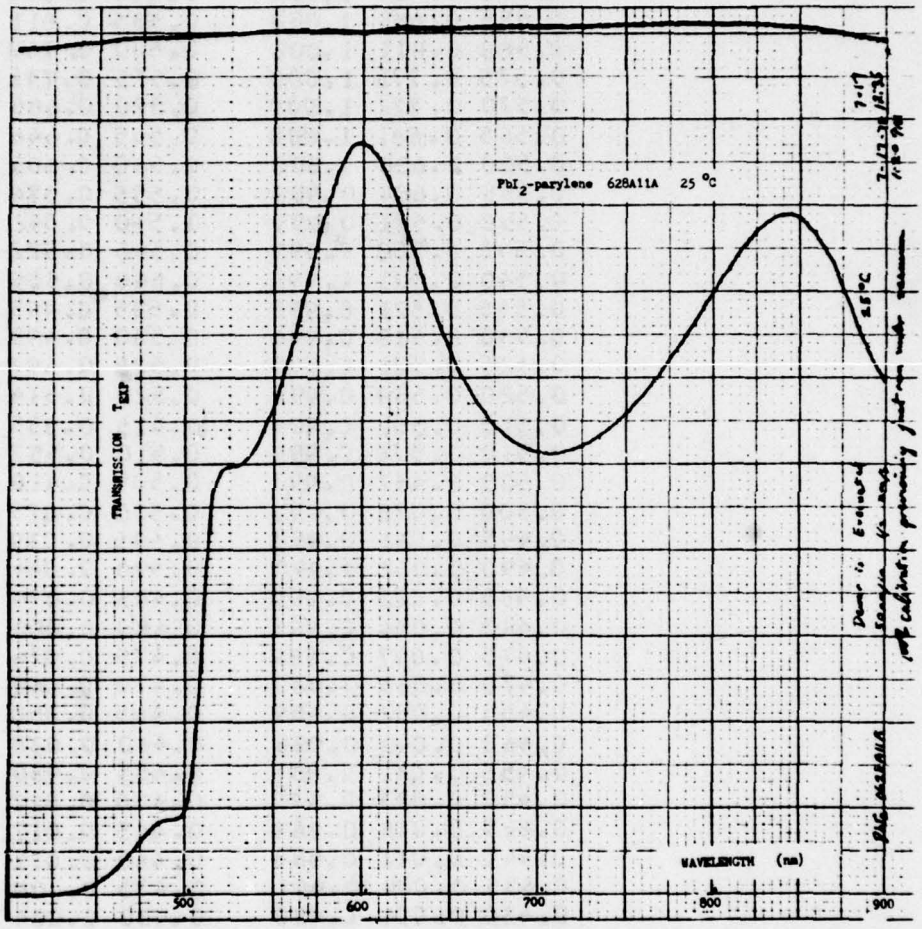

Figure 2.5-60. Transmission of PbI_2-parylene No. 628A11A at 25°C (4).

Table 2.5-24. High-resolution transmission scan, PbI_2-parylene No. 628A11A at 25°C.

TEMP= 25. PBI2 PARY 628A 11-A 7-17 1.50

WL EXP	T EXP	CALIB	WL	TRANS
0.525	0.498	1.000	0.525	0.497
0.524	0.498	1.000	0.524	0.497
0.523	0.498	1.000	0.523	0.497
0.522	0.497	0.999	0.522	0.496
0.521	0.494	0.999	0.521	0.494
0.520	0.493	0.999	0.520	0.493
0.519	0.490	0.999	0.519	0.490
0.518	0.488	0.999	0.518	0.488
0.517	0.481	0.998	0.517	0.481
0.516	0.475	0.998	0.516	0.475
0.515	0.466	0.998	0.515	0.466
0.514	0.452	0.998	0.514	0.452
0.513	0.433	0.998	0.513	0.433
0.512	0.410	0.998	0.512	0.410
0.511	0.379	0.998	0.511	0.379
0.510	0.344	0.998	0.510	0.344
0.509	0.310	0.998	0.509	0.310
0.508	0.277	0.998	0.508	0.277
0.507	0.245	0.998	0.507	0.245
0.506	0.216	0.997	0.506	0.216
0.505	0.189	0.997	0.505	0.189
0.504	0.164	0.997	0.504	0.164
0.503	0.141	0.997	0.503	0.141
0.502	0.124	0.997	0.502	0.124
0.501	0.111	0.997	0.501	0.111
0.500	0.103	0.997	0.500	0.103
0.499	0.098	0.997	0.499	0.098
0.498	0.092	0.997	0.498	0.092
0.497	0.090	0.997	0.497	0.090
0.496	0.090	0.997	0.496	0.090
0.495	0.089	0.997	0.495	0.089
0.494	0.089	0.997	0.494	0.089
0.493	0.089	0.997	0.493	0.089
0.492	0.088	0.996	0.492	0.088
0.491	0.088	0.996	0.491	0.088
0.490	0.088	0.996	0.490	0.088
0.489	0.088	0.996	0.489	0.088
0.488	0.088	0.996	0.488	0.088
0.487	0.088	0.995	0.487	0.088
0.486	0.086	0.995	0.486	0.086
0.485	0.084	0.995	0.485	0.084
0.484	0.082	0.995	0.484	0.082
0.483	0.080	0.995	0.483	0.080
0.482	0.080	0.994	0.482	0.080
0.481	0.079	0.994	0.481	0.079
0.480	0.076	0.994	0.480	0.076

Table 2.5-25. High-resolution transmission scan, PbI_2-parylene No. 628A11A, at 2°C.

TEMP= 2. PBI2 PARY 628A 11-A 7-17 2.1C

WL EXP	T EXP	CALIB	WL	TRANS
0.525	0.493	1.000	0.525	0.497
0.524	0.493	1.000	0.524	0.497
0.523	0.493	1.000	0.523	0.497
0.522	0.495	0.999	0.522	0.500
0.521	0.496	0.999	0.521	0.501
0.520	0.497	0.999	0.520	0.502
0.519	0.496	0.999	0.519	0.501
0.518	0.495	0.999	0.518	0.500
0.517	0.493	0.998	0.517	0.498
0.516	0.489	0.998	0.516	0.494
0.515	0.483	0.998	0.515	0.488
0.514	0.474	0.998	0.514	0.479
0.513	0.462	0.998	0.513	0.467
0.512	0.442	0.998	0.512	0.446
0.511	0.422	0.998	0.511	0.426
0.510	0.394	0.998	0.510	0.398
0.509	0.360	0.998	0.509	0.364
0.508	0.320	0.998	0.508	0.323
0.507	0.280	0.998	0.507	0.283
0.506	0.236	0.997	0.506	0.239
0.505	0.200	0.997	0.505	0.202
0.504	0.168	0.997	0.504	0.170
0.503	0.140	0.997	0.503	0.142
0.502	0.120	0.997	0.502	0.121
0.501	0.105	0.997	0.501	0.106
0.500	0.094	0.997	0.500	0.095
0.499	0.088	0.997	0.499	0.089
0.498	0.082	0.997	0.498	0.083
0.497	0.080	0.997	0.497	0.081
0.496	0.080	0.997	0.496	0.081
0.495	0.080	0.997	0.495	0.081
0.494	0.079	0.997	0.494	0.080
0.493	0.080	0.997	0.493	0.081
0.492	0.080	0.996	0.492	0.081
0.491	0.080	0.996	0.491	0.081
0.490	0.080	0.996	0.490	0.081
0.489	0.082	0.996	0.489	0.083
0.488	0.082	0.996	0.488	0.083
0.487	0.082	0.995	0.487	0.083
0.486	0.082	0.995	0.486	0.083
0.485	0.081	0.995	0.485	0.082
0.484	0.081	0.995	0.484	0.082
0.483	0.080	0.995	0.483	0.081
0.482	0.080	0.994	0.482	0.081
0.481	0.078	0.994	0.481	0.079
0.480	0.077	0.994	0.480	0.078

Table 2.5-26. High-resolution transmission scan, PbI_2-parylene No. 628A11A, at 5°C.

TEMP= 5. PBI2 PARY 628A 11-A 7-17 2.46

WL EXP	T EXP	CALIB	WI	TRANS
0.525	0.497	1.000	0.525	0.497
0.524	0.498	1.000	0.524	0.498
0.523	0.498	1.000	0.523	0.498
0.522	0.498	0.999	0.522	0.498
0.521	0.499	0.999	0.521	0.499
0.520	0.498	0.999	0.520	0.498
0.519	0.498	0.999	0.519	0.498
0.518	0.497	0.999	0.518	0.497
0.517	0.494	0.998	0.517	0.495
0.516	0.490	0.998	0.516	0.491
0.515	0.483	0.998	0.515	0.484
0.514	0.474	0.998	0.514	0.475
0.513	0.459	0.998	0.513	0.460
0.512	0.440	0.998	0.512	0.441
0.511	0.413	0.998	0.511	0.414
0.510	0.389	0.998	0.510	0.390
0.509	0.352	0.998	0.509	0.353
0.508	0.314	0.998	0.508	0.315
0.507	0.271	0.998	0.507	0.272
0.506	0.231	0.997	0.506	0.232
0.505	0.198	0.997	0.505	0.199
0.504	0.168	0.997	0.504	0.169
0.503	0.143	0.997	0.503	0.143
0.502	0.121	0.997	0.502	0.121
0.501	0.109	0.997	0.501	0.109
0.500	0.098	0.997	0.500	0.098
0.499	0.090	0.997	0.499	0.090
0.498	0.086	0.997	0.498	0.086
0.497	0.082	0.997	0.497	0.082
0.496	0.080	0.997	0.496	0.080
0.495	0.080	0.997	0.495	0.080
0.494	0.080	0.997	0.494	0.080
0.493	0.080	0.997	0.493	0.080
0.492	0.080	0.996	0.492	0.080
0.491	0.081	0.996	0.491	0.081
0.490	0.082	0.996	0.490	0.082
0.489	0.082	0.996	0.489	0.082
0.488	0.083	0.996	0.488	0.083
0.487	0.083	0.995	0.487	0.083
0.486	0.083	0.995	0.486	0.083
0.485	0.082	0.995	0.485	0.082
0.484	0.081	0.995	0.484	0.081
0.483	0.080	0.995	0.483	0.080
0.482	0.080	0.994	0.482	0.080
0.481	0.079	0.994	0.481	0.079
0.480	0.078	0.994	0.480	0.078

Table 2.5-27. High-resolution transmission scan, PbI_2-parylene No. 628A11A, at 10°C.

TEMP= 10. PBI2 PARY 628A 11-A 7-17 3.18

WL EXP	T EXP	CALIB	WL	TRANS
0.525	0.496	1.000	0.525	0.497
0.524	0.496	1.000	0.524	0.497
0.523	0.497	1.000	0.523	0.498
0.522	0.497	0.999	0.522	0.499
0.521	0.497	0.999	0.521	0.499
0.520	0.497	0.999	0.520	0.499
0.519	0.496	0.999	0.519	0.497
0.518	0.494	0.999	0.518	0.495
0.517	0.490	0.998	0.517	0.492
0.516	0.486	0.998	0.516	0.488
0.515	0.480	0.998	0.515	0.482
0.514	0.470	0.998	0.514	0.472
0.513	0.455	0.998	0.513	0.457
0.512	0.435	0.998	0.512	0.437
0.511	0.407	0.998	0.511	0.409
0.510	0.379	0.998	0.510	0.381
0.509	0.339	0.998	0.509	0.340
0.508	0.307	0.998	0.508	0.308
0.507	0.267	0.998	0.507	0.268
0.506	0.229	0.997	0.506	0.230
0.505	0.192	0.997	0.505	0.193
0.504	0.164	0.997	0.504	0.165
0.503	0.141	0.997	0.503	0.142
0.502	0.122	0.997	0.502	0.123
0.501	0.109	0.997	0.501	0.110
0.500	0.098	0.997	0.500	0.098
0.499	0.091	0.997	0.499	0.091
0.498	0.088	0.997	0.498	0.088
0.497	0.084	0.997	0.497	0.084
0.496	0.083	0.997	0.496	0.083
0.495	0.082	0.997	0.495	0.082
0.494	0.081	0.997	0.494	0.081
0.493	0.082	0.997	0.493	0.082
0.492	0.082	0.996	0.492	0.082
0.491	0.083	0.996	0.491	0.084
0.490	0.084	0.996	0.490	0.085
0.489	0.084	0.996	0.489	0.085
0.488	0.084	0.996	0.488	0.085
0.487	0.084	0.995	0.487	0.085
0.486	0.084	0.995	0.486	0.085
0.485	0.082	0.995	0.485	0.083
0.484	0.081	0.995	0.484	0.082
0.483	0.080	0.995	0.483	0.081
0.482	0.080	0.994	0.482	0.081
0.481	0.079	0.994	0.481	0.080
0.480	0.076	0.994	0.480	0.077

Table 2.5-28. High-resolution transmission scan, PbI_2-parylene No. 62A11A, at 15°C.

TEMP= 15. PBI2 PARY 628A 11-A 7-17 3.45

WL EXP	T EXP	CALIB	WL	TRANS
0.525	0.496	1.000	0.525	0.497
0.524	0.496	1.000	0.524	0.497
0.523	0.495	1.000	0.523	0.496
0.522	0.495	0.999	0.522	0.496
0.521	0.496	0.999	0.521	0.497
0.520	0.494	0.999	0.520	0.495
0.519	0.493	0.999	0.519	0.494
0.518	0.491	0.999	0.518	0.492
0.517	0.488	0.998	0.517	0.490
0.516	0.482	0.998	0.516	0.484
0.515	0.473	0.998	0.515	0.475
0.514	0.461	0.998	0.514	0.463
0.513	0.445	0.998	0.513	0.447
0.512	0.425	0.998	0.512	0.427
0.511	0.399	0.998	0.511	0.401
0.510	0.366	0.998	0.510	0.367
0.509	0.330	0.998	0.509	0.331
0.508	0.296	0.998	0.508	0.297
0.507	0.260	0.998	0.507	0.261
0.506	0.223	0.997	0.506	0.224
0.505	0.190	0.997	0.505	0.191
0.504	0.165	0.997	0.504	0.166
0.503	0.140	0.997	0.503	0.141
0.502	0.124	0.997	0.502	0.125
0.501	0.111	0.997	0.501	0.112
0.500	0.100	0.997	0.500	0.101
0.499	0.094	0.997	0.499	0.094
0.498	0.091	0.997	0.498	0.091
0.497	0.088	0.997	0.497	0.088
0.496	0.087	0.997	0.496	0.087
0.495	0.084	0.997	0.495	0.084
0.494	0.084	0.997	0.494	0.084
0.493	0.084	0.997	0.493	0.084
0.492	0.085	0.996	0.492	0.086
0.491	0.085	0.996	0.491	0.086
0.490	0.086	0.996	0.490	0.087
0.489	0.086	0.996	0.489	0.087
0.488	0.086	0.996	0.488	0.087
0.487	0.086	0.995	0.487	0.087
0.486	0.086	0.995	0.486	0.087
0.485	0.085	0.995	0.485	0.086
0.484	0.083	0.995	0.484	0.084
0.483	0.082	0.995	0.483	0.083
0.482	0.081	0.994	0.482	0.082
0.481	0.080	0.994	0.481	0.081
0.480	0.079	0.994	0.490	0.080

Table 2.5-29. High-resolution transmission scan, PbI_2-parylene No. 628A11A, at 20°C.

TEMP= 20. PBI2 PARY 628A 11-A 7-17 4.00

WL EXP	T EXP	CALIB	WL	TRANS
0.525	0.497	1.000	0.525	0.497
0.524	0.496	1.000	0.524	0.496
0.523	0.496	1.000	0.523	0.496
0.522	0.496	0.999	0.522	0.496
0.521	0.494	0.999	0.521	0.494
0.520	0.494	0.999	0.520	0.494
0.519	0.492	0.999	0.519	0.492
0.518	0.490	0.999	0.518	0.490
0.517	0.484	0.998	0.517	0.485
0.516	0.479	0.998	0.516	0.480
0.515	0.469	0.998	0.515	0.470
0.514	0.456	0.998	0.514	0.457
0.513	0.439	0.998	0.513	0.440
0.512	0.416	0.998	0.512	0.417
0.511	0.388	0.998	0.511	0.389
0.510	0.359	0.998	0.510	0.360
0.509	0.322	0.998	0.509	0.323
0.508	0.287	0.998	0.508	0.288
0.507	0.253	0.998	0.507	0.254
0.506	0.217	0.997	0.506	0.218
0.505	0.189	0.997	0.505	0.190
0.504	0.161	0.997	0.504	0.161
0.503	0.140	0.997	0.503	0.140
0.502	0.125	0.997	0.502	0.125
0.501	0.113	0.997	0.501	0.113
0.500	0.103	0.997	0.500	0.103
0.499	0.096	0.997	0.499	0.096
0.498	0.094	0.997	0.498	0.094
0.497	0.090	0.997	0.497	0.090
0.496	0.089	0.997	0.496	0.089
0.495	0.088	0.997	0.495	0.088
0.494	0.087	0.997	0.494	0.087
0.493	0.086	0.997	0.493	0.086
0.492	0.086	0.996	0.492	0.086
0.491	0.087	0.996	0.491	0.087
0.490	0.088	0.996	0.490	0.088
0.489	0.087	0.996	0.489	0.087
0.488	0.086	0.996	0.488	0.086
0.487	0.085	0.995	0.487	0.085
0.486	0.084	0.995	0.486	0.084
0.485	0.083	0.995	0.485	0.083
0.484	0.081	0.995	0.484	0.081
0.483	0.080	0.995	0.483	0.080
0.482	0.080	0.994	0.482	0.080
0.481	0.079	0.994	0.481	0.079
0.480	0.076	0.994	0.480	0.076

Table 2.5-30. High-resolution transmission scan, PbI_2-parylene No. 628A11A, at 30°C.

TEMP= 30. PBI2 PARY 628A 11-A 7-17 4.31

WL EXP	T EXP	CALIB	WL	TRANS
0.525	0.497	1.000	0.525	0.497
0.524	0.497	1.000	0.524	0.497
0.523	0.496	1.000	0.523	0.496
0.522	0.494	0.999	0.522	0.494
0.521	0.493	0.999	0.521	0.493
0.520	0.490	0.999	0.520	0.490
0.519	0.489	0.999	0.519	0.489
0.518	0.484	0.999	0.518	0.484
0.517	0.479	0.998	0.517	0.480
0.516	0.470	0.998	0.516	0.471
0.515	0.459	0.998	0.515	0.460
0.514	0.443	0.998	0.514	0.444
0.513	0.426	0.998	0.513	0.427
0.512	0.401	0.998	0.512	0.402
0.511	0.373	0.998	0.511	0.374
0.510	0.344	0.998	0.510	0.345
0.509	0.310	0.998	0.509	0.311
0.508	0.277	0.998	0.508	0.278
0.507	0.244	0.998	0.507	0.244
0.506	0.212	0.997	0.506	0.213
0.505	0.187	0.997	0.505	0.188
0.504	0.162	0.997	0.504	0.162
0.503	0.142	0.997	0.503	0.142
0.502	0.127	0.997	0.502	0.127
0.501	0.114	0.997	0.501	0.114
0.500	0.107	0.997	0.500	0.107
0.499	0.100	0.997	0.499	0.100
0.498	0.096	0.997	0.498	0.096
0.497	0.093	0.997	0.497	0.093
0.496	0.091	0.997	0.496	0.091
0.495	0.090	0.997	0.495	0.090
0.494	0.090	0.997	0.494	0.090
0.493	0.090	0.997	0.493	0.090
0.492	0.090	0.996	0.492	0.090
0.491	0.089	0.996	0.491	0.089
0.490	0.089	0.996	0.490	0.089
0.489	0.088	0.996	0.489	0.088
0.488	0.088	0.996	0.488	0.088
0.487	0.087	0.995	0.487	0.087
0.486	0.086	0.995	0.486	0.086
0.485	0.084	0.995	0.485	0.084
0.484	0.082	0.995	0.484	0.082
0.483	0.081	0.995	0.483	0.081
0.482	0.080	0.994	0.482	0.080
0.481	0.078	0.994	0.481	0.078
0.480	0.077	0.994	0.480	0.077

Table 2.5-31. High-resolution transmission scan, PbI_2-parylene No. 628A11A, at 35 °C.

TEMP= 35. PBI2 PARY 628A 11-A 7-17 4.57

WL EXP	T EXP	CALIB	WL	TRANS
0.525	0.497	1.000	0.525	0.497
0.524	0.497	1.000	0.524	0.497
0.523	0.496	1.000	0.523	0.496
0.522	0.495	0.999	0.522	0.495
0.521	0.493	0.999	0.521	0.493
0.520	0.490	0.999	0.520	0.490
0.519	0.489	0.999	0.519	0.489
0.518	0.482	0.999	0.518	0.482
0.517	0.479	0.998	0.517	0.480
0.516	0.469	0.998	0.516	0.470
0.515	0.458	0.998	0.515	0.459
0.514	0.442	0.998	0.514	0.443
0.513	0.421	0.998	0.513	0.422
0.512	0.398	0.998	0.512	0.399
0.511	0.370	0.998	0.511	0.371
0.510	0.340	0.998	0.510	0.341
0.509	0.304	0.998	0.509	0.305
0.508	0.272	0.998	0.508	0.273
0.507	0.240	0.998	0.507	0.240
0.506	0.213	0.997	0.506	0.214
0.505	0.183	0.997	0.505	0.184
0.504	0.162	0.997	0.504	0.162
0.503	0.143	0.997	0.503	0.143
0.502	0.129	0.997	0.502	0.129
0.501	0.118	0.997	0.501	0.118
0.500	0.109	0.997	0.500	0.109
0.499	0.101	0.997	0.499	0.101
0.498	0.099	0.997	0.498	0.099
0.497	0.095	0.997	0.497	0.095
0.496	0.092	0.997	0.496	0.092
0.495	0.090	0.997	0.495	0.090
0.494	0.090	0.997	0.494	0.090
0.493	0.090	0.997	0.493	0.090
0.492	0.090	0.996	0.492	0.090
0.491	0.090	0.996	0.491	0.090
0.490	0.090	0.996	0.490	0.090
0.489	0.090	0.996	0.489	0.090
0.488	0.089	0.996	0.488	0.089
0.487	0.088	0.995	0.487	0.088
0.486	0.087	0.995	0.486	0.087
0.485	0.085	0.995	0.485	0.085
0.484	0.083	0.995	0.484	0.083
0.483	0.080	0.995	0.483	0.080
0.482	0.079	0.994	0.482	0.079
0.481	0.078	0.994	0.481	0.078
0.480	0.076	0.994	0.480	0.076

Table 2.5-32. High-resolution transmission scan, PbI_2-parylene No. 628A11A, at 40°C.

TEMP= 40. PBI2 PARY 628A 11-A 7-17 5.15

WL EXP	T EXP	CALIB	WL	TRANS
0.525	0.497	1.000	0.525	0.497
0.524	0.497	1.000	0.524	0.497
0.523	0.495	1.000	0.523	0.495
0.522	0.494	0.999	0.522	0.494
0.521	0.492	0.999	0.521	0.492
0.520	0.489	0.999	0.520	0.489
0.519	0.487	0.999	0.519	0.487
0.518	0.480	0.999	0.518	0.480
0.517	0.473	0.998	0.517	0.474
0.516	0.464	0.998	0.516	0.465
0.515	0.452	0.998	0.515	0.453
0.514	0.435	0.998	0.514	0.436
0.513	0.416	0.998	0.513	0.417
0.512	0.391	0.998	0.512	0.392
0.511	0.361	0.998	0.511	0.362
0.510	0.330	0.998	0.510	0.331
0.509	0.301	0.998	0.509	0.302
0.508	0.268	0.998	0.508	0.269
0.507	0.237	0.998	0.507	0.237
0.506	0.210	0.997	0.506	0.211
0.505	0.182	0.997	0.505	0.183
0.504	0.160	0.997	0.504	0.160
0.503	0.143	0.997	0.503	0.143
0.502	0.128	0.997	0.502	0.128
0.501	0.119	0.997	0.501	0.119
0.500	0.110	0.997	0.500	0.110
0.499	0.104	0.997	0.499	0.104
0.498	0.100	0.997	0.498	0.100
0.497	0.098	0.997	0.497	0.098
0.496	0.095	0.997	0.496	0.095
0.495	0.093	0.997	0.495	0.093
0.494	0.092	0.997	0.494	0.092
0.493	0.091	0.997	0.493	0.091
0.492	0.090	0.996	0.492	0.090
0.491	0.090	0.996	0.491	0.090
0.490	0.090	0.996	0.490	0.090
0.489	0.090	0.996	0.489	0.090
0.488	0.089	0.996	0.488	0.089
0.487	0.088	0.995	0.487	0.088
0.486	0.087	0.995	0.486	0.087
0.485	0.085	0.995	0.485	0.085
0.484	0.083	0.995	0.484	0.083
0.483	0.081	0.995	0.483	0.081
0.482	0.080	0.994	0.482	0.080
0.481	0.078	0.994	0.481	0.078
0.480	0.076	0.994	0.480	0.076

Table 2.5-33. High-resolution transmission scan, PbI_2-parylene No. 628A11A at 45°C.

TEMP= 45. PBI2 PARY 628A 11-A 7-17 5.41

WL EXP	T EXP	CALIB	WL	TRANS
0.525	0.497	1.000	0.525	0.497
0.524	0.496	1.000	0.524	0.496
0.523	0.494	1.000	0.523	0.494
0.522	0.493	0.999	0.522	0.493
0.521	0.490	0.999	0.521	0.490
0.520	0.488	0.999	0.520	0.488
0.519	0.483	0.999	0.519	0.483
0.518	0.478	0.999	0.518	0.478
0.517	0.470	0.998	0.517	0.471
0.516	0.460	0.998	0.516	0.461
0.515	0.448	0.998	0.515	0.449
0.514	0.429	0.998	0.514	0.430
0.513	0.409	0.998	0.513	0.410
0.512	0.377	0.998	0.512	0.378
0.511	0.355	0.998	0.511	0.356
0.510	0.324	0.998	0.510	0.325
0.509	0.292	0.998	0.509	0.293
0.508	0.265	0.998	0.508	0.266
0.507	0.233	0.998	0.507	0.233
0.506	0.205	0.997	0.506	0.206
0.505	0.182	0.997	0.505	0.183
0.504	0.159	0.997	0.504	0.159
0.503	0.144	0.997	0.503	0.144
0.502	0.130	0.997	0.502	0.130
0.501	0.120	0.997	0.501	0.120
0.500	0.112	0.997	0.500	0.112
0.499	0.107	0.997	0.499	0.107
0.498	0.102	0.997	0.498	0.102
0.497	0.100	0.997	0.497	0.100
0.496	0.098	0.997	0.496	0.098
0.495	0.096	0.997	0.495	0.096
0.494	0.094	0.997	0.494	0.094
0.493	0.093	0.997	0.493	0.093
0.492	0.091	0.996	0.492	0.091
0.491	0.090	0.996	0.491	0.090
0.490	0.090	0.996	0.490	0.090
0.489	0.090	0.996	0.489	0.090
0.488	0.090	0.996	0.488	0.090
0.487	0.089	0.995	0.487	0.089
0.486	0.088	0.995	0.486	0.088
0.485	0.087	0.995	0.485	0.087
0.484	0.084	0.995	0.484	0.084
0.483	0.082	0.995	0.483	0.082
0.482	0.080	0.994	0.482	0.080
0.481	0.078	0.994	0.481	0.078
0.480	0.076	0.994	0.480	0.076

Table 2.5-34. High-resolution transmission scan, PbI_2-parylene No. 628A11A, at 50°C.

TEMP= 50. PBI2 PARY 628A 11-A 7-17 6.00

WL EXP	T EXP	CALIB	WL	TRANS
0.525	0.497	1.000	0.525	0.497
0.524	0.496	1.000	0.524	0.496
0.523	0.493	1.000	0.523	0.493
0.522	0.490	0.999	0.522	0.490
0.521	0.489	0.999	0.521	0.489
0.520	0.487	0.999	0.520	0.487
0.519	0.480	0.999	0.519	0.480
0.518	0.475	0.999	0.518	0.475
0.517	0.466	0.998	0.517	0.467
0.516	0.454	0.998	0.516	0.455
0.515	0.440	0.998	0.515	0.441
0.514	0.424	0.998	0.514	0.425
0.513	0.400	0.998	0.513	0.401
0.512	0.377	0.998	0.512	0.378
0.511	0.350	0.998	0.511	0.351
0.510	0.018	0.998	0.510	0.018
0.509	0.287	0.998	0.509	0.288
0.508	0.258	0.998	0.508	0.259
0.507	0.230	0.998	0.507	0.230
0.506	0.201	0.997	0.506	0.202
0.505	0.179	0.997	0.505	0.180
0.504	0.160	0.997	0.504	0.160
0.503	0.144	0.997	0.503	0.144
0.502	0.131	0.997	0.502	0.131
0.501	0.121	0.997	0.501	0.121
0.500	0.113	0.997	0.500	0.113
0.499	0.108	0.997	0.499	0.108
0.498	0.104	0.997	0.498	0.104
0.497	0.101	0.997	0.497	0.101
0.496	0.099	0.997	0.496	0.099
0.495	0.097	0.997	0.495	0.097
0.494	0.097	0.997	0.494	0.097
0.493	0.094	0.997	0.493	0.094
0.492	0.093	0.996	0.492	0.093
0.491	0.093	0.996	0.491	0.093
0.490	0.091	0.996	0.490	0.091
0.489	0.090	0.996	0.489	0.090
0.488	0.090	0.996	0.488	0.090
0.487	0.090	0.995	0.487	0.090
0.486	0.089	0.995	0.486	0.089
0.485	0.087	0.995	0.485	0.087
0.484	0.085	0.995	0.484	0.085
0.483	0.082	0.995	0.483	0.082

Table 2.5-38. High-resolution transmission scan, PbI_2-parylene No. 628A11A, at 25°C (at end of temperature cycling).

TEMP= 25. PBI2 PARY 628A 11-A 7-17 6.33

WL EXP	T EXP	CALIB	WL	TRANS
0.525	0.499	1.000	0.525	0.498
0.524	0.498	1.000	0.524	0.497
0.523	0.497	1.000	0.523	0.496
0.522	0.497	0.999	0.522	0.496
0.521	0.495	0.999	0.521	0.495
0.520	0.494	0.999	0.520	0.494
0.519	0.491	0.999	0.519	0.491
0.518	0.489	0.999	0.518	0.489
0.517	0.483	0.998	0.517	0.483
0.516	0.476	0.998	0.516	0.476
0.515	0.468	0.998	0.515	0.468
0.514	0.455	0.998	0.514	0.455
0.513	0.439	0.998	0.513	0.439
0.512	0.413	0.998	0.512	0.413
0.511	0.384	0.998	0.511	0.384
0.510	0.351	0.998	0.510	0.351
0.509	0.317	0.998	0.509	0.317
0.508	0.283	0.998	0.508	0.283
0.507	0.251	0.998	0.507	0.251
0.506	0.221	0.997	0.506	0.221
0.505	0.195	0.997	0.505	0.195
0.504	0.170	0.997	0.504	0.170
0.503	0.149	0.997	0.503	0.149
0.502	0.130	0.997	0.502	0.130
0.501	0.116	0.997	0.501	0.116
0.500	0.106	0.997	0.500	0.106
0.499	0.099	0.997	0.499	0.099
0.498	0.094	0.997	0.498	0.094
0.497	0.091	0.997	0.497	0.091
0.496	0.090	0.997	0.496	0.090
0.495	0.090	0.997	0.495	0.090
0.494	0.089	0.997	0.494	0.089
0.493	0.089	0.997	0.493	0.089
0.492	0.089	0.996	0.492	0.089
0.491	0.089	0.996	0.491	0.089
0.490	0.088	0.996	0.490	0.088
0.489	0.088	0.996	0.489	0.088
0.488	0.088	0.996	0.488	0.088
0.487	0.087	0.995	0.487	0.087
0.486	0.086	0.995	0.486	0.086
0.485	0.084	0.995	0.485	0.084
0.484	0.082	0.995	0.484	0.082
0.483	0.081	0.995	0.483	0.081
0.482	0.080	0.994	0.482	0.080
0.481	0.078	0.994	0.481	0.078
0.480	0.075	0.994	0.480	0.075

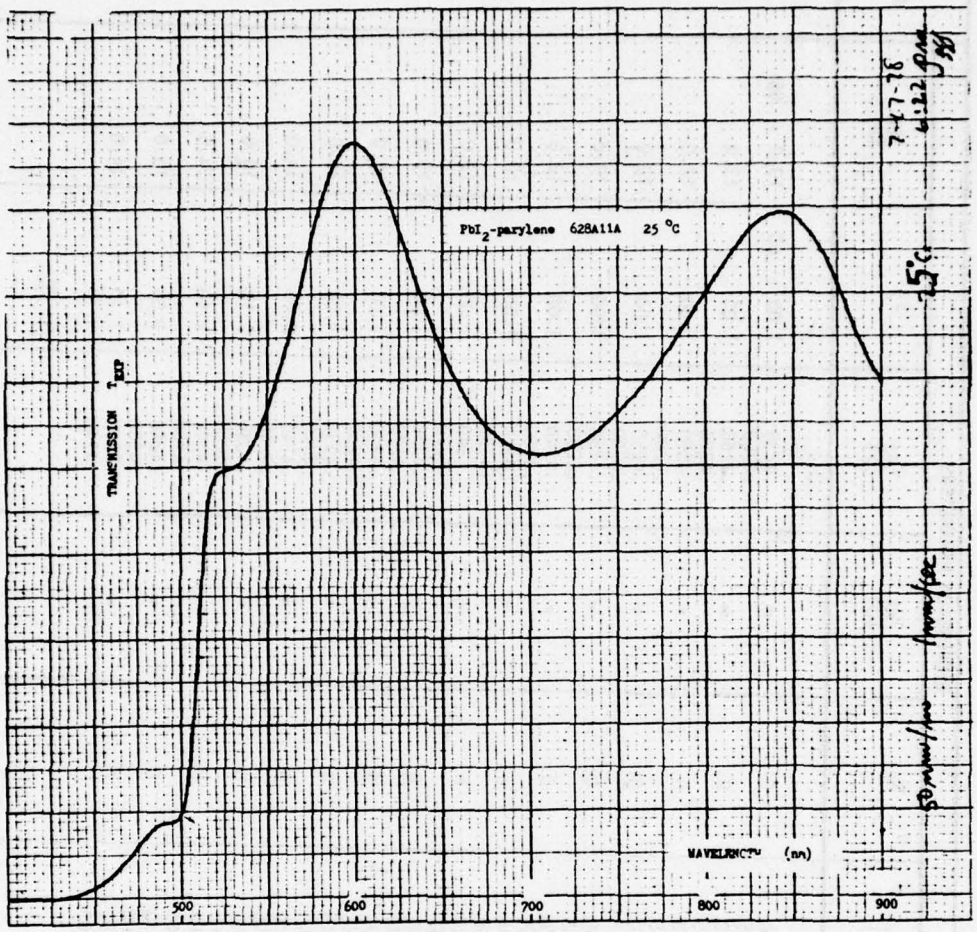

Figure 2.5-61. Transmission of PbI_2-parylene No. 628A11A at 25°C (5).

TABLE 2.5-36. Thickness, Refractive Index, and Dispersion Parameters for PbI_2-parylene Sample 628A11A, by Computer Analysis of Transmission Curves.

TRANSMISSION SCAN NO. ON 7-10-78	TEMPERATURE °C	PbI_2 THICKNESS $D_2(\mu) \pm .0025$	DISPERSION PARAMETERS							SUM OF SQUARED DEVIATIONS Σ
			$n_o^2 \pm .05$	λ_{01} (μ)	S_1	λ_{G1} (μ)	λ_{02} (μ)	S_2	λ_{G2} (μ)	
9.32	Calibration Scan									
9.45	25	.2350	4.00	.4960	0.	∞	.4230	1.00 ± .05	13.0 ± .05	.01075
9.59 *	25	"		.4965			.4260			
10.47	20	"	"	.4960	0.	∞	.4250	1.00	13.0	.009568
10.57 *	20	"		.4955			.4230			
11.08	15	"	"	.4950	0.	∞	.4250	1.00	12.0	.01035
11.18 *	15	"		.4950			.4280			
11.30	10	"	"	.4950	0.	∞	.4250	1.00	12.0	.009784
11.40 *	10	"		.4950			.4230			
11.58	2	"	"	.4950	0.	∞	.4250	1.00	12.0	.01024
12.08 *	2	"		.4955			.4280			
12.31	35	"	"	.4970	0.	∞	.4240	1.00	12.0	.01208
12.43 *	35	"		.4955			.4280			
1.01	40	"	"	.4970	0.	∞	.4250	1.00	12.0	.01025
1.12 *	40	"		.4950			.4280			
1.26	45	"	"	.4940	0.	∞	.4240	1.00	13.0	.01594
1.39 *	45	"		.4942			.4270			
1.57	50	"	"	.4940	0.	∞	.4250	1.00	13.0	.01049
2.07 *	50	"		.4940			.4270			
2.43	25	"	"	.4970	0.	∞	.4240	1.00	12.0	.009285
2.53 *	25	"		.4956			.4250			
3.37	-175	"	4.20	.4940	0.	∞	.4230	1.00	14.0	.01650
3.48 *	-175	"		.4950			.4260			
4.03	-150	"	4.20	.4970	0.	∞	.4240	0.90	14.0	0.4196
4.15 *	-150	"		.4956			.4240			
4.50	- 75	"	4.10	.4960	0.	∞	.4240	1.10	14.0	.01073
5.06 *	- 75	"		.4966			.4260			
5.21	- 50	"	4.20	.4960	0.	∞	.4240	1.10	14.0	.02863
5.31 *	- 50	"		.4966			.4260			
6.07	25	"	4.00	.4970	0.	∞	.4240	1.00	13.0	.008604
6.18 *	25	"		.4960			.4280			
8.00	-112	"	4.00	.4960	0.	∞	.4230	1.10	14.0	.008500
8.08 *	-112	"		.4963			.4230			
9.00	Calibration Scan									

* Absorption-edge Scan from 600 nm to 420 nm, with Higher Resolution.

TABLE 2.5-37. Thickness, Refractive Index, and Dispersion Parameters from Analysis of High-Resolution Absorption Edge Transmission Data for PbI_2-parylene Sample No. 628A11A.

TRANSMISSION SCAN NO. ON 7-17-78	TEMPERATURE °C	PbI_2 THICKNESS $D_2(\mu) \pm .0025$	DISPERSION PARAMETERS							SUM OF SQUARED DEVIATIONS Σ
			$n_0^2 \pm .05$	λ_{01} (μ)	S_1	λ_{G1} (μ)	λ_{02} (μ)	S_2	λ_{G2} (μ)	
12.35	25	Calibration Scan		----	----	----	----	----	----	----
1.20 ‡	25	.2350	4.10	.4970	0.	∞	.4340	.90 ± .05	13.0 ± .05	.01182
1.50 *	25	"		.4960			.4340			
2.10 *	2	"		.4940			.4340			
2.46 *	5	"		.4940			.4340			
3.18 *	10	"		.4940			.4340			
3.45 *	15	"		.4940			.4340			
4.00 *	20	"		.4940			.4340			
4.31 *	30	"		.4940			.4340			
4.57 *	35	"		.4930			.4340			
5.19 *	40	"		.4920			.4340			
5.41 *	45	"		.4900			.4340			
6.00 *	50	"		.4900			.4340			
6.22 ‡	25	"	"	.4970	0.	∞	.4340	.90	13.0	.01133
6.33 †	25	"	"	.4960	0.	∞	.4340	.90	13.0	.01480

NOTE:

‡ Low-resolution Scan from 900 nm to 400 nm.
* High-resolution Scans; 1 nm/inch, 1/16 nm/second.
† High-resolution Scan; 10 nm/inch, 1/2 nm/second.

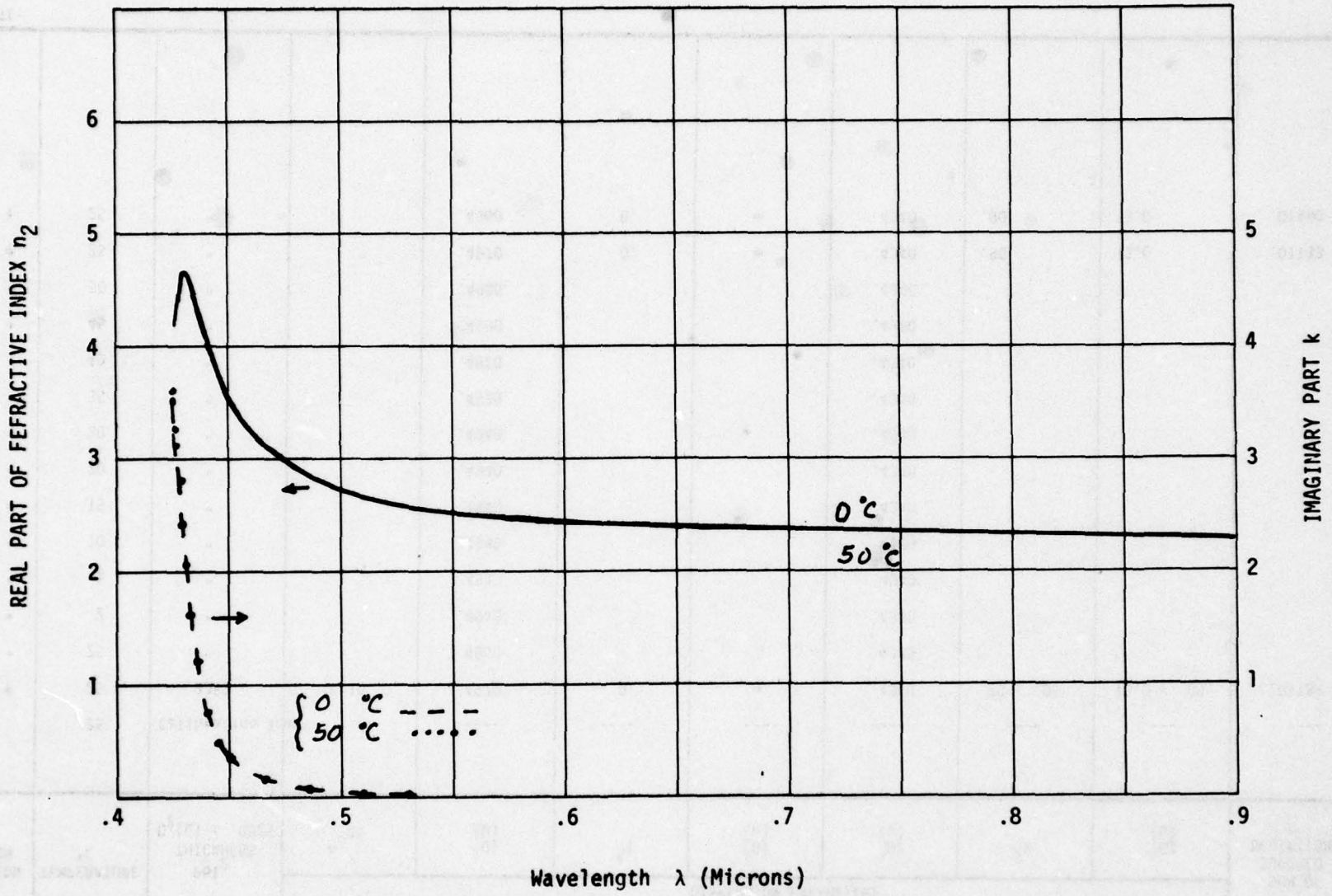

FIGURE 2.5-62. Variation of Complex Refractive Index n+ik with Wavelength for PbI_2-parylene Sample No. 628A11A at 0°C and 50°C.

The refractive index for PbI_2 is considerably lower for Sample 628A11A on parylene than for Sample 210A9 on glass. At 0.6μ wavelength n ≃ 3.19 for Sample 210A9 and n ≃ 2.5 for Sample 628A11A. This indicates a substantial difference between the physical characteristics of the two films, both in density and in degree of polycrystalline orientation. The PbI_2 film 628A11A on parylene was deposited at a rate of 70 Å per minute with a substrate temperature of 23°C. The PbI_2 film 210A9 on glass was deposited at a rate of 167 Å per minute with a substrate temperature of 150°C. Apparently, the higher substrate temperature is critical to the growth of highly oriented PbI_2 films. Unfortunately, the parylene membranes are not likely to survive 150°C temperatures without sagging, so that re-mounting onto a smaller support ring would become necessary.

Transmission curves were also run for PbI_2-parylene Sample 808B2J, as shown in Figures 2.5-64 through -72, and the accompanying Tables of high-resolution data for the absorption edge. A single transmission scan was made for Sample 809A2K at 25°C, shown in Figure 2.5-63, and for Sample 707A2D as shown in Figures 2.5-73 through -75. These curves have not been analyzed by computer at present, but some qualitative features are noteable. The thickness of the PbI_2 film is apparently somewhat larger for 808B2J than for previous samples, as evidenced by the relatively closely spaced extrema. Of particular interest is the sharp transmission peak located just at the long-wavelength side of the absorption edge, at 515 nm for 25°C temperature. This peak drops from 3.10 percent at 0°C to 2.55 percent at 50°C. This peak appears to shift toward the minimum at 530 nm with increasing temperature. If interference did not contribute to the transmission curves at all, the absorption edge would shift to longer wavelengths, causing the transmission at 515 nm to drop with increasing temperature. Therefore, the interference phenomenon is enhancing the temperature shift of the fundamental absorption edge by causing the transmittivity at 515 nm to drop more strongly with increasing temperature. The location of interference extrema in the long-wavelength portion of the absorption edge will be an important design parameter, influencing the thickness of thermo-optic transducer films.

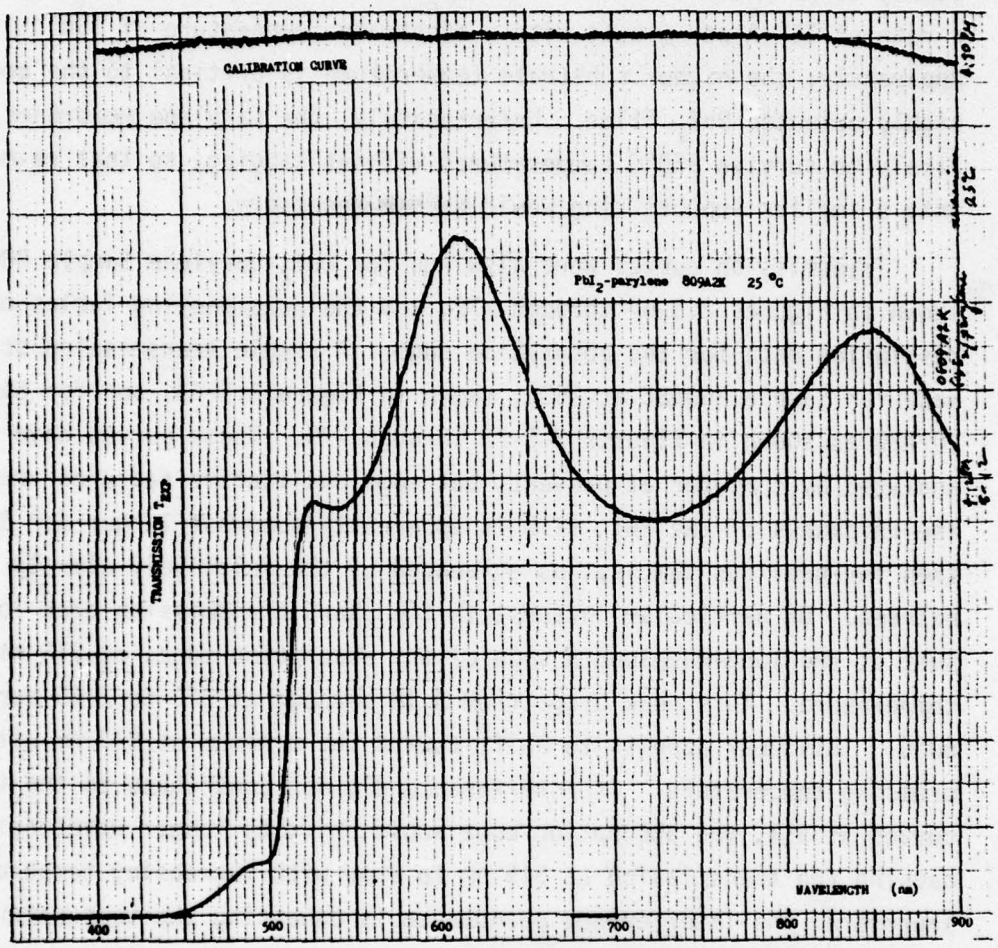

FIGURE 2.5-63. Transmission of PbI_2-parylene No. 809A2K at 25°C.

TEMP= 25. PBI2 PARY 808B -2J 8.12 3.55

WL	EXP T	EXP CALIB	WL	TRANS
0.900	0.655	C.975	0.898	0.677
0.895	0.644	C.978	0.893	0.666
0.890	0.628	0.979	0.888	0.647
0.885	0.606	C.980	0.883	0.623
0.880	0.581	C.982	0.878	0.596
0.875	0.558	0.985	0.873	0.571
0.870	0.532	C.990	0.868	0.542
0.865	0.509	0.991	0.863	0.518
0.860	0.487	0.996	0.858	0.493
0.855	0.466	C.999	0.853	0.470
0.850	0.440	1.000	0.848	0.444
0.845	0.421	1.001	0.843	0.424
0.840	0.407	1.001	0.838	0.410
0.835	0.394	1.002	0.833	0.396
0.830	0.387	1.003	0.828	0.389
0.825	0.382	1.004	0.823	0.384
0.820	0.380	1.005	0.818	0.381
0.815	0.378	1.006	0.813	0.380
0.810	0.382	1.005	0.808	0.383
0.805	0.388	1.007	0.803	0.388
0.800	0.396	1.007	0.798	0.396
0.795	0.406	1.005	0.793	0.407
0.790	0.421	1.008	0.788	0.421
0.785	0.436	1.009	0.783	0.436
0.780	0.456	1.010	0.778	0.455
0.775	0.474	1.009	0.773	0.474
0.770	0.500	1.009	0.768	0.501
0.765	0.525	1.004	0.763	0.527
0.760	0.547	1.004	0.758	0.550
0.755	0.569	1.004	0.753	0.571
0.750	0.626	1.005	0.748	0.628
0.745	0.661	1.004	0.743	0.664
0.740	0.705	1.004	0.738	0.708
0.735	0.745	1.003	0.733	0.749
0.730	0.785	1.003	0.728	0.789
0.725	0.819	1.005	0.723	0.821
0.720	0.852	1.005	0.718	0.855
0.715	0.874	1.008	0.713	0.874
0.710	0.890	1.007	0.708	0.891
0.705	0.890	1.007	0.703	0.891
0.700	0.877	1.008	0.698	0.877
0.695	0.860	1.007	0.693	0.861
0.690	0.826	1.007	0.688	0.827
0.685	0.790	1.008	0.683	0.790
0.680	0.748	1.007	0.678	0.749
0.675	0.710	1.008	0.673	0.710
0.670	0.665	1.009	0.668	0.664
0.665	0.629	1.009	0.663	0.628
0.660	0.594	1.009	0.658	0.593
0.655	0.565	1.009	0.653	0.564
0.650	0.540	1.009	0.648	0.539
0.645	0.524	1.009	0.643	0.523
0.640	0.510	1.007	0.638	0.511
0.635	0.501	1.007	0.633	0.501
0.630	0.501	1.005	0.628	0.502
0.625	0.506	1.010	0.623	0.505
0.620	0.520	1.009	0.618	0.519
0.615	0.540	1.008	0.613	0.540
0.610	0.572	1.007	0.608	0.573
0.605	0.605	1.004	0.603	0.607
0.600	0.656	1.004	0.598	0.659
0.595	0.705	1.005	0.593	0.707
0.590	0.761	1.003	0.588	0.765
0.585	0.794	1.004	0.583	0.797
0.580	0.794	1.005	0.578	0.796
0.575	0.750	1.004	0.573	0.751
0.570	0.664	1.006	0.568	0.665
0.565	0.573	1.006	0.563	0.574
0.560	0.460	1.005	0.558	0.461
0.555	0.390	1.004	0.553	0.392
0.550	0.317	1.004	0.548	0.318
0.545	0.270	1.004	0.543	0.271
0.540	0.231	1.002	0.538	0.232
0.535	0.210	1.001	0.533	0.211
0.530	0.200	1.000	0.528	0.202
0.525	0.206	1.000	0.523	0.208
0.520	0.239	1.000	0.518	0.241
0.515	0.272	1.000	0.513	0.274
0.510	0.142	1.000	0.508	0.143
0.505	0.045	1.000	0.503	0.045
0.500	0.018	0.999	0.498	0.018
0.495	0.015	0.999	0.493	0.015
0.490	0.014	1.000	0.488	0.014
0.485	0.014	1.000	0.483	0.014
0.480	0.011	1.000	0.478	0.011
0.475	0.009	1.000	0.473	0.009
0.470	0.005	1.000	0.468	0.005
0.465	0.003	1.000	0.463	0.003
0.460	0.001	1.000	0.458	0.001
0.455	0.0	0.999	0.453	0.0
0.450	-.001	0.999	0.448	-.001
0.445	-.002	0.999	0.443	-.002
0.440	-.002	0.994	0.438	-.002
0.435	-.003	0.992	0.433	-.003
0.430	-.003	0.992	0.428	-.003
0.425	-.003	0.990	0.423	-.003

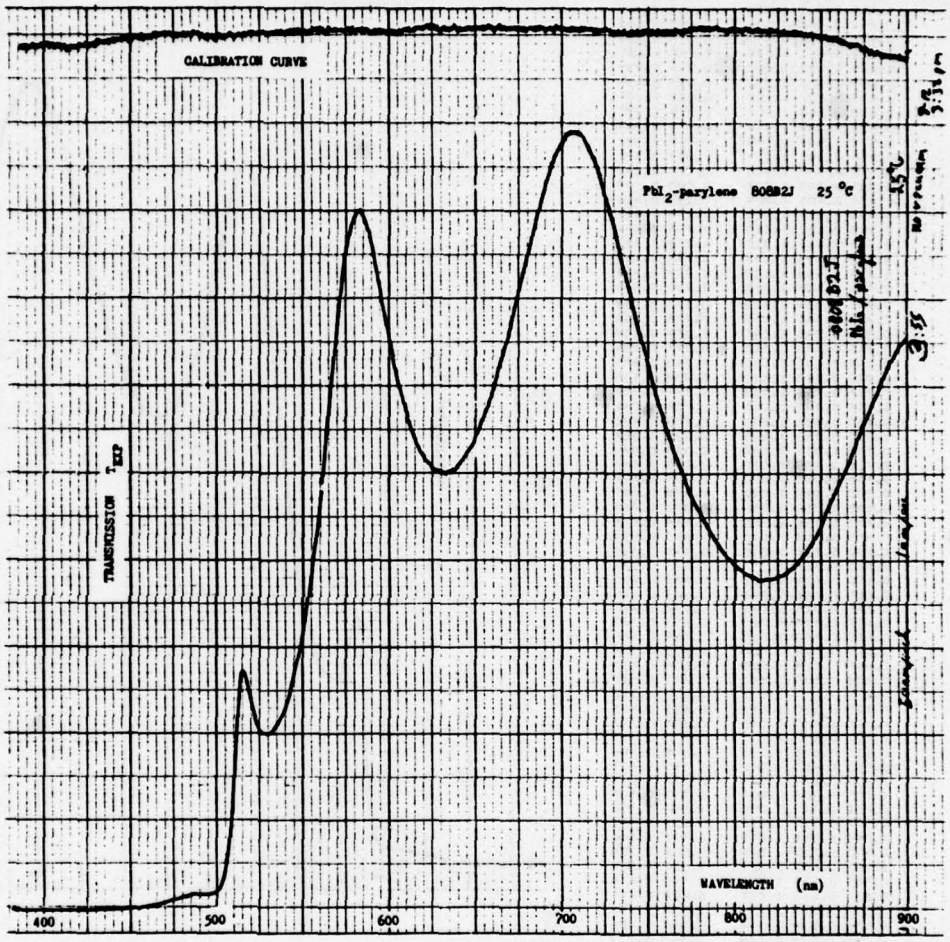

FIGURE 2.5-64. Transmission of PbI_2-parylene No. 808B2J at 25°C (1).

TEMP= 25. PBI2 PAPY 8098 -2J 8.13 3.30

WL EXP	T EXP	CALIB	WL	TRANS
0.900	0.462	0.972	0.899	0.491
0.895	0.468	0.973	0.893	0.478
0.890	0.475	0.975	0.888	0.483
0.885	0.465	0.977	0.883	0.830
0.880	0.502	0.980	0.878	0.457
0.875	0.505	0.982	0.873	0.475
0.870	0.511	0.985	0.868	0.525
0.865	0.497	0.986	0.859	0.499
0.855	0.478	0.988	0.852	0.489
0.850	0.447	0.990	0.848	0.456
0.845	0.427	1.000	0.843	0.435
0.840	0.411	1.000	0.838	0.418
0.835	0.401	1.001	0.833	0.409
0.830	0.393	1.002	0.828	0.399
0.825	0.389	1.003	0.823	0.395
0.820	0.387	1.005	0.818	0.392
0.815	0.387	1.004	0.813	0.392
0.810	0.390	1.006	0.809	0.395
0.805	0.395	1.008	0.803	0.399
0.800	0.404	1.009	0.798	0.408
0.795	0.414	1.010	0.793	0.417
0.790	0.430	1.010	0.788	0.433
0.785	0.445	1.010	0.783	0.449
0.780	0.464	1.010	0.778	0.468
0.775	0.484	1.010	0.773	0.488
0.770	0.509	1.010	0.768	0.513
0.765	0.534	1.010	0.763	0.538
0.760	0.565	1.010	0.758	0.569
0.755	0.595	1.010	0.753	0.600
0.750	0.633	1.010	0.748	0.638
0.745	0.670	1.010	0.743	0.675
0.740	0.713	1.010	0.738	0.719
0.735	0.749	1.010	0.733	0.755
0.730	0.790	1.010	0.728	0.796
0.725	0.824	1.010	0.723	0.831
0.720	0.855	1.010	0.718	0.862
0.715	0.876	1.010	0.713	0.883
0.710	0.890	1.010	0.708	0.897
0.705	0.890	1.010	0.703	0.897
0.700	0.880	1.010	0.698	0.887
0.695	0.861	1.010	0.693	0.868
0.690	0.831	1.010	0.688	0.838
0.685	0.797	1.010	0.683	0.803
0.680	0.754	1.010	0.678	0.760
0.675	0.716	1.010	0.673	0.722
0.670	0.674	1.011	0.668	0.679
0.665	0.642	1.011	0.663	0.646
0.660	0.603	1.011	0.658	0.607
0.655	0.578	1.010	0.653	0.583
0.650	0.552	1.010	0.648	0.556
0.645	0.534	1.010	0.643	0.538
0.640	0.521	1.010	0.638	0.525
0.635	0.515	1.010	0.633	0.519
0.630	0.515	1.012	0.628	0.518
0.625	0.520	1.012	0.623	0.523
0.620	0.534	1.013	0.618	0.537
0.615	0.553	1.011	0.613	0.557
0.610	0.585	1.010	0.608	0.590
0.605	0.620	1.010	0.603	0.625
0.600	0.670	1.010	0.598	0.675
0.595	0.720	1.010	0.593	0.726
0.590	0.770	1.010	0.588	0.776
0.585	0.799	1.011	0.583	0.805
0.580	0.798	1.010	0.578	0.804
0.575	0.750	1.010	0.573	0.756
0.570	0.670	1.011	0.568	0.675
0.565	0.575	1.012	0.563	0.578
0.560	0.475	1.017	0.558	0.475
0.555	0.399	1.016	0.553	0.404
0.550	0.324	1.015	0.548	0.329
0.545	0.278	1.014	0.543	0.279
0.540	0.240	1.015	0.538	0.241
0.535	0.220	1.014	0.533	0.221
0.530	0.219	1.011	0.528	0.219
0.525	0.220	1.012	0.523	0.221
0.520	0.260	1.011	0.518	0.262
0.515	0.273	1.011	0.513	0.275
0.510	0.116	1.010	0.508	0.117
0.505	0.035	1.010	0.503	0.035
0.500	0.019	1.010	0.498	0.019
0.495	0.018	1.010	0.493	0.018
0.490	0.018	1.010	0.488	0.018
0.485	0.016	1.010	0.483	0.016
0.480	0.013	1.010	0.478	0.013
0.475	0.010	1.009	0.473	0.010
0.470	0.007	1.010	0.468	0.007
0.465	0.004	1.010	0.463	0.004
0.460	0.003	1.005	0.458	0.003
0.455	0.001	1.005	0.453	0.001
0.450	0.0	1.004	0.448	0.0
0.445	0.0	1.002	0.443	0.0
0.440	0.0	1.002	0.438	0.0
0.435	0.0	1.001	0.433	0.0
0.430	0.0	1.000	0.428	0.0
0.425	0.0	1.000	0.423	0.0

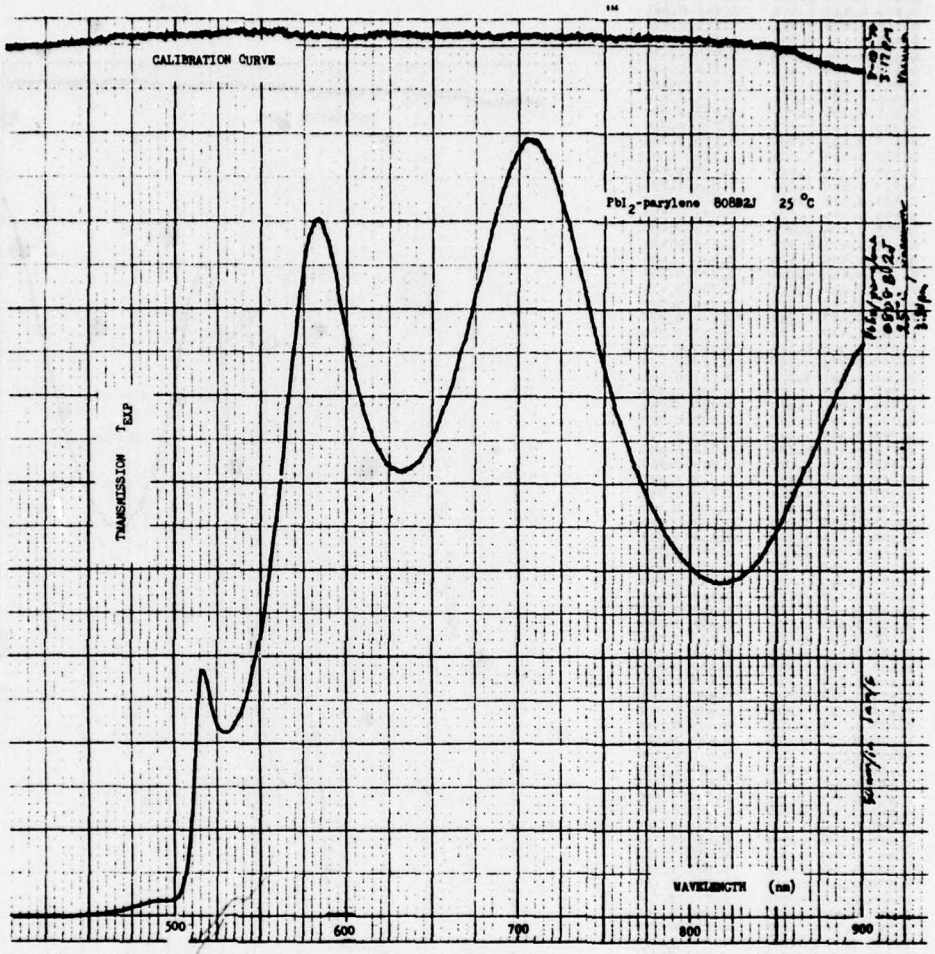

FIGURE 2.5-65. Transmission of PbI_2-parylene No. 808B2J at 25°C (2).

Table 2,5-38, High-resolution Transmission Scan of PbI_2-parylene No. 808B2J at 25°C.

TEMP= 25. PBI2 PARY 808B -2J 8.13 4.00

WL EXP	T EXP	CALIB	WL	TRANS
0.530	0.212	1.013	0.530	0.213
0.529	0.211	1.013	0.529	0.212
0.528	0.212	1.013	0.528	0.213
0.527	0.213	1.012	0.527	0.214
0.526	0.213	1.012	0.526	0.214
0.525	0.216	1.012	0.525	0.217
0.524	0.220	1.012	0.524	0.221
0.523	0.224	1.012	0.523	0.225
0.522	0.230	1.012	0.522	0.231
0.521	0.237	1.012	0.521	0.238
0.520	0.245	1.012	0.520	0.246
0.519	0.254	1.012	0.519	0.256
0.518	0.264	1.012	0.518	0.266
0.517	0.273	1.012	0.517	0.275
0.516	0.280	1.012	0.516	0.282
0.515	0.283	1.012	0.515	0.285
0.514	0.280	1.012	0.514	0.282
0.513	0.265	1.012	0.513	0.267
0.512	0.240	1.011	0.512	0.242
0.511	0.207	1.011	0.511	0.208
0.510	0.172	1.011	0.510	0.173
0.509	0.135	1.011	0.509	0.136
0.508	0.105	1.011	0.508	0.106
0.507	0.081	1.011	0.507	0.082
0.506	0.063	1.011	0.506	0.063
0.505	0.049	1.011	0.505	0.049
0.504	0.039	1.011	0.504	0.039
0.503	0.031	1.011	0.503	0.031
0.502	0.027	1.011	0.502	0.027
0.501	0.023	1.011	0.501	0.023
0.500	0.021	1.011	0.500	0.021
0.499	0.020	1.011	0.499	0.020
0.498	0.019	1.011	0.498	0.019
0.497	0.018	1.010	0.497	0.018
0.496	0.018	1.010	0.496	0.018
0.495	0.018	1.010	0.495	0.018
0.494	0.018	1.010	0.494	0.018
0.493	0.018	1.010	0.493	0.018
0.492	0.018	1.010	0.492	0.018
0.491	0.018	1.010	0.491	0.018
0.490	0.018	1.010	0.490	0.018
0.489	0.017	1.010	0.489	0.017
0.488	0.017	1.010	0.488	0.017
0.487	0.017	1.010	0.487	0.017
0.486	0.017	1.010	0.486	0.017
0.485	0.016	1.010	0.485	0.016
0.484	0.016	1.010	0.484	0.016
0.483	0.015	1.010	0.483	0.015
0.482	0.014	1.010	0.482	0.014
0.481	0.014	1.010	0.481	0.014
0.480	0.013	1.010	0.480	0.013

TEMP= 0. PBI2 PARY 9080 -2J 8.13 9.35

WL EXP	T EXP	CALIP	WL	TRANS
0.900	0.655	C.572	0.898	0.686
0.895	0.648	0.973	0.893	0.678
0.890	0.619	C.975	0.888	0.646
0.885	0.598	C.977	0.883	0.623
0.880	0.572	0.980	0.878	0.596
0.875	0.545	0.982	0.873	0.565
0.870	0.526	0.985	0.868	0.542
0.865	0.502	C.988	0.863	0.516
0.860	0.481	C.994	0.858	0.493
0.855	0.459	0.995	0.853	0.470
0.850	0.437	C.998	0.848	0.446
0.845	0.422	1.CCC	0.843	0.430
0.840	0.408	1.CC0	0.838	0.415
0.835	0.398	1.CC1	0.833	0.405
0.830	0.390	1.CC2	0.828	0.396
0.825	0.386	1.003	0.823	0.392
0.820	0.382	1.CC5	0.818	0.387
0.815	0.383	1.CC4	0.813	0.388
0.810	0.389	1.CC6	0.808	0.394
0.805	0.393	1.CC8	0.803	0.397
0.800	0.403	1.CC9	0.798	0.407
0.795	0.414	1.C10	0.793	0.417
0.790	0.429	1.C10	0.788	0.432
0.785	0.445	1.C10	0.783	0.449
0.780	0.464	1.C1C	0.778	0.468
0.775	0.485	1.010	0.773	0.489
0.770	0.510	1.C10	0.768	0.514
0.765	0.536	1.010	0.763	0.540
0.760	0.570	1.010	0.758	0.575
0.755	0.600	1.C1C	0.753	0.605
0.750	0.639	1.010	0.748	0.644
0.745	0.680	1.010	0.743	0.685
0.740	0.720	1.010	0.738	0.726
0.735	0.759	1.010	0.733	0.765
0.730	0.798	1.C10	0.728	0.804
0.725	0.830	1.010	0.723	0.837
0.720	0.857	1.C10	0.718	0.864
0.715	0.877	1.C10	0.713	0.884
0.710	0.883	1.010	0.708	0.890
0.705	0.883	1.C1C	0.703	0.890
0.700	0.867	1.C10	0.698	0.874
0.695	0.845	1.010	0.693	0.852
0.690	0.812	1.C10	0.688	0.818
0.685	0.776	1.010	0.683	0.782
0.680	0.738	1.C10	0.678	0.744
0.675	0.700	1.C10	0.673	0.706
0.670	0.659	1.011	0.668	0.664
0.665	0.624	1.011	0.663	0.628
0.660	0.593	1.011	0.658	0.597
0.655	0.564	1.010	0.653	0.568
0.650	0.543	1.C1C	0.648	0.547
0.645	0.528	1.C10	0.643	0.532
0.640	0.513	1.C10	0.638	0.517
0.635	0.509	1.C1C	0.633	0.513
0.630	0.509	1.012	0.628	0.512
0.625	0.515	1.C12	0.623	0.518
0.620	0.530	1.C13	0.618	0.533
0.615	0.550	1.011	0.613	0.554
0.610	0.585	1.C1C	0.608	0.590
0.605	0.622	1.010	0.603	0.627
0.600	0.670	1.010	0.598	0.675
0.595	0.720	1.C10	0.593	0.726
0.590	0.766	1.010	0.588	0.772
0.585	0.793	1.C11	0.583	0.798
0.580	0.785	1.C10	0.578	0.791
0.575	0.739	1.010	0.573	0.745
0.570	0.650	1.C11	0.568	0.655
0.565	0.560	1.C12	0.563	0.563
0.560	0.458	1.C17	0.558	0.458
0.555	0.380	1.C1A	0.553	0.381
0.550	0.332	1.019	0.548	0.333
0.545	0.766	1.C14	0.543	0.767
0.540	0.234	1.015	0.538	0.235
0.535	0.216	1.C14	0.533	0.217
0.530	0.212	1.013	0.528	0.213
0.525	0.228	1.012	0.523	0.229
0.520	0.280	1.C11	0.518	0.282
0.515	0.290	1.C11	0.513	0.292
0.510	0.100	1.C10	0.508	0.101
0.505	0.025	1.C1C	0.503	0.025
0.500	0.014	1.010	0.498	0.014
0.495	0.014	1.C10	0.493	0.014
0.490	0.015	1.C10	0.488	0.015
0.485	0.014	1.010	0.483	0.014
0.480	0.011	1.C1C	0.478	0.011
0.475	0.009	1.0C9	0.473	0.009
0.470	0.006	1.010	0.468	0.006
0.465	0.003	1.C10	0.463	0.003
0.460	0.001	1.005	0.458	0.001
0.455	0.0	1.0C5	0.453	0.0
0.450	0.0	1.003	0.448	0.0
0.445	0.0	1.002	0.443	0.0
0.440	0.0	1.CC2	0.438	0.0
0.435	0.0	1.001	0.433	0.0
0.430	0.0	1.000	0.428	0.0
0.425	0.0	1.CCC	0.423	0.0

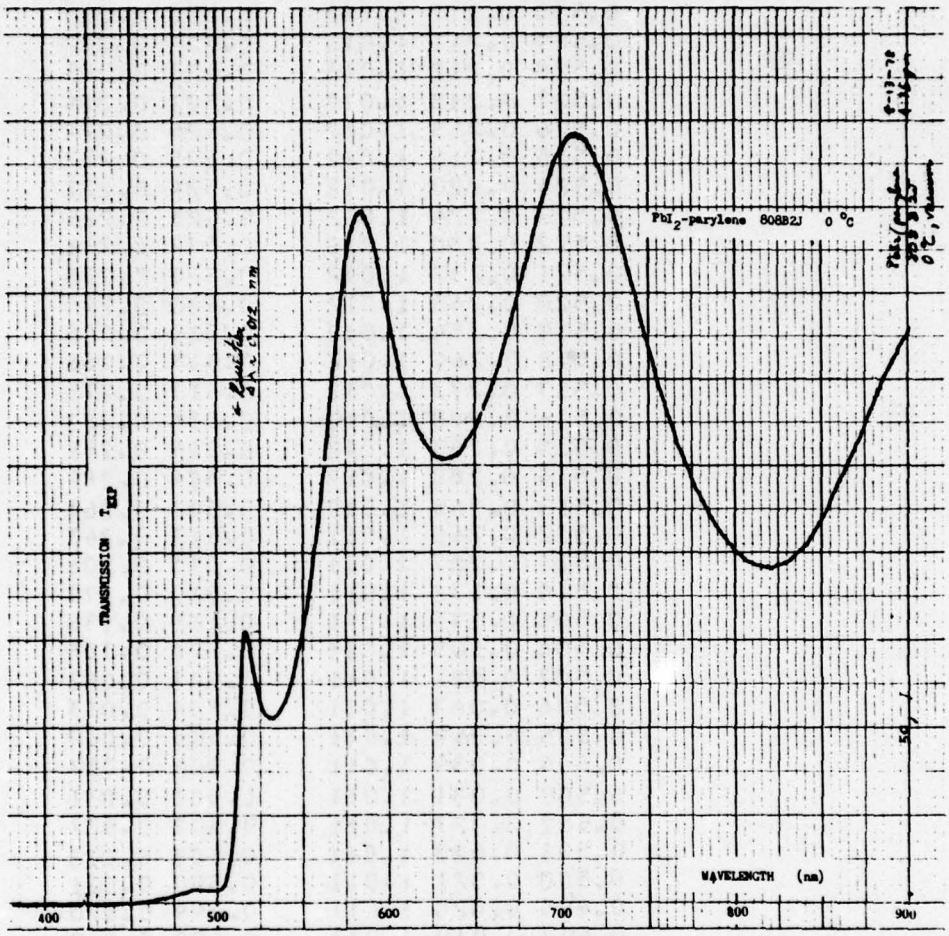

FIGURE 2.5-66. Transmission of PbI_2-parylene No. 808B2J at 0°C.

Table 2.5-39. High-resolution Transmission Scan of PbI_2-parylene No. 808B2J at 0°C.

TEMP= 0. PBI2 PARY 808B -2J 8.13 4.45

WL EXP	T EXP	CALIB	WL	TRANS
0.530	0.212	1.013	0.530	0.213
0.529	0.211	1.013	0.529	0.212
0.528	0.210	1.013	0.528	0.211
0.527	0.212	1.012	0.527	0.213
0.526	0.213	1.012	0.526	0.214
0.525	0.216	1.012	0.525	0.217
0.524	0.219	1.012	0.524	0.220
0.523	0.224	1.012	0.523	0.225
0.522	0.230	1.012	0.522	0.231
0.521	0.238	1.012	0.521	0.239
0.520	0.247	1.012	0.520	0.248
0.519	0.257	1.012	0.519	0.259
0.518	0.269	1.012	0.518	0.271
0.517	0.281	1.012	0.517	0.283
0.516	0.294	1.012	0.516	0.296
0.515	0.305	1.012	0.515	0.307
0.514	0.311	1.012	0.514	0.313
0.513	0.308	1.012	0.513	0.310
0.512	0.290	1.011	0.512	0.292
0.511	0.256	1.011	0.511	0.258
0.510	0.213	1.011	0.510	0.214
0.509	0.169	1.011	0.509	0.170
0.508	0.129	1.011	0.508	0.130
0.507	0.096	1.011	0.507	0.097
0.506	0.071	1.011	0.506	0.071
0.505	0.052	1.011	0.505	0.052
0.504	0.039	1.011	0.504	0.039
0.503	0.030	1.011	0.503	0.030
0.502	0.024	1.011	0.502	0.024
0.501	0.020	1.011	0.501	0.020
0.500	0.018	1.011	0.500	0.018
0.499	0.017	1.011	0.499	0.017
0.498	0.015	1.011	0.498	0.015
0.497	0.015	1.010	0.497	0.015
0.496	0.015	1.010	0.496	0.015
0.495	0.015	1.010	0.495	0.015
0.494	0.015	1.010	0.494	0.015
0.493	0.015	1.010	0.493	0.015
0.492	0.015	1.010	0.492	0.015
0.491	0.015	1.010	0.491	0.015
0.490	0.015	1.010	0.490	0.015
0.489	0.015	1.010	0.489	0.015
0.488	0.015	1.010	0.488	0.015
0.487	0.015	1.010	0.487	0.015
0.486	0.015	1.010	0.486	0.015
0.485	0.015	1.010	0.485	0.015
0.484	0.015	1.010	0.484	0.015
0.483	0.015	1.010	0.483	0.015
0.482	0.015	1.010	0.482	0.015
0.481	0.014	1.010	0.481	0.014
0.480	0.013	1.010	0.480	0.013

TEMP= 10. PBI2 PARY 808B -2J 8.13 5.07

WL EXP	T EXP	CALIB	WL	TRANS
0.900	0.655	C.977	0.898	0.646
0.895	0.640	0.973	0.893	0.670
0.890	0.620	C.979	0.888	0.647
0.885	0.600	0.977	0.883	0.625
0.880	0.576	C.980	0.878	0.596
0.875	0.550	C.982	0.873	0.570
0.870	0.526	0.985	0.868	0.542
0.865	0.503	C.990	0.863	0.517
0.860	0.484	0.994	0.858	0.496
0.855	0.463	0.995	0.853	0.474
0.850	0.440	C.998	0.848	0.449
0.845	0.423	1.000	0.843	0.431
0.840	0.409	1.000	0.838	0.416
0.835	0.399	1.001	0.833	0.406
0.830	0.390	1.002	0.828	0.396
0.825	0.085	1.003	0.823	0.086
0.820	0.382	1.005	0.818	0.387
0.815	0.382	1.004	0.813	0.387
0.810	0.386	1.006	0.808	0.391
0.805	0.391	1.008	0.803	0.395
0.800	0.400	1.009	0.798	0.404
0.795	0.410	1.010	0.793	0.413
0.790	0.424	1.010	0.788	0.427
0.785	0.440	1.010	0.783	0.443
0.780	0.460	1.010	0.778	0.464
0.775	0.479	1.010	0.773	0.483
0.770	0.503	1.010	0.768	0.507
0.765	0.530	1.010	0.763	0.534
0.760	0.559	1.010	0.758	0.563
0.755	0.590	1.010	0.753	0.595
0.750	0.629	1.010	0.748	0.634
0.745	0.664	1.010	0.743	0.669
0.740	0.703	1.010	0.738	0.709
0.735	0.743	1.010	0.733	0.749
0.730	0.785	1.010	0.728	0.791
0.725	0.815	1.010	0.723	0.821
0.720	0.849	1.010	0.718	0.854
0.715	0.869	1.010	0.713	0.876
0.710	0.890	1.010	0.708	0.897
0.705	0.882	1.010	0.703	0.889
0.700	0.870	1.010	0.698	0.877
0.695	0.852	1.010	0.693	0.859
0.690	0.871	1.010	0.688	0.878
0.685	0.787	1.010	0.683	0.793
0.680	0.745	1.010	0.678	0.751
0.675	0.709	1.010	0.673	0.715
0.670	0.669	1.011	0.668	0.674
0.665	0.632	1.011	0.663	0.636
0.660	0.598	1.011	0.658	0.602
0.655	0.570	1.010	0.653	0.575
0.650	0.548	1.010	0.648	0.552
0.645	0.528	1.010	0.643	0.532
0.640	0.515	1.010	0.638	0.519
0.635	0.510	1.010	0.633	0.514
0.630	0.510	1.012	0.628	0.513
0.625	0.517	1.012	0.623	0.520
0.620	0.530	1.013	0.618	0.533
0.615	0.550	1.011	0.613	0.554
0.610	0.584	1.010	0.608	0.589
0.605	0.620	1.010	0.603	0.625
0.600	0.666	1.010	0.598	0.671
0.595	0.719	1.010	0.593	0.725
0.590	0.764	1.010	0.588	0.770
0.585	0.792	1.011	0.583	0.797
0.580	0.789	1.010	0.578	0.795
0.575	0.742	1.010	0.573	0.748
0.570	0.660	1.011	0.568	0.665
0.565	0.570	1.012	0.563	0.573
0.560	0.465	1.017	0.558	0.465
0.555	0.388	1.016	0.553	0.389
0.550	0.320	1.015	0.548	0.325
0.545	0.275	1.014	0.543	0.278
0.540	0.238	1.015	0.538	0.239
0.535	0.219	1.014	0.533	0.220
0.530	0.211	1.013	0.528	0.212
0.525	0.223	1.012	0.523	0.224
0.520	0.268	1.011	0.518	0.270
0.515	0.293	1.011	0.513	0.295
0.510	0.120	1.010	0.508	0.121
0.505	0.033	1.010	0.503	0.033
0.500	0.017	1.010	0.498	0.017
0.495	0.016	1.010	0.493	0.016
0.490	0.017	1.010	0.488	0.017
0.485	0.016	1.010	0.483	0.016
0.480	0.012	1.010	0.478	0.012
0.475	0.010	1.009	0.473	0.010
0.470	0.007	1.010	0.468	0.007
0.465	0.006	1.010	0.463	0.006
0.460	0.002	1.009	0.458	0.002
0.455	0.001	1.005	0.453	0.001
0.450	0.0	1.003	0.448	0.0
0.445	0.0	1.002	0.443	0.0
0.440	0.0	1.002	0.438	0.0
0.435	0.0	1.001	0.433	0.0
0.430	0.0	1.000	0.428	0.0
0.425	0.0	1.000	0.423	0.0

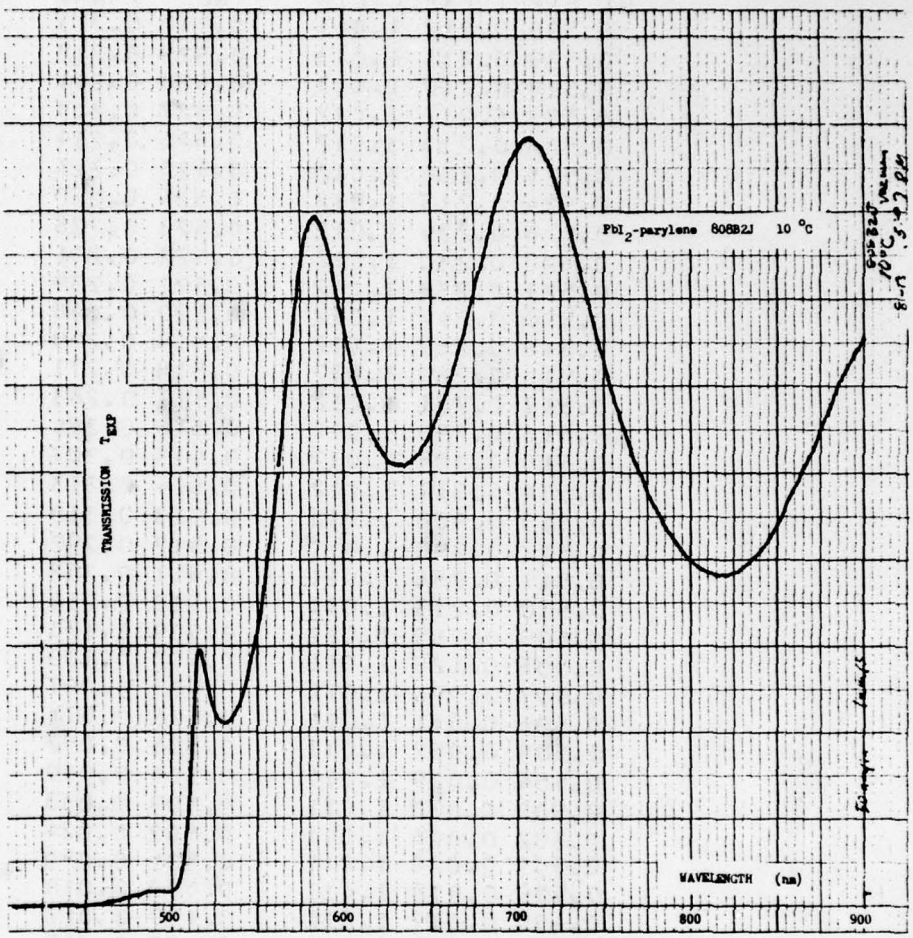

FIGURE 2.5-67. Transmission of PbI_2-parylene No. 808B2J at 10°C.

Table 2.5-40. High-resolution Transmission Scan of PbI_2-parylene No. 808B2J at 10°C.

TEMP= 10. PBI2 PARY 808B -2J 8.13 5.15

WL EXP	T EXP	CALIB	WL	TRANS
0.530	0.211	1.013	0.530	0.212
0.529	0.210	1.013	0.529	0.211
0.528	0.210	1.013	0.528	0.211
0.527	0.211	1.012	0.527	0.212
0.526	0.212	1.012	0.526	0.213
0.525	0.217	1.012	0.525	0.218
0.524	0.219	1.012	0.524	0.220
0.523	0.223	1.012	0.523	0.224
0.522	0.229	1.012	0.522	0.230
0.521	0.237	1.012	0.521	0.238
0.520	0.246	1.012	0.520	0.247
0.519	0.255	1.012	0.519	0.257
0.518	0.267	1.012	0.518	0.269
0.517	0.278	1.012	0.517	0.280
0.516	0.288	1.012	0.516	0.290
0.515	0.295	1.012	0.515	0.297
0.514	0.295	1.012	0.514	0.297
0.513	0.285	1.012	0.513	0.287
0.512	0.263	1.011	0.512	0.265
0.511	0.228	1.011	0.511	0.230
0.510	0.190	1.011	0.510	0.191
0.509	0.149	1.011	0.509	0.150
0.508	0.113	1.011	0.508	0.114
0.507	0.086	1.011	0.507	0.087
0.506	0.065	1.011	0.506	0.065
0.505	0.050	1.011	0.505	0.050
0.504	0.039	1.011	0.504	0.039
0.503	0.030	1.011	0.503	0.030
0.502	0.025	1.011	0.502	0.025
0.501	0.021	1.011	0.501	0.021
0.500	0.019	1.011	0.500	0.019
0.499	0.018	1.011	0.499	0.018
0.498	0.017	1.011	0.498	0.017
0.497	0.016	1.010	0.497	0.016
0.496	0.016	1.010	0.496	0.016
0.495	0.016	1.010	0.495	0.016
0.494	0.016	1.010	0.494	0.016
0.493	0.016	1.010	0.493	0.016
0.492	0.016	1.010	0.492	0.016
0.491	0.016	1.010	0.491	0.016
0.490	0.016	1.010	0.490	0.016
0.489	0.016	1.010	0.489	0.016
0.488	0.016	1.010	0.488	0.016
0.487	0.016	1.010	0.487	0.016
0.486	0.016	1.010	0.486	0.016
0.485	0.015	1.010	0.485	0.015
0.484	0.015	1.010	0.484	0.015
0.483	0.014	1.010	0.483	0.014
0.482	0.014	1.010	0.482	0.014
0.481	0.014	1.010	0.481	0.014
0.480	0.013	1.010	0.480	0.013

IEPP= 20. PB12 PARY 808B -2J 8.13 5.45

WL EXP	T EXP	CALIB	WL	TRANS
0.900	0.654	0.972	0.898	0.683
0.895	0.638	0.971	0.893	0.665
0.890	0.621	0.975	0.888	0.644
0.885	0.601	0.977	0.883	0.624
0.880	0.574	0.980	0.878	0.594
0.875	0.550	0.982	0.873	0.568
0.870	0.527	0.985	0.868	0.543
0.865	0.507	0.990	0.863	0.520
0.860	0.484	0.994	0.859	0.494
0.855	0.463	0.995	0.853	0.472
0.850	0.441	0.998	0.848	0.448
0.845	0.425	1.000	0.843	0.431
0.840	0.410	1.000	0.838	0.416
0.835	0.400	1.001	0.833	0.405
0.830	0.391	1.002	0.828	0.396
0.825	0.386	1.003	0.823	0.390
0.820	0.383	1.005	0.818	0.387
0.815	0.384	1.004	0.813	0.388
0.810	0.388	1.006	0.809	0.391
0.805	0.392	1.008	0.803	0.395
0.800	0.400	1.009	0.798	0.402
0.795	0.411	1.010	0.793	0.413
0.790	0.425	1.010	0.788	0.427
0.785	0.439	1.010	0.783	0.441
0.780	0.459	1.010	0.778	0.461
0.775	0.479	1.010	0.773	0.481
0.770	0.504	1.010	0.768	0.506
0.765	0.529	1.010	0.763	0.531
0.760	0.560	1.010	0.758	0.563
0.755	0.593	1.010	0.753	0.596
0.750	0.625	1.010	0.748	0.628
0.745	0.665	1.010	0.743	0.668
0.740	0.705	1.010	0.738	0.708
0.735	0.745	1.010	0.733	0.748
0.730	0.784	1.010	0.728	0.788
0.725	0.816	1.010	0.723	0.820
0.720	0.850	1.010	0.718	0.854
0.715	0.869	1.010	0.713	0.873
0.710	0.885	1.010	0.708	0.889
0.705	0.886	1.010	0.703	0.890
0.700	0.874	1.010	0.698	0.878
0.695	0.856	1.010	0.693	0.860
0.690	0.825	1.010	0.688	0.829
0.685	0.791	1.010	0.683	0.795
0.680	0.750	1.010	0.678	0.753
0.675	0.711	1.010	0.673	0.714
0.670	0.680	1.011	0.668	0.682
0.665	0.637	1.011	0.663	0.639
0.660	0.600	1.011	0.658	0.602
0.655	0.574	1.010	0.653	0.577
0.650	0.549	1.010	0.648	0.551
0.645	0.531	1.010	0.643	0.533
0.640	0.519	1.010	0.638	0.521
0.635	0.512	1.010	0.633	0.514
0.630	0.510	1.012	0.628	0.512
0.625	0.516	1.012	0.623	0.517
0.620	0.529	1.013	0.618	0.530
0.615	0.549	1.011	0.613	0.551
0.610	0.579	1.010	0.608	0.582
0.605	0.615	1.010	0.603	0.618
0.600	0.662	1.010	0.598	0.665
0.595	0.718	1.010	0.593	0.721
0.590	0.768	1.010	0.588	0.771
0.585	0.797	1.011	0.583	0.800
0.580	0.793	1.010	0.578	0.797
0.575	0.748	1.010	0.573	0.751
0.570	0.660	1.011	0.568	0.662
0.565	0.565	1.012	0.561	0.566
0.560	0.445	1.017	0.558	0.444
0.555	0.306	1.016	0.553	0.305

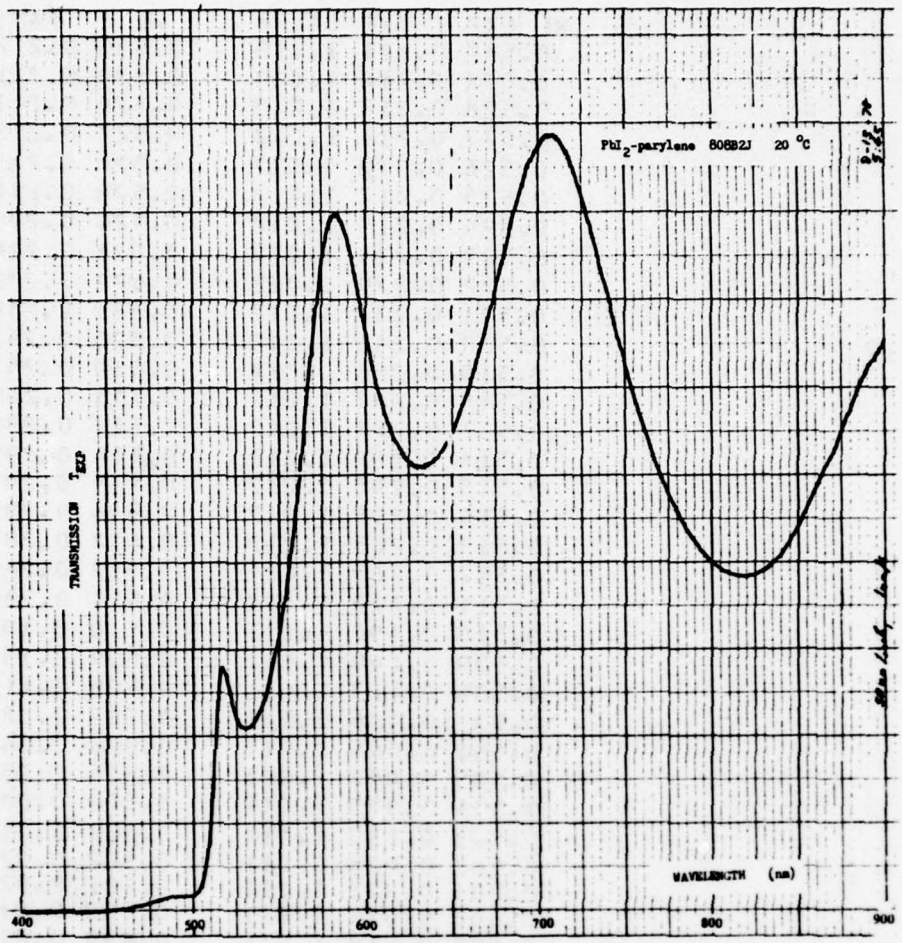

FIGURE 2.5-68. Transmission of PbI_2-parylene No. 808B2J at 20°C.

0.550	0.314	1.019	0.548	0.314
0.545	0.274	1.014	0.543	0.274
0.540	0.237	1.019	0.538	0.237
0.535	0.217	1.014	0.533	0.217
0.530	0.210	1.011	0.528	0.210
0.525	0.220	1.012	0.523	0.221
0.520	0.260	1.011	0.518	0.261
0.515	0.260	1.011	0.513	0.261
0.510	0.101	1.010	0.508	0.101
0.505	0.034	1.010	0.503	0.034
0.500	0.018	1.010	0.498	0.018
0.495	0.017	1.010	0.493	0.017
0.490	0.017	1.010	0.488	0.017
0.485	0.014	1.010	0.483	0.014
0.480	0.012	1.010	0.478	0.012
0.475	0.009	1.009	0.473	0.009
0.470	0.006	1.010	0.468	0.006
0.465	0.004	1.010	0.463	0.004
0.460	0.002	1.005	0.458	0.002
0.455	0.001	1.005	0.453	0.001
0.450	0.0	1.003	0.448	0.0
0.445	0.0	1.002	0.443	0.0
0.440	0.0	1.002	0.438	0.0
0.435	0.0	1.001	0.433	0.0
0.430	0.0	1.000	0.428	0.0
0.425	0.0	1.000	0.423	0.0

Table 2.5-41. High-resolution Transmission Scan of PbI_2-parylene No. 308B2J at 20°C.

TEMP= 20. PBI2 8088 -2J 8.13 6.10

WL EXP	T EXP	CALIB	WL	TRANS
0.530	0.211	1.013	0.530	0.211
0.529	0.211	1.013	0.529	0.211
0.528	0.211	1.013	0.528	0.211
0.527	0.212	1.012	0.527	0.213
0.526	0.213	1.012	0.526	0.214
0.525	0.217	1.012	0.525	0.218
0.524	0.220	1.012	0.524	0.221
0.523	0.224	1.012	0.523	0.225
0.522	0.230	1.012	0.522	0.231
0.521	0.237	1.012	0.521	0.238
0.520	0.245	1.012	0.520	0.246
0.519	0.255	1.012	0.519	0.256
0.518	0.264	1.012	0.518	0.265
0.517	0.273	1.012	0.517	0.274
0.516	0.280	1.012	0.516	0.281
0.515	0.282	1.012	0.515	0.283
0.514	0.278	1.012	0.514	0.279
0.513	0.263	1.012	0.513	0.264
0.512	0.235	1.011	0.512	0.236
0.511	0.202	1.011	0.511	0.203
0.510	0.167	1.011	0.510	0.168
0.509	0.133	1.011	0.509	0.133
0.508	0.104	1.011	0.508	0.104
0.507	0.080	1.011	0.507	0.080
0.506	0.062	1.011	0.506	0.062
0.505	0.049	1.011	0.505	0.049
0.504	0.039	1.011	0.504	0.039
0.503	0.031	1.011	0.503	0.031
0.502	0.027	1.011	0.502	0.027
0.501	0.023	1.011	0.501	0.023
0.500	0.021	1.011	0.500	0.021
0.499	0.020	1.011	0.499	0.020
0.498	0.020	1.011	0.498	0.020
0.497	0.019	1.010	0.497	0.019
0.496	0.018	1.010	0.496	0.018
0.495	0.018	1.010	0.495	0.018
0.494	0.018	1.010	0.494	0.018
0.493	0.018	1.010	0.493	0.018
0.492	0.018	1.010	0.492	0.018
0.491	0.018	1.010	0.491	0.018
0.490	0.018	1.010	0.490	0.018
0.489	0.017	1.010	0.489	0.017
0.488	0.017	1.010	0.488	0.017
0.487	0.017	1.010	0.487	0.017
0.486	0.017	1.010	0.486	0.017
0.485	0.017	1.010	0.485	0.017
0.484	0.016	1.010	0.484	0.016
0.483	0.015	1.010	0.483	0.015
0.482	0.015	1.010	0.482	0.015
0.481	0.014	1.010	0.481	0.014
0.480	0.013	1.010	0.480	0.013

IEPP= 32. P212 PARY 808B -2J 8.13 6.30

WL EXP	T EXP	CALIB	WL	TRANS
C.900	0.664	C.572	0.899	0.684
0.895	0.650	C.973	0.892	0.669
0.890	0.626	0.975	0.888	0.643
0.885	0.655	C.977	0.882	0.671
0.880	0.580	C.980	C.878	0.592
C.875	0.553	C.982	0.873	0.564
C.87C	0.530	C.985	0.868	0.539
0.865	0.509	C.990	0.863	0.515
C.860	0.487	C.994	0.858	0.490
C.855	0.465	0.995	C.853	0.468
C.850	0.445	C.998	0.848	0.446
0.845	0.429	1.000	0.843	0.429
0.840	0.412	1.CC0	0.838	0.412
0.835	0.401	1.CC1	C.833	0.401
0.830	0.393	1.CC2	0.828	0.393
0.825	0.385	1.CC3	0.823	0.383
0.820	0.388	1.CC5	0.818	0.386
0.815	0.388	1.CC6	0.813	0.387
C.810	0.391	1.CC6	C.808	C.389
0.805	0.397	1.CC8	0.803	0.396
0.800	0.405	1.CC9	0.798	0.402
0.795	0.416	1.C10	0.793	0.412
0.790	0.430	1.010	0.788	0.426
0.785	0.446	1.C1C	0.783	C.442
0.780	0.465	1.C10	0.778	0.461
0.775	0.487	1.C1C	0.773	0.483
0.770	0.510	1.C1C	0.768	C.505
0.765	0.535	1.C10	0.763	0.530
0.76C	0.579	1.C1C	0.758	0.574
0.755	0.598	1.010	0.753	0.593
0.750	0.639	1.C10	0.748	0.634
0.745	0.673	1.010	0.743	0.667
0.740	0.717	1.C10	0.738	0.711
0.735	0.754	1.C1C	C.733	C.747
0.730	0.798	1.C10	0.728	0.791
0.725	0.831	1.C1C	0.723	0.824
0.720	0.86C	1.C1C	0.718	0.852
0.715	0.882	1.010	0.713	0.874
0.710	0.895	1.C10	0.708	0.887
0.705	0.899	1.C10	0.703	0.891
0.700	0.896	1.010	0.698	0.888
C.695	0.866	1.C1C	C.693	0.858
0.690	0.835	1.C10	0.688	0.828
0.685	0.801	1.C1C	0.683	0.794
C.68C	0.76C	1.C1C	C.678	0.753
0.675	0.721	1.010	0.673	0.715
C.67C	0.675	1.C11	C.668	0.672
0.665	0.642	1.011	0.663	0.636
0.660	0.608	1.011	0.658	0.602
C.655	0.5PC	1.C1C	0.653	0.575
0.650	0.555	1.C10	0.648	0.552
0.645	0.549	1.C10	0.643	0.544
0.640	0.527	1.C1C	0.638	0.517
0.635	0.517	1.010	0.633	0.512
0.630	0.517	1.C12	0.628	0.511
0.625	0.523	1.C12	0.623	0.517
0.620	0.537	1.C13	0.618	0.531
C.615	0.555	1.C11	C.613	0.550
0.610	0.588	1.C10	0.608	0.583
0.605	0.622	1.C10	0.603	0.616
C.600	0.672	1.C1C	C.598	C.666
0.595	0.720	1.010	0.593	0.714
0.590	0.782	1.010	0.588	0.775
0.585	0.806	1.011	0.583	0.796
0.580	0.806	1.010	0.578	0.797
0.575	0.764	1.C1C	C.573	0.747
0.570	0.679	1.C11	C.568	0.672
0.565	0.580	1.C12	C.563	0.574
0.560	0.475	1.C17	C.558	0.468
0.555	0.399	1.016	0.553	0.393
0.550	0.328	1.C15	0.548	0.323
0.545	0.280	1.014	0.543	0.276
0.540	0.242	1.C15	C.538	0.239
0.535	0.220	1.C14	0.533	0.217
0.530	0.212	1.011	0.528	0.209
0.525	0.210	1.C12	0.523	0.207
0.520	0.209	1.C11	0.518	0.207
0.515	0.210	1.C11	0.513	0.207
0.510	0.174	1.C10	0.508	0.171
0.505	0.040	1.010	0.503	0.040
0.50C	0.020	1.01C	0.498	0.020
0.495	0.018	1.C10	0.493	0.018
0.490	0.018	1.010	0.488	0.018
0.485	0.015	1.C1C	C.483	0.015
0.480	0.012	1.010	0.478	0.012
0.475	0.009	1.CC9	0.473	0.009
0.47C	0.007	1.C1C	0.468	0.007
0.465	0.004	1.010	0.463	0.004
0.460	0.002	1.0C9	0.458	0.002
0.455	0.001	1.0C9	0.453	0.001
0.450	0.0	1.0C9	0.448	0.0
0.445	0.0	1.CC2	0.443	0.0
0.440	0.0	1.0C2	0.438	0.0
0.435	0.0	1.CC1	0.433	0.0
C.430	0.0	1.CCC	0.428	0.0
0.425	0.0	1.000	0.423	0.0

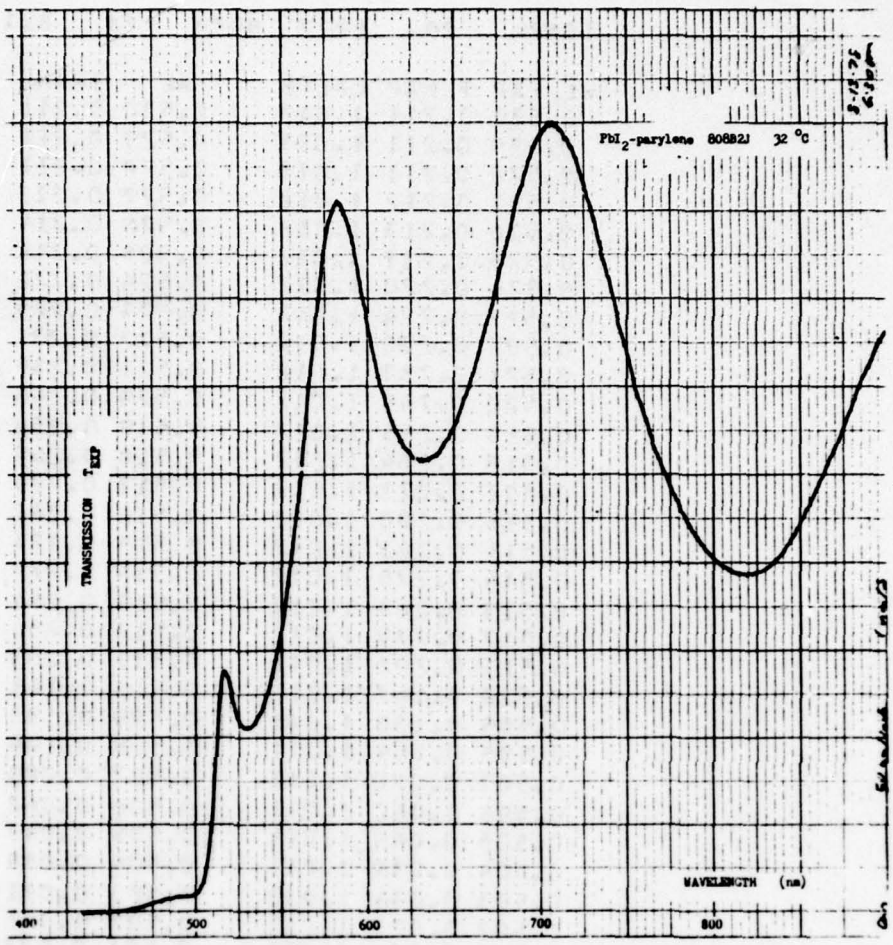

FIGURE 2.5-69. Transmission of PbI_2-parylene No. 808B2J at 32°C.

Table 2,5-42. High-resolution Transmission Scan of PbI_2-parylene No. 3088J at 32°C.

TEMP= 32. PBI2 PARY 8088 -2J 8.13 6

WL EXP	T EXP	CALIB	WL	TRANS
0.530	0.212	1.013	0.530	0.209
0.529	0.211	1.013	0.529	0.209
0.528	0.211	1.013	0.528	0.209
0.527	0.213	1.012	0.527	0.211
0.526	0.214	1.012	0.526	0.212
0.525	0.217	1.012	0.525	0.215
0.524	0.220	1.012	0.524	0.218
0.523	0.225	1.012	0.523	0.223
0.522	0.230	1.012	0.522	0.228
0.521	0.238	1.012	0.521	0.235
0.520	0.247	1.012	0.520	0.244
0.519	0.253	1.012	0.519	0.250
0.518	0.263	1.012	0.518	0.260
0.517	0.270	1.012	0.517	0.267
0.516	0.276	1.012	0.516	0.273
0.515	0.278	1.012	0.515	0.275
0.514	0.271	1.012	0.514	0.268
0.513	0.258	1.012	0.513	0.255
0.512	0.229	1.011	0.512	0.227
0.511	0.195	1.011	0.511	0.193
0.510	0.159	1.011	0.510	0.157
0.509	0.127	1.011	0.509	0.126
0.508	0.100	1.011	0.508	0.099
0.507	0.078	1.011	0.507	0.077
0.506	0.062	1.011	0.506	0.061
0.505	0.049	1.011	0.505	0.049
0.504	0.039	1.011	0.504	0.039
0.503	0.032	1.011	0.503	0.032
0.502	0.028	1.011	0.502	0.028
0.501	0.024	1.011	0.501	0.024
0.500	0.021	1.011	0.500	0.021
0.499	0.020	1.011	0.499	0.020
0.498	0.020	1.011	0.498	0.020
0.497	0.020	1.010	0.497	0.020
0.496	0.019	1.010	0.496	0.019
0.495	0.018	1.010	0.495	0.018
0.494	0.018	1.010	0.494	0.018
0.493	0.018	1.010	0.493	0.018
0.492	0.018	1.010	0.492	0.018
0.491	0.018	1.010	0.491	0.018
0.490	0.018	1.010	0.490	0.018
0.489	0.018	1.010	0.489	0.018
0.488	0.018	1.010	0.488	0.018
0.487	0.018	1.010	0.487	0.018
0.486	0.018	1.010	0.486	0.018
0.485	0.017	1.010	0.485	0.017
0.484	0.016	1.010	0.484	0.016
0.483	0.015	1.010	0.483	0.015
0.482	0.014	1.010	0.482	0.014
0.481	0.014	1.010	0.481	0.014
0.480	0.013	1.010	0.480	0.013

TEMP= 40. PBI2 PARY B08B -2J 9.13 7.05

WL	EXP T	EXP CALIB	WL	TRANS
0.900	0.666	0.972	0.898	0.693
0.895	0.654	0.971	0.893	0.670
0.890	0.635	0.975	0.888	0.649
0.885	0.613	0.977	0.883	0.625
0.880	0.588	0.980	0.878	0.598
0.875	0.561	0.982	0.873	0.569
0.870	0.547	0.985	0.868	0.553
0.865	0.519	0.990	0.863	0.518
0.860	0.492	0.994	0.858	0.493
0.855	0.472	0.995	0.853	0.473
0.850	0.450	0.998	0.848	0.449
0.845	0.431	1.000	0.843	0.430
0.840	0.417	1.000	0.838	0.416
0.835	0.403	1.001	0.833	0.401
0.830	0.394	1.002	0.828	0.392
0.825	0.390	1.003	0.823	0.387
0.820	0.386	1.005	0.818	0.383
0.815	0.386	1.004	0.813	0.383
0.810	0.389	1.006	0.808	0.385
0.805	0.393	1.008	0.803	0.389
0.800	0.400	1.009	0.798	0.395
0.795	0.411	1.010	0.793	0.406
0.790	0.425	1.010	0.788	0.419
0.785	0.440	1.010	0.783	0.434
0.780	0.459	1.010	0.778	0.453
0.775	0.479	1.010	0.773	0.473
0.770	0.502	1.010	0.768	0.495
0.765	0.528	1.010	0.763	0.521
0.760	0.560	1.010	0.758	0.553
0.755	0.591	1.010	0.753	0.583
0.750	0.631	1.010	0.748	0.623
0.745	0.664	1.010	0.743	0.655
0.740	0.710	1.010	0.738	0.701
0.735	0.748	1.010	0.733	0.738
0.730	0.789	1.010	0.728	0.779
0.725	0.825	1.010	0.723	0.814
0.720	0.860	1.010	0.718	0.849
0.715	0.882	1.010	0.713	0.870
0.710	0.895	1.010	0.708	0.887
0.705	0.903	1.010	0.703	0.891
0.700	0.895	1.010	0.698	0.883
0.695	0.878	1.010	0.693	0.866
0.690	0.846	1.010	0.688	0.835
0.685	0.810	1.010	0.683	0.799
0.680	0.768	1.010	0.678	0.758
0.675	0.726	1.010	0.673	0.716
0.670	0.687	1.011	0.668	0.672
0.665	0.648	1.011	0.663	0.639
0.660	0.610	1.011	0.658	0.601
0.655	0.583	1.010	0.653	0.575
0.650	0.558	1.010	0.648	0.551
0.645	0.540	1.010	0.643	0.533
0.640	0.526	1.010	0.638	0.519
0.635	0.519	1.010	0.633	0.512
0.630	0.515	1.012	0.628	0.507
0.625	0.520	1.012	0.623	0.512
0.620	0.535	1.013	0.618	0.526
0.615	0.551	1.011	0.613	0.543
0.610	0.583	1.010	0.608	0.575
0.605	0.620	1.010	0.603	0.612
0.600	0.666	1.010	0.598	0.657
0.595	0.718	1.010	0.593	0.709
0.590	0.770	1.010	0.588	0.760
0.585	0.805	1.011	0.583	0.796
0.580	0.807	1.010	0.578	0.796
0.575	0.775	1.010	0.573	0.769
0.570	0.695	1.011	0.568	0.689
0.565	0.600	1.012	0.563	0.591
0.560	0.490	1.012	0.558	0.480
0.555	0.410	1.010	0.553	0.402
0.550	0.336	1.010	0.548	0.330
0.545	0.286	1.010	0.543	0.281
0.540	0.249	1.010	0.538	0.241
0.535	0.223	1.010	0.533	0.219
0.530	0.211	1.010	0.528	0.208
0.525	0.214	1.012	0.523	0.211
0.520	0.248	1.011	0.518	0.244
0.515	0.269	1.011	0.513	0.261
0.510	0.140	1.010	0.508	0.138
0.505	0.040	1.010	0.503	0.047
0.500	0.028	1.010	0.498	0.028
0.495	0.019	1.010	0.493	0.019
0.490	0.017	1.010	0.488	0.017
0.485	0.015	1.010	0.483	0.015
0.480	0.012	1.010	0.478	0.012
0.475	0.110	1.005	0.473	0.109
0.470	0.006	1.010	0.468	0.006
0.465	0.003	1.010	0.463	0.003
0.460	0.001	1.005	0.458	0.001
0.455	0.0	1.005	0.453	0.0
0.450	0.0	1.003	0.448	0.0
0.445	0.0	1.002	0.443	0.0
0.440	0.0	1.002	0.438	0.0
0.435	0.0	1.001	0.433	0.0
0.430	0.0	1.000	0.428	0.0
0.425	0.0	1.000	0.423	0.0

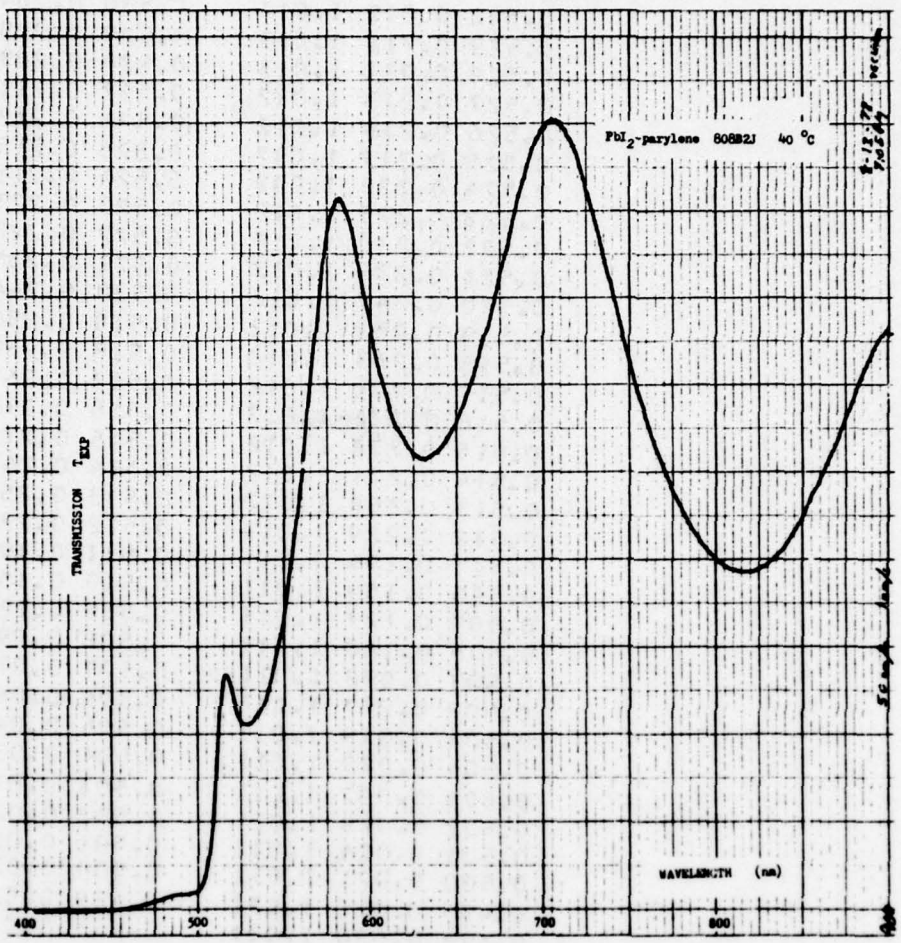

FIGURE 2.5-70. Transmission of PbI_2-parylene No. 808B2J at 40°C.

Table 2,5-43, High-resolution Transmission Scan of PbI_2-parylene No. 808B2J at 40°C.

TEMP= 40. PBI2 PARY 808B -2J 8.13 7.15

WL EXP	T EXP	CALIB	WL	TRANS
0.530	0.211	1.013	0.530	0.208
0.529	0.211	1.013	0.529	0.208
0.528	0.211	1.013	0.528	0.208
0.527	0.212	1.012	0.527	0.209
0.526	0.212	1.012	0.526	0.209
0.525	0.215	1.012	0.525	0.212
0.524	0.220	1.012	0.524	0.217
0.523	0.223	1.012	0.523	0.220
0.522	0.230	1.012	0.522	0.226
0.521	0.234	1.012	0.521	0.230
0.520	0.241	1.012	0.520	0.237
0.519	0.250	1.012	0.519	0.246
0.518	0.258	1.012	0.518	0.254
0.517	0.264	1.012	0.517	0.260
0.516	0.269	1.012	0.516	0.265
0.515	0.267	1.012	0.515	0.263
0.514	0.256	1.012	0.514	0.252
0.513	0.237	1.012	0.513	0.233
0.512	0.210	1.011	0.512	0.207
0.511	0.179	1.011	0.511	0.176
0.510	0.150	1.011	0.510	0.148
0.509	0.120	1.011	0.509	0.118
0.508	0.094	1.011	0.508	0.093
0.507	0.075	1.011	0.507	0.074
0.506	0.060	1.011	0.506	0.059
0.505	0.049	1.011	0.505	0.048
0.504	0.039	1.011	0.504	0.038
0.503	0.034	1.011	0.503	0.034
0.502	0.029	1.011	0.502	0.029
0.501	0.026	1.011	0.501	0.026
0.500	0.022	1.011	0.500	0.022
0.499	0.021	1.011	0.499	0.021
0.498	0.020	1.011	0.498	0.020
0.497	0.020	1.010	0.497	0.020
0.496	0.020	1.010	0.496	0.020
0.495	0.020	1.010	0.495	0.020
0.494	0.020	1.010	0.494	0.020
0.493	0.020	1.010	0.493	0.020
0.492	0.019	1.010	0.492	0.019
0.491	0.019	1.010	0.491	0.019
0.490	0.019	1.010	0.490	0.019
0.489	0.019	1.010	0.489	0.019
0.488	0.018	1.010	0.488	0.018
0.487	0.018	1.010	0.487	0.018
0.486	0.018	1.010	0.486	0.018
0.485	0.017	1.010	0.485	0.017
0.484	0.017	1.010	0.484	0.017
0.483	0.016	1.010	0.483	0.016
0.482	0.015	1.010	0.482	0.015
0.481	0.015	1.010	0.481	0.015
0.480	0.013	1.010	0.480	0.013

TEMP= 25. PBI2 PARY 808B ·2J 0.13 0.08

WL EXP	T EXP	CAL IR	WL	TRANS
0.900	0.664	C.972	0.898	0.685
0.895	0.642	C.973	0.893	0.662
0.890	0.621	0.975	0.888	0.639
0.885	0.600	C.977	0.883	0.616
0.88C	0.574	C.9EC	0.878	0.589
0.875	0.547	C.9E2	0.873	0.559
0.870	0.522	C.9E5	C.868	0.532
C.865	0.503	C.9EC	0.863	0.510
0.860	0.481	0.994	0.858	0.485
0.855	0.462	C.995	0.853	0.466
0.850	0.440	C.998	0.848	0.442
0.845	0.424	1.000	0.843	0.425
0.840	0.41C	1.CCC	0.838	C.411
0.835	0.398	1.0C1	0.833	0.399
0.830	0.391	1.CC2	0.828	0.391
0.825	0.387	1.CC3	C.823	0.387
0.820	0.387	1.005	0.818	0.386
0.815	0.388	1.CC6	C.813	0.389
0.810	0.390	1.0C6	0.808	0.389
0.805	0.397	1.0C8	0.803	0.395
0.80C	0.4C6	1.CC5	C.798	C.404
0.795	0.416	1.010	0.793	0.413
0.790	0.431	1.C1C	C.788	0.428
C.785	0.447	1.C1C	0.783	0.444
0.780	0.466	1.011	0.778	0.463
0.775	0.487	1.C10	0.773	0.484
0.770	0.511	1.C10	0.768	0.508
0.765	0.538	1.C1C	0.763	0.534
0.760	0.570	1.010	0.758	0.566
0.755	0.601	1.010	0.753	0.597
C.750	0.641	1.C1C	0.748	C.637
0.745	0.675	1.C10	0.743	0.670
0.740	0.719	1.C1C	C.738	0.714
0.735	C.758	1.C1C	C.733	0.753
C.730	0.798	1.C10	0.728	0.793
0.725	0.832	1.C10	0.723	0.826
0.720	0.862	1.C10	C.718	0.856
0.715	0.882	1.010	0.713	0.876
C.710	0.899	1.C1C	C.7C8	C.899
0.705	0.895	1.010	0.703	C.889
0.700	0.882	1.C10	0.698	0.876
0.695	0.861	1.C1C	0.693	0.855
C.690	0.832	1.010	0.688	0.826
0.685	0.799	1.C10	0.683	0.793
0.683	0.751	1.C10	0.678	0.746
0.675	0.712	1.010	0.673	0.707
C.67C	0.672	1.C11	0.668	0.667
0.665	0.638	1.C11	0.663	0.633
0.660	0.607	1.C11	0.658	0.597
0.655	0.576	1.C1C	C.653	0.572
0.650	0.550	1.010	0.648	0.546
0.645	0.534	1.C1C	0.643	0.530
0.640	0.522	1.010	0.638	0.518
0.635	0.514	1.012	0.633	0.511
0.630	0.514	1.C12	0.628	0.510
0.625	0.522	1.C12	0.623	0.517
0.620	0.537	1.C13	C.618	0.532
0.615	0.558	1.C11	0.613	0.554
C.610	0.584	1.010	0.608	0.585
0.605	0.625	1.C1C	0.603	0.621
0.600	0.675	1.C10	0.598	0.670
0.595	0.724	1.010	0.593	0.719
0.590	0.774	1.C1C	C.588	0.769
0.585	0.801	1.C11	0.583	0.797
0.580	0.802	1.C10	0.578	0.797
0.575	0.755	1.C1C	0.573	0.750
0.570	0.673	1.011	0.568	0.668
0.565	0.575	1.C12	0.563	0.570
0.560	0.473	1.C17	0.558	0.467
0.555	0.390	1.016	0.553	0.385
0.550	0.329	1.C15	0.548	0.321
0.545	0.277	1.C14	0.543	0.274
0.54C	0.24C	1.C15	C.538	C.237
0.535	0.220	1.C14	0.533	0.218
0.530	0.211	1.C13	0.528	0.209
0.525	0.210	1.C13	0.523	0.210
0.520	0.260	1.C11	0.518	0.258
0.515	0.274	1.C11	0.513	0.272
0.510	0.125	1.C10	0.508	0.124
0.505	0.038	1.010	0.503	0.038
0.50C	0.019	1.C1C	C.498	0.019
0.495	0.017	1.010	0.493	0.017
C.49C	0.016	1.C1C	0.488	0.016
0.485	0.014	1.C1C	C.483	0.014
0.480	0.011	1.010	0.478	0.011
0.475	0.009	1.CC9	0.473	0.009
0.470	0.006	1.010	0.468	0.006
0.465	0.003	1.C1C	0.463	0.003
0.460	0.002	1.CC9	0.458	0.002
0.455	0.0	1.CC9	0.453	0.0
0.450	0.0	1.CC3	0.448	0.0
0.445	0.0	1.CC2	0.443	0.0
0.440	0.0	1.002	0.438	0.0
0.435	0.0	1.CC1	0.433	0.0
0.430	0.0	1.CC0	0.428	0.0
0.425	0.0	1.000	0.423	0.0

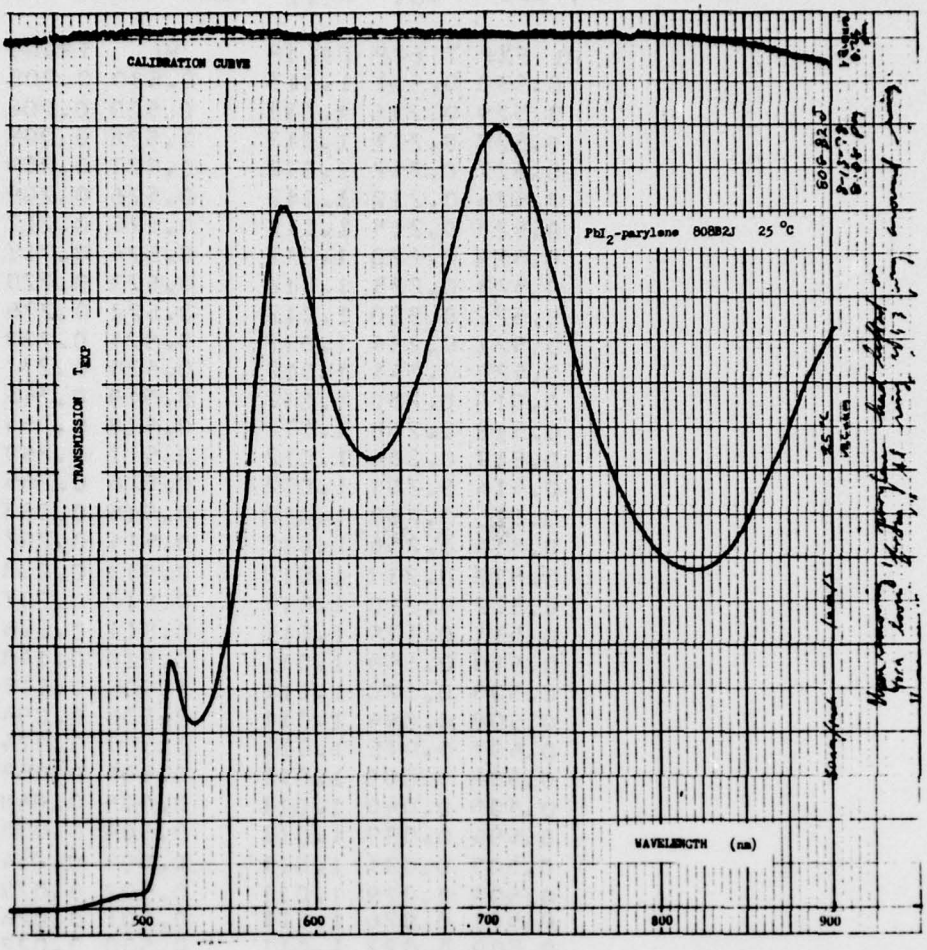

FIGURE 2.5-71. Transmission of PbI_2-parylene No. 808B2J at 25°C.

TEMP= 50. PBI2 PARY 808B -2J 8.13 8.35

WL EXP	T EXP	CALIB	WL	TRANS
0.900	0.656	C.572	0.898	0.599
0.895	0.643	C.573	C.893	C.587
0.890	0.622	0.575	0.888	0.566
0.885	0.600	C.577	0.883	0.565
0.880	0.574	C.580	0.878	0.520
0.875	0.549	C.582	0.873	0.496
0.870	0.524	C.585	0.868	C.472
0.865	0.504	C.550	0.863	0.452
0.860	0.471	C.554	0.858	0.421
0.855	0.461	C.555	C.853	0.411
0.850	0.438	0.558	0.848	0.390
0.845	0.421	1.CC0	0.843	0.374
0.840	0.406	1.CC0	0.838	0.361
0.835	0.397	1.001	0.833	0.352
0.830	0.390	1.CC2	C.828	0.344
0.825	0.384	1.CC3	0.823	C.340
0.820	0.383	1.CC5	0.818	0.338
C.815	0.384	1.CC4	0.813	0.340
0.810	0.388	1.CC6	0.808	0.342
0.805	0.394	1.CC8	0.803	0.347
0.800	0.403	1.CC9	0.798	0.355
0.795	0.414	1.C10	0.793	0.364
0.790	0.430	1.C1C	0.788	0.378
0.785	0.447	1.C10	0.783	0.393
0.780	0.467	1.C10	0.778	0.411
C.775	0.488	1.C1C	C.773	C.429
0.770	0.511	1.010	0.768	0.449
C.765	0.540	1.C1C	C.763	0.475
0.760	0.570	1.010	0.758	0.501
0.755	0.603	1.C10	0.753	0.530
0.750	0.642	1.010	0.748	0.564
0.745	0.684	1.010	0.743	0.601
0.740	0.725	1.C1C	0.738	C.637
0.735	0.769	1.010	0.733	0.673
0.730	0.806	1.C1C	0.728	0.709
0.725	0.841	1.C1C	C.723	0.739
0.720	0.872	1.010	0.718	0.767
0.715	0.890	1.C10	0.713	0.782
0.710	0.900	1.010	0.708	0.791
0.705	0.901	1.010	0.703	0.792
0.700	0.886	1.C1C	0.698	0.779
0.695	0.865	1.C10	0.693	0.761
0.690	0.83C	1.C10	0.688	0.730
0.685	0.793	1.C1C	C.683	0.697
0.680	0.750	1.010	0.678	0.659
0.675	0.710	1.C10	0.673	0.624
0.670	0.668	1.C11	0.668	0.587
0.665	0.634	1.011	0.663	0.557
0.660	0.599	1.C11	C.658	0.526
0.655	0.572	1.010	0.653	0.503
0.650	0.549	1.C10	0.648	0.483
0.645	0.531	1.C1C	0.643	0.467
0.640	0.519	1.C10	0.638	0.456
0.635	0.511	1.C10	0.633	0.449
0.630	0.513	1.C12	0.628	0.450
0.625	0.521	1.012	0.623	0.457
0.620	0.530	1.C13	C.618	0.472
0.615	0.559	1.C11	0.613	0.490
0.610	0.592	1.C10	0.608	0.520
0.605	0.631	1.C1C	0.603	0.555
0.600	0.686	1.010	0.598	0.601
0.595	0.735	1.C1C	0.593	0.646
0.590	0.784	1.010	0.588	0.689
0.585	0.810	1.011	0.583	0.711
0.580	0.800	1.C10	0.578	0.703
0.575	0.748	1.C10	0.573	0.658
0.570	0.659	1.C11	0.568	0.579
0.565	0.595	1.C12	C.563	0.487
0.560	0.450	1.017	0.558	0.393
0.555	0.370	1.C16	0.553	0.323
0.550	0.306	1.C15	0.548	0.268
0.545	0.260	1.C14	0.543	0.228
0.540	0.228	1.015	0.538	0.199
0.535	0.210	1.014	0.533	0.184
0.530	0.200	1.C13	0.528	0.182
0.525	0.225	1.C12	0.523	0.197
0.520	0.254	1.C11	0.518	0.223
0.515	0.190	1.C11	0.513	0.167
0.510	0.068	1.010	0.508	0.060
0.505	0.029	1.C10	0.503	0.025
0.500	0.020	1.C10	0.498	0.018
0.495	0.019	1.010	0.493	0.017
C.490	0.017	1.C10	C.488	0.015
0.485	0.016	1.010	0.483	0.012
0.480	0.010	1.C10	0.478	0.009
0.475	0.008	1.CC9	0.473	0.007
0.470	0.004	1.010	0.468	0.004
0.465	0.002	1.C10	0.463	0.002
0.460	0.001	1.005	0.458	0.001
0.455	0.0	1.005	0.453	0.0
0.450	0.0	1.CC3	0.448	0.0
0.445	0.0	1.CC2	0.443	0.0
0.440	0.0	1.CC2	0.438	0.0
0.435	0.0	1.CC1	0.433	0.0
0.430	0.0	1.000	0.428	0.0
0.425	0.0	1.CC0	0.423	0.0

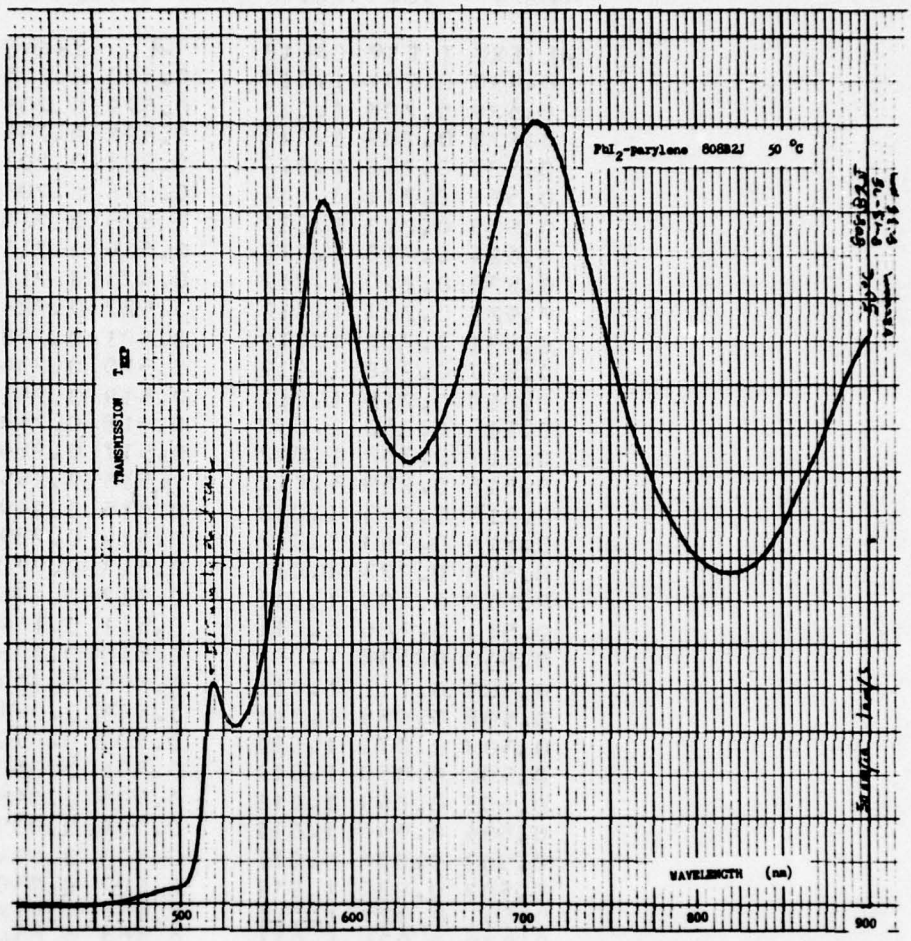

FIGURE 2.5-72. Transmission of PbI_2-parylene No. 808B2J at 50°C.

Table 2.5-44. High-resolution Transmission Scan of PbI_2-parylene No. 808B2J at 50°C.

TEMP= 50. PBI2 PARY 808B -2J 8.13 8.45

WL EXP	T EXP	CALIB	WL	TRANS
0.530	0.209	1.013	0.530	0.206
0.529	0.208	1.013	0.529	0.205
0.528	0.209	1.013	0.528	0.206
0.527	0.210	1.012	0.527	0.207
0.526	0.211	1.012	0.526	0.208
0.525	0.213	1.012	0.525	0.210
0.524	0.218	1.012	0.524	0.215
0.523	0.220	1.012	0.523	0.217
0.522	0.227	1.012	0.522	0.224
0.521	0.232	1.012	0.521	0.228
0.520	0.238	1.012	0.520	0.234
0.519	0.245	1.012	0.519	0.241
0.518	0.252	1.012	0.518	0.248
0.517	0.258	1.012	0.517	0.254
0.516	0.259	1.012	0.516	0.255
0.515	0.253	1.012	0.515	0.249
0.514	0.243	1.012	0.514	0.239
0.513	0.223	1.012	0.513	0.220
0.512	0.198	1.011	0.512	0.195
0.511	0.166	1.011	0.511	0.164
0.510	0.138	1.011	0.510	0.136
0.509	0.111	1.011	0.509	0.109
0.508	0.089	1.011	0.508	0.088
0.507	0.071	1.011	0.507	0.070
0.506	0.059	1.011	0.506	0.058
0.505	0.049	1.011	0.505	0.048
0.504	0.040	1.011	0.504	0.039
0.503	0.034	1.011	0.503	0.034
0.502	0.030	1.011	0.502	0.030
0.501	0.027	1.011	0.501	0.027
0.500	0.024	1.011	0.500	0.024
0.499	0.022	1.011	0.499	0.022
0.498	0.020	1.011	0.498	0.020
0.497	0.020	1.010	0.497	0.020
0.496	0.020	1.010	0.496	0.020
0.495	0.020	1.010	0.495	0.020
0.494	0.020	1.010	0.494	0.020
0.493	0.020	1.010	0.493	0.020
0.492	0.020	1.010	0.492	0.020
0.491	0.019	1.010	0.491	0.019
0.490	0.019	1.010	0.490	0.019
0.489	0.018	1.010	0.489	0.018
0.488	0.018	1.010	0.488	0.018
0.487	0.017	1.010	0.487	0.017
0.486	0.016	1.010	0.486	0.016
0.485	0.016	1.010	0.485	0.016
0.484	0.015	1.010	0.484	0.015
0.483	0.014	1.010	0.483	0.014
0.482	0.014	1.010	0.482	0.014
0.481	0.013	1.010	0.481	0.013
0.480	0.012	1.010	0.480	0.012

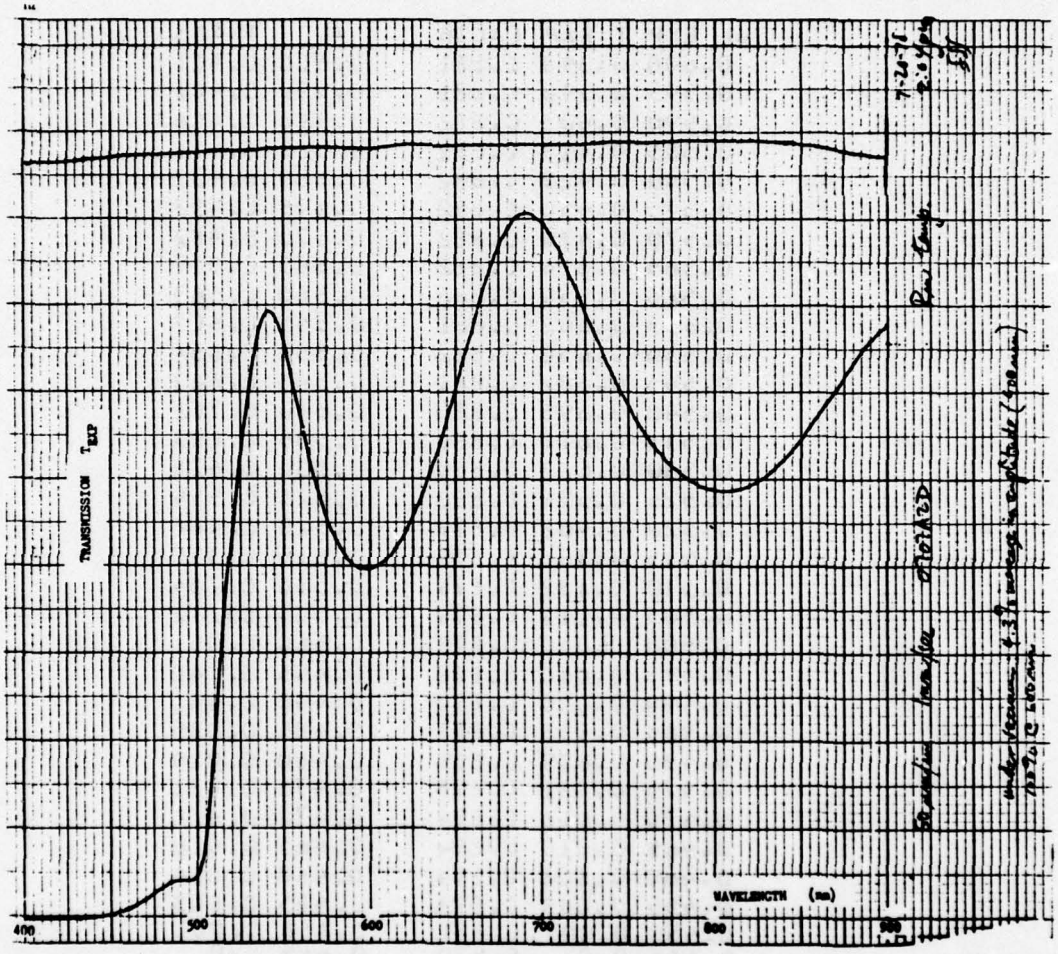

FIGURE 2.5-73. Transmission of PbI_2-parylene No, 707A2D at 25°C.

Table 2.5-45. Absorption Edge Transmission of PbI_2-parylene No. 707A2D at 25°C, from 600 nm to 440 nm.

TEMP= 25. PBI2 PARY 707A -2D 7.20 2.16

WL EXP	T EXP	CALIB	WL	TRANS
0.600	0.398	C.881	0.600	C.401
0.595	0.398	C.881	0.595	C.401
0.590	0.403	C.882	0.590	C.406
0.585	0.413	C.882	0.585	C.416
0.580	0.429	C.882	0.580	0.432
0.575	0.450	C.882	0.575	C.453
0.570	0.479	C.882	0.570	C.482
0.565	0.514	C.882	0.565	C.517
0.560	0.559	C.882	0.560	C.563
0.555	0.602	C.881	0.555	C.607
0.550	C.650	C.882	0.550	C.654
0.545	0.682	C.881	0.545	0.687
0.540	0.695	C.880	0.540	C.701
0.535	0.677	C.880	0.535	C.683
0.530	0.622	C.880	0.530	0.628
0.525	0.554	C.880	0.525	C.559
0.520	0.461	C.879	0.520	0.466
0.515	0.366	C.879	0.515	C.370
0.510	0.232	C.879	0.510	C.234
0.505	0.111	C.879	0.505	C.112
0.500	0.050	C.878	0.500	C.051
0.495	0.040	C.878	0.495	0.040
0.490	0.040	C.877	0.490	0.041
0.485	0.035	C.876	0.485	C.035
0.480	0.029	C.875	0.480	0.029
0.475	0.021	C.875	0.475	0.021
0.470	0.016	C.874	0.470	0.016
0.465	0.010	C.874	0.465	0.010
0.460	0.006	C.874	0.460	C.006
0.455	0.003	C.873	0.455	C.003
0.450	0.001	C.871	0.450	0.001
0.445	0.0	C.870	0.445	0.0
0.440	0.0	C.870	0.440	0.0
0.435	0.0	C.869	0.435	0.0
0.430	0.0	C.867	0.430	0.0

Table 2.5-46. High-resolution Transmission Scan of PbI_2-parylene No. 707A2D at 25°C.

TEMP= 25. PBI2 PARY 707A -2D 7.20 2.24

WL EXP	T EXP	CALIB	WL	TRANS
0.525	0.550	0.880	0.525	0.555
0.524	0.533	0.880	0.524	0.538
0.523	0.516	0.880	0.523	0.521
0.522	0.500	0.880	0.522	0.505
0.521	0.481	0.880	0.521	0.485
0.520	0.464	0.879	0.520	0.469
0.519	0.444	0.879	0.519	0.449
0.518	0.426	0.879	0.518	0.430
0.517	0.403	0.879	0.517	0.407
0.516	0.381	0.879	0.516	0.385
0.515	0.361	0.879	0.515	0.365
0.514	0.340	0.879	0.514	0.343
0.513	0.314	0.879	0.513	0.317
0.512	0.291	0.879	0.512	0.294
0.511	0.264	0.879	0.511	0.267
0.510	0.237	0.879	0.510	0.239
0.509	0.208	0.879	0.509	0.210
0.508	0.180	0.879	0.508	0.182
0.507	0.155	0.879	0.507	0.157
0.506	0.131	0.879	0.506	0.132
0.505	0.109	0.879	0.505	0.110
0.504	0.091	0.879	0.504	0.092
0.503	0.076	0.879	0.503	0.077
0.502	0.066	0.879	0.502	0.067
0.501	0.057	0.879	0.501	0.058
0.500	0.051	0.878	0.500	0.052
0.499	0.048	0.878	0.499	0.049
0.498	0.046	0.878	0.498	0.047
0.497	0.043	0.878	0.497	0.043
0.496	0.043	0.878	0.496	0.043
0.495	0.042	0.878	0.495	0.042
0.494	0.042	0.878	0.494	0.042
0.493	0.042	0.878	0.493	0.042
0.492	0.042	0.878	0.492	0.042
0.491	0.041	0.878	0.491	0.041
0.490	0.041	0.877	0.490	0.042
0.489	0.041	0.877	0.489	0.042
0.488	0.040	0.877	0.488	0.041
0.487	0.040	0.877	0.487	0.041
0.486	0.040	0.877	0.486	0.041
0.485	0.040	0.876	0.485	0.041
0.484	0.040	0.876	0.484	0.041
0.483	0.040	0.876	0.483	0.041
0.482	0.039	0.876	0.482	0.040
0.481	0.038	0.876	0.481	0.039
0.480	0.037	0.875	0.480	0.038

2.5.5 Optical Properties of HgI_2 Films on Glass

HgI_2 films were evaporated onto 200μ thick borosilicate glass substrates. Considerable difficulty was experienced in reproducibly obtaining HgI_2 films of good optical quality. Additionally, it was found that HgI_2 is unstable when stored in vacuum because of its high vapor pressure, so that a passivating overlayer is required for the intended thermal imaging application. Because of these problems, emphasis for this program was concentrated upon PbI_2 films. In this section, we report the results of optical transmission measurements performed upon some of the HgI_2 films, including temperature dependence of the absorption edge.

The transmission characteristic for HgI_2-glass sample No. 303A9 at 25°C is shown in Figure 2.5-74, along with the transmission curve for a bare glass substrate. This transmission curve is noteable for the absence of multiple-reflection interference structure and for the monotonic decrease in transmission with decreasing wavelengths, even for wavelengths considerably longer than absorption edge values.

The absence of interference structure indicates the film thickness may be considerably less than 0.8μ, or that the film is either quite non-uniform in thickness, or lossy, or both. The steady decrease in transmission most probably indicates propagation losses which increase with decreasing wavelength, although it is not established whether absorption or scattering is the dominant loss mechanism. Also, part of this monotonic decrease may be attributed to an interference minimum below 0.5μ. The absorption edge occurs for wavelengths between 550 nm and 570 nm, and is not sharply distinguishable. The HgI_2 film thickness is indicated to be about 0.8μ by a profilometer measurement. However, this data is not considered reliable because the stylus easily scratched the soft HgI_2.

The transmission of this sample at other temperatures between 25°C and 50°C is shown in Figures 2.5-74 through 2.5-77. The dewar was evacuated for these measurements. After the scan at 50°C was completed, an additional scan at 25°C revealed 5 percent transmission for wavelengths smaller than 520 nm, for which the sample had previously been opaque. A portion of the film around the circumference had evaporated away and 0.2 to 0.5 mm "pinholes" appeared in the sample, caused by evaporation of HgI_2 in the vacuum environment. Curiously, the transmission at 800 nm decreased with successive scans at higher temperatures, although the film was evaporating away. This

AD-A069 537 ROCKWELL INTERNATIONAL ANAHEIM CA ELECTRONICS RESEAR--ETC F/G 11/6
TEMPERATURE SENSITIVE OPTICAL PHENOMENA IN HEAVY METAL HALIDE F--ETC(U)
JAN 79 J D MCMULLEN, D M HEINZ, F S STEARNS DAAK70-77-C-0165

UNCLASSIFIED C79-8-501 NL

3 OF 4
AD A069537

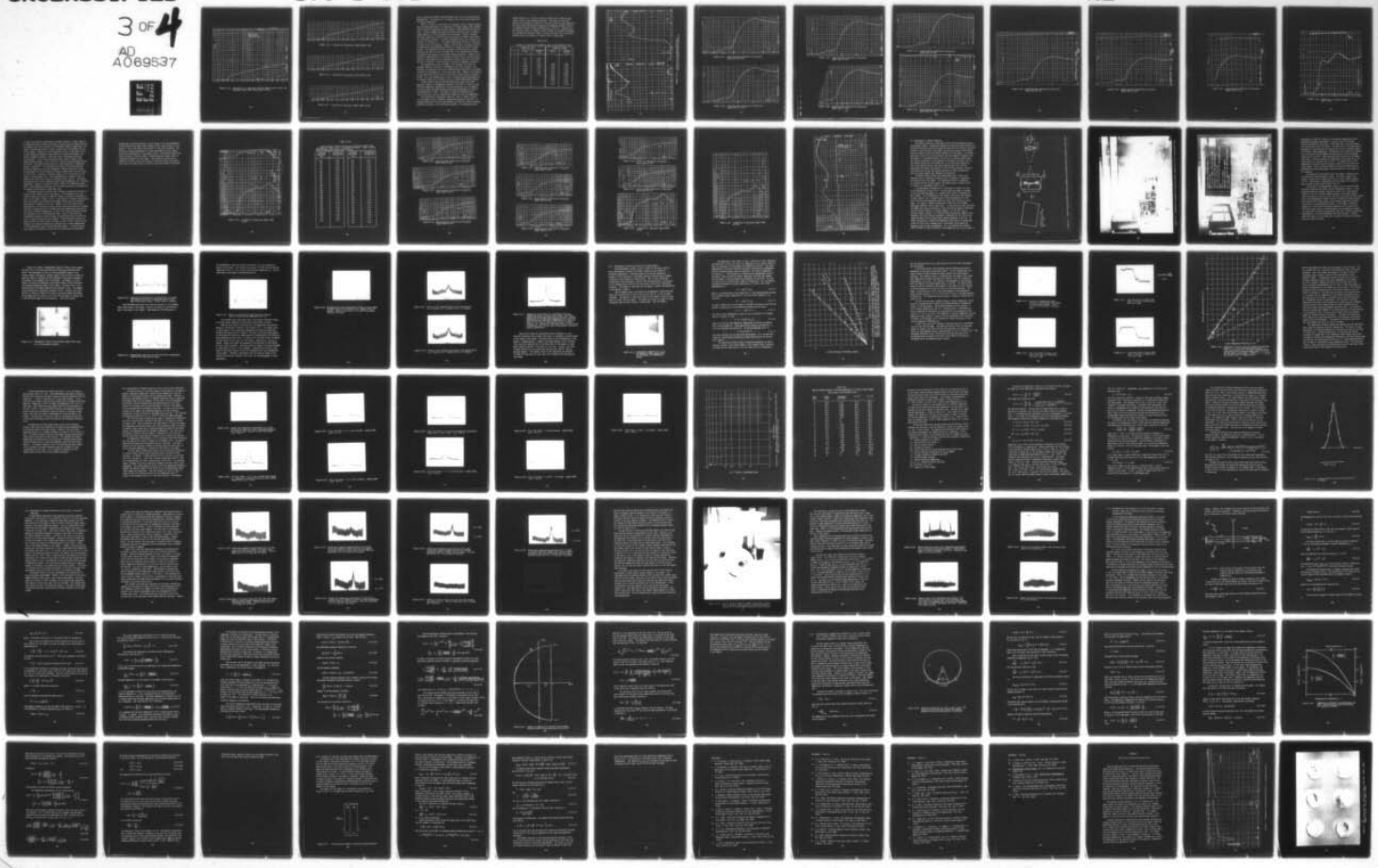

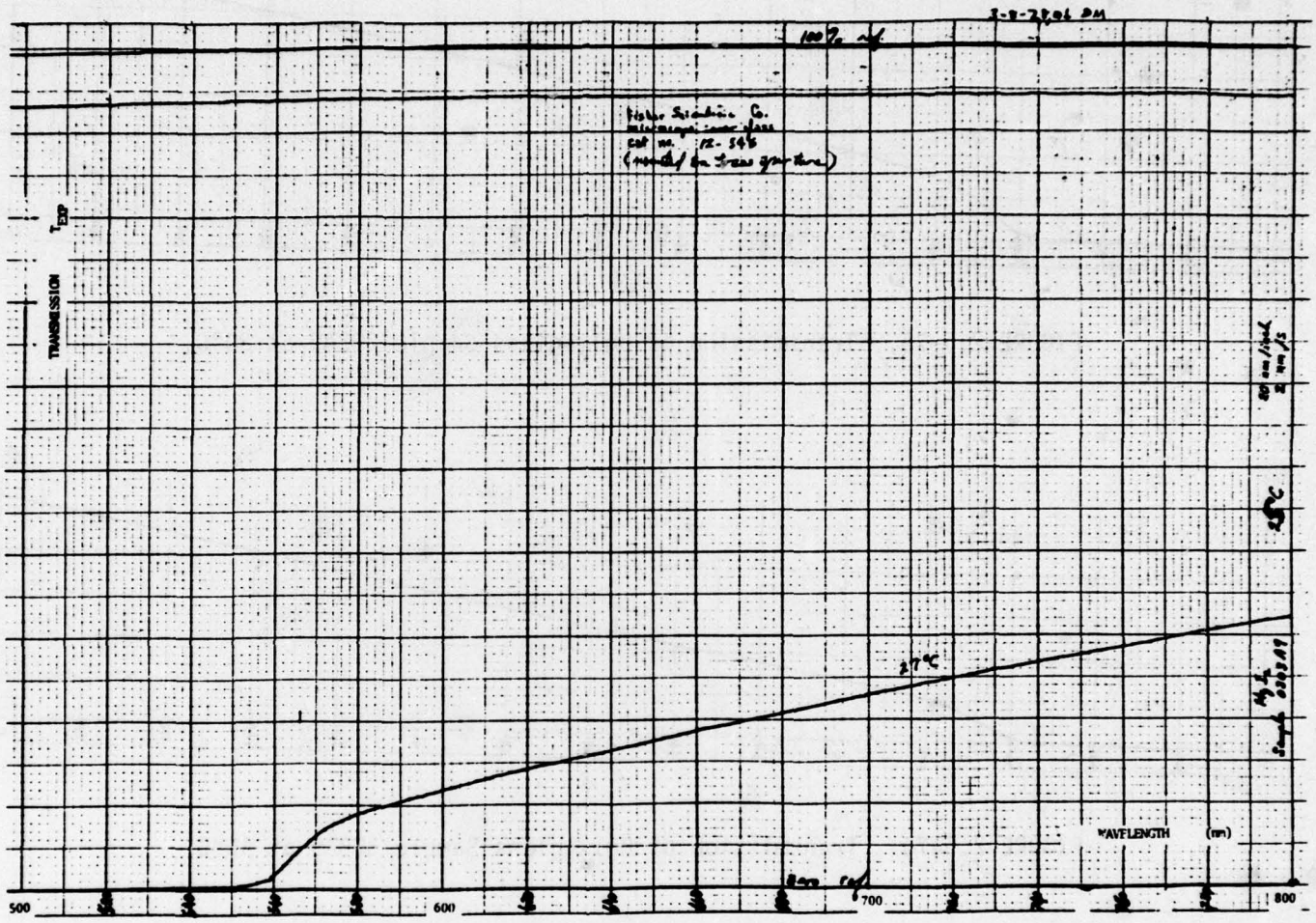

FIGURE 2.5-74. Transmission of a Bare Glass Substrate (Upper Curve) at 25°C, and HgI_2-glass Sample 303A9 (Lower Curve) at 25°C.

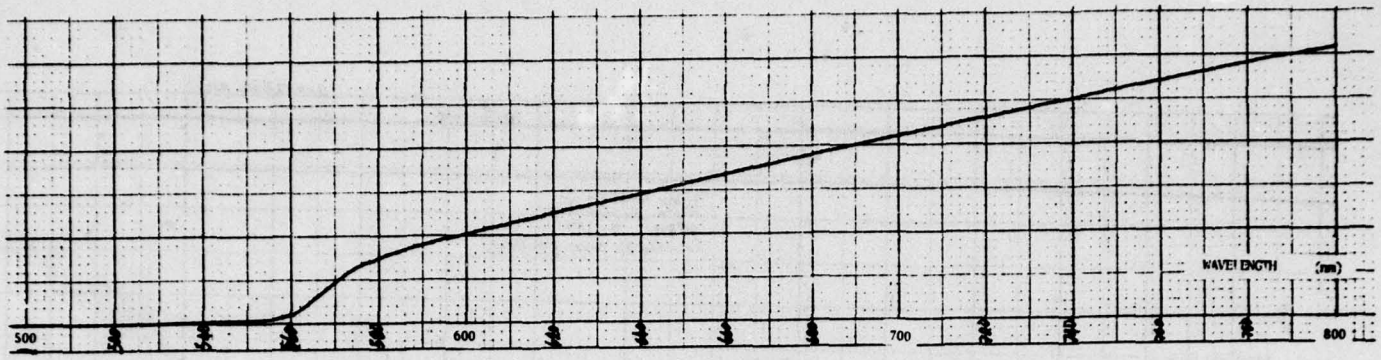

FIGURE 2.5-75. Transmission of HgI_2-glass Sample 303A9 at 30°C.

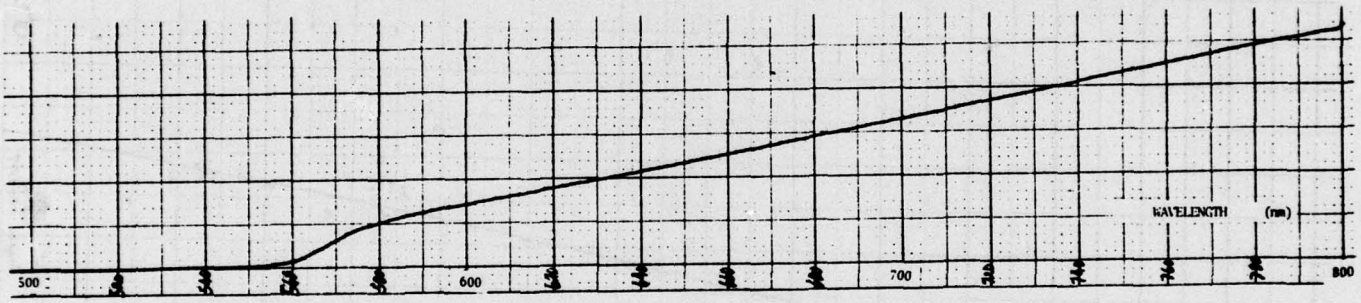

FIGURE 2.5-76. Transmission of HgI_2-glass Sample 303A9 at 50°C.

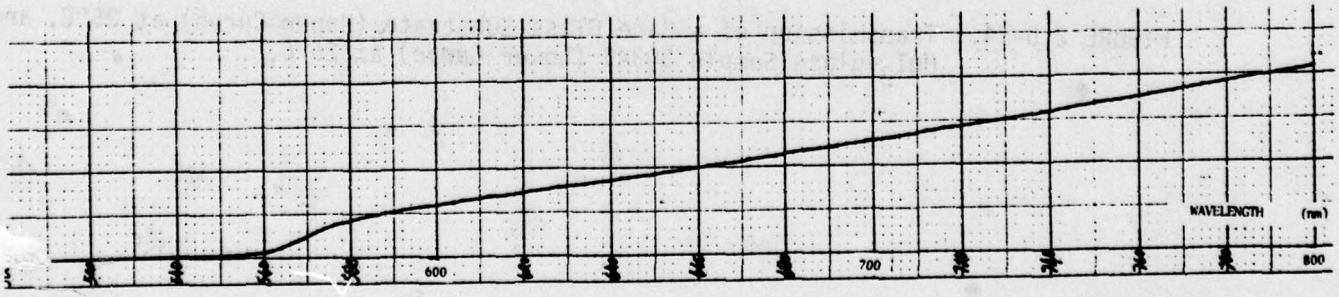

FIGURE 2.5-77. Transmission of HgI_2-glass Sample 303A9 at 50°C.

may be caused by the metallic Hg precipitate left in the film during vacuum decomposition. The condition of the sample at this point made further optical testing impossible.

Clearly, if HgI_2 is to be used as a transducer film for thermal imaging, with the requirement that it be contained in a vacuum chamber, then a method must be found to encapsulate the HgI_2 surface so that decomposition does not occur. Several attempts were made to overcoat these HgI_2 films, including vacuum deposition of SiO_2 and deposition of parylene. Results indicated that both vacuum and a radiative heat source must be avoided in any successful overcoating procedure. A coating of photoresist was spun to about 0.8μ thickness on one HgI_2 film. This sample showed good stability in vacuum for 50 hours at one torr pressure. However, after 50 hours the HgI_2 film began to deteriorate, and disappeared completely in another ten hours of vacuum storage. The overcoating for HgI_2, provided a suitable one can be found, should be less than 0.1μ thick in order that it not significantly increase the thermal time constant of the thermal imaging transducer. However, considerable experimentation will be needed to develop such a thin overcoating, applied at room temperature and atmospheric pressure, which will be uniform and free of pinholes, so that the HgI_2 film would be adequately protected.

The transmission curves of Figures 2.5-74 through 2.5-77 were not analyzed, because of the lack of knowledge of HgI_2 film thickness. The thickness and refractive index can be obtained by multiple angle of incidence reflectivity measurements of s and p polarized light. However, the condition of the sample after the 50°C scan did not permit further optical characterization. Also, the decomposition of HgI_2 in vacuum prevented measurement of the thermal properties of the HgI_2 films by infrared thermographic methods.

Further optical transmission measurements were made on two other HgI_2-glass samples for temperatures between 0°C and 50°C, in order to establish the temperature dependence of the absorption edge for this material. The optical dewar was <u>not</u> evacuated during these measurements in order to avoid evaporation of HgI_2. No evidence of moisture condensation was found on the HgI_2 films for temperatures between 0°C and room temperature.

The transmission of HgI_2/glass sample No. 323C1 is shown in Figures 2.5-78 through 2.5-88 at different temperatures between 0°C and 50°C. An improved transmission scan was made between 0.8μ and 2.0μ to more accurately establish the orders of the transmission extrema. The extrema and their

integer orders for T = 25°C are listed in Table 2.5-47. along with the product n(λ)D at each extremum wavelength. The theory for this data analysis was presented in Section 2.5.3 for PbI_2 films on glass substrates. The orders were established by comparing the frequency intervals (ratios) for adjacent extrema to those predicted by Eq. (2.5.3-5). Dispersion of the refractive index is evident as n(λ)D increases for shorter wavelengths. If we assume the refractive index is close to the value 2.65 as previously reported, then the thickness of film No. 323C1 is about 0.38μ.

TABLE 2.5-47

Analysis of Transmission Extrema for HgI_2 on Glass Samples at 25°C.

	SAMPLE NO. 323C1		SAMPLE NO. 329B1	
m	$\lambda^{(m)}_{(\mu)}$	$n\left(\lambda^{(m)}_{(\mu)}\right)D$	$\lambda^{(m)}_{(\mu)}$	$n\left(\lambda^{(m)}_{(\mu)}\right)D$
1				
2	1.96	0.980		
3	1.35	1.012		
4	1.05	1.050	1.960	1.960
5	0.840	1.050	1.540	1.925
6	0.745	1.118	1.294	1.941
7	0.650	1.138	1.120	1.960
8	0.605	1.210	1.010	2.020
9			0.888	1.998
10			0.846	2.115
11			0.752	2.068
12			0.716	2.148

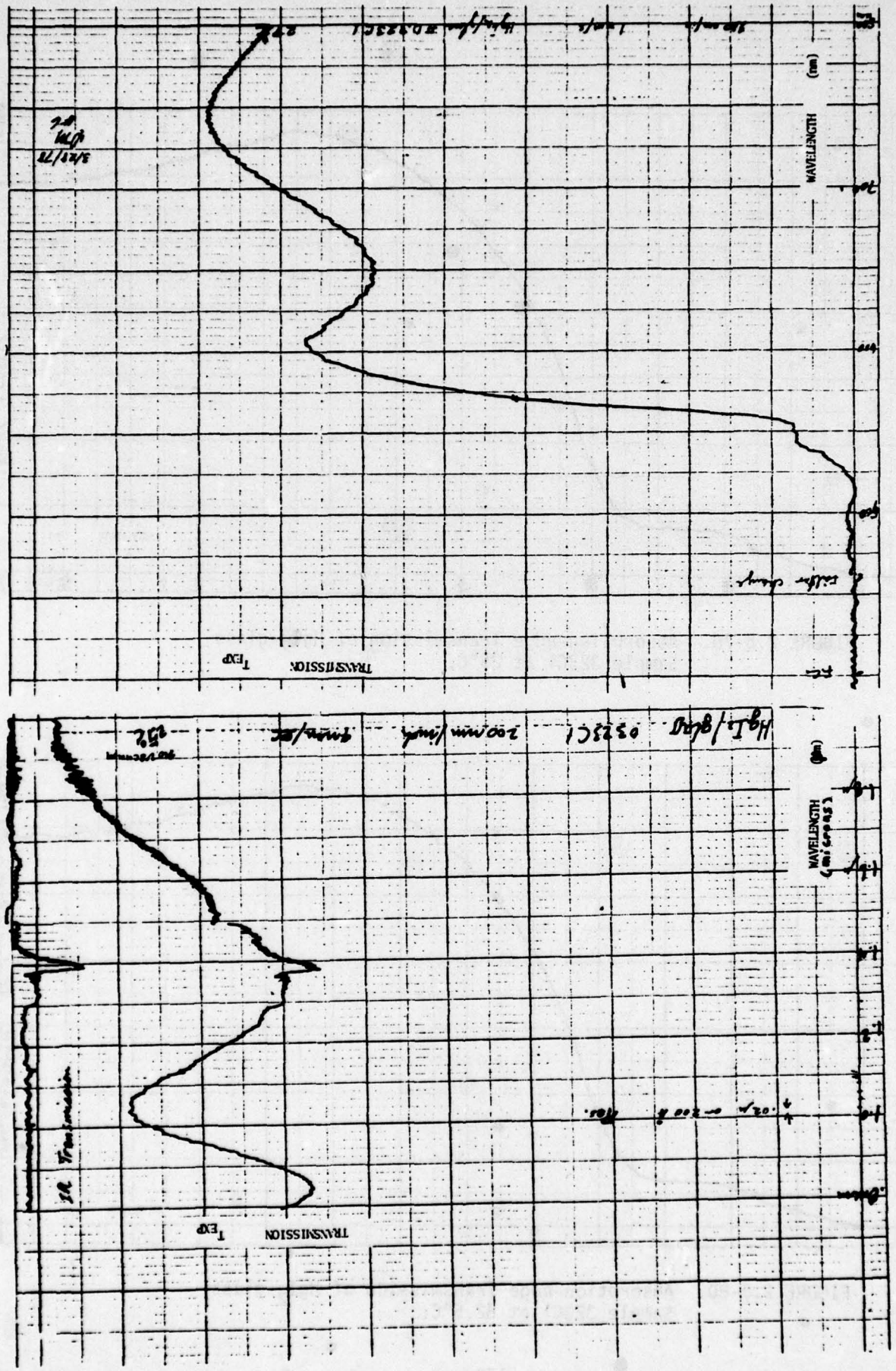

FIGURE 2.5-78. Transmission of HgI_2-glass Sample 323C1 at 25°C at Infrared and Visible Frequencies.

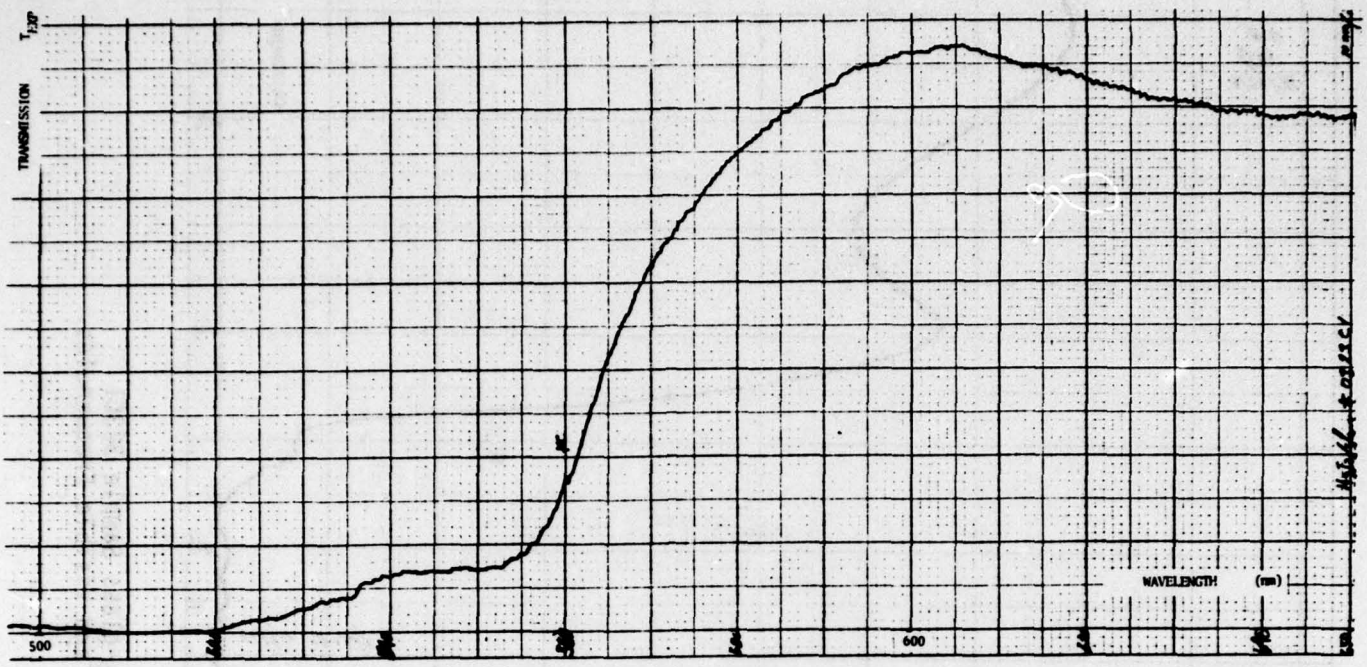

FIGURE 2.5-79. Absorption-edge Transmission of HgI_2-glass Sample 323C1 at 25°C.

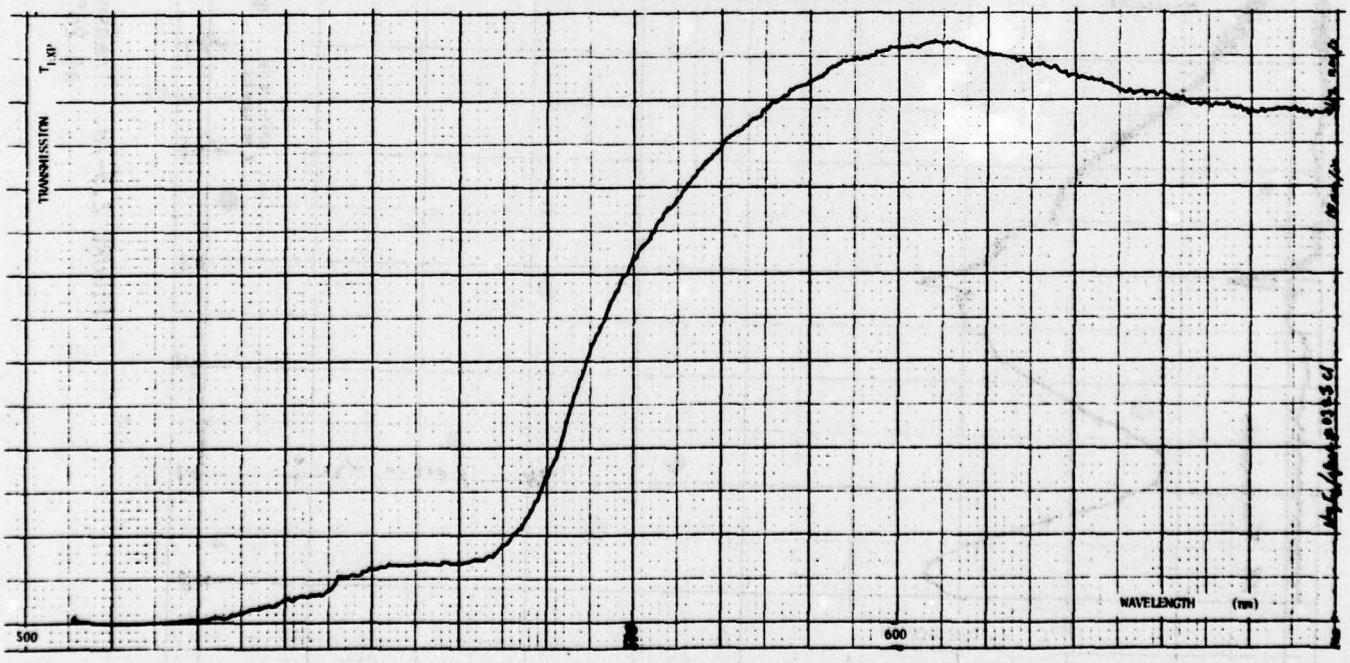

FIGURE 2.5-80. Absorption-edge Transmission of HgI_2-glass Sample 323C1 at 32.5°C.

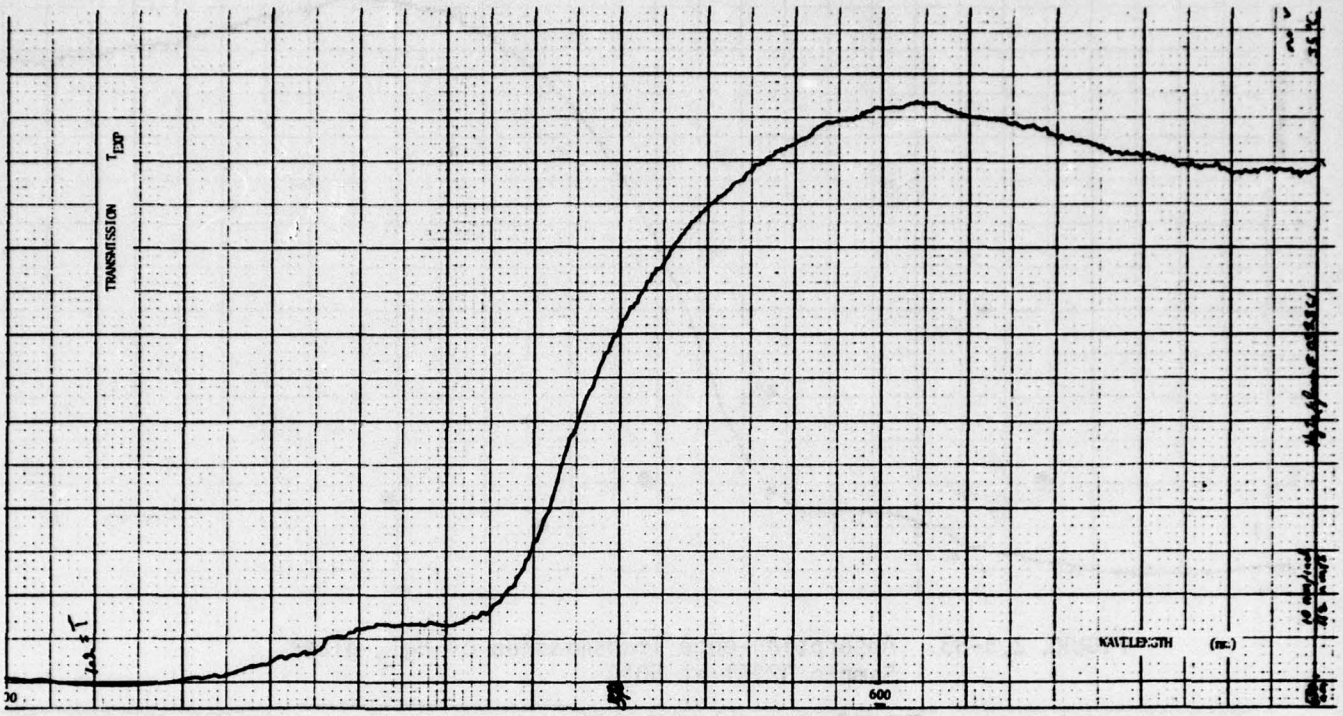

FIGURE 2.5-81. Absorption-edge Transmission of HgI_2-glass Sample 323C1 at 35°C.

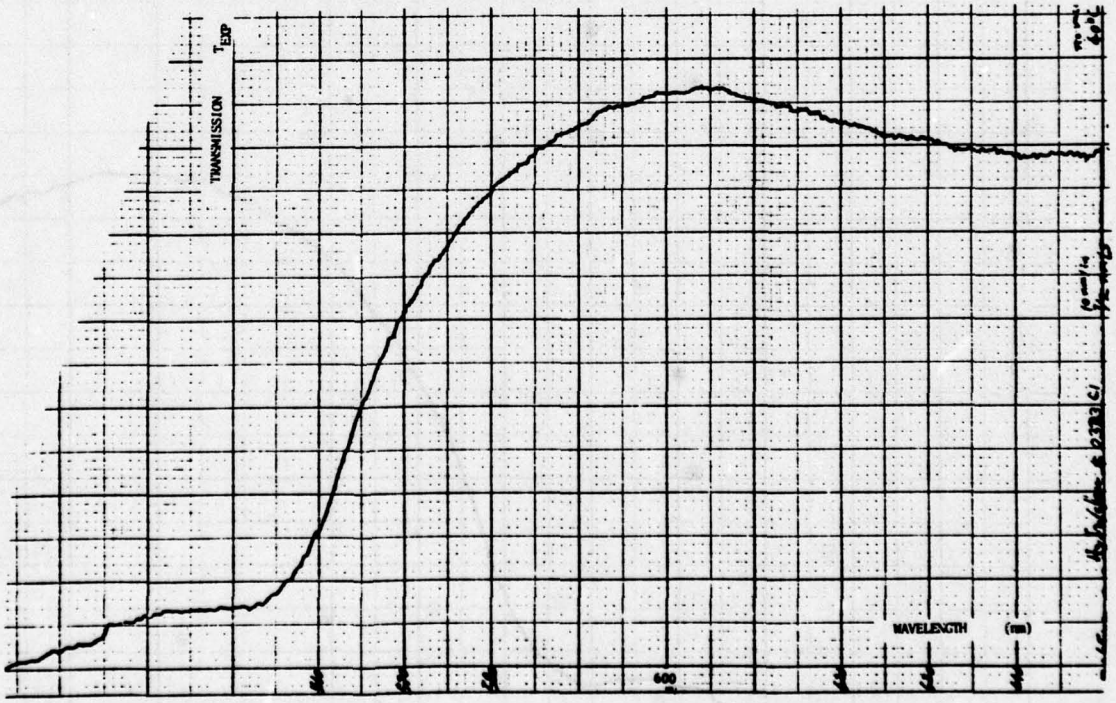

FIGURE 2.5-82. Absorption-edge Transmission of HgI_2-glass Sample 323C1 at 40°C.

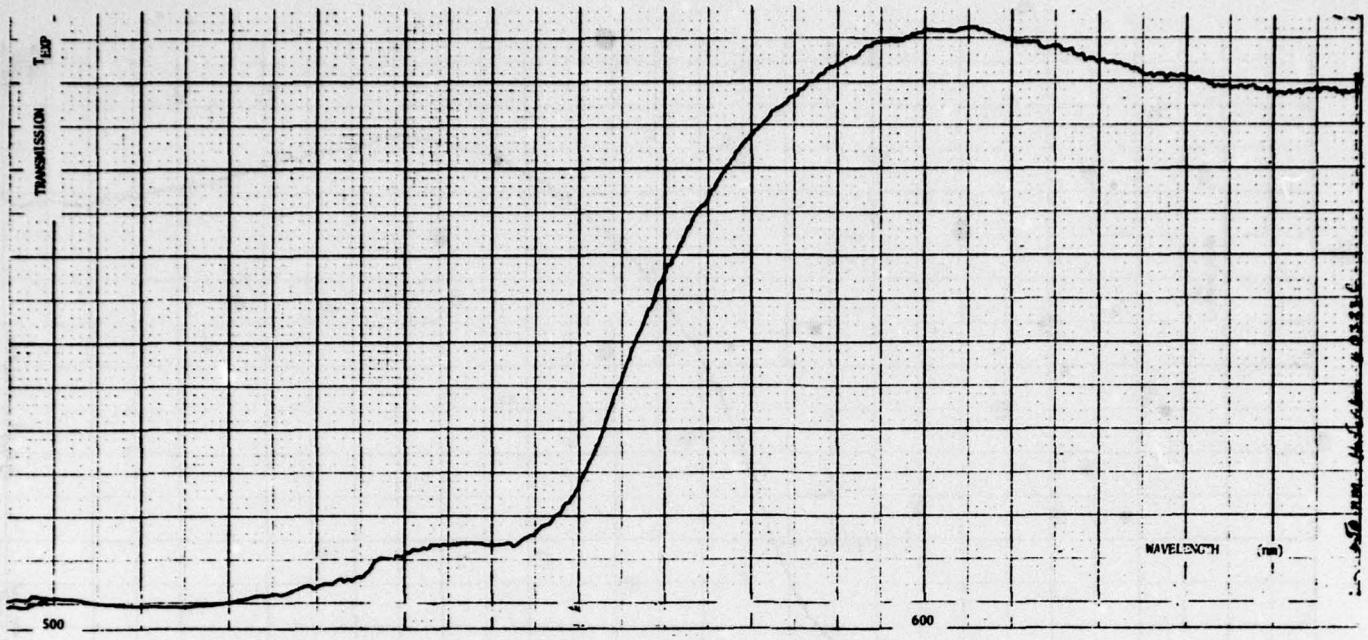

FIGURE 2.5-83. Absorption-edge Transmission of HgI_2-glass Sample 323C1 at 50°C.

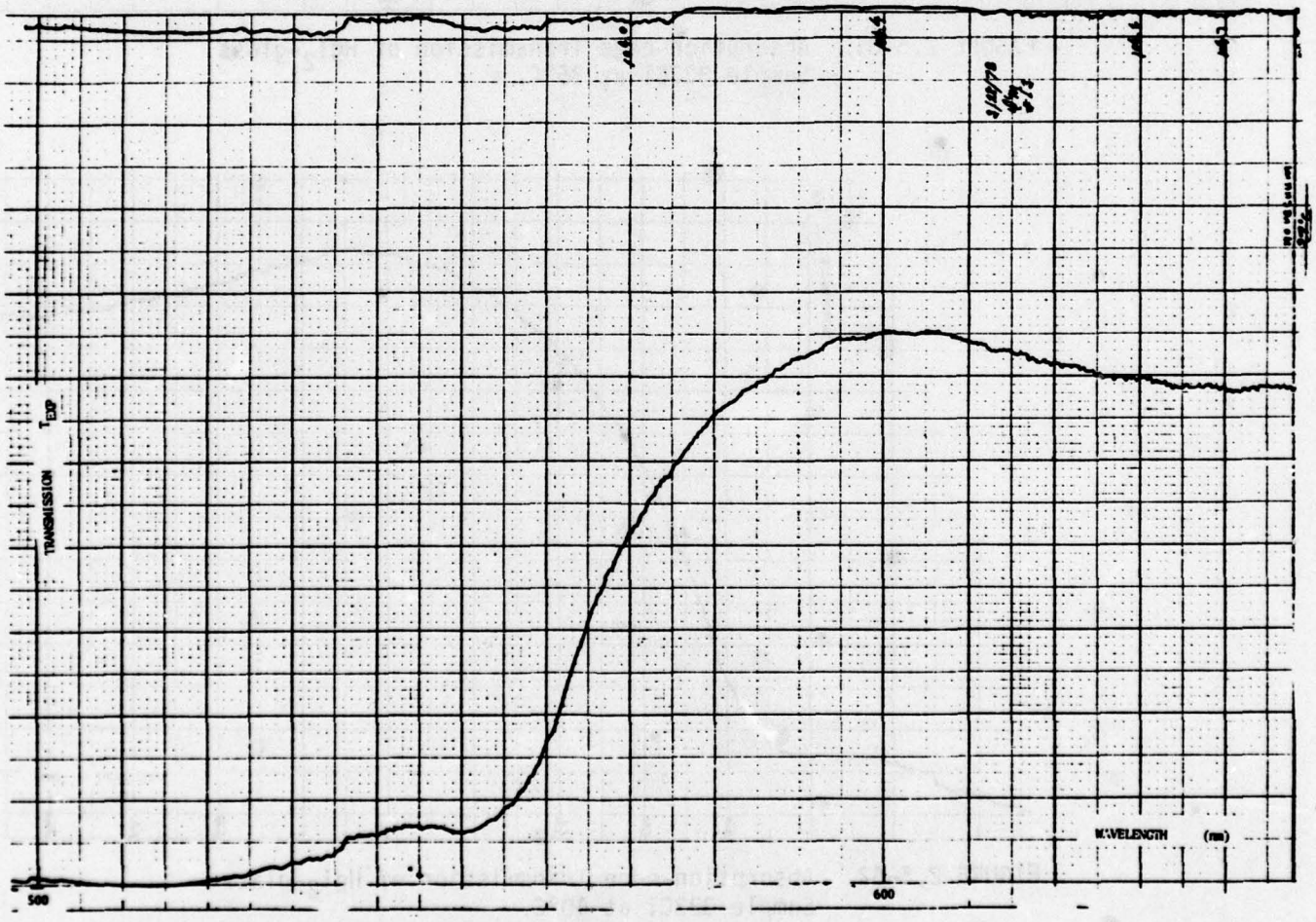

FIGURE 2.5-84. Absorption-edge Transmission of HgI_2-glass Sample 323C1 at 25°C.

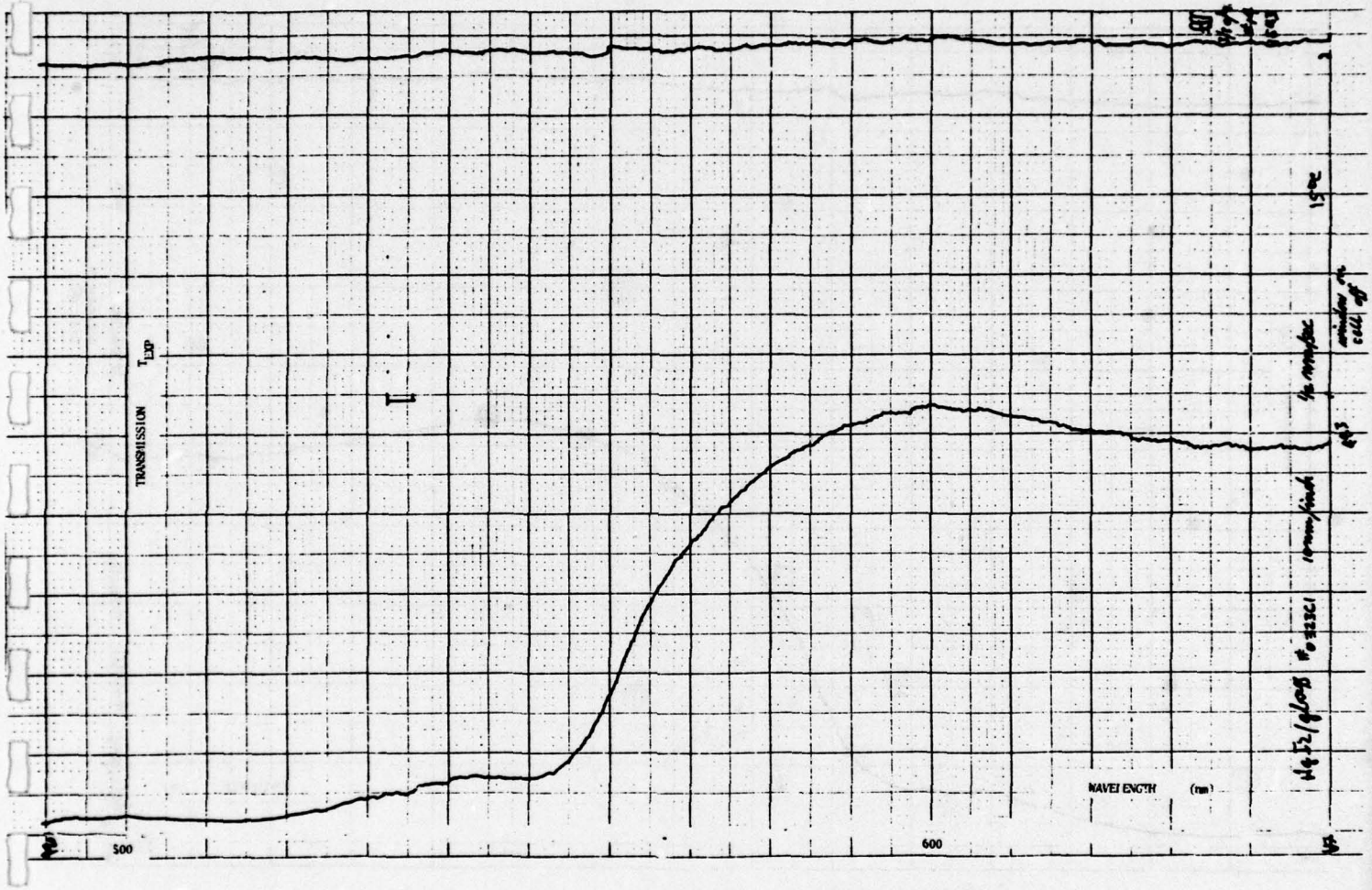

FIGURE 2.5-85. Absorption-edge Transmission of HgI_2-glass Sample 323C1 at 15°C.

FIGURE 2.5-86. Absorption-edge Transmission of HgI_2-glass Sample 323Cl at 20°C.

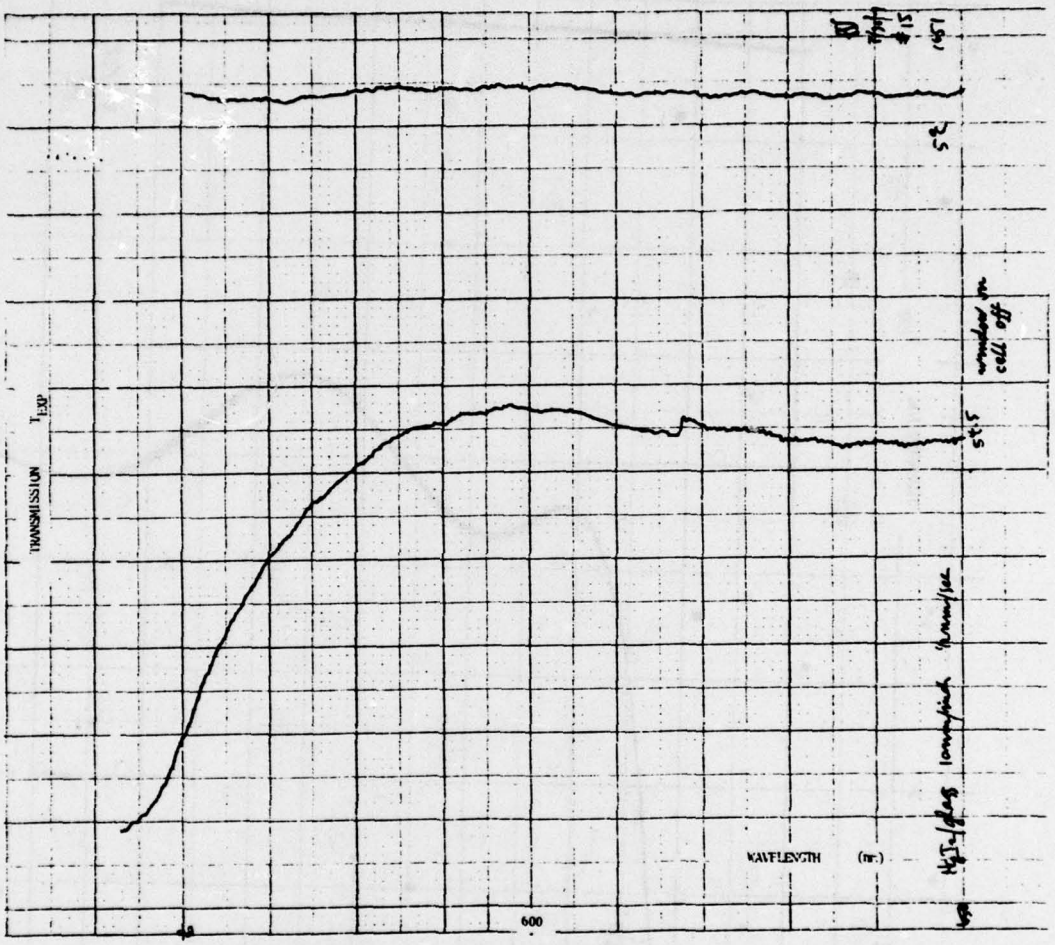

FIGURE 2.5-87. Absorption-edge Transmission of HgI_2-glass Sample 323Cl at 5°C.

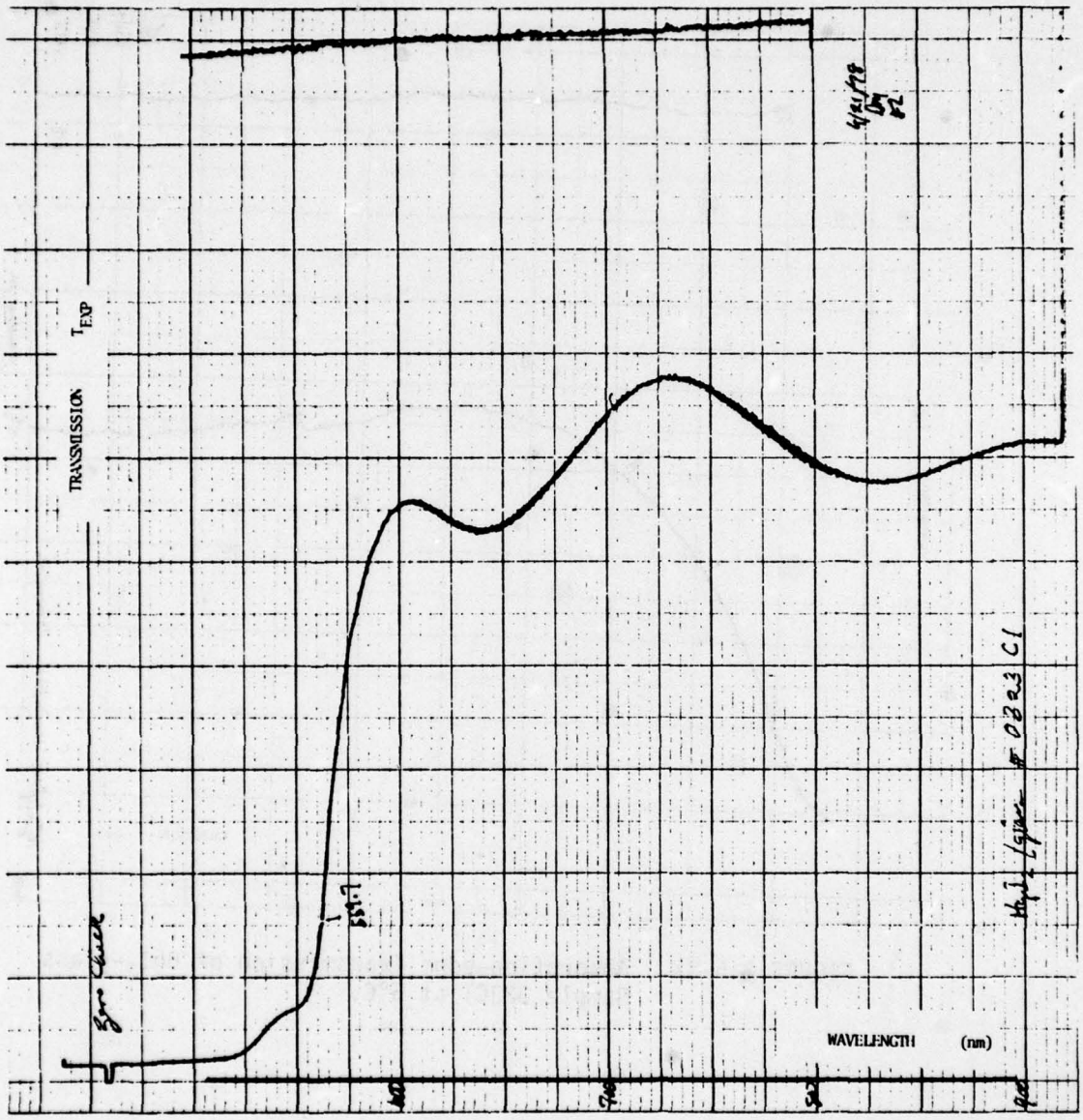

FIGURE 2.5-88. Transmission of HgI_2-glass Sample 323Cl at 25°C.

In view of the apparent nonuniformity in sample thickness, further reduction of transmission data to obtain the optical constants does not appear feasible. The transmission scans of Figures 2.5-78 through 2.5-88 for sample 323C1, are shown in chronological order, in order to keep track of the thermal cycling of this sample. Comparison of the transmission curves at 25°C shows a shift of the transmission maximum at about 605 nm to a smaller wavelength, indicating a permanent decrease in refractive index or thickness during the testing period. A scan taken three weeks later, shown in Figure 2.5-88, showed further decrease in nD, as well as a smaller amplitude between maxima and minima. The sample had been stored in a dark dessicator at atmospheric pressure. Therefore, it is concluded that the HgI_2 film deteriorated both during the temperature cycling at atmospheric pressure and during storage. The wavelengths for the transmission extrema of sample 329B1 are also listed in Table 2.5-47. Assuming a refractive index of 2.6, the thickness of this sample is approximately 0.77μ. More experimentation is needed in order to produce 0.2μ thick films of HgI_2 of acceptable optical quality. The absorption edge does shift quite observably toward longer wavelengths with increasing temperature. However, no attempt is made to quantify the temperature dependence of the absorption edge because of the large uncertainty in thickness and the apparent nonuniformity of these HgI_2 films.

An attempt was made to minimize the influence of nonuniform thickness by sampling a much smaller area of the samples. A 4 mm diameter area in the center of HgI_2-glass sample No. 329B1 was sampled, yielding the transmission curve at 25°C shown in Figure 2.5-89. A small amount of residual transmission, about one percent, was present for wavelengths shorter than the absorption edge because of pinholes in the film. However, since this effect can be accounted for in the analysis of data, and this was the best quality of sample remaining, transmission scans of higher resolution between 550 nm and 600 nm were run at different temperatures in order to at least qualitatively display the temperature shift of the absorption edge. Figure 2.5-89 shows that interference extrema are barely present, indicating poor optical quality for this film even over the small area sampled. A high resolution scan was repeated at 25°C, and those results are given in Table 2.5-48. Figures 2.5-89 through 2.5-99 show the transmission characteristics at other temperatures, in the chronological order in which they were scanned. It should be noted that ordinate or transmission values must be renormalized for wavelengths

between 560 nm and 460 nm because a filter change in the spectrophotometer shifted the beam and caused lower readings in this range by about 0.3 per percent. This is the cause of the "glitch" in the curves at 560 nm. This effect was removed experimentally in later measurements on PbI_2 samples, but must be corrected for in the present curves. The infrared transmission curve in Figure 2.5-100 was useful in establishing the integer orders of transmission extrema for this sample. The transmission curve for the sample was run with a full-scale range of 20 percent, whereas the calibration curve in the same figure is run with a full-scale range of 50 percent.

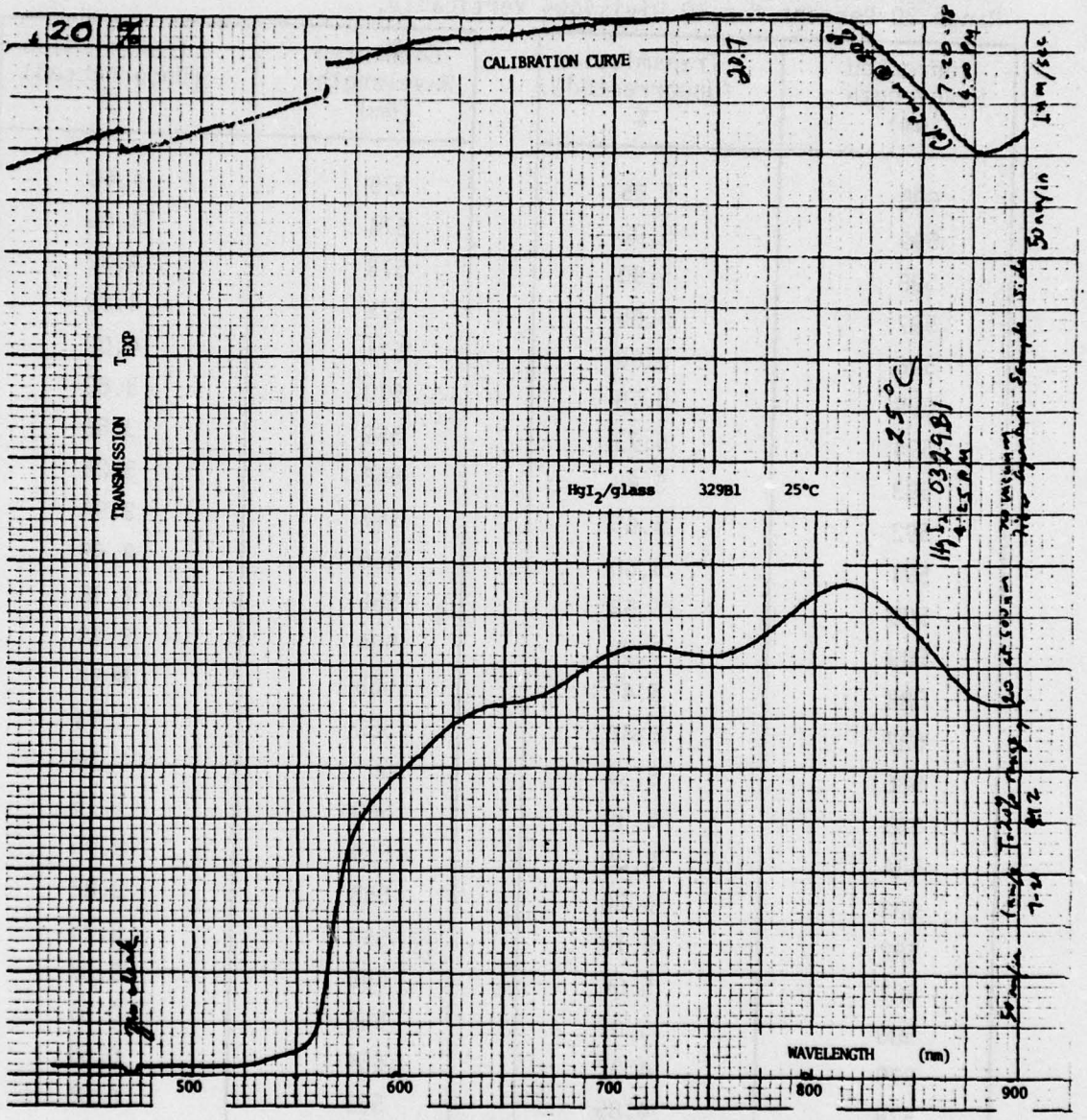

FIGURE 2.5-89. Transmission of HgI_2-glass Sample 329B1 at 25°C.

TABLE 2.5-48

High-resolution Transmission Scan Across Absorption Edge of HgI_2 for Sample No. 329B1 at 25°C. Scan Speed 1/16 nm/sec. Scale 1 nm/inch. Range 20 Percent for 10 Divisions Vertically.

Corrected Wavelength (nm)	Transmission (Uncorrected) %	Corrected Wavelength (nm)	Transmission (Uncorrected) %
600	5.96	575	4.60
599	5.92	574	4.46
598	5.90	573	4.32
597	5.85	572	4.20
596	5.80	571	4.00
595	5.79	570	3.80
594	5.73	569	3.58
593	5.68	568	3.26
592	5.65	567	2.98
591	5.60	566	2.69
590	5.58	565	2.38
589	5.50	564	2.08
588	5.43	563	1.80
587	5.40	562	1.53
586	5.37	561	1.30
585	5.30	560	1.15
584	5.25	559	0.95
583	5.20	558	0.82
582	5.14	557	0.75
581	5.06	556	0.67
580	5.02	555	0.61
579	4.97	554	0.59
578	4.85	553	0.55
577	4.80	552	0.51
576	4.70	551	0.49
		550	0.46

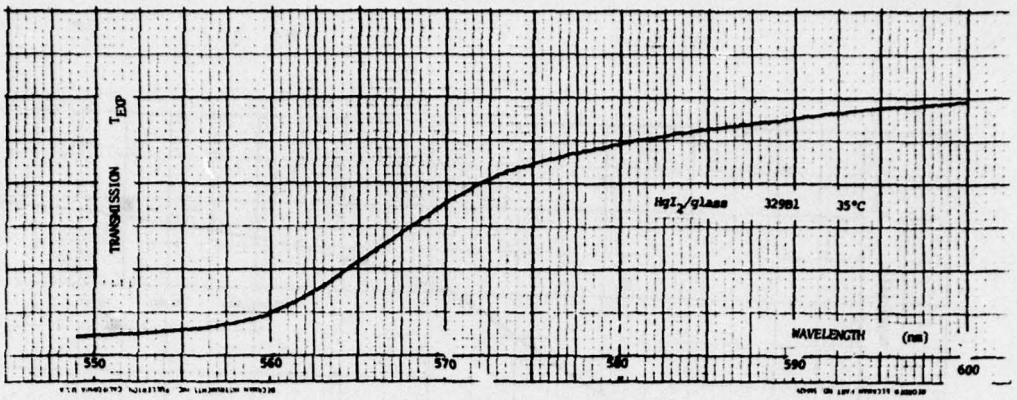

FIGURE 2.5-90. Absorption-edge Transmission of HgI_2-glass Sample 329B1 at 35°C.

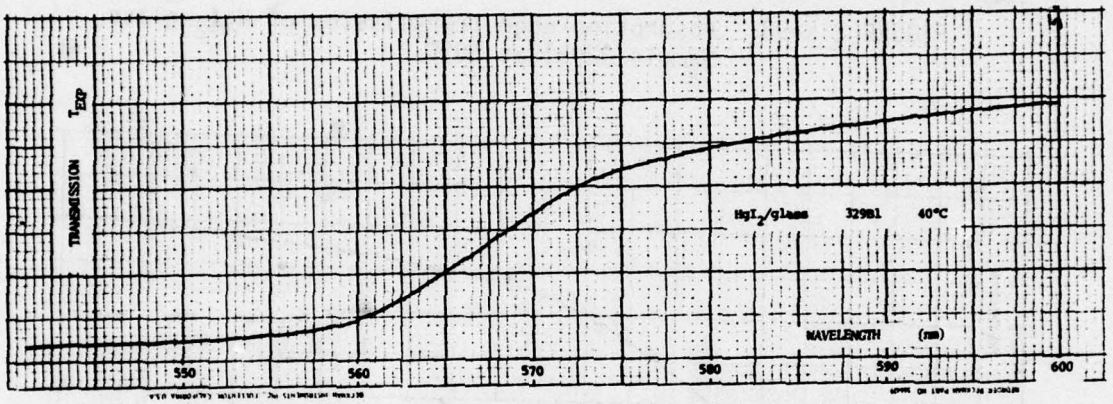

FIGURE 2.5-91. Absorption-edge Transmission of HgI_2-glass Sample 329B1 at 40°C.

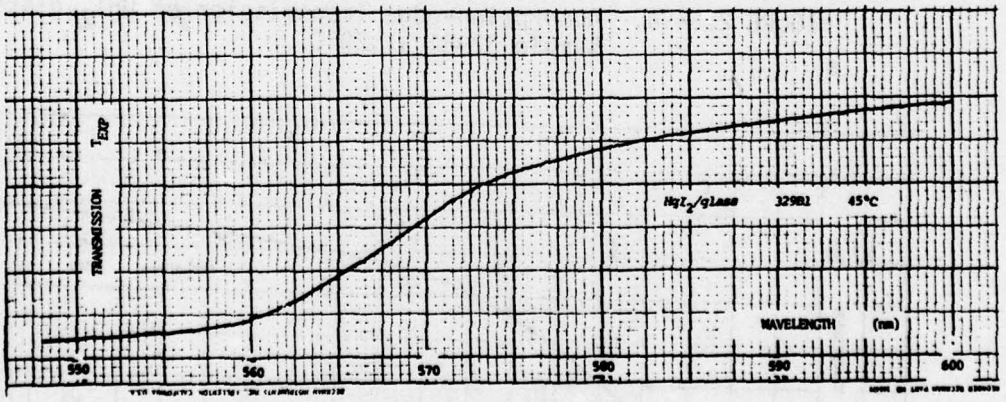

FIGURE 2.5-92. Absorption-edge Transmission of HgI_2-glass Sample 329B1 at 45°C.

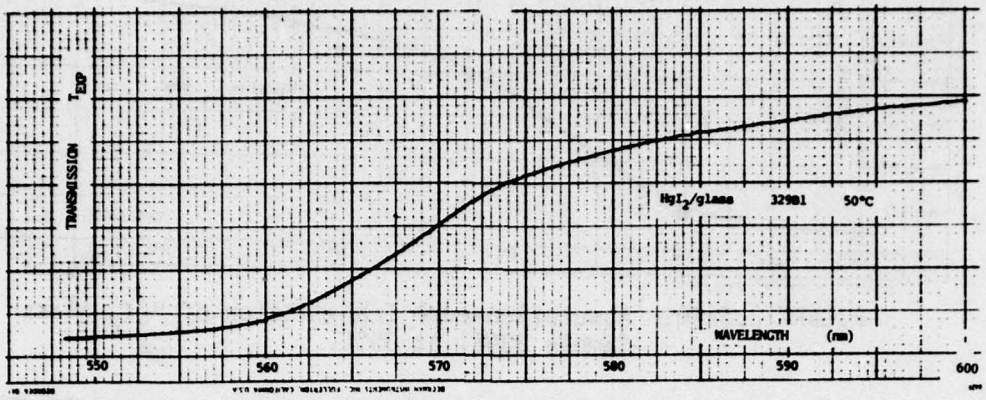

FIGURE 2.5-93. Absorption-edge Transmission of HgI_2-glass Sample 329B1 at 50°C.

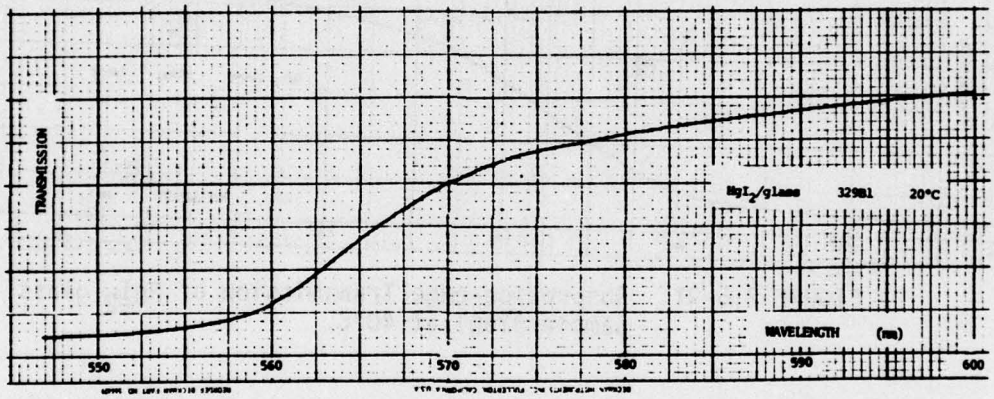

FIGURE 2.5-94. Absorption-edge Transmission of HgI_2-glass Sample 329B1 at 20°C.

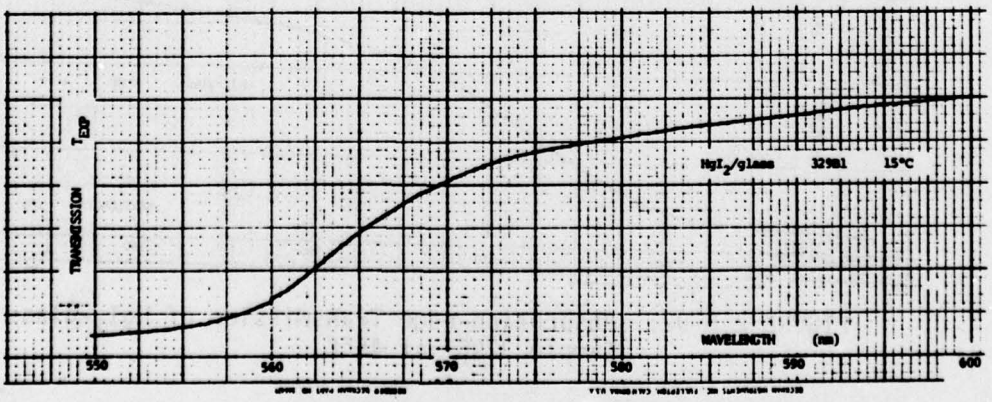

FIGURE 2.5-95. Absorption-edge Transmission of HgI_2-glass Sample 329B1 at 15°C.

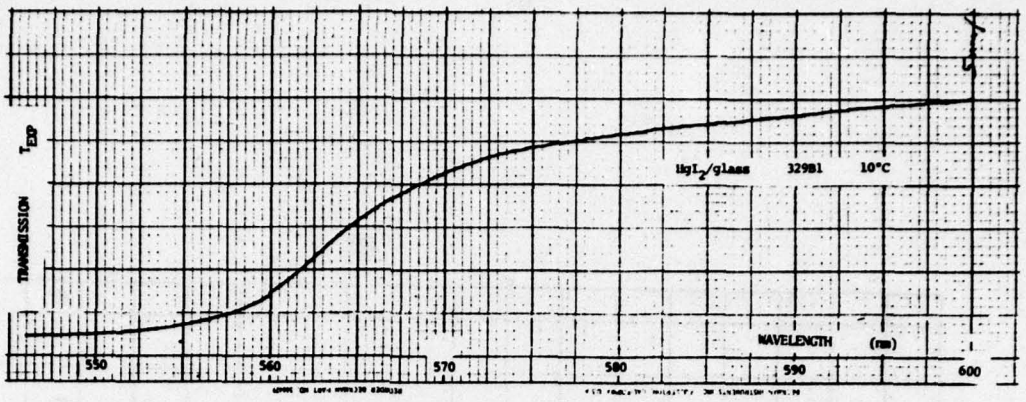

FIGURE 2.5-96. Absorption Transmission of HgI_2-glass Sample 329B1 at 10°C.

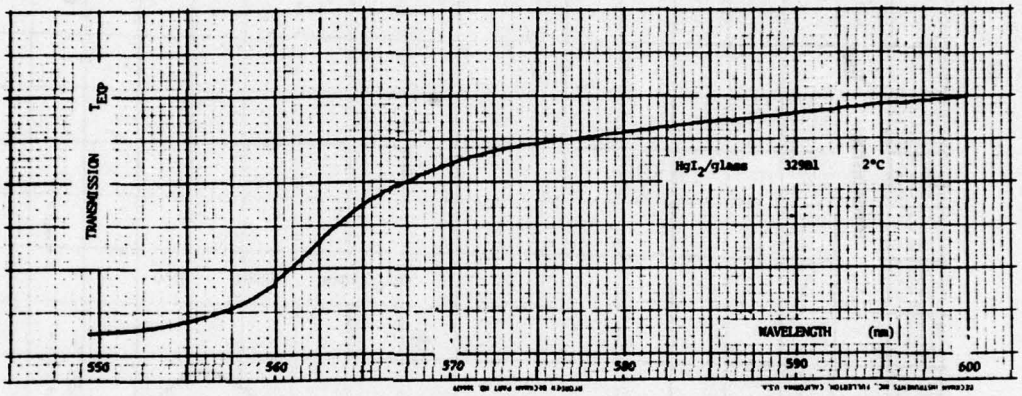

FIGURE 2,5-97. Absorption-edge Transmission of HgI_2-glass Sample 329B1 at 2°C.

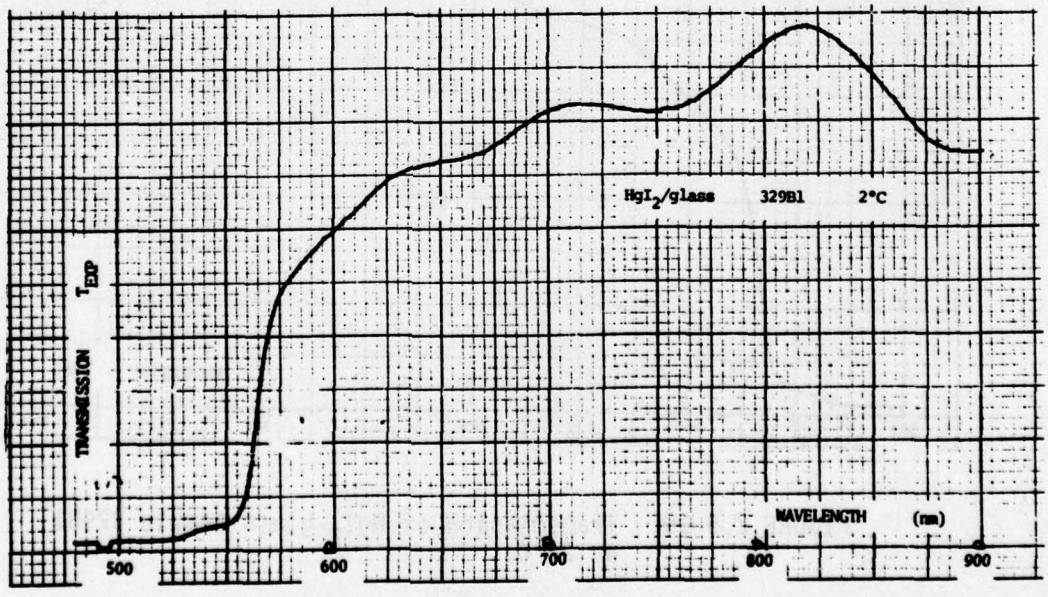

FIGURE 2.5-98. Transmission of HgI_2-glass Sample 329B1 at 2°C.

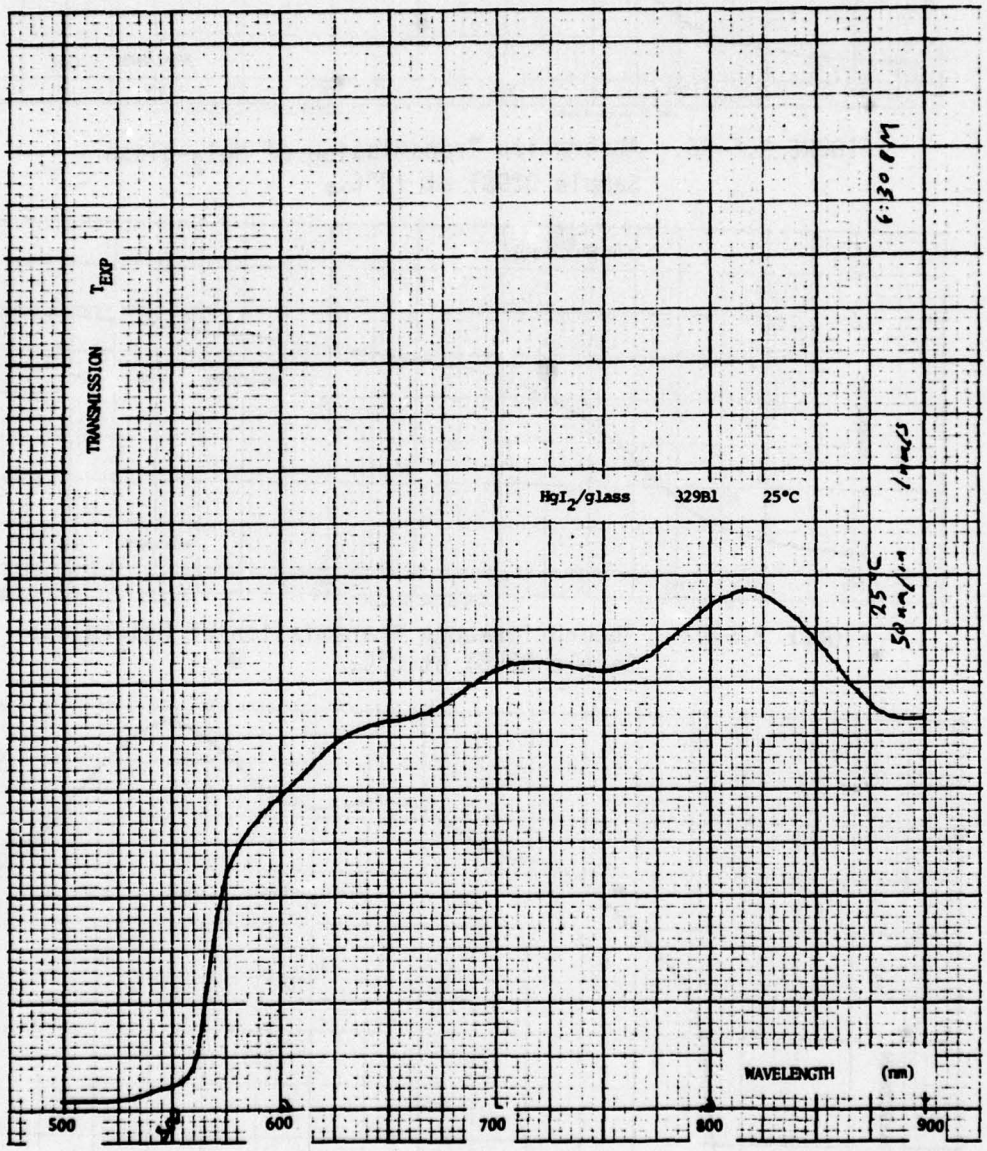

FIGURE 2.5-99. Transmission of HgI_2-glass Sample 329B1 at 25°C.

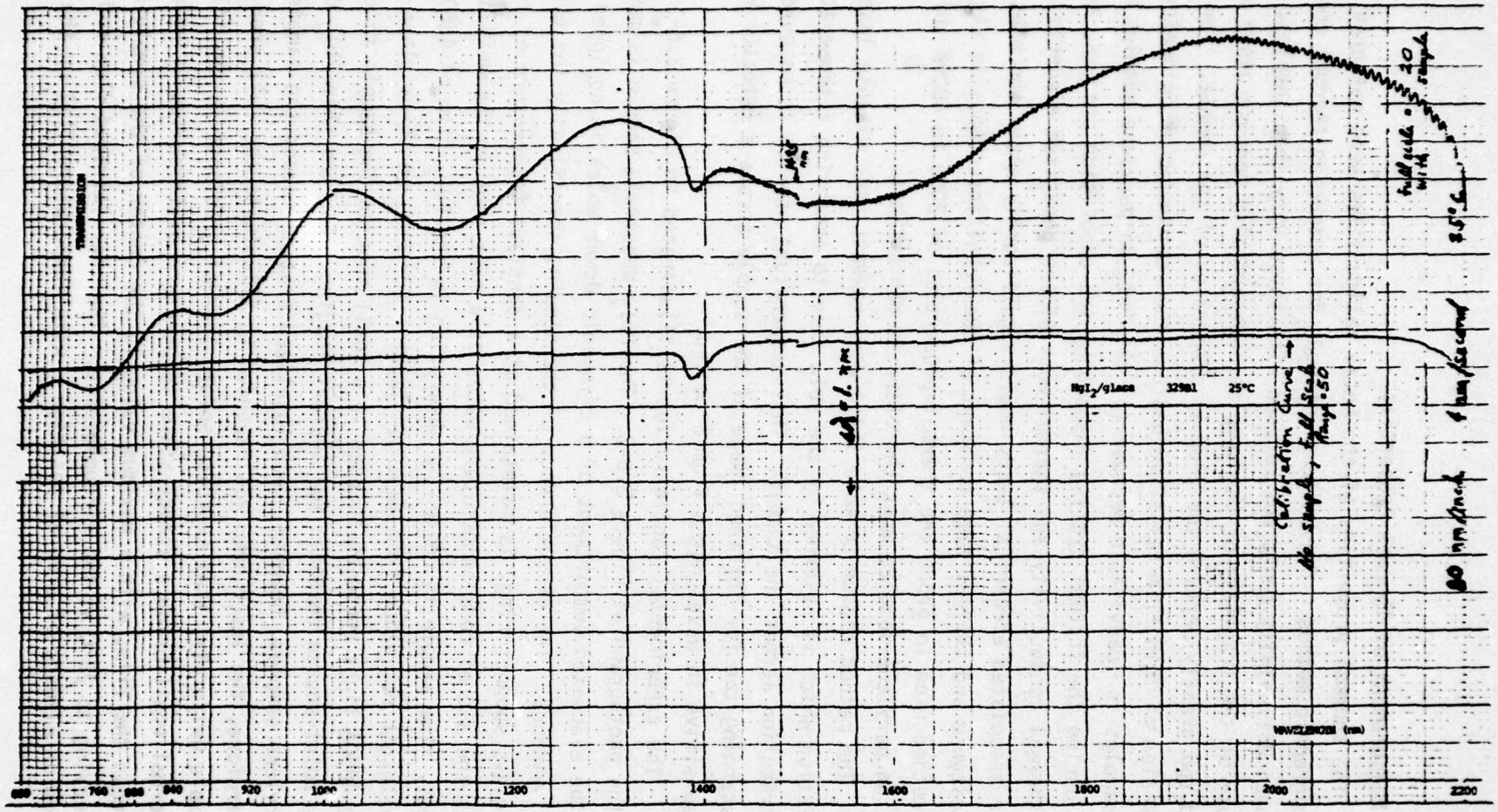

FIGURE 2.5-100. Infrared Transmission of HgI_2-glass Sample 329B1 at 25°C.

2.6 Measurement of Thermal Properties

The thermal properties of the metal halide films were measured using a thermographic method. Conventional methods for measuring thermal conductivity and heat diffusivity could not be used with these very thin samples, partially because of the fragility of the samples and partially because other methods would too greatly perturb the thermal properties of the sample. For example, deposition of thin film resistive heaters and semiconductor bolometers onto the samples is inadvisable because (1) the PbI_2 on parylene samples might tear during the thermal cycling imposed by the deposition process, and (2) the thermal conductivity and thermal mass of the deposited elements and their associated electrical leads would significantly alter the heat capacitance and thermal time constant of the resulting composite structure. The method used to probe the thermal properties of 2000 to 4000Å thick PbI_2 on parylene samples must therefore be contactless.

The method chosen to make these measurements uses visible laser radiation which is absorbed by the PbI_2 film to establish a temperature distribution across the sample. This temperature profile is measured by scanning the far-infrared image of the sample across a detector which is sensitive to wavelengths from 8 to 14μ.

The experimental configuration is illustrated in Figure 2.6-1 and in the photograph of Figure 2.6-2. The PbI_2-substrate sample is mounted in the evacuated compartment of a cryogenic dewar which is equipped with NaCl windows. The circumference of the sample, specifically the aluminum or glass support ring, is maintained at a constant temperature of 25°C with the aid of room temperature water as a heat sink in the well of the dewar. The sample is heated by absorption in the PbI_2 film of 4880Å wavelength radiation from an argon laser. For PbI_2 on thick glass substrates the 4880Å light could be focused to a small spot on the sample to determine the point-source response for thermal imaging. For the thin PbI_2 on parylene samples, however, such localized heating caused the sample to tear. Therefore, the laser beam was expanded to illuminate the full area of the sample uniformly, thus avoiding severe thermal gradients in the film. At thermal equilibrium a steady-state temperature distribution is established across the film, with a maximum value in the center of the sample and decaying to 25°C at the circumference. The far-infrared flux radiated from an element of area at position $\underline{r}$ with temperature $T(\underline{r})$ on the surface is

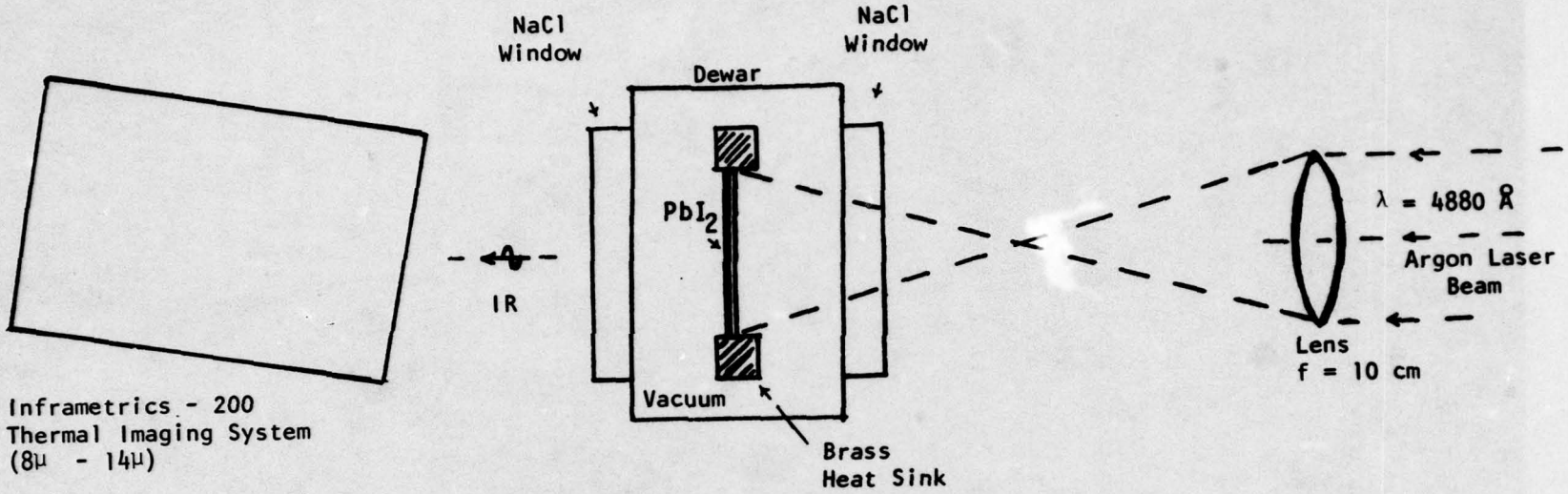

Figure 2.6-1. Thermal imaging experiment to measure temperature distribution along the surface of a PbI_2 film.

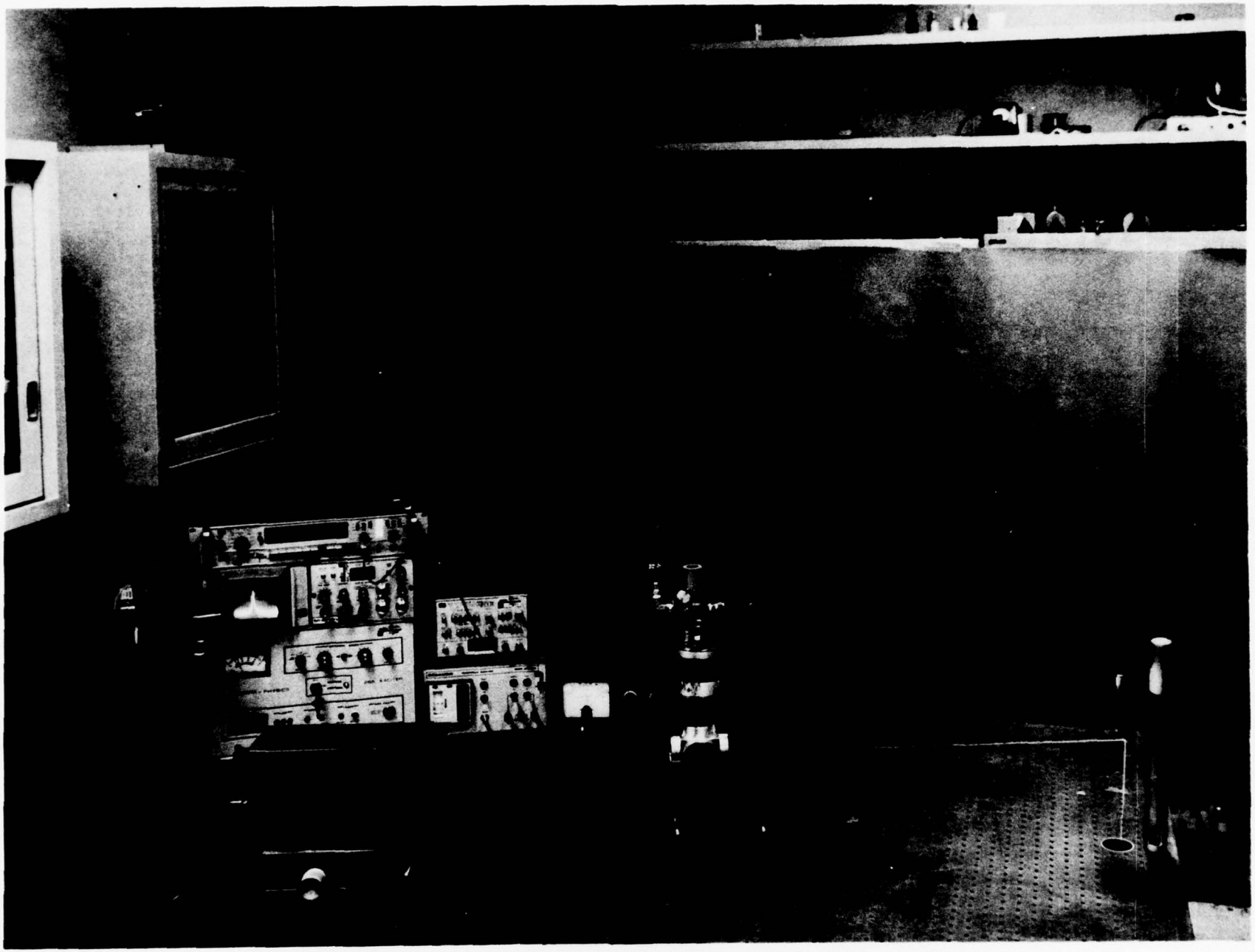

Figure 2.6-2. Experimental arrangement for measuring thermal properties of thin, rim-supported films.

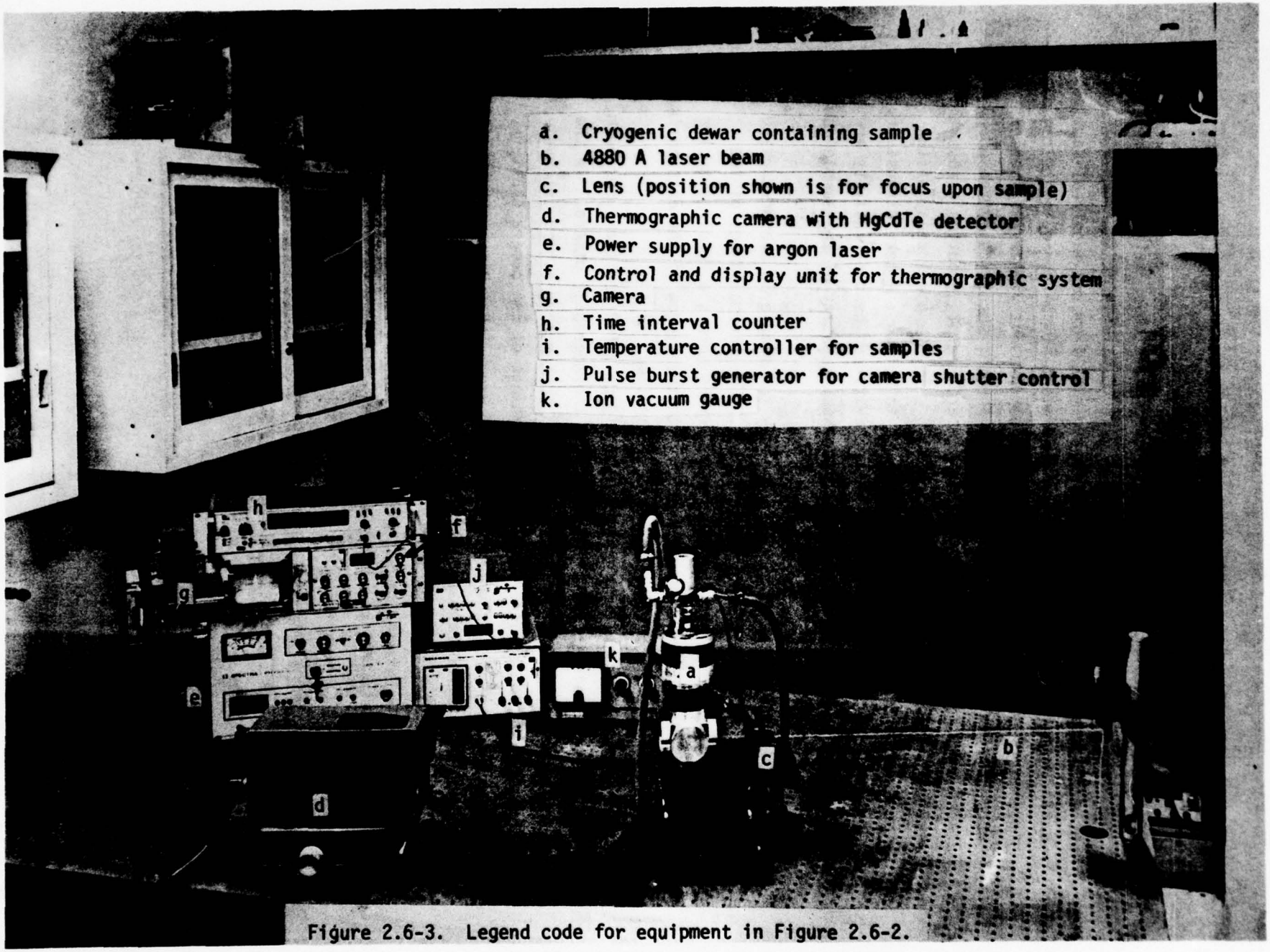

Figure 2.6-3. Legend code for equipment in Figure 2.6-2.

proportional to $T(x)^4-T_A^4$, where T_A is the ambient temperature of the surrounding laboratory environment. A spatial scan of the thermal radiation emitted from the surface of the sample then yields the temperature distribution across the surface. The emissivity of the sample may be determined by measuring the far-infrared flux from two identical samples at different, known temperatures. Measurement of the steady-state temperature distribution with the 4880Å laser beam present yields the thermal conductivity of the film. When the heat source, specifically the 4880Å laser beam, is abruptly removed, the temperature distribution across the sample decays to a constant value of 25°C. The temporal decay of the temperature distribution may be analyzed to obtain the heat diffusivity of the sample. Once the thermal conductivity and heat diffusivity are determined from these measurements, the heat capacity of the sample can be calculated.

The temperature distribution across the sample is measured using an Inframetrics 200 thermographic system. The thermal image of the sample is mechanically scanned by two mirrors across a HgCdTe detector at 77°K. The detector in combination with the window of the detector's dewar responds to wavelengths between 8 and 14μ.

Illustrated in the photograph of Figure 2.6-2 are the laser beam, the dewar containing the sample, and the thermographic camera. In the background behind the camera, from top to bottom, are a time interval counter to read the intervals between openings of the camera shutter after electronically shuttering the laser beam; the control and CRT display unit of the thermographic system to which is attached a camera equipped with electronically gated shutter; and the power supply for the argon laser which is located beneath the table. To the right, from top to bottom, are a controllable pulse-burst generator used to control the electronic camera shutter, and the automatic cyclic temperature control unit used both in emissivity measurements here and in optical transmission measurements in the spectrophotometer described elsewhere. Directly behind the dewar is an ion gauge used to monitor the vacuum in the dewar, typically about 200 microns.

Figure 2.6-4 shows a thermographic image of a PbI_2 on glass sample. The PbI_2 film is 0.2μ thick and the borosilicate glass substrate 200μ thick. Distinguishable in this (8 to 14μ wavelength) image are the circular sample, the annular aluminum support ring, the brass cylinder in which the sample is mounted, and the rectangular brass mount attached to the bottom of the cryogenic well of the dewar. The sample is at 25°C. Figure 2.6-5 shows the temperature distribution along a single horizontal line scanned through the center of the sample. The noise level is pronounced because the highest amplifier gain setting is used. The temperature distribution is essentially constant at 25°C. The dark spot above and left of center in Figure 2.6-4 moves as the angle between the normal to the sample and the optical axis of the infrared camera is varied, and is the reflected image of the cold detector (narcissus effect).

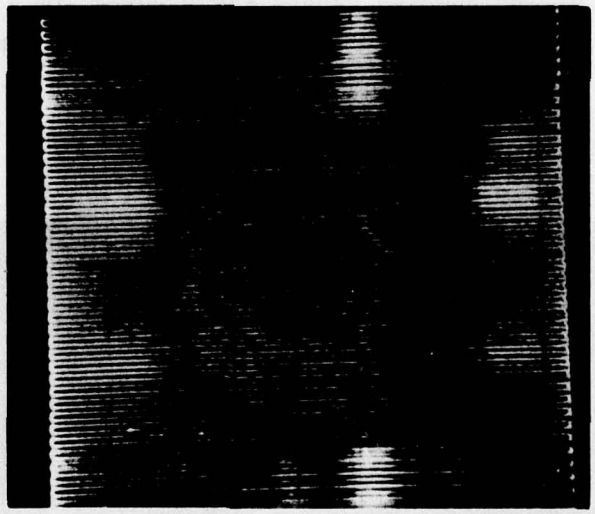

Figure 2.6-4. Thermographic image of PbI_2-on-glass sample taken using 8 to 14μ wavelength radiation.

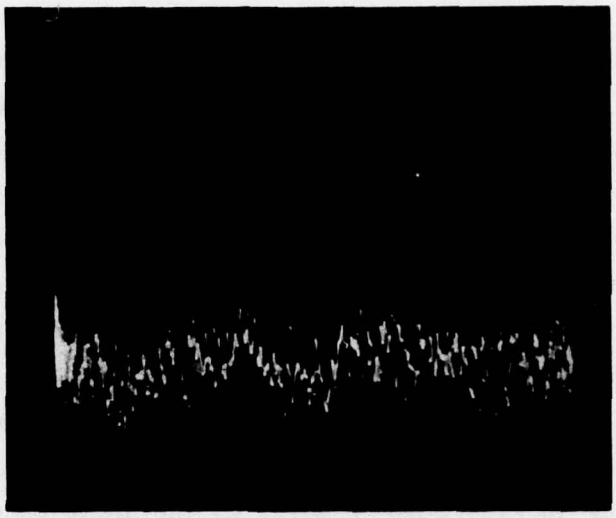

Figure 2.6-5. Temperature distribution is a constant 25°C on a single line scanned horizontally through the center of the above PbI_2-on-glass sample. No heat source is present.

With the 4880A wavelength laser beam now focused to a 10μ diameter spot in the center of the sample, Figure 2.6-6 shows the resulting hot spot in the center of the sample. Superimposed in this photograph is

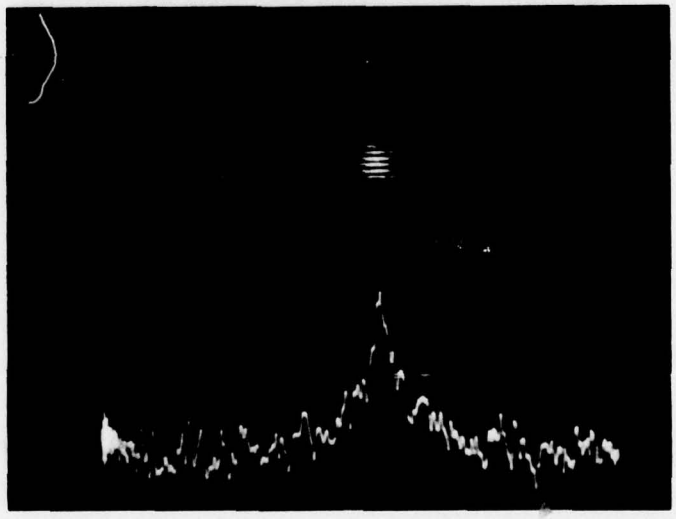

Figure 2.6-6. Thermographic image and line scan horizontally through the center of the PbI_2-on-glass sample.

the thermographic image just above a horizontal line scan through the center of the sample. The incident laser power is 25 mW, and the vertical temperature scale is 5 °C/5 cm for the emissivity temperature T_E. The circumference of the sample is maintained at 25°C.

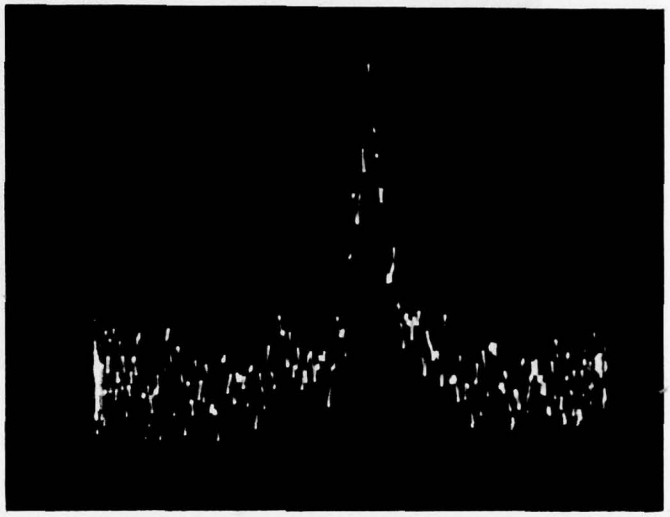

Figure 2.6-7. Similar to the previous figure but with a vertical scale of 3°C emissivity temperature per 5 cm.

The incident power given above takes into account reflection losses at the NaCl dewar window and at the glass and glass-PbI_2 surfaces.

When the laser beam is shuttered off, the temperature distribution decays as illustrated in Figures 2.6-8 through 2.6-11. The highest curve in each figure is the steady-state temperature distribution before the focused laser heat source is removed. The lower curves were photographed by electronically gating the camera shutter at predetermined time intervals after removing the laser beam. In Figure 2.6-8 the three curves correspond to time values of zero, one, and two seconds, respectively, from top to bottom. Figure 2.6-9 shows the temperature distributions at time values of zero, 5, and 10 seconds. The three curves of Figure 2.6-10 were recorded at time values of zero, 3, and 8 seconds. Superposition of noise in the wings of the curves results in loss of information near the circumference of the sample. Therefore, quantitative data for analysis taken on this sensitivity scale was limited to two curves for each photograph in later experiments.

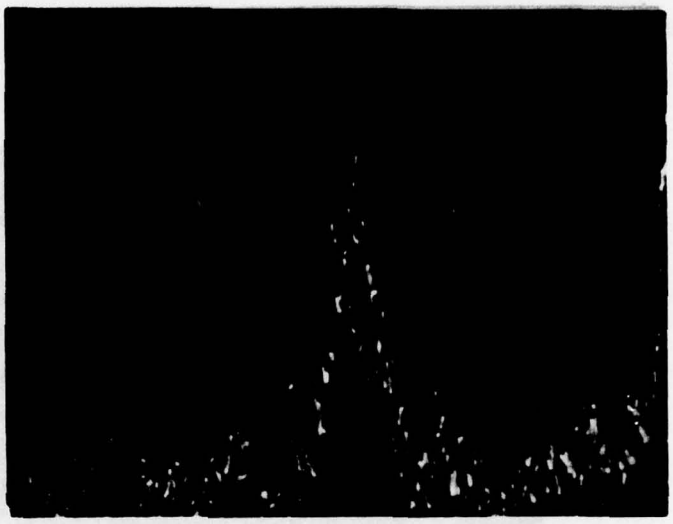

Figure 2.6-8. Horizontal line scan through center of PbI_2-on-glass sample at time values of (a) 0 seconds, (b) 1 second, and (c) 2 seconds. Vertical sensitivity is 3°C emissivity temperature per 5 divisions.

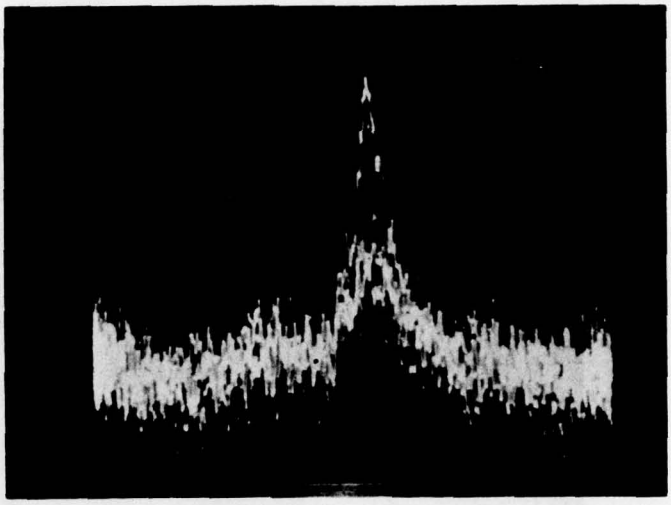

Figure 2.6-9. Similar to the preceding figure, with time values of (a.) 0 seconds, (b.) 5 seconds, and (c.) 10 seconds.

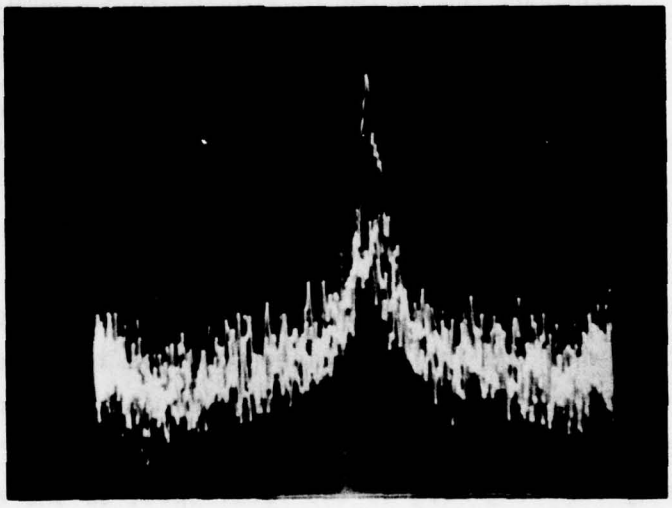

Figure 2.6-10. Similar to the preceding two figures, with time values of (a.) 0 seconds, (b.) 3 seconds, and (c.) 8 seconds.

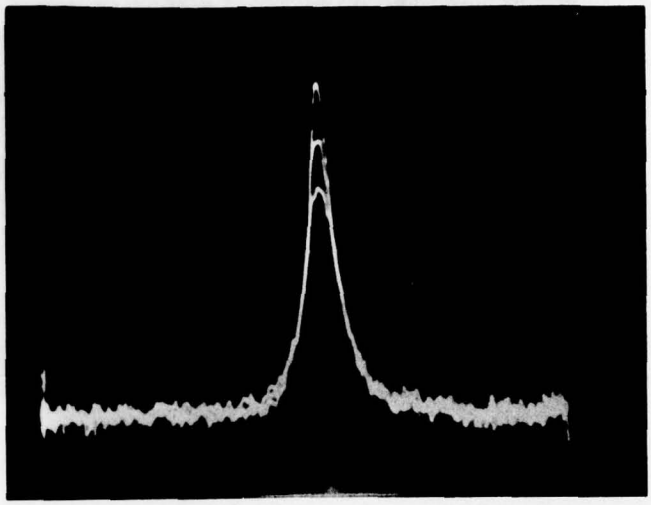

Figure 2.6-11. Temperature distribution for a horizontal line scan through the center of PbI_2-on-glass sample, with laser power of 60 mW incident upon the PbI_2 film and a vertical sensitivity of 5°C emissivity temperature per 5 divisions. Consecutive scans upon remal of heat source at times (a) zero, (b) one, and (c) two seconds from top to bottom, respectively. Consecutive scans upon removal of heat source at times (a) zero; (b) one, and (c) two seconds from top to bottom, respectively.

Figure 2.6-11 shows the temperature profile obtained on a less sensitive scale when the incident laser power is increased to 60 mW focused at the center of the sample. The noise level at the circumference of the sample is reduced greatly. However, this power density "burns" the PbI_2 film, partially removing PbI_2 at the focal spot, so the amount of laser power actually absorbed is not known for this case. Clearly, this type of power density must be avoided with the much more fragile PbI_2-on-parylene samples. The temporal decay of the temperature distribution is shown for time values of zero, one, and 2 seconds after removing the laser beam.

2.6.1 Thermograph Calibration and Emissivity Measurements

The thermographic system is used in either of two modes, both of which simultaneously compare the thermal radiance of two objects at different temperatures. Each mode requires calibration separately. A decrease in the resistance of the HgCdTe detector required that we change a resistor in the detector's bridge circuit. This in turn caused the calibration of the instrument to differ from the manufacturer's calibration so the isotherm scales and the line scan scales could not be interpreted literally. The change in resistance did not appear to affect the sensitivity of the detector, however.

The two samples used to calibrate the thermographic system were both water with an emissivity of 0.96, close to the limit of 1.0 for an ideal blackbody. Two beakers of water were placed in the camera's field of view, about 0.5 meter from the camera. The camera was aimed at an angle of about 45 degrees from the water surface, "looking down" upon the beakers.

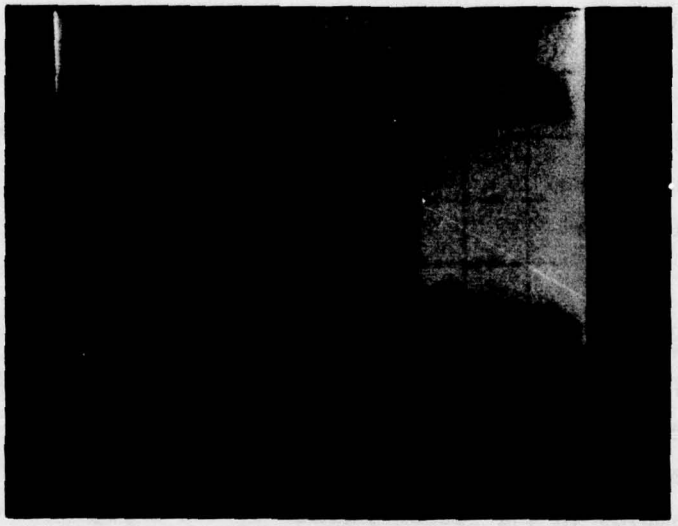

FIGURE 2.6.12 Thermographic Image (at 8 μ to 14 μ Wavelengths) of Water Samples Used for Calibration of Thermographic System.

The temperature of one beaker of water, referred to as the "reference," was maintained at about 23°C, while the temperature of the "sample" beaker of water was adjusted to values between room temperature and 65°C. The actual temperatures of the water reference and sample are measured by thermometers, and the difference between those two readings is the "actual temperature difference ΔT ." The procedure for calibrating the thermographic unit for each mode is then to read the radiant temperature difference ΔT_E between the two samples, using the appropriate procedures for each mode. The rate Q at which heat is radiated from a sample at temperature T to a surrounding blackbody environment at ambient temperature T_A is given in the linear approximation as

$$Q = \varepsilon \sigma 4 T_A^3 (T-T_A), \qquad (2.6.1\text{-}1)$$

where ε is the emissivity of the sample and σ is the Stefan-Boltzman constant. For a different sample temperature T' the rate of heat radiation Q' is, similarly,

$$Q' = \varepsilon \sigma 4 T_A^3 (T'-T_A). \qquad (2.6.1\text{-}2)$$

For both isotherm and line scan modes of operation the quantity read from the display is proportional to the difference between the flux levels

$$Q - Q' = \varepsilon \sigma 4 T_A^3 (T-T') \quad . \qquad (2.6.1\text{-}3)$$

The scales of the thermographic system are pre-calibrated for a blackbody source, for which $\varepsilon=1$ and

$$Q - Q' = \sigma 4 T_A^3 (T_E-T_E') \qquad (2.6.1\text{-}4)$$

where T_E and T_E' are the radiometric temperatures of the two blackbodies used in this calibration. Upon comparing the previous two equations, it is easily shown that the emissivity of the non-blackbody source is

$$\varepsilon = (T_E-T_E')/(T-T') \quad . \qquad (2.6.1\text{-}5)$$

This forms the basis for our emissivity measurements. It is assumed that convective losses do not significantly change these results for the two water samples.

The emissivity of PbI_2 or HgI_2 is measured by mounting two nearly identical samples in the vacuum chamber of the cryogenic dewar, adjusting and measuring the temperatures of the two samples both by thermocouples

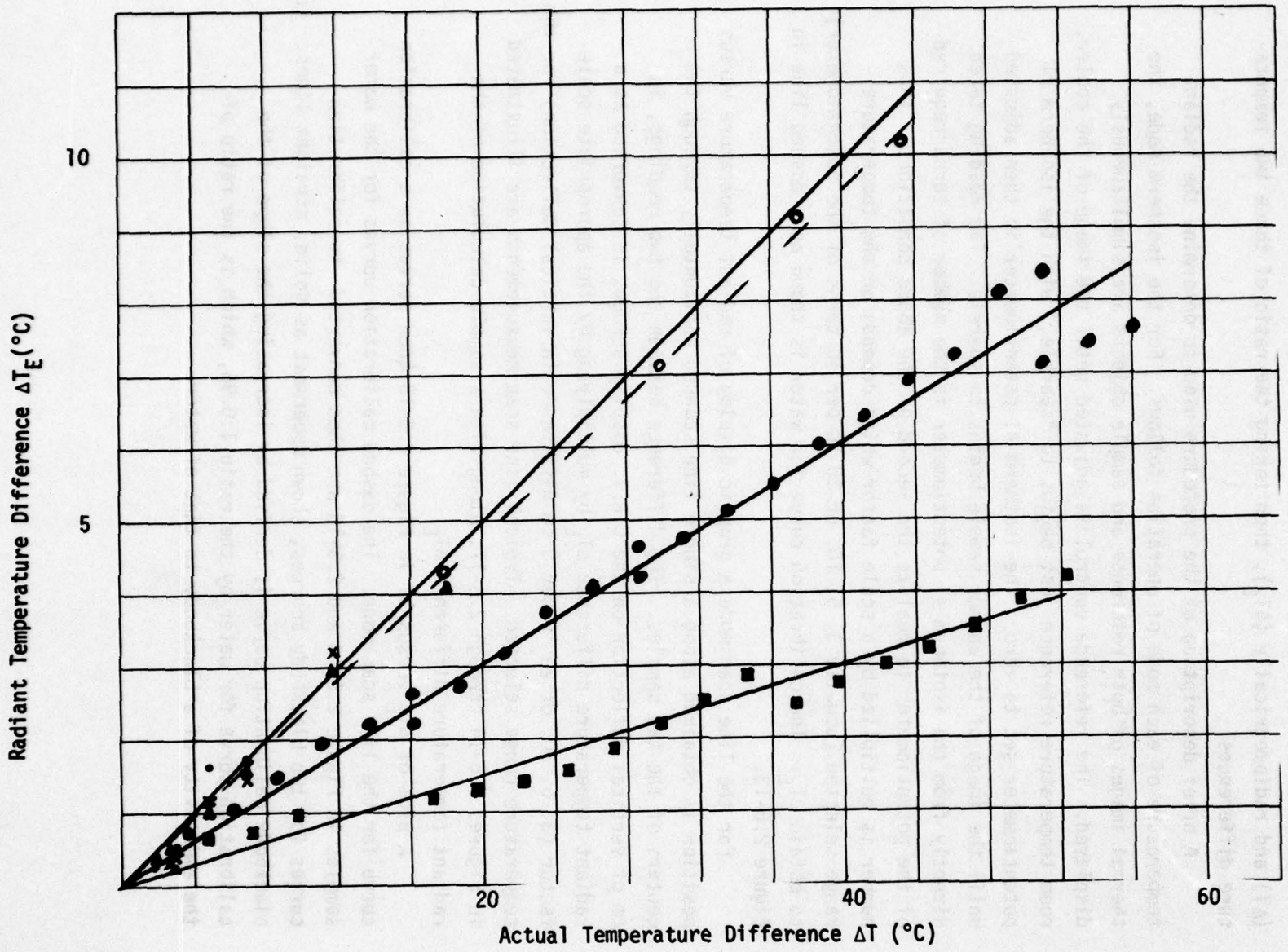

FIGURE 2.6.13. Calibration data for isotherm #1 using two water samples for temperature range scales 3 (·), 5 (Δ), 10 (x) and 20 (∘) °C per 10 turns. Dashed curve averages data for water samples. Upper solid curve is calibration curve for two blackbody samples. Lower two curves are for data on PbI_2 films (●) and HgI_2 crystals (■). Slopes $\Delta T_E/\Delta T$ are 0.2477, 0.2386, 0.150, and 0.075 from top to bottom, respectively.

(ΔT) and radiometrically (ΔT_E), then taking the ratio of these two temperature differences.

A brief description of the procedure used to determine the radiant temperature of each mode of operation follows. For the isotherm mode, the thermal images of both reference and sample objects are simultaneously displayed. The reference control is adjusted until the image of the cooler, room temperature reference just begins to "sparkle," with the isotherm #1 potentiometer set to zero. The isotherm #1 potentiometer is then adjusted until the image of the warmer sample begins to sparkle. The reading taken directly from the isotherm #1 potentiometer is the number of turns required of the potentiometer to realize the second of the above conditions. This number is multiplied by a scale factor which depends on the temperature range selected (usually 3, 5, 10, or 20 °C per 10 turns of the potentiometer) to obtain ΔT_E. The calibration curve for water is shown as a dashed line in Figure 2.6-13.

For the line scan mode a graphic display of radiant temperature versus position is obtained along a single line scanned horizontally through the centers of the two samples. The difference between the two readings, in cm of vertical deflection on the C.R.T. display screen, is converted to a radiant temperature difference ΔT_E by multiplying by the appropriate scale factor (3, 5, 10, or 20 °C per 5 cm difference in vertical deflection) for the temperature range selected. Typical line scan measurements are illustrated in Figures 2.6-14 through 2.6-17, along with a sample calculation of the radiant temperature difference ΔT_E.

A plot of ΔT_E versus ΔT in Figure 2.6-18 then serves as a calibration curve for the line scan mode. The dashed calibration curves for the water samples in Figure 2.6-13 and 2.6-18 are then converted to calibration curves for two blackbody sources, shown uppermost as solid, straight lines. Each blackbody calibration curve is derived by increasing the slope of the calibration curve for water by the ratio 1:0.96, which is the ratio of the emissivity of a blackbody to that of water.

FIGURE 2.6-14. Line scan of temperature versus position, scanned through the centers of the two water samples. Scale = 5°C per 5 cm vertically; line scan 1 mode.

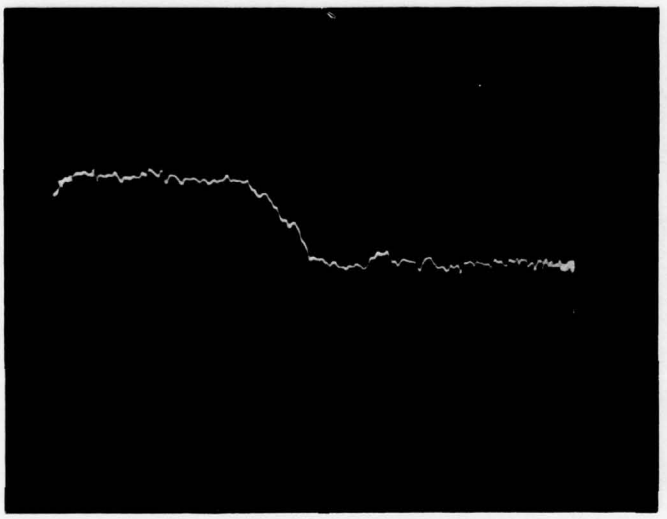

FIGURE 2.6-15. Line scan similar to above, with scale = 20°C per 5 cm vertically; line scan 1 mode

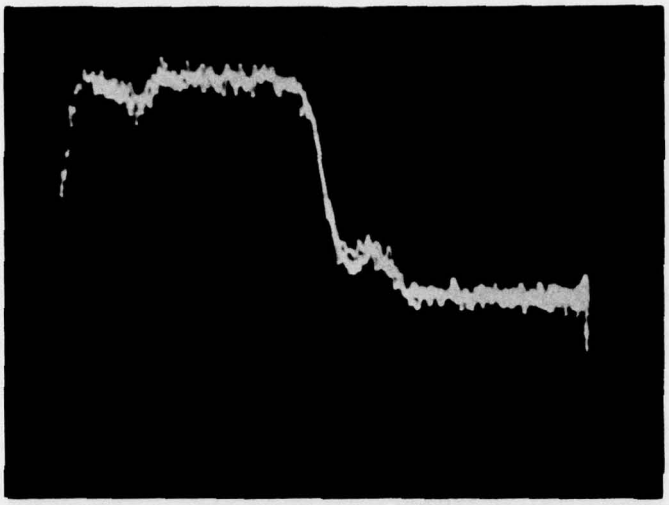

$$\Delta T_E = 3.5\text{cm} \times \frac{10°C}{5\text{ cm}}$$

$$= 7.0°C$$

FIGURE 2.6-16. Line scan similar to above, with scale = 10°C per 5 cm vertically; line scan 1 mode.

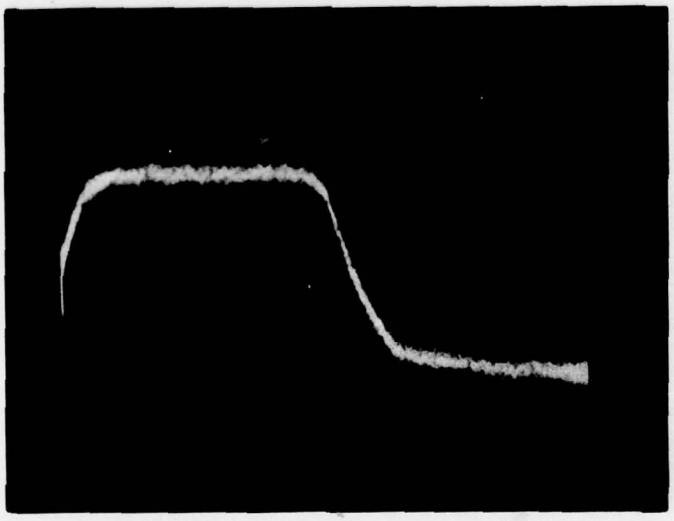

FIGURE 2.6-17. Line scan similar to above, with scale = 10°C per 5 cm vertically; line scan 2 mode.

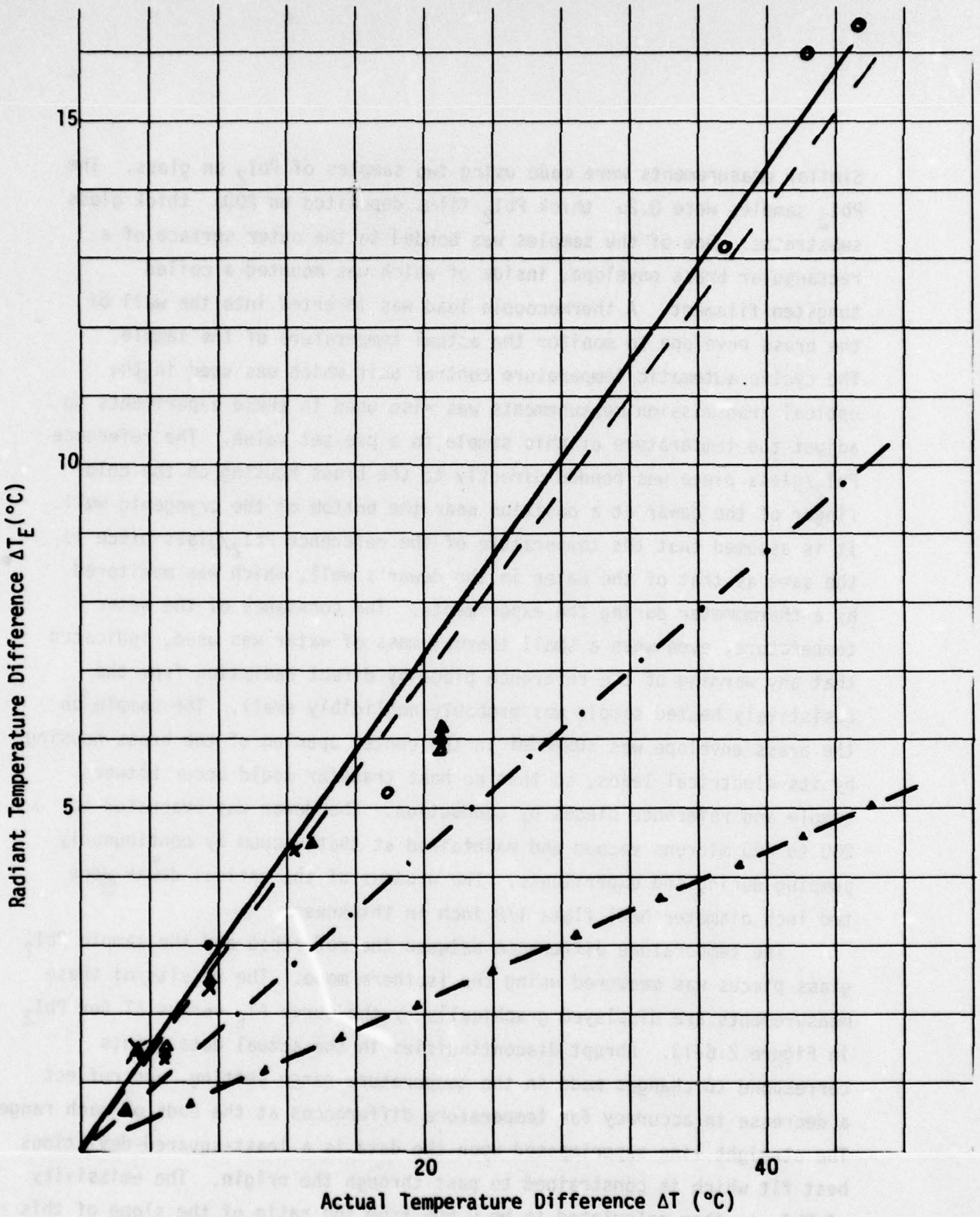

FIGURE 2.6-18. Calibration curves for line scan #2 mode using two water samples (-----), for temperature range scales 3 (·), 5 (Δ), 10 (x) and 20 (o). The other calibration curves constructed are for blackbody samples with $\varepsilon = 1$ (——), for PbI_2 films on glass with $\varepsilon = 0.606$ (-.-.-.-), and for HgI_2 crystals with $\varepsilon = 0.303$(-Δ-Δ-Δ-Δ).

Similar measurements were made using two samples of PbI_2 on glass. The PbI_2 samples were 0.2μ thick PbI_2 films deposited on 200μ thick glass substrates. One of the samples was bonded to the outer surface of a rectangular brass envelope, inside of which was mounted a coiled tungsten filament. A thermocouple lead was inserted into the wall of the brass envelope to monitor the actual temperature of the sample. The cyclic automatic temperature control unit which was used in the optical transmission measurements was also used in these experiments to adjust the temperature of this sample to a pre-set value. The reference PbI_2/glass piece was bonded directly to the brass housing on the cold finger of the dewar at a position near the bottom of the cryogenic well. It is assumed that the temperature of the reference PbI_2/glass piece is the same as that of the water in the dewar's well, which was monitored by a thermometer during the experiments. The constancy of the water temperature, even when a small thermal mass of water was used, indicated that any warming of the reference piece by direct radiation from the resistively heated sample was probably negligibly small. The sample on the brass envelope was suspended in the center opening of the brass housing by its electrical leads, so that no heat transfer could occur between sample and reference pieces by conduction. The dewar was evacuated to 200 to 400 microns vacuum and maintained at that vacuum by continuously pumping during the experiments. The windows of the optical dewar were two inch diameter NaCl flats 1/8 inch in thickness.

The temperature difference between the reference and the sample PbI_2 glass pieces was measured using the isotherm mode. The results of these measurements are displayed graphically by the curve ΔT_E versus ΔT for PbI_2 in Figure 2.6-13. Abrupt discontinuities in the actual data points correspond to changes made in the temperature range setting, and reflect a decrease in accuracy for temperature differences at the ends of each range. The straight line superimposed upon the data is a least-squared-deviations best fit which is constrained to pass through the origin. The emissivity of PbI_2 is then calculated to be 0.606 from the ratio of the slope of this curve to the slope of the blackbody calibration curve.

Similar measurements were made using two 5 x 5 x 0.1 cm plates of HgI_2 obtained from E.G.G. Corp. These measurements were made as rapidly as possible after evacuating the dewar, because of previous experience with the evaporation of HgI_2 in vacuum due to its high vapor pressure. It was noted that the surface of the warm HgI_2 sample begin to change to the yellow phase at a temperature of 67°C in vacuum, corresponding to $\Delta T = 44.7°C$ in the figure. Upon removing the HgI_2 sample after the last measurement at 75°C ($\Delta T = 52°C$), it was observed that the phase transformation evidenced by the yellow color extended well below the surface, a distance of about 0.5mm. With time, the crystal transformed back to the red phase at the surface. The emissivity of HgI_2 was 0.303, as calculated from the ratio of the slope of the HgI_2 curve to the slope for the blackbody calibration curve.

The emissivity for PbI_2 reported here is for a 0.2μ thick PbI_2 film on a 200μ thick glass substrate, with thermal emission measured from the direction normal to the PbI_2 surface. Actually, for such a thin sample, the emissivity is probably different from that of a thick crystal of PbI_2. The thermal radiation from the film samples contains contributions from multiple reflections at each interface. The radiated flux should depend upon the reflectivities of the PbI_2-glass interface and the glass-vacuum interface, as well as upon the absorption coefficient within each material. The thermal radiance of thin film structures has been treated in the literature, and these influences should be included in future investigations of this type. This is especially important for the samples which are thin films on thin polymer substrates.

2.6.2 Measurements of Thermal Properties of PbI_2 Films on Glass Substrates

In order to deliver a sufficient amount of laser power to the sample to produce a detectable temperature increase without damaging the film, the sample was illuminated uniformly with an expanded laser beam. Initially, a telescopic beam expander using a 3μ diameter pinhole was used to expand the 2mm diameter beam to one cm diameter, but the power loss was unacceptable. Sufficiently uniform illumination was obtained by moving a 10 cm focal length lens a distance of 60 cm from the sample to just fill the sample's 1/2 inch aperture with the diverging laser beam. For 342 mW of laser power incident on the sample, the transmitted power was 10.3 mW, yielding a transmission of about 3 percent for the 2000Å thick PbI_2 film. This indicates an absorption coefficient of 1.75×10^5 cm^{-1} for PbI_2 at 4880Å wavelength.

With the laser beam illuminating the sample, a steady-state temperature profile was observed with a maximum at the center of the sample, as shown in Figure 2.6-19. Upon blocking the laser beam before it strikes the sample, the temperature distribution decays with a time constant of about 20 seconds. In contrast, when a beam stop is inserted between the sample and the HgCdTe detector the temperature profile disappears immediately. This test ensures that thermal radiation from the sample is responsible for the line scan profile rather than a weak detector response to the visible laser radiation.

The temperature distributions T(r,t) at different times after shuttering the laser beam off are shown in Figures 2.6-19 through 2.6-27. The shutter speed from the camera was 1/30 second with the f stop open. The figure captions give the time after removal of the heat source for each curve, as well as the peak temperature T_c initially at the center of the sample.

The laser power incident upon the PbI_2 film, corrected for reflections at the NaCl window surfaces, glass substrate surface, and glass-to-PbI_2 interface, was 320 mW. A range setting of 20 °C of ΔT_E per 5 cm was used with line scan mode #2. Each line is scanned through the center of both the illuminated PbI_2 film and a reference PbI_2 film at 25°C. The reference sample is bonded to the brass housing and located to the left side in each photograph. The isotherm mode was used to verify the temperature difference between the reference sample and the center of the illuminated PbI_2 sample under steady-state conditions. From the straight line plot for PbI_2 in Figure 2.6-18, the calibration factor for the temperature scale in Figure 2.6-19 through 2.6-27 is ΔT = 16.6°C per division. The vertical

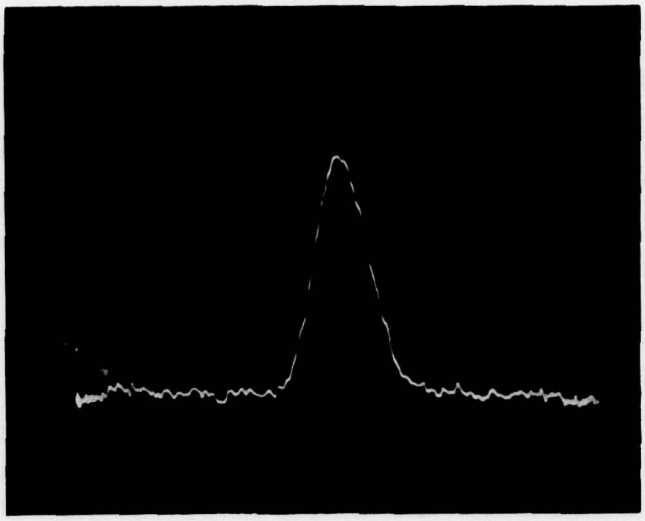

Figure 2.6-19. Steady-state temperature distribution $T(r,0)$ with PbI_2 on glass sample No. 412A9 illuminated uniformly by 320 mW of laser radiation at 4880 Å wavelength. $T_c(0) = 86.6°C$.

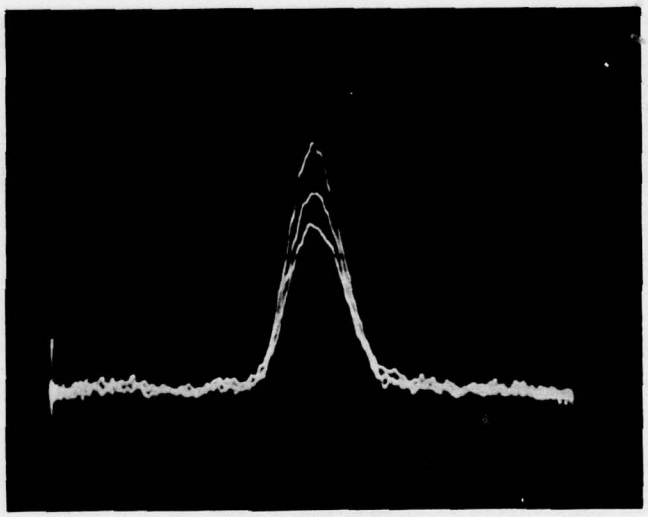

Figure 2.6-20. $T(r,t)$ for times t = 0, 2, and 4 seconds after removal of heat source, shown by successively lower curves. Sample 412A9. $T_c(0) = 88.6°C$

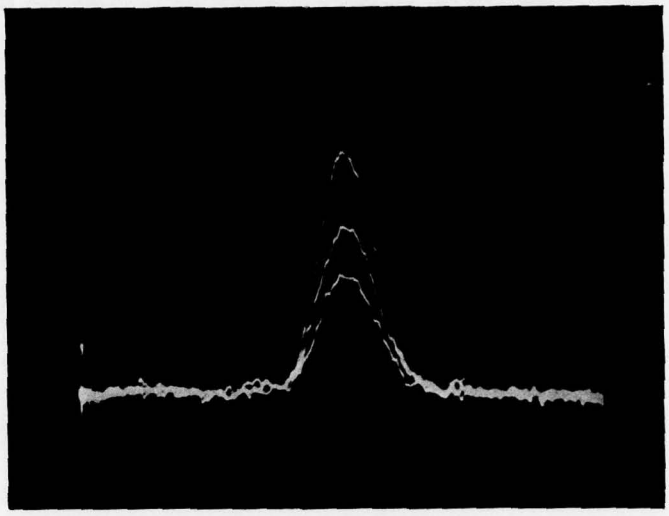

Figure 2.6-21. T(r,t) for times t = 0, 4, and 8 seconds. Sample 412A9. $T_c(0)$ = 87.3°C.

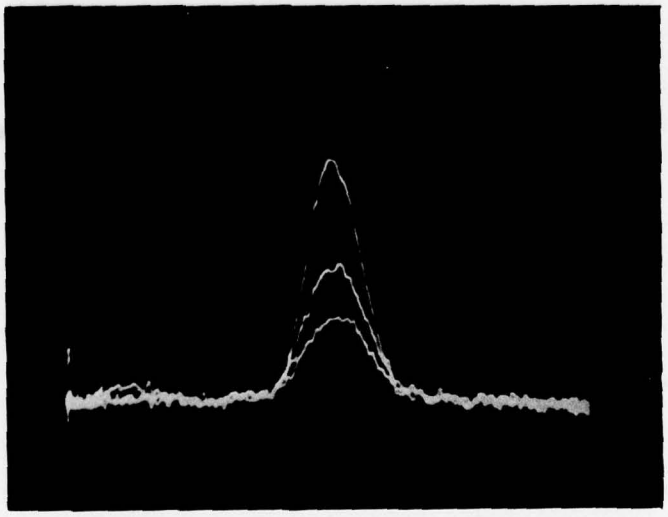

Figure 2.6-22. T(r,t) for times t = 0, 6, and 12 seconds. Sample 412A9. $T_c(0)$ = 86.4°C.

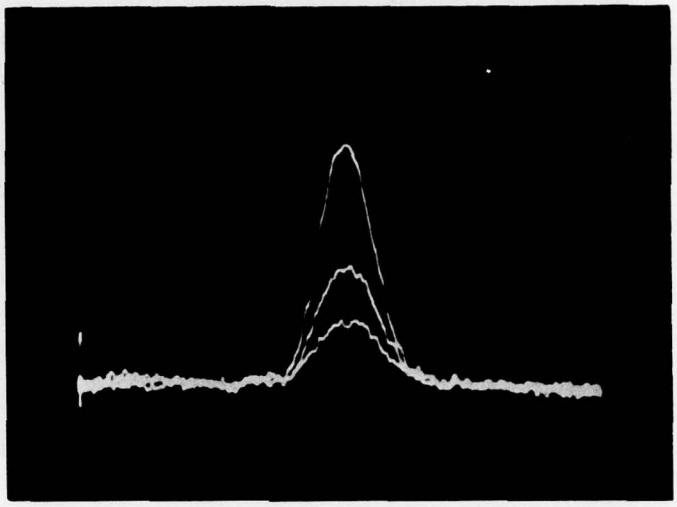

Figure 2.6-23. T(r,t) for times t = 0, 8, and 16 seconds for successively lower curves. Sample 412A9. $T_c(0)$ = 86.8°C.

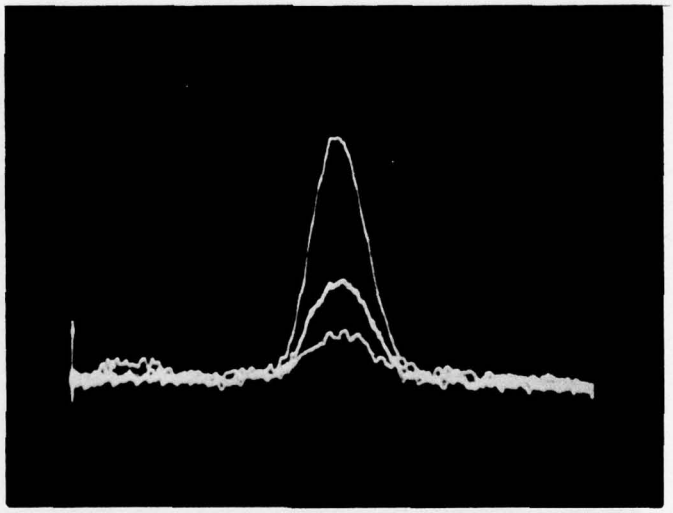

Figure 2.6-24. T(r,t) for times t = 0, 10, and 20 seconds. Sample 412A9. $T_c(0)$ = 86.8°C.

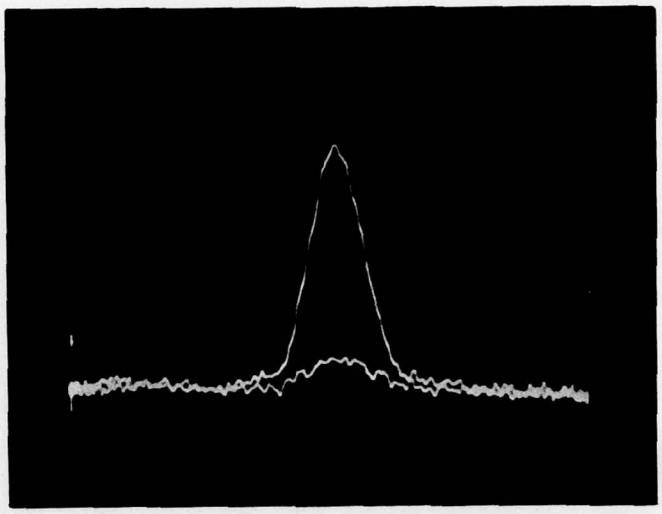

Figure 2.6-25. T(r,t) for times t = 0 and 25 seconds. Sample 412A9. $T_c(0)$ = 87.7°C.

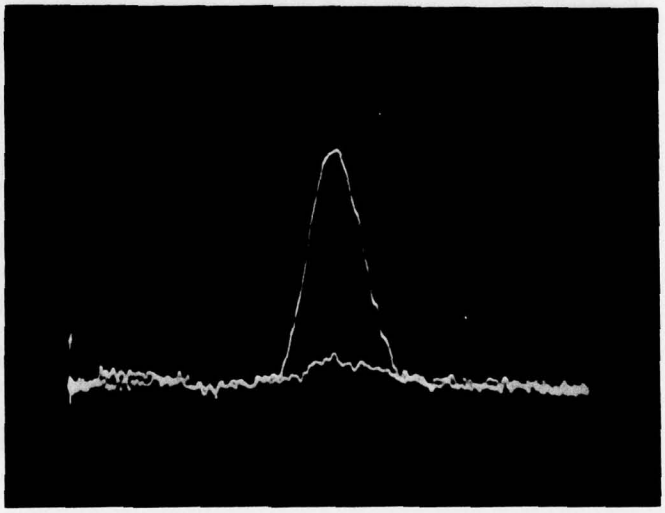

Figure 2.6-26. T(r,t) for times t = 0 and t = 30 seconds. Sample 412A9. $T_c(0)$ = 86.8°C.

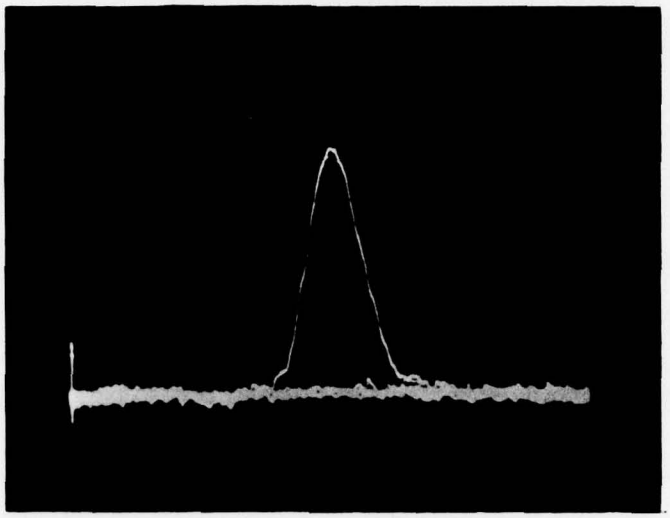

Figure 2.6-27. T(r,t) for t = 0 and t = 40 seconds. Sample 412A9. $T_c(0)$ = 88.1°C.

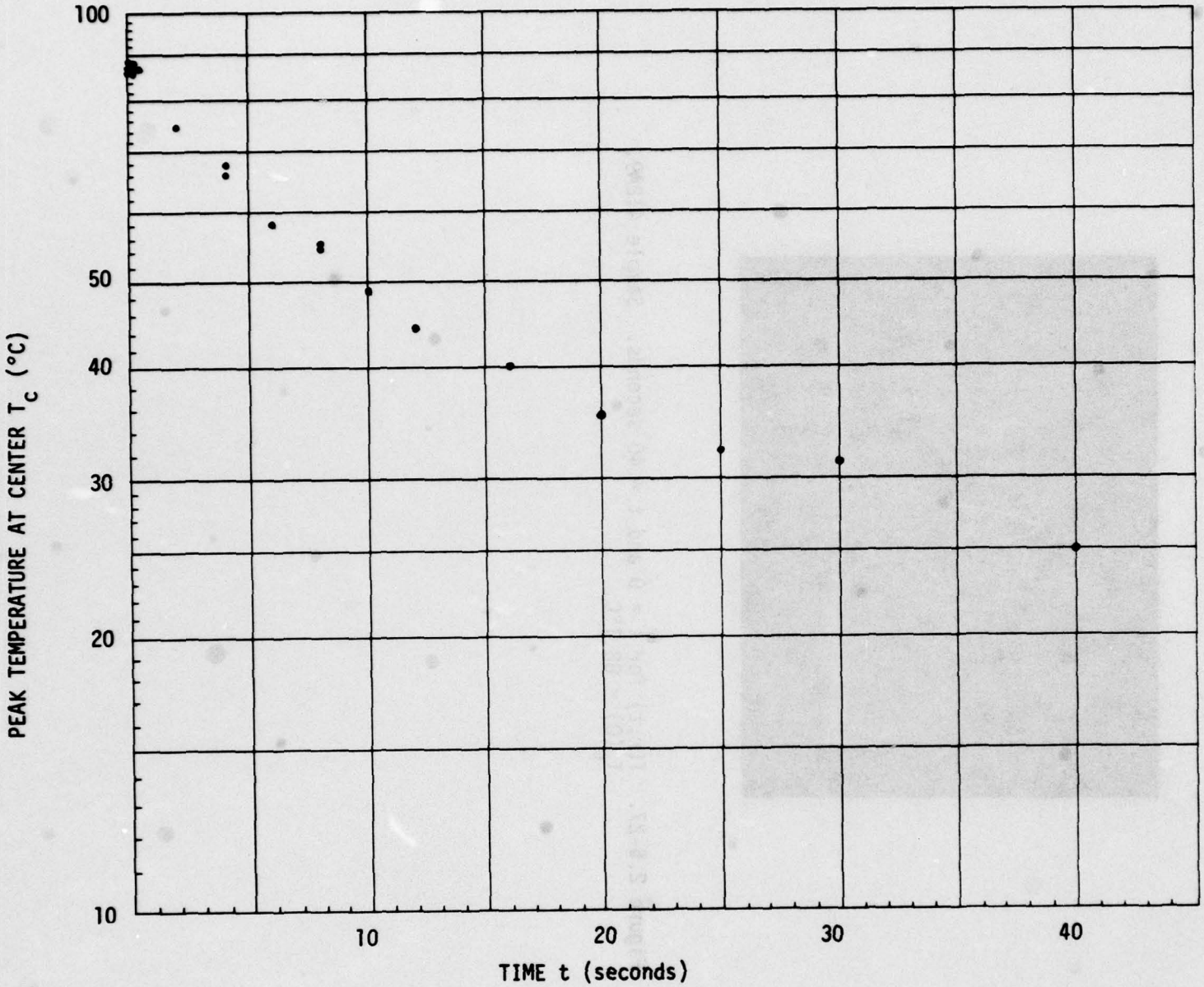

Figure 2.6-28. Temporal decay of peak temperature T_c at center of PbI_2 on glass sample upon removal of laser heat source at t=0.

Table 2.6-1

Data for temporal decay of the peak temperature T_c of PbI_2 on glass sample from Figures 2.6-19 through 2.6-27.

Time (sec)	Height (mm)	Divisions Vertically	ΔT (°C)	T_c (°C)
0	33.4	3.711	61.6	86.6
0	34.5	3.833	63.6	88.6
2	27.3	3.033	50.4	75.4
4	22.4	2.489	41.3	66.3
0	33.8	3.756	62.3	87.3
4	23.3	2.589	43.0	68.0
8	16.3	1.811	30.1	55.1
0	33.3	3.7	61.4	86.4
6	18.0	2.0	33.2	58.2
12	10.7	1.189	19.7	44.7
0	33.5	3.722	61.8	86.8
8	16.1	1.789	29.7	54.7
16	8.3	.922	15.3	40.3
0	33.5	3.722	61.8	86.8
10	13.0	1.444	24.0	49.0
20	5.7	.633	10.5	35.5
0	34.0	3.777	62.7	87.7
25	4.1	.4555	7.56	32.56
0	33.5	3.722	61.8	86.8
30	3.5	.389	6.46	31.46
0	34.2	3.8	63.1	88.1
40	0.	0.	0.	25.0

division of one cm referred to in this scaling is not necessarily one cm in the figure, because different magnifications were used with the camera. The scale distance of one cm on the CRT display is indicated by the marks on the right side of each photograph. As an example, the temperature difference from edge to center of the sample in Figure 2.6-19 is ΔT = 16.6 (°C/cm) x 3.7 (cm) = 62°C, giving a peak temperature of 87 °C.

The data in Figures 2.6-19 through 2.6-27 is partially summarized in Figure 2.6-28, which gives the peak temperature T_c at the center as a function of time after removal of the heat source. The data for T_c taken from the photographs is listed in Table 2.6-1. From Figure 2.6-28, the thermal time constant for the PbI_2 on glass sample is about 14 seconds for the peak temperature to decrease by a factor of 1/2. Figure 2.6-28 shows the temporal decay is not a simple exponential decay, but T_c varies more rapidly initially.

The thermal conductivity and heat diffusivity for the PbI_2 film are obtained from this data, using the theoretical results of sections 2.6.4, -.5, and -.6 which follow. The equations derived therein which apply to the present measurements are summarized here for convenience. In the discussion which follows, the following definitions of symbols are used:

Subscripts 1, 2 refer to the PbI_2 film and glass substrate, respectively,

k_i = thermal conductivity of region i,

α_i = heat diffusivity for region i,

c_i = specific heat of region i,

D_i = thickness of region i,

Q_V = rate of heat per unit volume generated by the laser source,

a = optical absorption coefficient of PbI_2 at 4880Å,

I_o = incident intensity at 4880Å in watts/cm^2,

σ = Stefan-Boltzman constant,

T_A = ambient laboratory temperature,

J_o, J_1, I_o = cylindrical Bessel functions,

a_m = m'th root of J_o, and

R = radius of circular sample.

The data just summarized in Table 2.6-1 and Figure 2.6-28 is analyzed by comparison to the theoretical temperature distributions

$$T(r,0) = T_R + \frac{Q_v}{k\beta^2}\left[1 - \frac{I_o(\beta r)}{I_o(\beta R)}\right] \qquad (2.6.2\text{-}1)$$

for steady state conditions, and

$$T(r,t) = T_R + \frac{2Q_v}{k\beta^2}\sum_{m=0}^{\infty} \frac{J_o(a_m r/R)\exp\left(-\alpha\beta t\left[1 + a_m^2/\beta^2R^2\right]\right)}{J_1(a_m)\, a_m\left[1 + a_m^2/\beta^2R^2\right]} \qquad (2.6.2\text{-}2)$$

for transient behavior. The derivation of these expressions is given in Sections 2.6.4 through 2.6.6, and only the useful results are presented here. It is assumed that the temperature T_R at the circumference r = R of the sample is the same as the temperature T_A of the surrounding environment. The parameters characterizing thermal properties of the materials are

$$k = (k_1 D_1 + k_2 D_2) / (D_1 + D_2), \qquad (2.6.2\text{-}3)$$

$$\alpha = (k_1 D_1 + k_2 D_2) / (\rho_1 c_1 D_1 + \rho_2 c_2 D_2), \qquad (2.6.2\text{-}4)$$

$$\beta^2 = (\varepsilon_f + \varepsilon_b)\,\sigma 4T_A^3 / (k_1 D_1 + k_2 D_2), \qquad (2.6.2\text{-}5)$$

$$k\beta^2 = (\varepsilon_f + \varepsilon_b)\,\sigma 4T_A^3 / (D_1 + D_2) \qquad (2.6.2\text{-}6)$$

and

$$Q_V = I_o\left[1 - \exp(-a D_2)\right] / (D_1 + D_2). \qquad (2.6.2\text{-}7)$$

Subscripts 1 and 2 refer to the substrate of thickness D_1 and the PbI_2 film of thickness D_2, respectively. Further definitions are fully covered in the theoretical sections which follow. For D_1 = 200μ, D_2 = 0.2μ, with 0.320 watts incident upon a 2.54 cm diameter sample, and an absorption coefficient at 4880Å wavelength measured to be $a = 1.75 \times 10^5 cm^{-1}$, the volumetric heat generation rate is $Q_V = 3.062$ watts/cm^3. The experimentally measured increase in temperature from edge to center of the sample is $T(0,0)-T_R = 62°K$. Using the previously measured values $\varepsilon_f = 0.606$ for PbI_2 and $\varepsilon_b = 0.95$ for glass, with $\sigma = 5.67 \times 10^{-12}$ watts $cm^{-2} - °K^{-4}$ and $T_A \simeq 300$ °K, Eq. 2.6.2-6 gives the result $k\beta^2 = 4.764 \times 10^{-2}$ watt - cm^{-3} - $°K^{-1}$, and therefore, $Q_V/k\beta^2 = 64.3$ °K. Eq. 2.6.2-1 then gives $\beta = 3.937\ cm^{-1}$ for the 1.27 cm radius. This value for β is larger than the allowed range of values β may assume, between 0 and

and $1/R = 0.7874\ cm^{-1}$. Consequently, the conductivity for the PbI_2 film, calculated from

$$k_2 = 10^3\ [1.001k - k_1]. \qquad (2.6.2\text{-}8)$$

will not be physically realistic. Because of the large difference between thickness of the film and the substrate, k_2 is calculated by subtracting two large numbers. The potential error in k_2 is large for a small error elsewhere in the above calculations. Therefore, this experimental procedure is recommended only for materials and thicknesses such that $k_1 D_1$ and $k_2 D_2$ are similar in magnitude. Besides the above mentioned sources of error, there also exists the possibility that the calibration of the thermographic display may have been incorrect, giving an incorrect value for the temperature at the center of the sample.

Fortunately, this last source of error can be eliminated by analyzing the shape of the temperature profile, rather than only the peak temperature. The temperature distribution of Eq. 2.6.2-1 may be rewritten in the form:

$$\eta \equiv \frac{T(r,0) - T_R}{T(0,0) - T_R} = \frac{[I_0(\beta R) - I_0(\beta r)]}{[I_0(\beta R) - I_0(0)\ ]} \qquad (2.6.2\text{-}9)$$

where $I_0(0) = 1$ and η is by definition the fractional difference in temperature as given above. The fractional change in $T(r,0)-T_R$ with respect to $T(0,0)-T_R$ can then be used to obtain the parameter β accurately, using a computerized curve fitting procedure. For the present, we determine an approximate value for β by using the radius $r=r_\eta$ at which the temperature decays to a fraction $(0<\eta<1)$ of the peak value. The parameter β must then satisfy

$$\frac{1}{\eta} I_0\ (\beta r_\eta) = 1 + [\frac{1}{\eta} - 1]\ I_0\ (\beta R). \qquad (2.6.2\text{-}10)$$

It is later shown in Figure 2.6-44 that β ranges over values from 0 to $1/R$ Consider specifically the radius for 1/2 of peak temperature, such that $\eta = 0.5$, and

$$2\ I_0\ (\beta r_{1/2}) = 1 + I_0\ (\beta R)\ . \qquad (2.6.2\text{-}11)$$

The curve of Figure 2.6-19 gives $r_{1/2} = 0.55$ cm, with $R = 1.27$ cm. Examination of Eq. 2.6.2-10 reveals that no non-trivial solution exists for β with $r_{1/2}$ this small. In fact, $r_{1/2}$ must be larger than $0.7/R$ if a solution is to be found for β in the allowed range.

The experimentally measured temperature profiles were too sharply peaked and steep along the sides to be described by the present theoretical model for T(r,t). Recall that the heat source is a 4880Å wavelength laser beam which has been focused and is incident upon the sample as a diverging beam of diameter 2.54 cm. This "beam diameter" was established by simply observing the laser beam displayed upon a black card at the position of the sample. Because of the above discrepancy between experiment and theory, the actual intensity profile of the laser beam was measured by scanning a slit-detector combination transversely across the beam. The slit aperture was 3μ wide and 3mm high. The measured beam profile is shown in Figure 2.6-29. It is clear that the half-power diameter of the beam is only about 1.0 cm rather than 2.54 cm, and the intensity is sharply peaked in the center. Our theoretical model assumes a heat source which is uniformly distributed across the sample. Clearly, this was not the case for the experiments. The theory is being revised to allow for a heat source with a Gaussian profile so the thermal properties of the materials can be extracted from these experimental data. This revision is the subject of further continuing studies.

Although the transient data cannot be analyzed by the present theoretical model, the approach to be used is outlined briefly. For the present theoretical model, the temperature $T(0,t) \equiv T_c(t)$ at the center of the sample is given by

$$\frac{T_c(t) - T_R}{T_c(0) - T_R} = \frac{\sum_{m=0}^{\infty} \exp(-\alpha\beta t\,[1+a_m^2/\beta^2R^2]) \left\{J_1(a_m)a_m[1+a_m^2/\beta^2R^2]\right\}^{-1}}{\sum_{n=0}^{\infty} \left\{J_1(a_n)a_n\,[1 + a_n^2/\beta^2R^2]\right\}^{-1}} \qquad (2.6.2\text{-}12)$$

The value of β must first be determined from the steady-state experiments. Then the heat diffusivity α can be found by comparing $T_c(t)-T_R$ with the curve in Figure 2.6-28.

Attempts were made to obain a more uniform beam cross-section using a beam expansion telescope, but losses were excessively high with the 3μ diameter pinhole required to produce a 2.5 cm diameter beam. This problem is not difficult to solve experimentally, and will be given specific attention in future work.

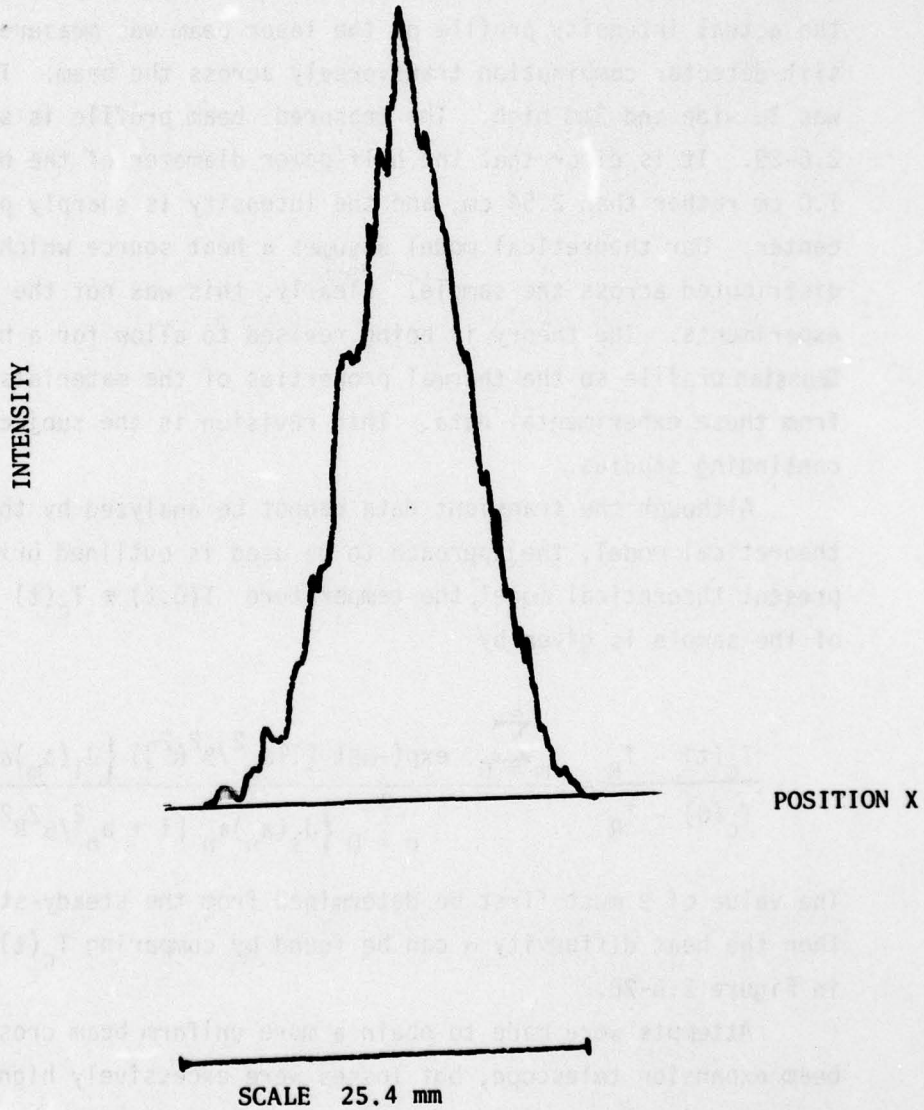

Figure 2,6-29. Intensity profile of laser beam at position of the sample.

2.6.3 Measurements of Thermal Properties of PbI_2 Films On Parylene-N Membranes.

The measurements described in the preceding section were repeated using samples consisting of a 0.2μ thick PbI_2 film on a 0.2μ thick parylene-N membrane. It was necessary to spread the laser beam intensity over the entire aperture of the sample in order to deliver sufficient power without burning a hole through these thin samples. This was accomplished using a single lens with the sample illuminated by the diverging laser beam, as illustrated in Figure 2.6-1. Sufficient incident laser power is required to generate an observable temperature increase at the center of the sample, but without damaging the sample. In practice, this turns out to be just possible to do with present equipment. Because of the small thermal mass of these thin samples, the incident power required to generate a temperature increase well above the infrared detector's noise level is rather close to the damage threshold of the sample. A number of PbI_2 on parylene samples were unavoidably destroyed in initial experiments while determining the optimum input power level. For incident powers of the order of 0.4 watts which did not damage the sample initially, the samples could not withstand thermal cycling. That is, when a sample had been illuminated with 0.4 watts continuously for a period of time, then the laser beam was blocked and the sample allowed to cool, re-introduction of the laser beam caused the sample to immediately rupture. This occurred even though there was no apparent sagging or wrinkling of the sample after the initial exposure. This result is consistent with our previous observations of tearing of parylene films upon thermal cycling up to 100°C in the PbI_2 film deposition chamber.

Experimental results of thermal measurements are reported here for PbI_2 on-parylene sample 809A2K. Because of the uncertainty of the precise damage threshold, which varied a small amount among samples, the laser power was increased in small increments and the steady-state temperature distribution for each laser power level was recorded. The incident power level given with each of the following figures is the power incident upon the parylene substrate, corrected for 92 percent transmission by the NaCl window.

Figure 2.6-30a shows the steady-state temperature distribution with an incident power of 0.166 watts at 4880Å wavelength. Approximately 10 percent of this amount is reflected and 90 percent absorbed by the PbI_2, although this proportion may vary significantly depending upon interference effects in the parylene substrate. For the most sensitive scale, 3°C of ΔT_E per 5 divisions of the line scan mode, the temperature increase at the center of the sample is just evident. Figure 2.6-30b shows the same conditions but with the laser heat source removed. The noise level of the detector and amplifier seriously limits quantitative data at this "safe" laser power level. Signal processing with a boxcar integrator is expected to give considerable improvement in these steady-state measurements. However, that method would not be useful for the transient measurements which follow. For the present, the laser power is increased in small increments to determine how much the temperature profile measurement can be improved before the sample is damaged.

Figure 2.6-31 shows the steady-state temperature distribution with 0.230 watts incident, and Figures 2.6-32 and 2.6-33 with 0.285 watts incident. The only difference between the latter two figures is a change in the vertical sensitivity scale. Figure 2.6-34 shows the temperature profile with the laser heat source blocked, for the sake of comparison. Recall that the calibration curve for PbI_2 in Figure 2.6-18 gives an actual temperature difference ΔT of 16.6°C per vertical division (cm of CRT display). The value of peak temperature T_c at the center of each line scan is indicated in each figure. Some freedom of interpretation must be admitted for peak temperature values because of the noise level. The disagreement between values of T_c = 73°C and T_c = 63°C obtained from scales 3 and 5 in Figures 2.6-32 and 33 is attributable to the noise level. Future experiments for steady-state measurements will use signal averaging techniques to yield more precise data.

The incident laser power was increased to 0.370 watts, yielding the temperature distribution of Figure 2.6-35 with a peak temperature of 81°C. This temperature profile was judged to be sufficient for quantitative analysis, and transient measurements were to be attempted with this incident power level. The incident power was below the 0.4 watt level at which most of the previously tested samples had been destroyed. However,

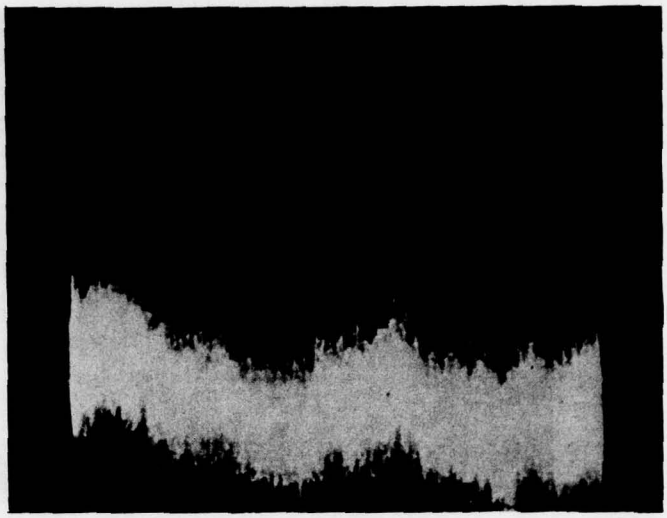

Figure 2.6-30a. Steady-state temperature distribution T(r) for PbI_2 on parylene sample No. 809A2K, with 4880 Å laser power of 166 mW incident upon the sample. Vertical sensitivity is 3 °C of ΔT_E per 5 divisions.

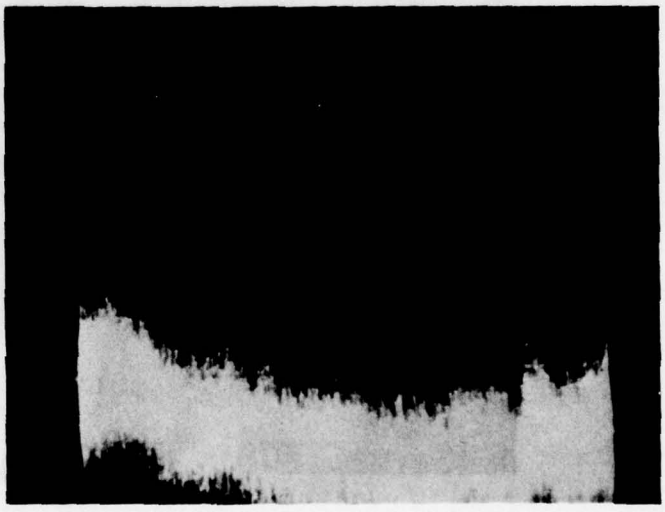

Figure 2,6-30b. Similar to previous figure but with laser heat source removed, showing ambient temperature and noise with room-temperature sample. Vertical sensitivity is 3 °C of ΔT_E per 5 divisions.

Figure 2.6-31. Steady-state temperature distribution T(r) for PbI_2 on parylene sample No. 809A2K with 230 mW of 4880 Å wavelength radiation incident upon the sample. Vertical sensitivity is 3 °C of ΔT_E per 5 divisions.

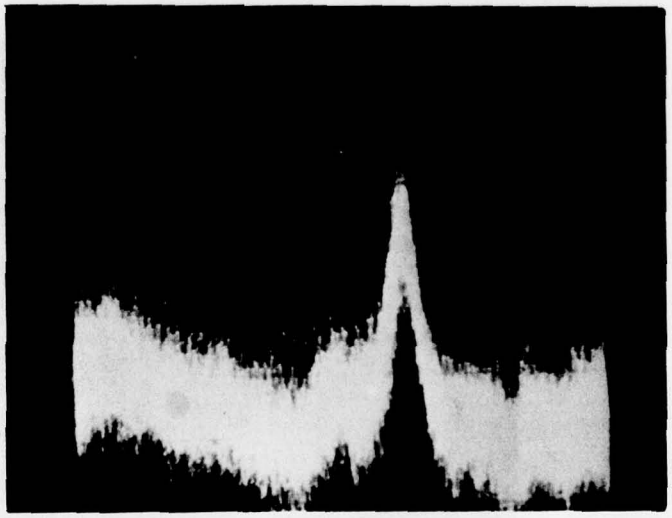

$\Delta T = 48°C$

$T_c = 73°C$

Figure 2.6-32. Steady-state temperature distribution T(r) for PbI_2 on parylene sample No. 809A2K with 285 mW of 4880 Å wavelength radiation incident upon the sample. Vertical sensitivity is 3 °C of ΔT_E per 5 divisions.

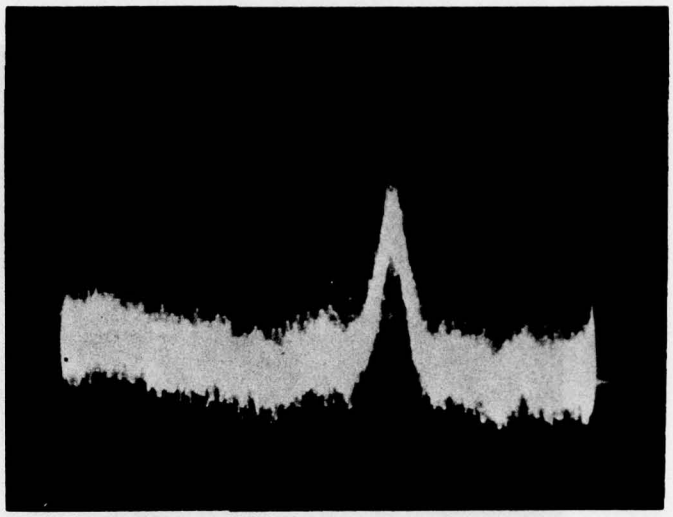

$\Delta T = 38°C$

$T_c = 63°C$

Figure 2.6-33. Steady-state temperature distribution T(r) for PbI_2 on parylene sample No. 809A2K with 285 mW of 4880 Å wavelength radiation incident upon the sample. Vertical sensitivity is 5 °C of ΔT_E per 5 divisions.

Figure 2.6-34. Similar to previous figure, but with laser beam blocked and sample at 25 °C. Vertical sensitivity is 5 °C of ΔT_E per 5 divisions.

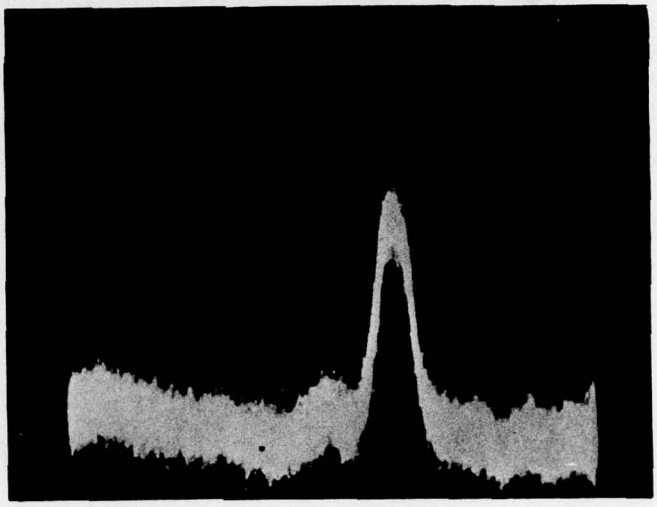

$\Delta T = 56°C$

$T_c = 81°C$

Figure 2.6-35. Steady-state temperature distribution T(r) for PbI_2 on parylene sample No. 809A2K, with 370 mW of 4880 Å wavelength laser radiation incident upon the sample. Vertical sensitivity is 5 °C of ΔT_E per 5 divisions.

when the laser beam was blocked then introduced again, a hole about 0.25 inches in diameter appeared suddenly in the center of the sample, as shown in Figure 2.6-36. It is interesting to note that this result is consistent with the rupture of samples which were thermally cycled up to 100°C in the PbI_2 deposition chamber. The temperature 81°C at which this thermal-cycling-related rupture occurred is also consistent with the "peculiar" transmission characteristics of uncoated parylene sample K at 75°K in Figure 2.5-13.

This was the last of the PbI_2 on parylene samples, the others having been similarly ruptured in measurements of this type. Therefore, this sample was used in this condition to perform transient measurements of the temperature distribution T(r,t) and obtain the heat diffusivity of the PbI_2 film. A taut area about 0.5 inches wide to the left of the rupture in Figure 2.6-36 was used for these measurements. This procedure is justified in spite of the irregular thermal boundary conditions for the torn sample, because the transfer of heat from the sample is nearly entirely radiative during the period after the removal of the laser beam. In section 2.6.4 it is shown that the time required for conduction of heat to the edges of such a thin sample is about 10 seconds, whereas the radiative time constant is typically less than one millisecond. Therefore, we assume the irregularity produced by the tear does not seriously alter the transient temperature decay rate upon removal of the heat source. Further, this was the only sample remaining with which to test the measurement technique.

An incident laser power of 0.370 watts was used in the following measurements, without further apparent damage to the sample. The experiment had to be modified because of the relatively fast thermal decay time for the thin sample, which was of the order of only a few milliseconds. The horizontal-sweep ramp voltage and intensity were taken from output terminals on the control and display unit of the thermographic system and displayed on an oscilloscope, using single-sweep and storage capabilities. The sweep time of the oscilloscope was adjusted so that several consecutive line scans of the thermal image appeared in a single oscilloscope trace. The oscilloscope trace stored on the CRT display was then photographed.

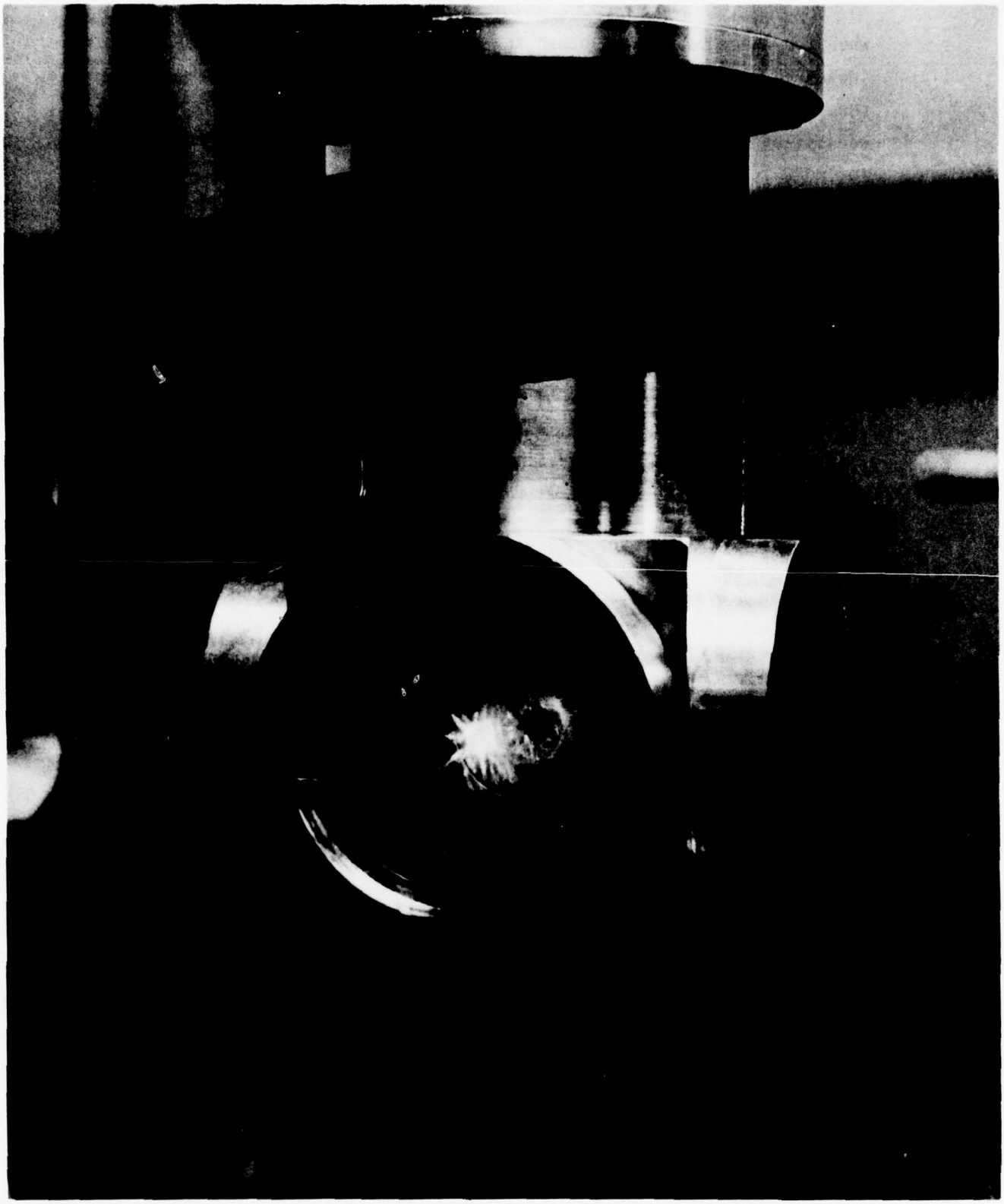

Figure 2.6-36. PbI_2 on parylene sample No. 809A2K inside dewar, showing hole in center of sample caused by repeated temperature cycling with 370 mW of 4880 Å wavelength laser radiation.

The laser beam is shuttered using an electromechanical shutter. The closing of the shutter is synchronized with the oscilloscope trigger, and a single sweep displays a number of consecutive temperature scans on the storage screen of the CRT. Figure 2.6-37 shows three such temperature scans during the first 500 microseconds after shuttering the laser beam off. The decrease in peak temperature is barely discernable during this interval. Figure 2.6-38 shows 60 consecutive thermal scans after shuttering off the laser beam. There is a 3 KHz modulation which must be subtracted from the data. However, the temporal decay of the envelope of peak temperatures is obvious in this figure.

Upon increasing the oscilloscope sweep time to 2 ms per division, the transient decay of the peak temperature is fully displayed in Figure 2.6-39. Each "spike" represents a single line scan of the thermal image. Similarly, Figure 2.6-40 shows the decay envelope for an oscilloscope sweep time of 5 ms per division. From these data, the peak temperature decays to 0.5 times its initial value in about 16 milliseconds, and to the ambient level of 25°C in 25 to 30 ms.

Consider the steady-state temperature distribution shown in Figure 2.6-35. For 0.370 watts incident upon the 2.54 cm diameter sample, with $D_1 = D_2 = 0.2\mu$ and an absorption coefficient $a = 1.75 \times 10^5 cm^{-1}$ at 4880Å, the volumetric heat generation rate is $Q_V = 1770$ watts/cm^3. Using $\varepsilon_f = 0.606$ for PbI_2 and $\varepsilon_b \simeq 0.9$ for parylene-N (value for ε_b is assumed for parylene-N in absence of data), we obtain $k\beta^2 = 23.055$ watt - cm^{-3} - $°K^{-1}$ and $Q_V/k\beta^2 = 73.8°K$. The peak temperature difference $T_C - T_R = 56°K$ experimentally, so that Eq. 2.6.2-1 gives a value for β of $\beta = 2.205\ cm^{-1}$. Just as for the PbI_2 on glass sample previously, β is larger than 1/R and therefore cannot yield a physically correct value for k_2. The radius $r_{1/2}$ at which the temperature decays to about one-half the peak value is $r_{1/2} \simeq 0.5R$ in Figure 2.6-35. Again, the temperature distribution decays too steeply to be described by the present theory. Future analysis will take into account the actual spatial distribution of energy in the defocused laser beam which supplies heat to the film.

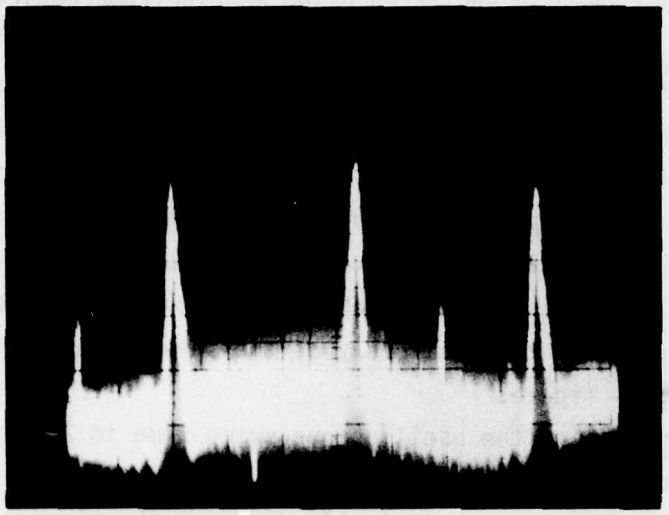

Figure 2.6-37. Three consecutive traces of the temperature distribution T(r,t) across PbI_2 on parylene sample No. 809A2K after removal of 4880 Å wavelength laser beam. Horizontal time scale is 50 μs per division.

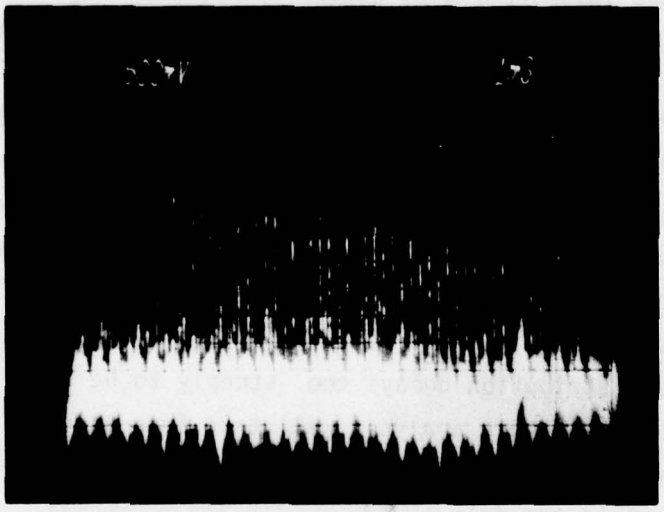

Figure 2.6-38. Temporal decay of the temperature distribution T(r,t) for successive line scans (each spike represents one line scan) across damaged PbI_2 on parylene sample 809A2K upon removal of 4880 Å wavelength laser beam. Time scale is 1 ms per division.

Figure 2.6-39. Similar to the previous figure, with horizontal time scale of 2 ms per division.

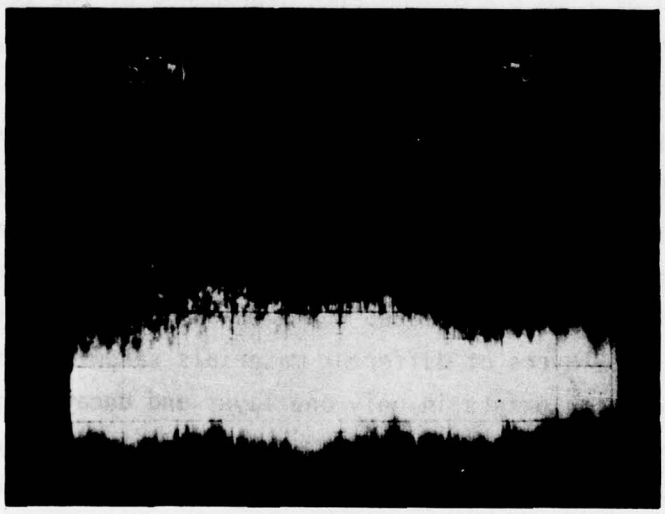

Figure 2.6-40. Similar to previous figure, with horizontal time scale of 5 ms per division.

2.6.4 One-Dimensional Heat Conduction in a Thin Plate With a Uniform Volumetric Heat Source, Radiative Surface Cooling, and Constant Temperature At The Edges

In this section the temperature distribution within a thin plate is derived for conditions which approximate those used in our thermal imaging experiments. The purpose of this analysis is to obtain analytic expressions which can be used to extract physical parameters such as thermal conductivity, heat diffusivity, and heat capacity of the metal halide films used in these experiments. The simplest theoretical model, albeit an imprecise model for our experiments, is one for which one-dimensional heat conduction occurs in a thin plate, as illustrated in Figure 2.6-41.[2] The model may be later generalized to radial heat conduction in a thin circular plate. The advantage of the present one-dimensional model is the analytic simplicity of the temperature distribution and its spatial Fourier transform, which is closely related to the modulation transfer function (MTF) of the infrared-to-visible transducer

As a first step, we derive the partial differential equation which describes temporal evolution of the temperature distribution $T(x,t)$ in the sample. Solutions are then found for the steady-state case which exists for times $t < 0$. During this period a constant heat source is uniformly distributed throughout the volume of the plate. Upon removal of the volumetric heat source at time $t = 0$, the time dependence of the temperature distribution is obtained as it decays from $T(x,0)$ to a constant value, determined by the fixed temperature at the ends of the plate and the temperature of the surrounding medium.

Certain simplifying assumptions are made in this "first-cut analysis", so that the sample shown in Figure 2.6-41 differs somewhat from those used in the experiments. First, it is assumed that the material bounded by the planes $z = +D/2$ and $z = -D/2$ is homogeneous and that the heat source is distributed uniformly throughout the plate. Samples actually used in the experiments consist of two layers of different materials sandwiched together, with a heat source which exists in only one layer and decays exponentially to zero within a few hundred angstroms from the material interface. Secondly, it is assumed that the temperature inside the plate is a function of only one coordinate and that heat conduction occurs in the $+\hat{x}$ and $-\hat{x}$ directions parallel to the surfaces. This assumption is reasonable for a sufficiently thin plate with radiative cooling at the surfaces, such as our PbI_2-on-parylene

samples. However, this assumption may not be valid for our PbI_2 and HgI_2 films on 200 μ thick glass substrates. Temperature variations along the $\hat{z}$ direction may be significant in the thicker glass substrates.

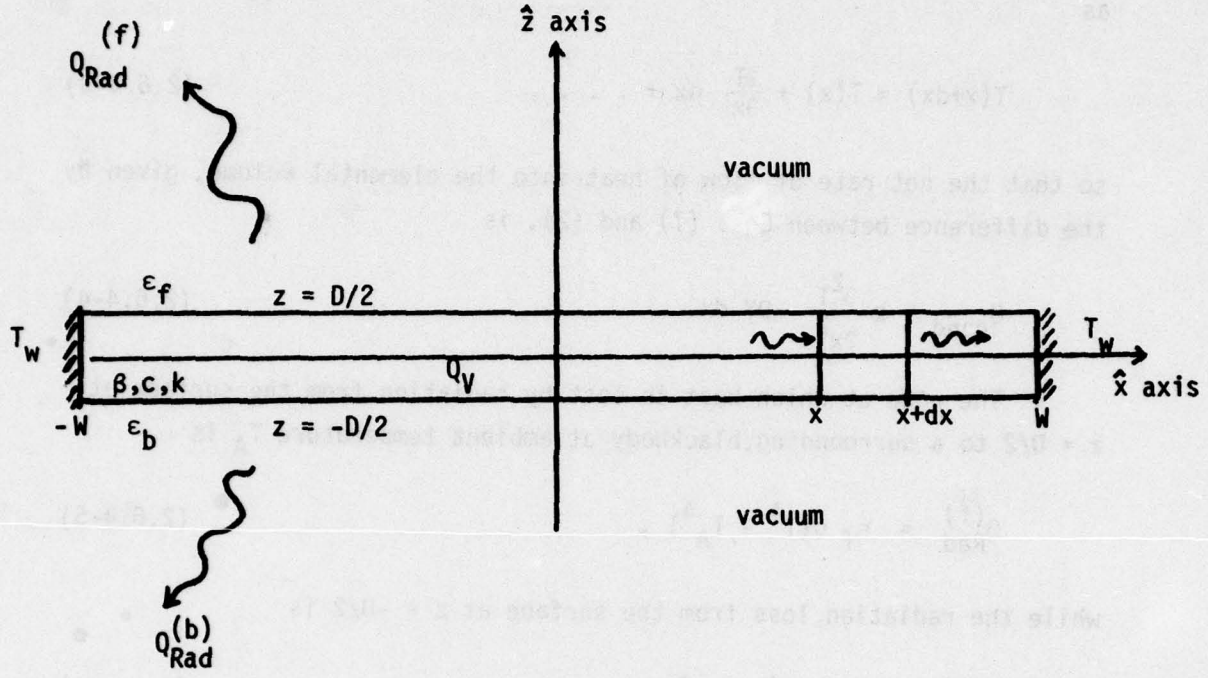

Figure 2.6-41. Cross section of thin plate in the y=0 plane, with ends fixed at constant temperature T_w and radiative heat transfer from the surface to a surrounding blackbody at temperature T_A

Consider the element of volume of height D along the $\hat{z}$ axis, width Y along the $\hat{y}$ axis, and located between the planes x and x+dx in Figure 2.6-41. The rate at which heat flows into this region across the plane at x is

$$-k \frac{\partial T(x)}{\partial x} \quad DY \quad , \qquad (2.6.4\text{-}1)$$

while the rate at which heat flows out of this volume by conduction across the boundary at x+dx is

$$-k \frac{\partial}{\partial x} T(x+dx)\ DY\ . \qquad (2.6.4\text{-}2)$$

The temperature at the exit face x+dx is given by a Taylor series expansion as

$$T(x+dx) \simeq T(x) + \frac{\partial T}{\partial x}\ dx + \ldots , \qquad (2.6.4\text{-}3)$$

so that the net rate of flow of heat into the elemental volume, given by the difference between Eqs. (1) and (2), is

$$Q_{cond} = k \frac{\partial^2 T}{\partial x^2}\ DY\ dx. \qquad (2.6.4\text{-}4)$$

The rate at which heat is lost by radiation from the surface at $z = D/2$ to a surrounding blackbody at ambient temperature T_A is

$$Q_{Rad}^{(f)} = \varepsilon_f \sigma(T^4 - T_A^4) , \qquad (2.6.4\text{-}5)$$

while the radiation loss from the surface at $z = -D/2$ is

$$Q_{Rad}^{(b)} = \varepsilon_b \sigma(T^4 - T_A^4) . \qquad (2.6.4\text{-}6)$$

The emissivities are ε_f and ε_b for front and back surfaces, respectively, and $\sigma = 5.67 \times 10^{-12}$ W-cm^{-2}(°K)$^{-4}$ is the Stefan-Boltzman constant.

A uniformly distributed source is assumed to generate heat within the plate at a constant rate Q_V. The contribution of this source to the rate of change of heat contained within the elemental volume is

$$Q_{source} = Q_V\ DY\ dx\ \theta(-t) , \qquad (2.6.4\text{-}7)$$

where $\theta(t)$ is the Heaviside unit step function.

$$\theta(-t) = \begin{cases} 1, & \text{for } t < 0 \\ 0, & \text{for } t \geq 0 \end{cases} . \qquad (2.6.4\text{-}8)$$

The net rate of change of internal energy for the element of volume is

$$Q_{net} = \frac{\partial}{\partial t} (\rho c T)\, DY\, dx \ , \qquad (2.6.4\text{-}9)$$

where ρ is the mass density and c is the specific heat of the material.

Upon writing the complete heat balance equation for the net rate of heat generation in the element of volume, we obtain after factorization of common parameters

$$\rho c \frac{\partial T}{\partial t} = k \frac{\partial^2 T}{\partial x^2} - (\varepsilon_f + \varepsilon_b) \frac{\sigma}{D} (T^4 - T_A{}^4) + Q_V \ . \qquad (2.6.4\text{-}10)$$

The nonlinear term proportional to $(T^4 - T_A{}^4)$ may be expanded in the following form:

$$T^4 - T_A{}^4 = 4T_A{}^3(T-T_A) + 6T_A{}^2(T-T_A)^2 + 4T_A(T-T_A)^3 + (T-T_A)^4 . \qquad (2.6.4\text{-}11)$$

If the temperature difference $T-T_A$ between the plate surface and the surrounding blackbody is sufficiently small, only the first term on the right side of Eq. (10) is of significant magnitude. With this simplification, the differential equation for temperature is linearized to the form:

$$\frac{1}{\alpha} \frac{\partial T}{\partial t} = \frac{\partial^2 T}{\partial x^2} - \beta^2 (T-T_A) + \frac{Q_V}{k} \ , \qquad (2.6.4\text{-}12)$$

where α is the heat diffusivity defined by

$$\alpha \equiv \frac{k}{\rho c} \ , \qquad (2.6.4\text{-}13)$$

and β is defined as the positive square root of

$$\beta^2 \equiv (\varepsilon_f + \varepsilon_b) \frac{\sigma}{kD} 4T_A^3 \ . \qquad (2.6.4\text{-}14)$$

The boundary conditions are that the edges of the plate at x = W and x = -W be maintained at a constant temperature T_W at all times, or

$$T(W,t) = T(-W,t) \equiv T_W . \qquad (2.6.4\text{-}15)$$

The initial temperature distribution $T(x,0)$ is given by the solution to the steady-state problem for which $\partial T/\partial t = 0$, assuming that the source was applied at time $t = -\infty$.

$$\frac{\partial^2}{\partial x^2} T(x,0) - \beta^2[T(x,0) - T_A] + \frac{Q_V}{k} = 0 \qquad (2.6.4\text{-}16)$$

The steady-state temperature distribution which simultaneously satisfies Eqs. (16) and (15) is

$$T(x,0) - T_A = \left(T_W - T_A - \frac{Q_V}{k\beta^2}\right)\frac{\cosh(\beta x)}{\cosh(\beta W)} + \frac{Q_V}{k\beta^2} \; . \qquad (2.6.4\text{-}17)$$

If $T_A = T_W$, as was the case for our experiments, the steady-state temperature distribution becomes

$$\lim_{T_A=T_W} T(x,0) = T_W + \frac{Q_V}{k\beta^2}\left[1 - \frac{\cosh(\beta x)}{\cosh(\beta W)}\right] \; . \qquad (2.6.4\text{-}18)$$

The peak temperature T_c at the center of the sample is then given by

$$\lim_{T_A=T_W} T_c = T_W + \frac{Q_V}{k\beta^2}\left[1 - \frac{1}{\cosh(\beta W)}\right] \; . \qquad (2.6.4\text{-}19)$$

T_c is now expressed in terms of T_W, the rate of heat generation Q_V, the material properties k, ε_f and ε_b contained within β, and the physical dimensionsD and W of the plate. The center temperature T_c given by Eq. (19) is always greater than the edge temperature T_W by an amount proportional to Q_V, as expected. Upon rewriting Eq. (17) in the form

$$T(x,0) = T_A + \frac{Q_V}{k\beta^2}\left[1 - \frac{\cosh(\beta x)}{\cosh(\beta W)}\right] + (T_W - T_A)\frac{\cosh(\beta x)}{\cosh(\beta W)} \; , \qquad (2.6.4\text{-}20)$$

it is apparent that the plate temperature $T(x,0)$ is always greater than T_A if $T_W > T_A$. If, however, T_W is maintained sufficiently far below T_A, then $T(x,0)$ may actually be smaller than T_A and the plate "receives" radiated heat from the surrounding blackbody rather than vice versa.

At this point, we may make an order-of-magnitude estimate of the temperature increase in our experiments. The heat source is typically 0.025 watts of continuous output from an argon laser at a wavelength of 4880Å, well above the absorption edge of PbI_2 and HgI_2. Allowing for a reflectivity of 4 percent at the glass substrate-to-vacuum interface, 4 percent reflectivity at each face of the input NaCl window of the vacuum dewar, and 11 percent reflectivity at the PbI_2-glass interface, approximately 78 percent of the incident power, or 0.0195 watts may be absorbed within the PbI_2 or HgI_2 film. Of course, it is assumed here that the glass substrate is sufficiently thick that interference effects do not significantly change the amount of power transmitted into the absorbing film.

Both the heat sink at the edges of the sample and the surrounding environment are at room temperature, so that $T_A=T_W=25°C$. Eq. (18) predicts a temperature rise at the center of the sample of

$$T_c - T_W = \frac{Q_V}{k\beta^2}\left[1 - \frac{1}{\cosh(\beta W)}\right] \quad . \qquad (2.6.4\text{-}21)$$

Since the incident power is assumed in this model to be uniformly distributed throughout the(2.5cm diameter by 0.2 micron thick)metal-halide film, the rate of heat generation Q_V is 198 watts-cm^{-3}. If we assume emissivities of $\varepsilon_f \simeq 0.2$ for the metal-halide surface and $\varepsilon_b \simeq .05$for the highly reflective glass substrate surface then $k\beta^2 \simeq 7.5$ W-cm^{-3}-$°K^{-1}$. Also, assuming for the present that the heat conductivity is $k = 10^{-4}$ W-cm^{-1}-$°K^{-1}$ we obtain $\beta W = 342$. The temperature increase predicted at the center of the sample is then about 26°C for the steady-state experiment.

Transient Temperature Distribution:

The initial temperature distribution across the plate is the steady-state distribution given by Eq. (17). Assume that at time t=0 the heat source is suddenly removed so that $Q_V=0$. The time-dependent temperature distribution then must satisfy

$$\frac{1}{\alpha}\frac{\partial}{\partial t}T(x,t) = \frac{\partial^2}{\partial x^2}T(x,t) - \beta^2\left[T(x,t) - T_A\right] \quad , \qquad (2.6.4\text{-}22)$$

along with the initial distribution $T(x,0)$ and the boundary conditions $T(W,t) = T(-W,t) = T_W$, constant for all time. Upon defining

$$w(x,t) \equiv [T(x,t) - T_A] \exp(\alpha\beta^2 t) \quad , \tag{2.6.4-23}$$

the differential equation simplifies to the form

$$\frac{\partial}{\partial t} w(x,t) = \alpha \frac{\partial^2}{\partial x^2} w(x,t) \quad , \tag{2.6.4-24}$$

subject to the initial condition

$$w(x,0) = T(x,0) - T_A \tag{2.6.4-25}$$

and the boundary conditions

$$w(W,t) = w(-W,t) \equiv (T_W - T_A) \exp(\alpha\beta^2 t) \quad . \tag{2.6.4-26}$$

The heat diffusion equation (23) is readily solved by first taking the Laplace transform of the time variable to obtain

$$\frac{\partial^2}{\partial x^2} \tilde{w}(x,s) - \frac{s}{\alpha} \tilde{w}(x,s) = -\frac{1}{\alpha} w(x,0) \quad , \tag{2.6.4-27}$$

subject to the two boundary conditions

$$\tilde{w}(W,s) = \tilde{w}(-W,s) = \frac{(T_W - T_A)}{(s - \alpha\beta^2)} \quad . \tag{2.6.4-28}$$

The solution for the Laplace transform is

$$\tilde{w}(x,s) = \frac{Q_V}{k\beta^2} \left[\frac{1}{(s-\alpha\beta^2)} - \frac{1}{s}\right] \frac{\cosh\left(x\sqrt{\frac{s}{\alpha}}\right)}{\cosh\left(W\sqrt{\frac{s}{\alpha}}\right)} +$$

$$\left[T_W - T_A - \frac{Q_V}{k\beta^2}\right] \frac{\cosh(\beta x)}{\cosh(\beta W)} \frac{1}{(s-\alpha\beta^2)} + \frac{Q_V}{k\beta^2} \frac{1}{s} \tag{2.6.4-29}$$

Upon performing the inverse Laplace transformation, then multiplying through by $\exp(-\alpha\beta^2 t)$, we obtain

$$T(x,t) - T_A = \frac{Q_V}{k\beta^2} e^{-\alpha\beta^2 t} \mathcal{L}^{-1}\left\{\left[\frac{1}{(s-\alpha\beta^2)} - \frac{1}{s}\right] \frac{\cosh\left(x\sqrt{\frac{s}{\alpha}}\right)}{\cosh\left(W\sqrt{\frac{s}{\alpha}}\right)}\right\}$$

$$+ \left[T_W - T_A - \frac{Q_V}{k\beta^2}\right] \frac{\cosh(\beta x)}{\cosh(\beta W)} + \frac{Q_V}{k\beta^2}\, \theta(t)\, \exp(-\alpha\beta^2 t)\,. \qquad (2.6.4\text{-}30)$$

In order to evaluate the inverse Laplace transformation of the first term, Heaviside's method of partial fractions is employed to make the expansions

$$\frac{1}{s} \frac{\cosh\left(x\sqrt{\frac{s}{\alpha}}\right)}{\cosh\left(W\sqrt{\frac{s}{\alpha}}\right)} = \frac{1}{s} - \frac{2}{\pi} \sum_{m=0}^{\infty} \frac{(-1)^m}{(m+\frac{1}{2})} \frac{\cos[\pi(m+1/2)x/W]}{\left[s+\alpha\pi^2(m+\frac{1}{2})^2/W^2\right]} \qquad (2.6.4\text{-}31)$$

$$\frac{1}{\left(s-\alpha\beta^2\right)} \frac{\cosh\left(x\sqrt{\frac{s}{\alpha}}\right)}{\cosh\left(W\sqrt{\frac{s}{\alpha}}\right)} = \frac{\cosh(\beta x)}{\cosh(\beta W)} \frac{1}{\left(s-\alpha\beta^2\right)} - 2\pi \sum_{m=0}^{\infty} \frac{(-1)^m (m+\frac{1}{2}) \cos[\pi(m+\frac{1}{2})x/W]}{\left[\beta^2 W^2 + \pi^2 (m+\frac{1}{2})^2\right]\left[s+\alpha\pi^2(m+\frac{1}{2})^2/W^2\right]}$$

(2.6.4-32)

with simple poles at $s = 0$ and $s_m = -\alpha\pi^2(m+\frac{1}{2})^2/W^2$ $(m = 0, 1, 2, 3, \ldots)$.

The inverse Laplace transform may now be performed for each term in Eqs (31) and (32). The method is illustrated in some detail for Eq. (32) only. The contour of integration in the complex s plane, shown in Figure 2.6-42, is closed by the line $s = a + i\,\mathrm{Im}(s)$ where $a > \alpha\beta^2$ and by the semicircle of infinite radius centered at $s = a + i0$. Integrating along each path, we obtain

$$\int_{a-i\infty}^{a+i\infty} ds\, e^{st}\, \tilde{f}(s) + \int_{\mathscr{C}_\infty} ds\, e^{st}\, \tilde{f}(s) = i2\pi \frac{\cosh(\beta x)}{\cosh(\beta W)} e^{\alpha\beta^2 t} + i2\pi \sum_{m=0}^{\infty} C_m e^{s_m t} \qquad (2.6.4\text{-}33)$$

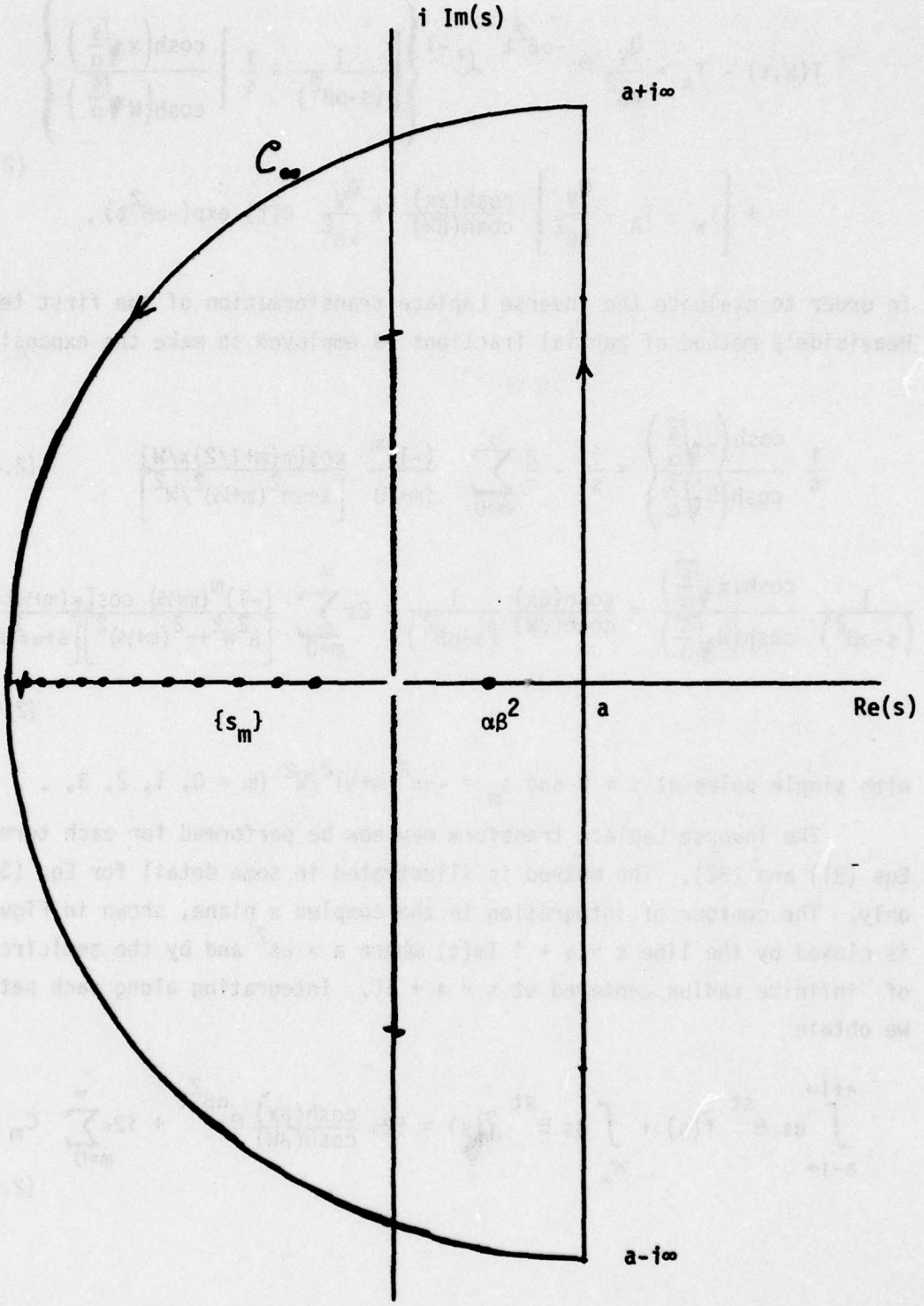

Figure 2.6-42. Contour of integration to evaluate inverse Laplace transform of $\tilde{w}(x,s)$ term containing Eq. (2.6.4-32).

where $\tilde{f}(s)$ is the expression on the left side of Eq. (32) and c_m and s_m are the summation coefficients and simple poles in the series on the right side of Eq. (32). The terms on the right above are residues of the simple poles inside the contour. The integral over the contour at infinity vanishes with the magnitude of $\tilde{f}(s)$. We then have

$$\frac{1}{2\pi i}\int_{a-i\infty}^{a+i\infty} ds\, e^{st}\,\tilde{f}(s) \equiv \mathcal{L}^{-L}[\tilde{f}(s)] = \frac{\cosh(\beta x)}{\cosh(\beta W)}\, e^{\alpha\beta^2 t} + \sum_{m=0}^{\infty} c_m e^{s_m t} . \qquad (2.6.4\text{-}34)$$

The inverse Laplace transform of Eq. (31) is evaluated similarly, with the contour closed to the right of the simple pole at s = 0. Upon combining these results, the temperature distribution is given by

$$T(x,t) - T_A = \frac{Q_V 2}{k\beta^2} \sum_{m=0}^{\infty} \frac{(-1)^m \cos[\pi(m+\tfrac{1}{2})x/W]}{\pi(m+\tfrac{1}{2})\left[1+\frac{\pi^2(m+\tfrac{1}{2})^2}{\beta^2 W^2}\right]} \exp\left(-\alpha\beta^2 t\left[1+\frac{\pi^2(m+\tfrac{1}{2})^2}{\beta^2 W^2}\right]\right)$$

$$+ (T_W - T_A)\frac{\cosh(\beta x)}{\cosh(\beta W)} \quad . \qquad (2.6.4\text{-}35)$$

Close inspection reveals that T(x,t) does reduce to the appropriate forms in the limits that t approaches zero and infinity.

The functional form of T(x,t) above suggests two characteristic time constants for the decay of the temperature profile in the thin plate. One of these time constants, defined as

$$\tau_{Rad} \equiv \frac{1}{\alpha\beta^2} = \frac{\rho c D}{(\epsilon_f+\epsilon_b)\sigma 4 T_A^3} \qquad (2.6.4\text{-}36)$$

is associated with heat loss by radiation from the surfaces. The other characteristic decay time $\tau^{(m)}$ for the m'th order contribution in the series is defined as

$$\tau_{Cond}^{(m)} \equiv \frac{W^2}{\alpha\pi^2(m+\tfrac{1}{2})^2} \quad (m = 0, 1, 2 \ldots) \quad . \qquad (2.6.4\text{-}37)$$

This decay time is associated exclusively with heat conduction to the walls at x = W and -W. For the example considered earlier, with $k\beta^2$=7.5 W-cm^{-3}-°K^{-1}, k=10^{-4}W-cm^{-1}-°K^{-1}, W=1.25 cm, and assuming a density ρ=2.5 gm-cm^{-3} and a specific heat c=2x10^{-4} Joules-gm^{-1}-°K^{-1}, then α=0.2cm^2/sec and the characteristic decay times are τ_{Rad}=0.07 msec and $\tau^{(0)}_{Cond}$=3.17 sec. It is obvious that radiative heat transfer will dominate the transient decay of the temperature profile because of the large surface area and thinness of the sample.

2.6.5 Two-dimensional, radial heat conduction in a thin, circular plate with a uniform volumetric heat source, radiative surface cooling, and constant temperature around the circumference.

The thin samples used in our thermal imaging experiments are circular films with a heat sink maintained at constant temperature T_R around the circumference of the sample. The one-dimensional heat conduction problem of the previous section provided physical insight to the heat transfer processes involved in the evolution of the temperature distribution. However, important quantitative differences are expected for the circular samples, so that, in this section, we analyze this more complicated problem. The basic difference arises from the fact that as heat is conducted radially outward from the center of the circular sample the thermal resistance decreases by an amount proportional to the radial distance from the center. This occurs because of the increase in cross-sectional area subtended by a constant angle as the radial distance from the center becomes larger. Because of this geometric influence, the steady-state temperature distribution is expected to exhibit a lower peak temperature and be more sharply peaked at the center of the sample. Upon removal of the heat source, the combined influences of the larger temperature gradient and the radially increasing heat conductance should cause the temperature distribution to decay more rapidly than for the one-dimensional case.

Consider the sample illustrated in Figure 2.6-43. The rate at which heat is conducted across the surface of the incremental volume at radius r is

$$-k \frac{\partial T}{\partial r} \quad r \, d\phi \, D \quad , \tag{2.6.5.1}$$

while the rate at which heat flows outward through the curved surface at r+dr is

$$-k \left.\frac{\partial T}{\partial r}\right|_{r+dr} \quad (r+dr) \, d\phi \, D \quad . \tag{2.6.5.2}$$

The temperature of the isothermal surface at r+dr is expressed by the Taylor series expansion

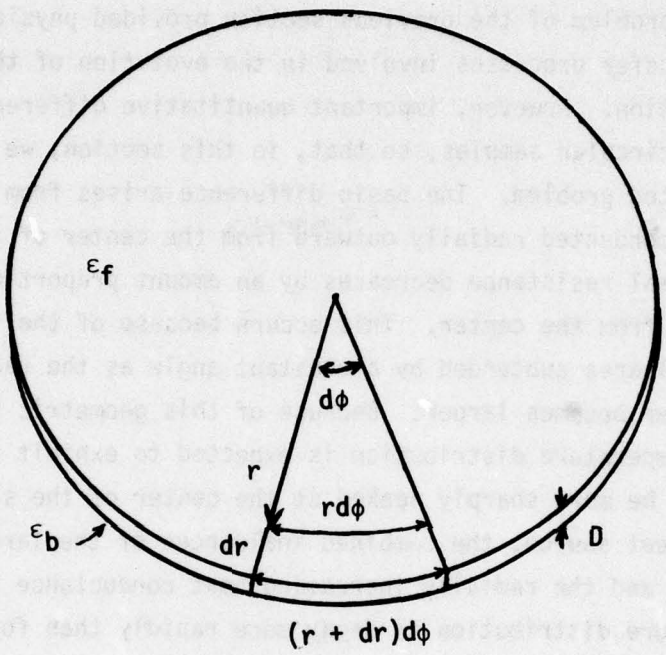

Figure 2.6-43. Radial heat conduction in a thin, circular plate, with radiative cooling from both surfaces and constant temperature T_R maintained around the circumference.

$$T(r+dr) = T(r) + \frac{\partial T}{\partial r}\, dr + \ldots \qquad (2.6.5\text{-}3)$$

The net rate of conduction of heat into the element is then given by Eq. (1) minus Eq. (2), or

$$Q_{Cond} = k\, \frac{\partial^2 T}{\partial r^2}\, r\, dr\, d\phi\, D + k\, \frac{\partial T}{\partial r}\, dr\, d\phi\, D \qquad (2.6.5\text{-}4)$$

since terms proportional to $(dr)^2$ may be neglected. It is assumed that there is no circulatory heat conduction in the $\hat{\phi}$ directions.

Heat is radiated from the front ($z=+D/2$) surface to the surrounding blackbody of temperature T_A at a rate

$$Q^{(f)}_{Rad} = \varepsilon_f\, \sigma \left[T(r)^4 - T_A{}^4\right] r\, d\phi\, dr\ , \qquad (2.6.5\text{-}5)$$

and from the back surface at a rate

$$Q^{(b)}_{Rad} = \varepsilon_b\, \sigma \left[T(r)^4 - T_A{}^4\right] r\, d\phi\, dr\ . \qquad (2.6.5\text{-}6)$$

The rate at which heat is generated by the uniform volumetric source is

$$Q_{Source} = Q_V\, r d\phi\, dr\, D\, \theta(-t). \qquad (2.6.5\text{-}7)$$

The net rate of change of heat within the volume element covered by these combined processes is

$$Q_{net} = \frac{\partial}{\partial t}\, (\rho c T)\, r d\phi\, dr\, D. \qquad (2.6.5\text{-}8)$$

The dynamic heat balance equation for the elemental volume may be written in the following form:

$$\rho c\, \frac{\partial}{\partial t}\, T = \frac{k}{r}\, \frac{\partial}{\partial r} \left(r\, \frac{\partial T}{\partial r}\right) - (\varepsilon_f + \varepsilon_b)\, \frac{\sigma}{D}\, (T^4 - T_A{}^4) + Q_V\, \theta(-t). \qquad (2.6.5\text{-}9)$$

Equation (9) may be linearized using the approximation

$$T^4 - T_A{}^4 \simeq 4 T_A{}^3\, (T - T_A) \qquad (2.6.5\text{-}10)$$

which is valid for small values of $|T-T_A|$. Upon defining the parameter β as the positive square root of

$$\beta^2 = (\varepsilon_f + \varepsilon_b) \frac{\sigma}{kD} 4T_A^3 \qquad (2.6.5\text{-}11)$$

and using the definition of the heat diffusivity α, given by

$$\alpha = k/(\rho c) \qquad (2.6.5\text{-}12)$$

the dynamic heat balance equation becomes

$$\frac{1}{\alpha}\frac{\partial}{\partial t} T = \frac{1}{r}\frac{\partial}{\partial r}\left(r \frac{\partial T}{\partial r}\right) - \beta^2(T - T_A) + \frac{Q_V}{k}\ \theta(-t). \qquad (2.6.5\text{-}13)$$

Solutions to Eq. (13) are required which satisfy the boundary condition

$$T(R,t) = T_R\ , \qquad (2.6.5\text{-}14)$$

where T_R is constant for all time, and the initial distribution $T(r,0)$ at zero time. $T(r,0)$, in turn, is the solution for the steady-state problem with a uniform, constant volumetric heat source Q_V. Assuming this heat source was applied at time $t = -\infty$, the steady-state temperature distribution satisfies

$$\frac{1}{r}\frac{\partial}{\partial r}\left(r \frac{\partial T}{\partial r}\right) - \beta^2\,[T - T_A] + \frac{Q_V}{k} = 0\ , \qquad (2.6.5\text{-}15)$$

with the boundary conditions $T(R)=T_R$ and finite temperature over the entire plate. The steady-state temperature distribution $T(r,0)$ which satisfies Eq. (15) and the boundary conditions is given by

$$T(r,0) - T_A = \left(T_R - T_A - \frac{Q_V}{k\beta^2}\right)\frac{I_o(\beta r)}{I_o(\beta R)} + \frac{Q_V}{k\beta^2}\ , \qquad (2.6.5\text{-}16)$$

where I_o is the modified Bessel function of the first kind of order zero. If $T_R=T_A$ as in our experiments, then $T(r,0)$ may be written in the form

$$\lim_{T_R=T_A} T(r,0) = T_R + \frac{Q_V}{k\beta^2}\left[1 - \frac{I_o(\beta r)}{I_o(\beta R)}\right]\ . \qquad (2.6.5\text{-}17)$$

The peak temperature T_c at the center of the sample, given by

$$\lim_{T_A=T_R} T_c = T_R + \frac{Q_V}{k\beta^2}\left[1 - \frac{1}{I_o(\beta R)}\right] , \qquad (2.6.5\text{-}18)$$

is directly proportional to the rate of heat generation Q_V by the volumetric source.

It is of interest to compare the steady-state temperature distribution $T(r,0)$ for the circular plate with that previously obtained for one-dimensional heat conduction in a thin plate. For large values of βR, the increase in temperature from edge to center is $Q_V/(k\beta^2)$ for both configurations. The significant difference is in the shape of the temperature distribution curve, which is given by $\cosh(\beta x)$ for the one-dimensional problem and $I_o(\beta r)$ for the radial-conduction problem. These two profiles are illustrated in Figure 2.6-44 for the case where $T_W=T_A$ and $T_R=T_A$. For the sake of making quantitative comparison, we have assumed $\beta W=\beta R\approx 1$ in this example. As anticipated, the temperature at the center of the plate is significantly lower for the two-dimensional, radial heat flow problem. However, the two temperature profiles do not vary much in shape. The distance from center to a temperature $T_c/2$ is about $\beta x\approx\beta r = 0.72$ for both cases. Therefore, the temperature does not drop more rapidly toward the edge of the plate as previously anticipated for the radial case, at least not for this choice of β.

At time t=0, the heat source is removed from the sample. The temperature distribution $T(r,t)$ must then obey the equation

$$\frac{1}{\alpha}\frac{\partial}{\partial t}T = \frac{1}{r}\frac{\partial}{\partial r}\left(r\frac{\partial T}{\partial r}\right) - \beta^2(T-T_A) , \qquad (2.6.5\text{-}19)$$

subject to the initial distribution $T(r,0)$ and the boundary condition $T(R,t) = T_R$ for all t. Upon making a substitution of variables

$$u(r,t) \equiv [T(r,t) - T_A]\exp(\alpha\beta^2 t) \qquad (2.6.5\text{-}20)$$

and then taking the Laplace transform of Eq. (19), the dynamic heat balance equation becomes

$$\frac{1}{r}\frac{\partial}{\partial r}\left(r\frac{\partial}{\partial r}\tilde{u}(r,s)\right) - \frac{s}{\alpha}\tilde{u}(r,s) = -\frac{1}{\alpha}u(r,0) , \qquad (2.6.5\text{-}21)$$

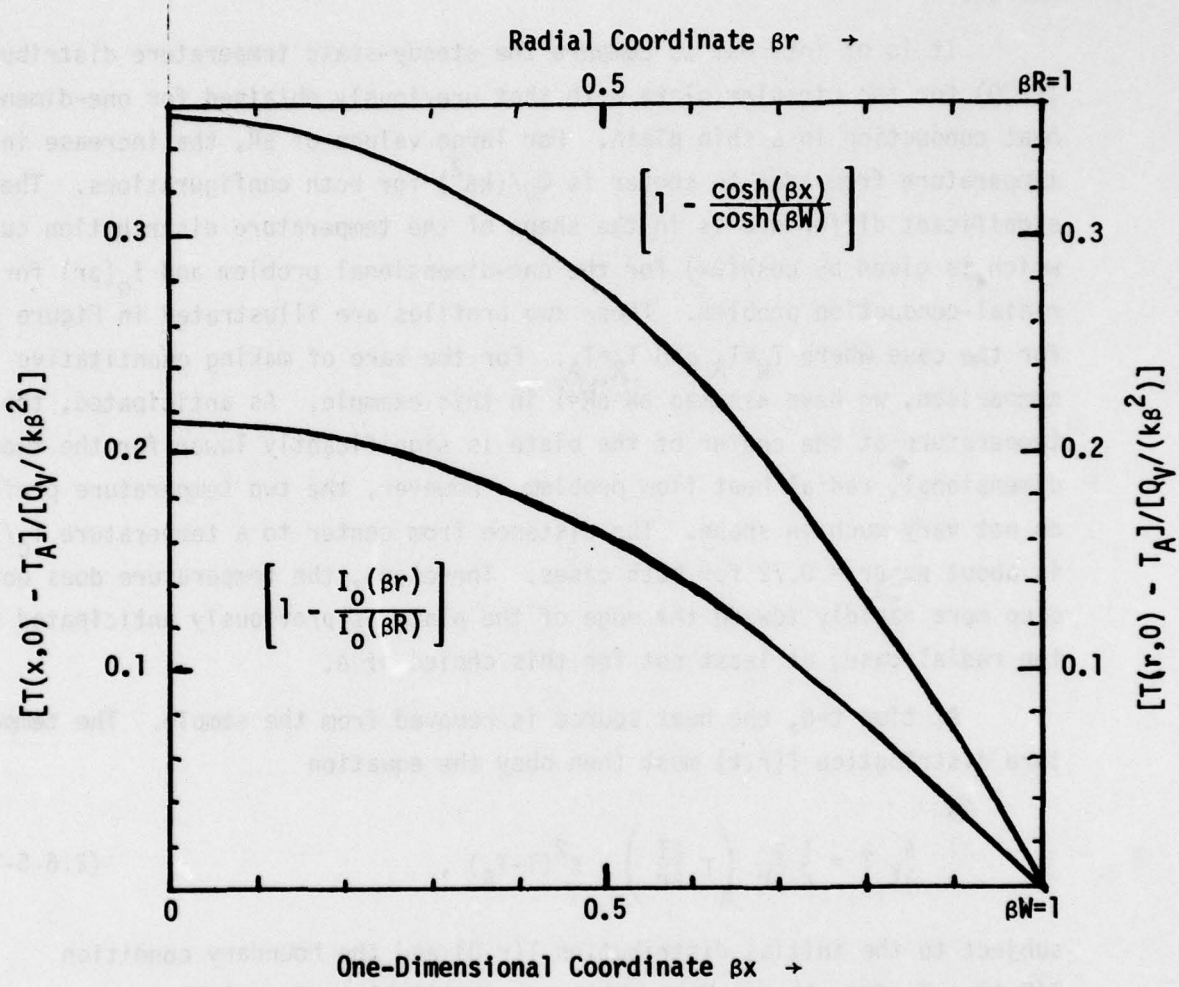

Figure 2.6-44. Temperature distribution in one-dimensional and radial steady-state heat conduction problems, with $T_W=T_R=T_A$ and $\beta W=\beta R=1$.

where $\tilde{u}(r,s) = \mathcal{L}\{u(r,t)\}$ and $u(r,0)$ is the initial distribution $T(r,0)-T_A$ given previously for the steady-state problem. The solution to Eq. (21) which satisfies the boundary condition

$$\tilde{u}(R,s) = (T_R - T_A)/(s - \alpha\beta^2) \tag{2.6.5-22}$$

is given by

$$\tilde{u}(r,s) = \frac{Q_V}{k\beta^2} \frac{I_o\left(r\sqrt{\frac{s}{\alpha}}\right)}{I_o\left(R\sqrt{\frac{s}{\alpha}}\right)}\left[\frac{1}{(s-\alpha\beta^2)} - \frac{1}{s}\right] + \left[T_R - T_A - \frac{Q_V}{k\beta^2}\right]\frac{I_o(\beta r)}{I_o(\beta R)} \frac{1}{(s-\alpha\beta^2)} + \frac{Q_V}{k\beta^2}\frac{1}{s} \quad . \tag{2.6.5-23}$$

It now remains to obtain the inverse Laplace transforms.

The temperature distribution $T(r,t)$ is then given by

$$T(r,t) - T_A = \frac{Q_V}{k\beta^2}\exp(-\alpha\beta^2 t)\,\mathcal{L}^{-1}\left\{\frac{I_o\left(r\sqrt{\frac{s}{\alpha}}\right)}{I_o\left(R\sqrt{\frac{s}{\alpha}}\right)}\left[\frac{1}{(s-\alpha\beta^2)} - \frac{1}{s}\right]\right\} + \left[T_R - T_A - \frac{Q_V}{k\beta^2}\right]\frac{I_o(\beta r)}{I_o(\beta R)} + \frac{Q_V}{k\beta^2}\exp(-\alpha\beta^2 t) \, , \tag{2.6.5-24}$$

where the inverse Laplace transform indicated in the first term is yet to be evaluated. This is accomplished by first expanding the two terms, recognizing the existance of simple poles at $s=\alpha\beta^2$, $s=-\alpha a_m^2/R$, and $s=0$, where a_m is the m'th root of $J_o(a)$ (m=1, 2, 3, 4, ...).

$$\frac{1}{(s-\alpha\beta^2)}\frac{I_o\left(r\sqrt{\frac{s}{\alpha}}\right)}{I_o\left(R\sqrt{\frac{s}{\alpha}}\right)} = \frac{I_o(\beta r)}{I_o(\beta R)}\frac{1}{(s-\alpha\beta^2)} - i2\sum_{m=0}^{\infty}\frac{a_m}{[\beta^2R^2+a_m^2]}\frac{I_o(ia_m r/R)}{I_1(ia_m)}\frac{1}{\left[s+\alpha\frac{a_m^2}{R^2}\right]} \tag{2.6.5-25}$$

$$\frac{1}{s}\frac{I_o\left(r\sqrt{\frac{s}{\alpha}}\right)}{I_o\left(R\sqrt{\frac{s}{\alpha}}\right)} = \frac{1}{s} - i2\sum_{m=0}^{\infty}\frac{1}{a_m}\frac{I_o(ia_m r/R)}{I_1(ia_m)}\frac{1}{[s+\alpha a_m^2/R^2]} \tag{2.6.5-26}$$

The inverse Laplace transformations are now easily evaluated for each term in the series above. With the assistance of the following identities,

$$I_0^{\,1}(\xi) = I_1(\xi), \tag{2.6.5-27a}$$

$$I_1(i\xi) = iJ_1(\xi), \tag{2.6.5-27b}$$

and

$$I_0(i\xi) = J_0(\xi), \tag{2.6.5-27c}$$

the temperature distribution T(r,t) may be written in the form

$$T(r,t) - T_A = \frac{2Q_v}{k\beta^2} \sum_{m=0}^{\infty} \frac{J_0(a_m r/R)\, \exp\left(-\alpha\beta t\left[1 + \frac{a_m^2}{\beta^2 R^2}\right]\right)}{J_1(a_m)\, a_m \left[1 + \frac{a_m^2}{\beta^2 R^2}\right]} + (T_R - T_A)\frac{I_0(\beta r)}{I_0(\beta R)} \,. \tag{2.6.5-28}$$

It is reassuring to note that this result reduces to the correct form in the limits t=0 and t=∞, and, except for the use of cylinder functions, qualitatively agrees with the equivalent result obtained previously for the one-dimensional problem. The characteristic times for decay of the temperature profile are defined as

$$\tau_{Rad} \equiv \frac{1}{\alpha\beta^2} = \frac{\rho c D}{(\varepsilon_f + \varepsilon_b)\sigma 4 T_A^{\,3}} \tag{2.6.5-29}$$

for radiative cooling and

$$\tau_{Cond}^{(m)} = \frac{R^2}{\alpha a_m^{\,2}} \tag{2.6.5-30}$$

for conduction of heat to the boundary at r=R. The geometric contribution due to cylindrical symmetry is apparent as the root a_m of the Bessel function replaces $\pi(m+\frac{1}{2})$ in the one-dimensional problem. The conduction time constant $\tau_{Cond}^{(1)}$ for the cylindrical case is smaller than $\tau_{Cond}^{(0)}$ for the one-dimensional problem by a factor of $[(\pi/(2a_1)]^2 = 0.427$. Except for this

correction factor, numerical results for the example discussed at the end of the one-dimensional analysis remain the same.

2.6.6 Influence of Two-Layer Structure upon Dynamic Heat Flow Measurements

The samples used in the experiments were layered structures, circular in cross section, consisting of two types; (a) a 0.2μ thick metal halide film on a 200μ thick borosilicate glass substrate, and (b) a 0.2μ thick metal halide film on a 0.2μ thick pellicle of N-type parylene. Each sample was supported around the circumference on an aluminum ring of inner diameter 0.5 inches. In the preceeding analyses the sample is assumed to be a single, uniform film. In this section the influence of the layered structure of the medium is examined. Appropriate modifications are made in the theory by introducing changes in the definitions of thermal parameters, appropriately weighting material properties such as thermal conductivity and specific heat to properly account for the geometry of the samples.

The geometry of the samples is illustrated in cross-section in Figure 2.6-45. It is assumed that the total thickness $D_1 + D_2$ of the

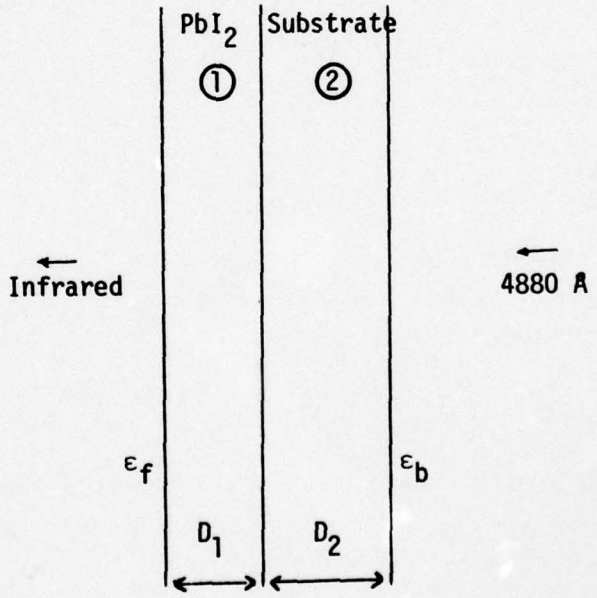

Figure 2.6-45. Cross-section of samples illustrating layered structure.

sample is much smaller than the heat conduction or diffusion distance for any time scale of interest in the experiments. Therefore, the temperature inside the sample is independent of the z coordinate and varies only in the radial direction, as previously. This assumption must be re-examined closely in evaluating the experiments on 200μ thick glass substrates.

The net rate of change of heat within a volume element at position r in cylindrical coordinates is

$$Q_{net} = \rho_1 c_1 \frac{\partial T}{\partial t} r\, d\phi\, dr\, D_1 + \rho_2 c_2 \frac{\partial T}{\partial t} r\, d\phi\, dr\, D_2 . \qquad (2.6.6\text{-}1)$$

Heat is generated by absorption of laser light which is incident from the substrate side of the sample. If the illuminating beam is uniform in cross-section across the sample, then the rate at which heat is generated is given by

$$Q_{source} = I_o [1 - \exp(-aD_2)]\, r\, d\phi\, dr, \qquad (2.6.6\text{-}2)$$

where I_o (watt/cm^2) is the incident intensity and $a(cm^{-1})$ is the absorption coefficient of the metal halide. The incident intensity I_o is specified just inside the PbI_2 layer, after refelction losses at the substrate-vacuum and PbI_2-substrate interfaces and standing wave effects in the substrate have been accounted for.

The rate at which heat is radiated from each surface is

$$Q_{Rad}^{(f)} = \varepsilon_f \sigma [T(r)^4 - T_A^4]\, r\, d\phi\, dr \qquad (2.6.6\text{-}3)$$

at $z = D_2$ and

$$Q_{Rad}^{(b)} = \varepsilon_b \sigma [T(r)^4 - T_A^4]\, r\, d\phi\, dr \qquad (2.6.6\text{-}4)$$

at $z = D_1$, just as previously.

Radial conduction of heat inside the sample gives a net flow of heat into the element of volume given by

$$-k_1 \frac{\partial T}{\partial r} r\, d\phi\, D_1 - k_2 \frac{\partial T}{\partial r} r\, d\phi\, D_2, \qquad (2.6.6\text{-}5)$$

while the rate at which heat is conducted outward through the surface at r + dr is

$$-k_1 \frac{\partial T(r + dr)}{\partial r} (r + dr)\, d\phi\, D_1 - k_2 \frac{\partial T(r + dr)}{\partial r} (r + dr)\, d\phi\, D_2. \qquad (2.6.6\text{-}6)$$

Upon expanding T(r+dr) in a Taylor series as before, the net rate of heat conduction into the volume element is found to be

$$Q_{cond} = (k_1 D_1 + k_2 D_2)\, r\, d\phi\, dr \frac{\partial^2 T}{\partial r^2} + (k_1 D_1 + k_2 D_2)\, dr\, d\phi \frac{\partial T}{\partial r} \quad . \qquad (2.6.6\text{-}7)$$

The dynamic heat balance equation formed from these contributions may be written in the form

$$(\rho_1 c_1 D_1 + \rho_2 c_2 D_2) \frac{\partial T}{\partial t} = (k_1 D_1 + k_2 D_2) \frac{1}{r} \frac{\partial}{\partial r} \left(r \frac{\partial T}{\partial r}\right) - (\varepsilon_f + \varepsilon_b)\, \sigma 4 T_A^3\, [T - T_A] + I_o\, [1 - \exp(-aD_2)]\, \Theta(-t). \qquad (2.6.6\text{-}8)$$

For the two-layer structure we may define average values k and α for the thermal conductivity and diffusivity as

$$k \equiv (k_1 D_1 + k_2 D_2) \,/\, (D_1 + D_2) \qquad (2.6.6\text{-}9)$$

and

$$\alpha \equiv \frac{(k_1 D_1 + k_2 D_2)}{(\rho_1 c_1 D_1 + \rho_2 c_2 D_2)} \quad . \qquad (2.6.6\text{-}10)$$

The rate of heat generation per unit volume is defined as

$$Q_v = I_o\, [1 - \exp(-aD_2)] \,/\, (D_1 + D_2), \qquad (2.6.6\text{-}11)$$

and the parameter β^2 is defined for the two layer structure as

$$\beta^2 = \frac{(\varepsilon_f + \varepsilon_b)\, \sigma 4 T_A^3}{(D_1 + D_2)\, k} \qquad (2.6.6\text{-}12)$$

with average k defined above. The dynamic heat balance equation may then be written as

$$\frac{1}{\alpha} \frac{\partial T}{\partial t} = \frac{1}{r} \frac{\partial}{\partial r} \left(r \frac{\partial T}{\partial r}\right) - \beta^2 (T - T_A) + \frac{Q_v}{k}\, \Theta(-t). \qquad (2.6.6\text{-}13)$$

This is precisely the same form which was solved for the previous one-layer problem, with α, β^2, k and Q_v redefined for two layers and exponential absorption.

The thermal properties of the substrate materials parylene - N and borosilicate glass are well known, and the thicknesses of each layer are determined by optical transmission measurements. The values of α and β^2 are found by analyzing the experimental data by computer to obtain the

best least-squared-deviation fit to the theoretical temperature distributions T(r,t). The emissivity of the metal halide film is measured independently. The properties α_2 and k_2 of the metal halide layer are then calculated directly from α and β^2 of the two-layer structure.

REFERENCES:

1. W. R. Harding, C. Hilsum, and D. C. Northrop, "A New Thermal Image-Converter," Nature 181, 691 (1958).

2. C. Hilsum and W. R. Harding, "The Theory of Thermal Imaging, and Its Application to the Absorption-Edge Image-Tube," Infrared Physics 1, 67 (1961).

3. J. K. Barr, "Spectral Emissivity by Interferometric Spectroscopy," Infrared Physics 9, 97 (1969).

4. J. O. White, T. R. Kirst and J. Tauc, "Amorphous Silicon as a Selective Absorber of Solar Energy: A Spectral Emissivity Study," Appl. Optics 17, 2427 (1978).

5. A. I. Carlson, "Transient Temperature Response of Thin Film Thermal Detectors in Infrared Imaging Systems," Appl. Optics 8, 243 (1969).

6. T. Minagawa, "Common Polytypes of PbI_2 at Low and High Temperatures and the 2H-12R Transformation," Acta Cryst. A31, 823 (1975).

7. M. Chand and G. C. Trigunayat, "Study of Structural Transformations During Growth of Lead Iodide Polytypes." J. Crystal Growth 30. 61 (1975).

8. E. Doni, G. Grosso, G. Harbeke, E. Meier, and E. Tosatti, "Interlayer Interaction and Optical Properties of Layer Semiconductors: 2H and 4H Polytypes of PbI_2," Phys. Stat. Sol. 68, 569 (1975).

9. M. R. Tubbs, "The Optical Properties and Chemical Decomposition of Lead Iodide," Proc. Roy. Soc. A280, 566 (1964).

10. M. R. Tubbs, "Dispersion Studies of Ionic Crystals with Layer Structures," J. Phys. Chem. Solids 27, 1667 (1966).

11. H. Y. Fan, "Temperature Dependence of the Energy Gap in Monatomic Semiconductors," Phys. Rev. 78, 808 (1950).

12. J. C. Zahner and H. G. Drickamer, "The Effect of Pressure on the Absorption Edge in Heavy-Metal Halides," J. Phys. Chem. Solids 11, 92 (1959).

13. I. Imai, "Experimental Study of Exciton Absorption in PbI_2," J. Phys. Chem. Solids 22, 81 (1961).

REFERENCES - (Cont'd.)

14. M. R. Tubbs and A. J. Forty, "The Exciton Spectrum of Lead Iodide," J. Phys. Chem. Solids 26, 711 (1965).

15. V. K. Miloslavskii, A. I. Rybalka, and L. A. Ageev, "Some Features of the Exciton Spectrum of Thin PbI_2 Films," Sov. Phys. Solid State 17, 733 (1975).

16. S. Nikitine and G. Perny, "Etude du Spectre de Raies d'absorption de PbI_2 aux Très Basses Temperatures," Comptes Rendus 240, 64 (1955).

17. S. Nikitine, J. Burckel, J. Biellmann, and R. Reiss, "Sur Quelques Observations Nouvelles Concernant les Spectres d'absorption, Réflexion et Photoluminescence de Monocristaux de PbI_2 à 4°K," Comptes Rendus 251, 935 (1960).

18. A. E. Dugan and H. K. Henisch, "Dielectric Properties and Index of Refraction of Lead Iodide Single Crystals," J. Phys. Chem. Solids 28, 971 (1967).

19. M. R. Tubbs, "The Optical Properties and Chemical Decomposition of Halides with Layer Structures," Phys. Stat. Sol. 67, 11 (1975).

20. A. B. Buckman and N. H. Hong, "Large Refractive Index Change in PbI_2 Films by Photolysis at 150-180°C," J. Opt. Soc. Am. 65, 914 (1975).

21. A. B. Buckman and N. H. Hong, "On the Origin of the Large Refractive Index Change in Photolyzed PbI_2 Films," J. Opt. Soc. A,. 67, 1123 (1977).

22. R. I. Dawood and A. J. Forty, "The Formation of Photographic Images in Single Crystals of Lead Iodide," Phil. Mag. 8, 1003 (1963).

23. M. G. Albrecht and M. Green, "The Kinetics of the Photolysis of Thin Films of Lead Iodide," J. Phys. Chem. Solids 38, 297 (1977).

24. J. B. Newkirk, "A Crystallographic Study of Mercuric Iodide," Acta Metallurgica 4, 316 (1956).

25. R. H. Bube, "Opto-Electronic Properties of Mercuric Iodide," Phys. Rev. 106, 703 (1957).

26. C. C. Coleman, "Growth of Large HgI_2 Single Crystals," J. Crystal Growth 6, 203 (1970).

27. J. P. Ponpon, R. Stuck and P. Siffert, "Properties of Vapor Phase Grown Mercuric Iodide Single Crystal Detectors," IEEE Trans. Nuclear Science NS-22, 182 (1975).

28. M. Slapa, G. C. Huth and W. Seibt, "Capabilities of Mercuric Iodide as a Room Temperature X-Ray Detector," IEEE Trans. Nuclear Science NS-23, 102 (1976).

29. S. P. Swierkowski, G. A. Armantrout and R. Wichner, "Recent Advances with HgI_2 X-Ray Detectors," IEEE Trans. Nuclear Science NS-21, 302 (1974).

30. S. P. Swierkowski, "High-Resolution HgI_2 X-Ray Spectrometers," Appl. Phys. Letters 23, 281 (1973).

31. K. Kanzaki and I. Imai, "The Optical Spectrum of HgI_2," J. Phys. Soc. Japan 32, 1003 (1972).

32. R. S. Scott and G. E. Fredericks, "Evaporative Degradation of HgI_2 X-Ray Detectors," Appl. Phys. Letters 27, 99 (1975).

33. M. R. Tubbs, "The Optical Properties and Chemical Decomposition of Halides with Layer Structures," Phys. Stat. Sol. 49, 11 (1972).

34. B. V. Novikov and M. M. Pimonenko, "Exciton Absorption and Luminescence of Tetragonal HgI_2 at Low Temperatures," Sov. Phys. Semiconductors 4, 1785 (1971).

35. M. K. Chung and S. W. Cho, "Preliminary Studies on Mercuric Iodide Soft-Gamma-Ray Detector," IEEE Trans. Nuclear Science NS-23, 112 (1976).

36. M. Schieber, R. C. Carlston, H. A. Lamonds, P. T. Randtke and F. W. Schnepple, "Purification, Growth and Characterization of Alpha Mercuric-Iodide Crystals for Gamma-Ray Detection," J. Crystal Growth 24/25, 205 (1974).

37. V. V. Mussil, V. K. Miloslaviskii, and V. V. Karmazin, "Exciton-Phonon Interaction and Faraday Effect in PbI_2," Sov. Phys. Solid State 17, 545 (1975).

38. A. Euken and E. Buchner, Z. Phys. Chem. B27, 321 (1934).

39. R. Minder, G. Ottaviani and C. Canali, "Charge Transport in Layer Semiconductors," J. Phys. Chem. Solids 37, 417 (1976).

40. International Critical Tables, Vol. III, (McGraw-Hill, New York, 1928) p. 44.

41. O. Kubaschewski and E. L. Evans, Metallurgical Thermochemistry (Permagon Press, Oxford, 1958).

42. "Parylene Pellicles for Space Applications," Union Carbide Corporation, Technical Report No. 10, October 1977.

43. F. Urbach, "The Long-Wavelength Edge of Photographic Sensitivity and of the Electronic Absorption of Solids," Phys. Rev. 92, 1324 (1953).

44. H. Mahr, "Ultraviolet Absorption of KI Diluted in KCl Crystals," Phys. Rev. 125, 1510 (1962).

APPENDIX A

PbI_2 Films on Nitrocellulose Pellicles

PbI_2 was deposited onto six nitrocellulose pellicles which were supplied by Night Vision Laboratories. The nitrocellulose pellicles were less than 450 Å thick, as shown by the optical transmission curves of pellicle No. IV in Figure A-1. The first order transmission minimum occurs at a wavelength smaller than 2500 Å, indicating that the product $n(\lambda)D$ of refractive index times thickness is smaller than 625 Å. Two of the nitrocellulose pellicles, designated as Samples V and VI, had a gold black absorption coating on the back surfaces, reportedly 1.0 optical density at 10 μm wavelength. All the pellicles were taut when received. They were stored inside a dessicator, because N.V.L. reports they sag when exposed to humidity for a long period of time. A few pinholes were noted in the two samples which had the gold black coatings. Also, these two samples sere slightly less taut than the others, as evidenced by large vibration amplitudes of the membrane during handling.

The samples had been mounted on 3 cm i.d. aluminum rings. Our sample holder was modified to accommodate this sample size, somewhat larger than our previous samples. The following labeling system is used to identify individual samples after the PbI_2 depositions: Month-day-deposition run order for that day - substrate label. For example, Sample No. 1005AI indicates a PbI_2 deposition made on October 5, run number A or the first run of the day, onto nitrocellulose substrate I.

Previous experience in depositing PbI_2 onto parylene indicates the optimum procedure should be a slow growth rate at the highest substrate temperature possible to obtain oriented polycrystalline PbI_2 films. N.V.L. reports that nitrocellulose pellicles are stable to about 110°C, and have survived as high a temperature as 120°C. Our first PbI_2 deposition was attempted with a substrate temperature of 90°C. The coated pellicles sagged, as shown in the photograph of Figure A-2. For lower substrate temperatures, the samples still sagged, although less severely. The thermocouple in the substrate holder did not register a temperature increase during the deposition at 25°C.

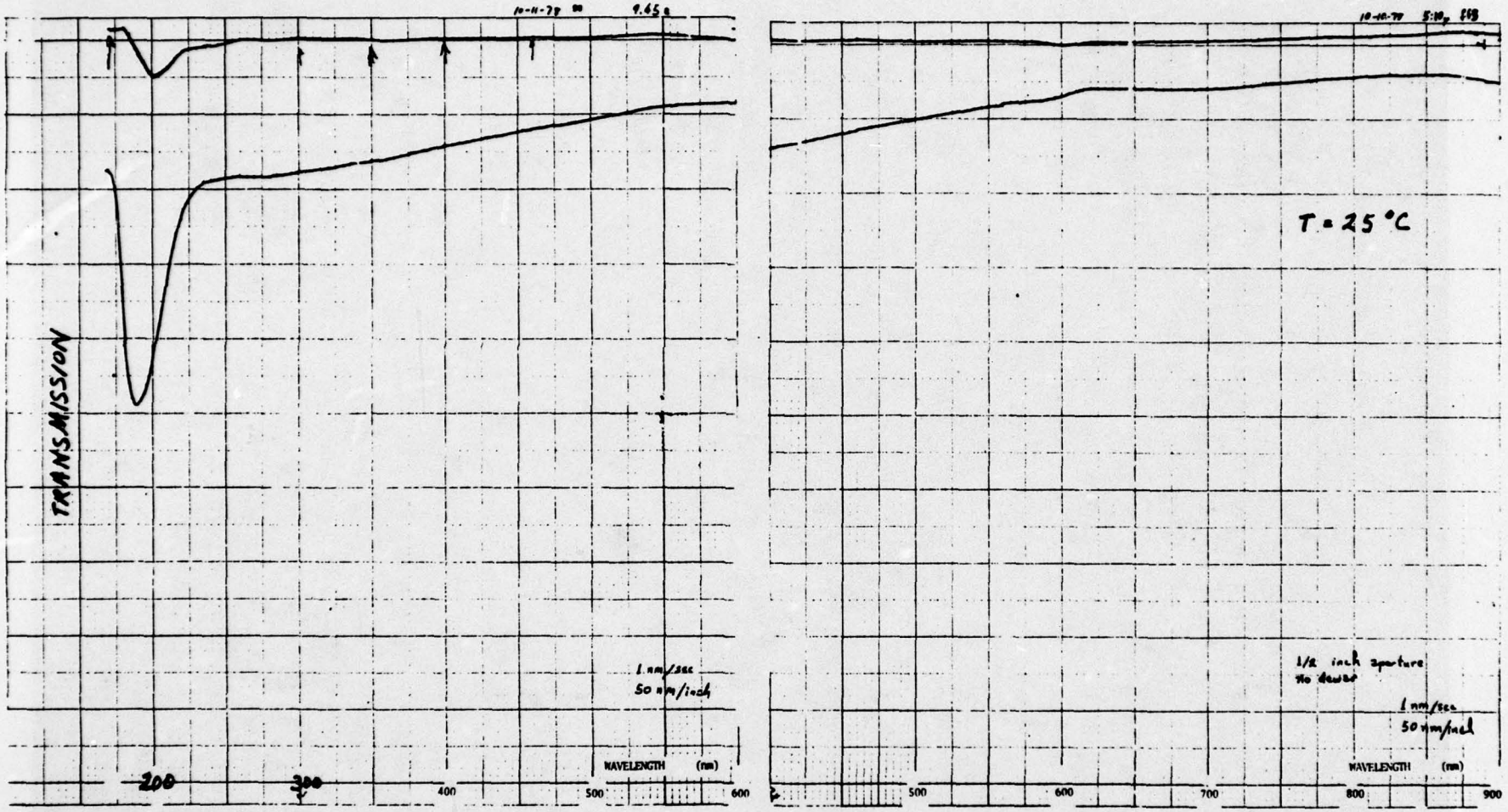

Figure A-1. Transmission of Nitrocellulose Pellicle No. IV from 900 nm to 200 nm.

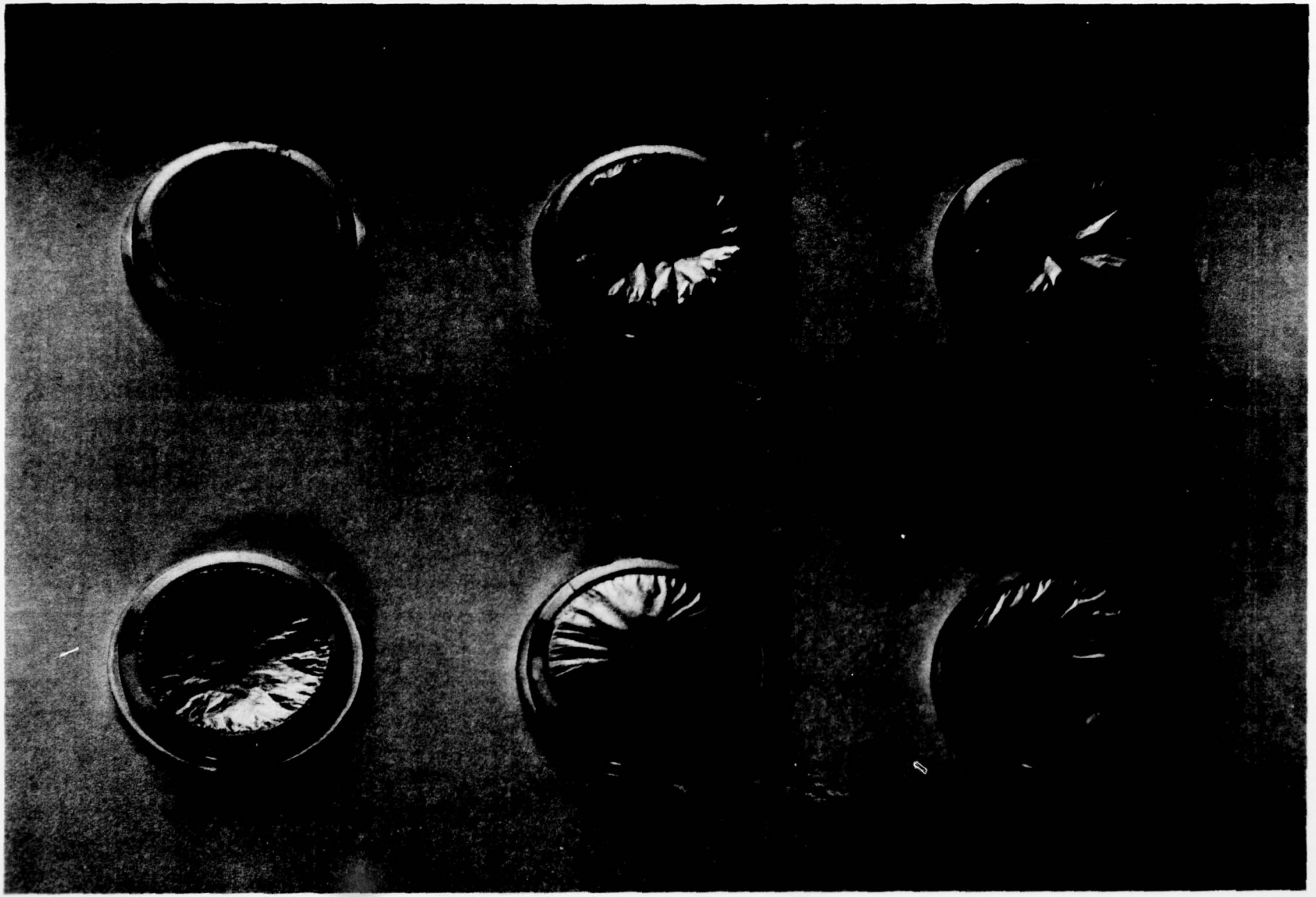

FIGURE A-2. PbI_2 on Nitrocellulose. From Left to Right, Bottom Row: 1005AI, 1005BII, 1006AIII, Top Row: 1011AIV, 1009AV, 1010AVI.

AD-A069 537 ROCKWELL INTERNATIONAL ANAHEIM CA ELECTRONICS RESEAR--ETC F/G 11/6
TEMPERATURE SENSITIVE OPTICAL PHENOMENA IN HEAVY METAL HALIDE F--ETC(U)
JAN 79 J D MCMULLEN, D M HEINZ, F S STEARNS DAAK70-77-C-0165

UNCLASSIFIED C79-8-501 NL

4 OF 4
AD. A069537

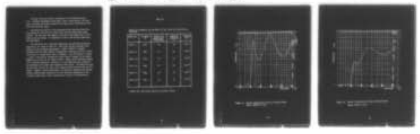

END
DATE FILMED
7-79
DDC

The PbI_2 films are visually transparent, with thicknesses about 0.2μ. Thickness measurements were made, using a Sloan Decktak, on three glass substrates which were exposed to the PbI_2 source simultaneously with each nitrocellulose sample.

Nitrocellulose pellicle IV was punctured during handling before the PbI_2 deposition, and pellicle V burst after the PbI_2 deposition during cooling. The very fact that Sample IV survived a PbI_2 deposition at 110°C without tearing further, is remarkable in view of our previous experience with parylene-N.

The deposition rate, substrate temperature, and pressure during each deposition are listed in Table A-1, along with the PbI_2 thickness indicated by the profilometer measurements. Sample 1011AIV is markedly different from the other samples in appearance, exhibiting a duller surface finish with an "orange peel" type of roughness. This difference is further apparent in the optical transmission curves shown in Figure A-3 for sample 1006AIII and Figure A-4 for sample 1011AIV. Sample 1011AIV exhibits greater loss, caused by absorption, scattering, or both absorption and scattering at wavelengths much longer than absorption edge values. The deposition rate may have been too fast to form a well ordered, polycrystalline film for this sample. However, further experiments are required to determine the optimum balance needed between deposition rate and substrate temperature to consistently produce PbI_2 films of good optical quality on nitrocellulose.

TABLE A-1

Deposition parameters and thickness of PbI_2 films on nitrocellulose pellicles.

SAMPLE NO.	THICKNESS Å	AVERAGE PbI_2 GROWTH RATE Å PER MINUTE	SUBSTRATE TEMPERATURE °C	PRESSURE torr
1005 A I	2100	42	90	$4x10^{-7}$
1005 B II	2000	47	50	$4x10^{-6}$
1006 A III	2100	60	24	$2x10^{-8}$
1011 A IV	2000	111	110	$4x10^{-8}$
1009 A V*	2000	67	24	$3x10^{-8}$
1010 A VI*	2100	83	24	$2x10^{-8}$

* Sample had a gold black coating on the back surface.

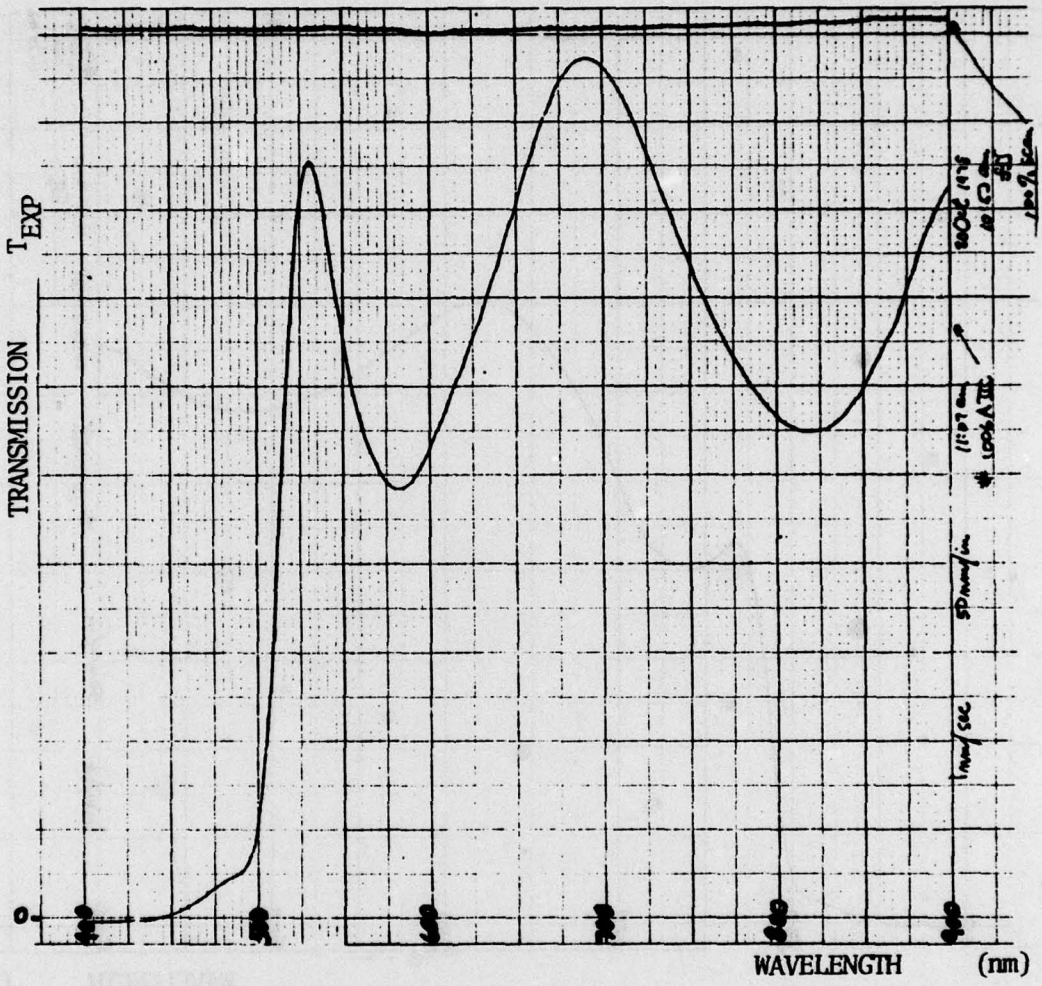

FIGURE A-3. Optical Transmission of PbI_2 on Nitrocellulose Sample 1006AIII at 25°C.

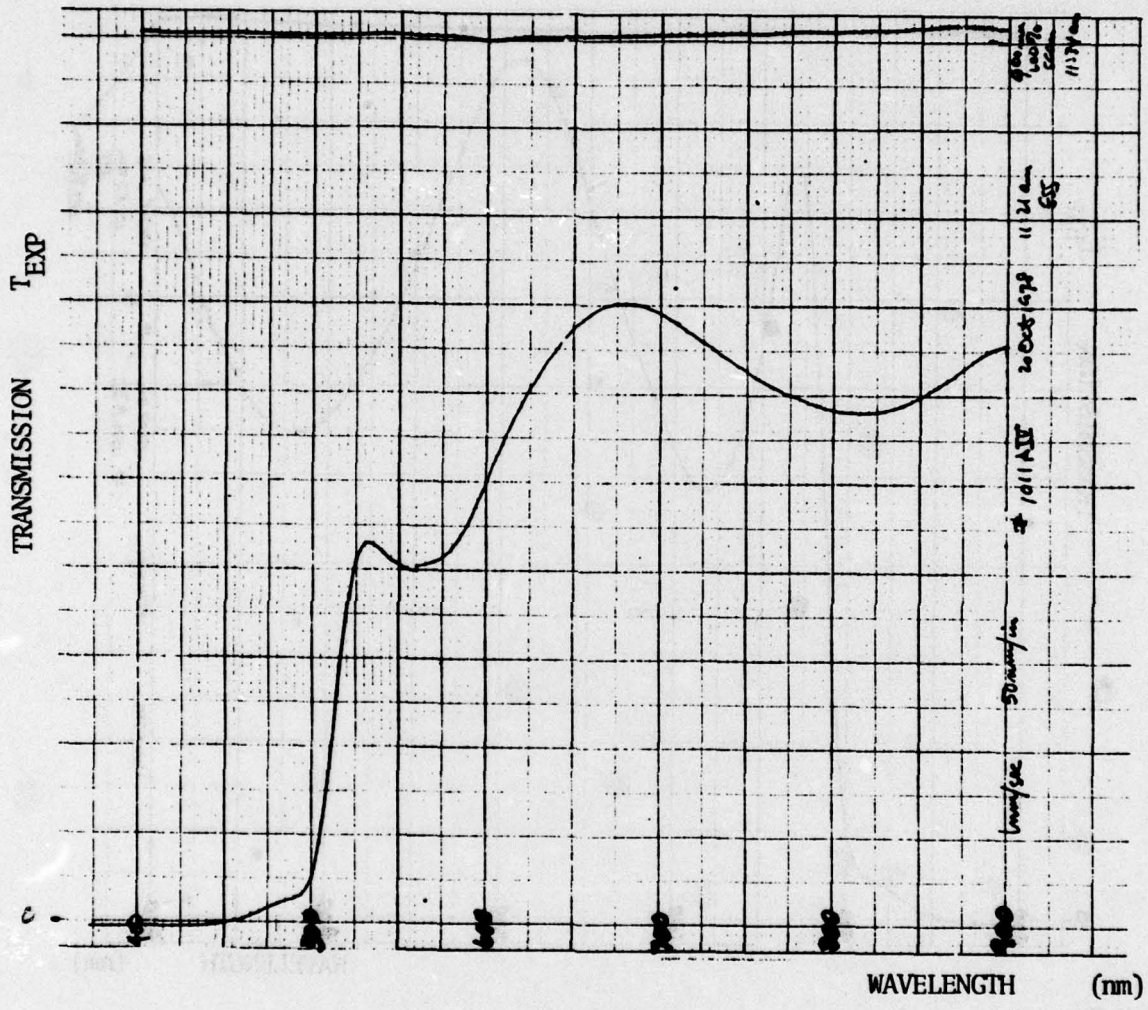

FIGURE A-4. Optical Transmission of PbI_2 on Nitrocellulose Sample 1011AIV at 25°C.